

**BIOMIMETIC INTEGRIN-SPECIFIC SURFACES TO DIRECT
OSTEOBLASTIC FUNCTION AND TISSUE HEALING**

A Dissertation
Presented to
The Academic Faculty

by

Timothy Andrew Petrie

In Partial Fulfillment
of the Requirements for the Degree
Doctor of Philosophy in the
School of Biomedical Engineering

Georgia Institute of Technology
August 2009

**BIOMIMETIC INTEGRIN-SPECIFIC SURFACES TO DIRECT
OSTEOBLASTIC FUNCTION AND TISSUE HEALING**

Approved by:

Dr. Andrés J. García, Advisor
School of Mechanical Engineering
Georgia Institute of Technology

Dr. Todd C. McDevitt
School of Biomedical Engineering
Georgia Institute of Technology

Dr. Barbara D. Boyan
School of Biomedical Engineering
Georgia Institute of Technology

Dr. Johnna S. Temenoff
School of Biomedical Engineering
Georgia Institute of Technology

Dr. Andrew Lyon
School of Chemistry and Biochemistry
Georgia Institute of Technology

Date Approved: May 14, 2009.

This dissertation is dedicated to my Mom, my Dad, and my big Bro, all without which my terrorizing IBB would not have been possible.

ACKNOWLEDGEMENTS

I have enjoyed my time here immensely at Georgia Tech, despite my west coast roots, and I can only attribute this fantastic and educational experience to the great many friends, colleagues, and professors with which I have been able to interact. Above all, and before thanking all of these people, I must acknowledge the superb advising of my advisor, Andres Garcia, who has, contrary to popular belief, represented to me more than just a “signature” and a ‘walking wallet’. Andres has been my surrogate Dad in the South, a strong individual who has taken me under his wing and closely guided my transformation from a messy post-undergrad to a messy PhD. Like a father, he has been there to let me know quite robustly when I screw up, but also has continuously provided encouragement and congratulations with each little success I have achieved. His boisterous laugh and our never-ending quips ranging from the merits (or demerits) of Bezerkeleyisms, baseball, football, SuperMax, etc. have always picked me up when I am feeling the monotony of graduate life. Lab has always been fun (and less productive) when he is around joking with us. I cannot seriously imagine a better advisor, colleague, and friend as Andres has been for the past (almost) six years. From our first meeting in wonderful Reno in the back room of a shady restaurant through our time together in the Dirty South, I will fondly look back at this time almost entirely due to his presence and guidance – and I look warmly to future work, encounters, and wasting of time with Andres.

I would also like to thank my committee for their time, patience, and effort. I have gotten to know each of my thesis members very well the past 5-6 years, and this

interaction has made me a better scientist, and, I hope, person. Dr. Barbara Boyan has always been so supportive, but firm as well when she needed to be, and I am very thankful she is in my corner. Dr. Todd McDevitt has assisted me with various experimental setups as well as providing a sounding board for career aspirations and questions. Dr. Johnna Temenoff has provided sound support for my career plans and provided key critiques of many of my experiments, making them more sound ultimately. Dr. Andrew Lyon has helped me greatly in the chemistry portion of the thesis, as well as by providing a non-biomaterials perspective of a large number of issues.

I would be remiss (and a fool) not to take this opportunity to thank my Real parents now as well, who have had to deal with my shenanigans a full 3 times as much time as Andres – without getting paid for any of it too. My Dad, Thomas, and Mom, Marlene, have gone through the same graduate process back in more fun times in the ‘70s, and have always been there to help me and hear me out through my time here. Without them, I would not be even closer to where I am today. Also, their house in San Diego provides me the extra motivation to work hard so I can vacation back in paradise. Please, Mom and Dad, do not sell the house!

The last 9 months have been my most enjoyable primarily because of my girlfriend, Rachel Horak, who has been going through this PhD journey step-by-step as well. You have been a great friend and companion, and introduced me to many cool, new things. I have felt extremely lucky to be with you during this time. A shoutout to Pancho Leon, Tomasa, and Mr. Stinky, our ferrets, for the stress releasers that they have been.

My brother, Jon, who has been deemed even more “unique” than me, has been my rock and best friend throughout my life. He is undergoing this same journey at Cornell,

and he gives me an outlet to experience snow for short periods of time when I visit. I am sure we will stay close, and, one magical day, he will even be able to meet Supermax in person. Until that day, I wish my most excellent brother all the best in getting his PhD done, and thank him profusely for always being there to help me out in any way I need, and, finally, being the best San Diego Charger Super Fan compatriot ever (and getting kicked out of hostile stadiums during road games).

I think anyone who has enjoyed their PhD journey will attribute much of the success to the laboratory social environment. Working 70 + hour weeks can take its toll over time, but when the lab is so fun to be in, time does really fly. Many past members, now Doctors themselves, were instrumental in helping me early on. Cathy Reyes and Charlie Gersbach were two of my earliest friends in the lab, and Cathy especially was my partner in crime for 3 years in the biomimetic project. She is still the only genius I have ever met who can come in at 11, take a 2 hour “Starbucks” break, and leave at 4 and achieve better results than I can only dream of. She and her husband, Charlie, will forever be my good friends, and I wish them all the best starting their new life on the east coast (after a few years in my hometown). Dr. Jenn Phillips has been a great role model for me as she has spent a few years undertaking a postdoc appointment in biology, which I have planned to do. I have had the pleasure to get to know her even better over the last year or two while collaborating on a paper. I cannot think of a more competent, driven, intelligent, and, when finally coaxed, silly, individual than Jenn, and I hope she keeps following (cliché alert) her heart to the great many successes that surely await her down the road. Dr. Benjamin Keselowsky was my predecessor in a way, since I observed from his exploits that charm and ingenuity can go a long way in the face of absurd messiness

and eccentricity. I always look forward to meeting him at conferences, and he was instrumental in getting me firmly situated in the lab my first year or two, as well as introducing me to the merits of GTA, music downloading, and napping in the microscope room. I must thank Dr. Nathan Gallant for showing me micropatterning techniques, and providing the all-around laid back presence that was so nice in the lab. Dr. Kristin Michael was a great colleague to have for scientific discussions, Starbucks breaks, and travel stories. I wish her all the best internationally in her synergistic role as a research scientist/007 American spy. Dr. Jeffery Capadona was a huge positive influence on me early on in the lab, and we have collaborated on several papers. He remains one of the best analysts and thinkers I have met, and is having tremendous success in his backup job as a scientist at Case Western (ever since his ideal stay-at-home Dad occupation didn't quite do it for him). I hope to continue to see him at conferences and correspond with him in the future. I thank Dr. Amanda Walls for putting up with me for 4 years as my deskmate, through all the paper avalanches, 4 'o clock Tuna Trains, and keyboard jelly she was cool as a cat. Her dry and witty repertoire with me kept me going through some dull afternoons, and I hope and trust she is doing great in her consulting job in Phoenix. Dr. Jenny Raynor, who worked in Dr. David Collard's lab in Chemistry, was a challenging joy to work with, collaborating on several papers and was an essential individual for my thesis. Despite past non-rosy chemistry collaborations, I look up to chemists now because of my work with her and Dr. David Collard, who has been tremendously supportive as well.

The last few years have been especially fun and productive for me in lab, and I am more than happy to thank the current individuals who have entertained and assisted

me during this time. The person most responsible for me not blowing the lab up and keeping my butt in line has been Kellie Burns, our ultra-competent, employee of the millennium lab manager. I will always value our friendship and both the stern and light-hearted face-to-faces we have had over the years. We have grown up in the lab together and I feel extremely lucky to have worked with a colleague like Kellie my entire time here. I know you “got my back” and cannot thank her enough for the hard work she has invested in the lab. She is the Atlas of this production factory, and if I had to choose just one person to run a lab, she would be it. It has been a true pleasure.

My primary partner-in-crime the last 3 years, helping me light up the sky-yyy-yyy whenever we can, and providing thunderbolts of lightning of pain during basketball and football IM games, David Dumbauld, despite his humble pandering to the contrary, is one of the most intelligent and grounded people I have met in my 27 years. We have had numerous conversations that, within one single conversation, have touched on important research experiments, philosophical meanderings, Cincy Bengals and Ocho Cinco, Ohio State vs. Cal, soul-less children of certain hair color, and so on. Whatever he decides to do down the road with respect to his career, he and his wife Kelly will enjoy life as usual and succeed brilliantly, also as usual (hopefully on the west coast, but doubtful). I look forward to much more trash-talking and science musing for a long time, big man.

I have had the joy of working with another intelligent ginger-colored individual, Dr. Abbey Wojtowicz, who I don't believe has ever NOT had a smile on her face. She and Dr. Joe Charest have been great pals to go out, talk shop, and collaborate with, and I cannot count the number of times she has picked me up with her fantastic smile and happy demeanor. I am sure I will see her many times again, and I wish both of them the

very best in Boston. Sean Coyer, now the veteran of the lab, has been very fun to work, eat, and play basketball with during my tenure. He is the Cool Hand Luke of the lab, and I always feel about 10 Rick James shades ‘sauver’ after talking with him. I hope we interact heartily in the future, as he is a top notch problem solver and all-around fun guy. I have only gotten to know Edward Phelps for the past several years, but in just that short amount of time he has established himself in the ‘Cathy Reyes’ level of experimental expertise. Ed is one of the most likeable guys I know, is a natural-born scientific genius, has the best dog eh-ver, and I am truly saddened I will not be present to watch his career bloom even more. Nonetheless, I am very thankful for his assistance in our German collaboration and treasure our friendship. Ed, we need to climb a mountain soon! Rachel Whitmire has been a great friend and labmate, and I appreciate so much her helping keep the lab in tiptop shape. We are like the YinYang of the lab cleanliness. I wish her, Jay, and Emma all the best in the rest of your graduate career and new abode. Nduka E. (for I still cannot pronounce his lat name, my apologies, bud) has Abbey Syndrome – he simply always has a gleaming and great smile on his face. I have never failed to laugh when I am around him for more than 5 seconds. He is an absolute attribute to the lab and to my life herein, and is one of the all-around best and brightest people I have had the pleasure to meet and work with. I am also thankful I will never have to play bball with him again, as he makes me feel old, slow, and lazy. Asha is the quick and sharp wit in the lab, the fastest jab-slinger in the east, and I have enjoyed being kept on my toes the past few years with her. In addition, she has carefully assisted me with rat surgeries and other experiments. I’d like to thank the “newbies” in the lab, Chi-Chi, Ram, Stacey, for respecting their elders (for the most part) and not lacking discipline. They are extremely

polite and are good people. I am sure the new generation in the lab will be just as successful and hopefully even more, than our generation has been.

I have also had the opportunity to collaborate and be entertained by a wide range of students in the Orthopedic Wing 2D, IBB, and Whitaker in general. Special thanks to Jay Sy for DLS assistance, Andrew Raines, Cool Cat Cornellian Chris Lee, Kevin Wong, Srin Nagaraja, Angela Lin, Ken Dupont and everyone else in 2D. The architectural setup is fantastic for social interaction, and everyone has taken advantage to all of our benefit.

Although not related directly to research, I think intramural sports teams contribute mightily to fostering our competitive edge and mental health that allows students such as myself to enjoy the PhD journey so much more. I would like to thank Meg McDevitt and Colly Mitchell for allowing me to put together so many sports teams over the years, and I feel we have represented IBB and Bioengineering in general robustly, attaining several championships and becoming the powerhouse of awesomeness that we are currently. I'd like to thank some of the close group of athletes who have chosen to become part of this greatness of man: the One, the Only, the Crazy, Andres Bratt-Leal, whose Cheshire-like smile belies the tenacious freight train fury that lies underneath; Richard Carpenedo, my running nemesis and all-around superb athlete; Matt Magnuson, the Swedish Rock of Cajunville; Ken Dupont, the Caucasian Shaq and all-around gentle giant, Nduka, who always embarrasses me on the bball court; Blaine Zern, Downtown Brown from Philadelphia; David Dumbauld, who somehow is a great athlete despite his colorific handicap and elongated frame, and, of course, Bryan Bell, who always was tied for me for the league lead in technical fouls. A pleasure to play with you Bryan, despite our "competitiveness", and with everyone else of course too.

I'd also like to thank all my friends over the years who have given me support when I have needed it and a welcome respite from lab work: Vincent Fiore, Adan, The Forum Athletic Club Crew, Chris Lee, Brent-Time (Kansas styley), Erin, and everyone else that has temporarily skipped my mind. I am grateful for the friendship of every one of you.

TABLE OF CONTENTS

	Page
ACKNOWLEDGEMENTS	iv
LIST OF FIGURES	xvi
LIST OF SYMBOLS AND ABBREVIATIONS	xx
SUMMARY	xxii
<u>CHAPTER</u>	
1 INTRODUCTION	1
2 BACKGROUND AND LITERATURE REVIEW	6
Extracellular Matrix-Derived Ligands	6
ECM: Composition and Role	6
Cell-ECM Adhesive Interactions	7
Engineering Biomaterial Surface Properties	14
ECM-mimetic Surface Strategies	17
Advanced ECM-mimetic Surface Strategies	33
Orthopedic Implant Surface Technologies	37
Bone Function and Formation	37
Bone Growth and Differentiation Factors	38
Osseointegration of Bone-Anchored Implants	39
Host and Material Response at the Bone Interface	39
Orthopedic Surface Strategies	41
Biomolecular Delivery Approaches	43
Summary	44

3	INTEGRIN SPECIFICITY AND ENHANCED CELLULAR ACTIVITIES ASSOCIATED WITH SURFACES PRESENTING A RECOMBINANT FIBRONECTIN FRAGMENT COMPARED TO RGD SUPPORTS	46
	Introduction	46
	Materials and Methods	48
	Reagents, Antibodies, and Cells	48
	Recombinant FNIII ₇₋₁₀ Production	50
	Model Biomaterial Surfaces	51
	Enzyme-Linked Immunosorbent Assay (ELISA) and Surface Density Measurements	52
	Centrifugation Cell Adhesion Assay	53
	Immunofluorescence Staining for Integrins and Focal Adhesions	53
	FAK Phosphorylation Assay	54
	Cell Proliferation Rate	55
	Statistics	55
	Results	56
	Recombinant FNIII ₇₋₁₀ has Equivalent Biological Activity as Plasma FN	56
	FNIII ₇₋₁₀ Displays Enhanced Cell Adhesive Activity Compared to RGD Peptides	58
	FNIII ₇₋₁₀ Surfaces Exhibit Different Integrin Specificity than RGD Supports	64
	FNIII ₇₋₁₀ Interfaces Trigger Enhanced Signaling and Cell Proliferation	68
	Discussion	71
	Summary	74
4	THE EFFECT OF INTEGRIN-SPECIFIC BIOACTIVE COATINGS ON TISSUE HEALING AND IMPLANT OSSEOINTEGRATION	75
	Introduction	75

Materials and Methods	77
Poly(OEGMA) Polymer Brush Preparation and Peptide Tethering Titanium	on 77
Cell Adhesion and Integrin Binding Assays	78
Osteogenic Differentiation Assays	79
Implantation Procedure and Analysis	79
Statistics	80
Results	80
Bio-functionalized Implant Coatings to Convey Integrin Binding Specificity	80
Effects of Integrin-Specific Implant Surfaces in Modulating Osteoblastic Differentiation and Mineralization	90
Integrin Specificity Modulates Functional Implant Osseointegration In Vivo	92
Discussion	96
Summary	99
5 SIMPLE APPLICATION OF FIBRONECTIN-MIMETIC COATING TO ENHANCE OSSEOINTEGRATION OF TITANIUM IMPLANTS	101
Introduction	101
Materials and Methods	103
Bioadhesive Ligands and Preparation of Surfaces	103
Cell Adhesion, Integrin Binding, and Signaling Assays	104
Proliferation Assay	106
Osteoblast-Specific Gene Expression	106
Alkaline Phosphatase (ALP) Activity and Matrix Mineralization Assays	107
Implantation Procedure and Functional Analysis	107
Statistics	109

Results	109
FN-mimetic Ligand Coatings	109
FN-mimetic Ligand Surfaces Promote Integrin-Specific Cell Adhesion and Signaling	110
Integrin-Specific Ti Coatings Modulate In Vitro Osteogenic Activities	114
Integrin $\alpha_5\beta_1$ -Specific Bioactive Coatings Enhance Implant Osseointegration	118
Discussion	122
Summary	125
6 NANOSCALE CLUSTERING OF INTEGRIN-SPECIFIC LIGANDS MODULATES ADHESIVE ACTIVITIES AND IMPLANT OSSEOINTEGRATION	126
Introduction	126
Materials and Methods	128
Multimer Preparation and Ligand Characterization	128
Cell Source and Culture	130
Binding Site Accessibility and Integrin Binding Assays	130
Spinning Disk Adhesion Strength Assay	132
Implantation Procedure and Functional Analysis	133
Statistics	134
Results	135
FNIII ₇₋₁₀ Multimeric Ligand Purification and Assembly	135
Multivalent FN-mimetic Ligands Enhance Integrin-Specific Binding and Adhesion	137
Multivalent FN-mimetic Ligand Coatings Enhance Early and Longer-Term Implant Osseointegration	143
Discussion	148

Summary	152
7. SUMMARY AND FUTURE CONSIDERATIONS	154
Introduction	154
Discussion	155
Fine-Tuning Integrin Specificity	155
Exploring Clustered Ligand Presentation	157
Elucidating In Vitro and In Vivo Mechanisms	158
Expanding Beyond 2D: Three-Dimensional Cell-Material Interactions	164
Assessing Clinical Coating Stability	165
Summary	166
APPENDIX A: PROTOCOLS	167
APPENDIX B: MICROPATTERNED SURFACES WITH CONTROLLED LIGAND TETHERING	173
APPENDIX C: CONTROLLING CELL ADHESION TO TITANIUM: FUNCTIONALIZATION OF POLY(OLIGO(ETHYLENE GLYCOL) METHACRYLATE) BRUSHES WITH CELL ADHESIVE PEPTIDES	197
REFERENCES	212
VITA	237

LIST OF FIGURES

	Page
Figure 2.1: General key roles of the extracellular matrix in regulating cellular response in tissue	8
Figure 2.2: Integrins link the extracellular and intracellular environments	11
Figure 2.3: Focal adhesion (FA) formation	12
Figure 2.4: List of selected native ECM proteins and known associated binding epitopes	13
Figure 2.5: Different modes of adsorption to biomaterial surfaces for integrin binding ligands	15
Figure 2.6: ECM-derived surfaces to direct integrin specificity to direct a focused cell response	19
Figure 2.7: Integrin-specific ligand clustering may augment integrin-mediated cell functions	36
Figure 3.1: Monobiotinylated FNIII ₇₋₁₀	57
Figure 3.2: Monobiotinylated FNIII ₇₋₁₀ exhibits equivalent biological activity as pFN	60
Figure 3.3: Bioadhesive ligand tethering to mixed SAMs	62
Figure 3.4: MC3T3-E1 cell adhesion strength to SAMs presenting controlled densities of bioadhesive ligands	63
Figure 3.5: Surfaces presenting FNIII ₇₋₁₀ display integrin binding specificity compared to RGD supports	65
Figure 3.6: Immunofluorescence staining for bound integrins and vinculin in MC3T3-E1 cells seeded for 4 h on FNIII ₇₋₁₀ and RGD-tethered SAMs	67
Figure 3.7: Phosphorylation of site-specific tyrosine residues of focal adhesion kinase (FAK) in MC3T3-E1 seeded cells on saturated density RGD and FNIII ₇₋₁₀ -tethered surfaces	69
Figure 3.8: Proliferation for MC3T3-E1 cells cultured for 20 h on RGD and FNIII ₇₋₁₀ -tethered surfaces for two different peptide densities	70
Figure 4.1: Poly(OEGMA) brushes with ligand tethered on titanium	82

Figure 4.2: Bioresistance and ligand tethering on poly(OEGMA) brushes on titanium (Ti)	84
Figure 4.3: Poly(OEGMA) brushes on Ti functionalized with integrin ligands display integrin specificity	87
Figure 4.4: FAK activation on equimolar ligand-tethered brush surfaces and serum-treated titanium is integrin-dependent	89
Figure 4.5: FNIII ₇₋₁₀ -functionalized surfaces enhance osteoblastic differentiation and mineralization in bone marrow stromal cultures at 7 days	91
Figure 4.6: Integrin specificity modulates <i>in vivo</i> implant osseointegration	95
Figure 5.1: Surface density and accessibility of bioactive integrin ligands adsorbed on titanium surfaces	112
Figure 5.2: Titanium surfaces functionalized with bioactive integrin ligands display integrin specificity	113
Figure 5.3: Initial cell signaling (FAK activation) and proliferation on equimolar ligand-treated and serum-treated Ti surfaces is integrin-dependent	116
Figure 5.4: FNIII ₇₋₁₀ -treated surfaces enhance expression of osteoblast-specific genes in bone marrow stromal cultures at 7 days post-seeding	117
Figure 5.5: Bone marrow stromal cells on FNIII ₇₋₁₀ -treated surfaces exhibit higher levels of markers for osteoblastic differentiation after 7 days in culture and more advanced matrix mineralization than pFN-treated or serum-treated Ti (14d)	119
Figure 5.6: Biomimetic ligand coatings targeting specific integrin receptors modulate <i>in vivo</i> implant osseointegration	121
Figure 6.1: Multimeric integrin ligands with varying FNIII ₇₋₁₀ valency	137
Figure 6.2: Nanoclustering integrin ligands augments integrin-specific binding	140
Figure 6.3: Nano-clustered integrin-specific ligands enhance cell adhesive strength	142
Figure 6.4: Nano-clustered ligand coatings targeting specific integrin receptors modulate early time-point (10 d) <i>in vivo</i> implant osseointegration	145
Figure 6.5: Nano-clustered ligand coatings targeting specific integrin receptors enhance functional <i>in vivo</i> implant osseointegration at 4 and 12 wks	147
Figure 7.1: Preliminary paracrine experiment examining osteogenic role of media soluble factors of cells on different integrin-specific surfaces	160

Figure 7.2: Caged cyclo(RGD) peptide system for assessing time-dependent effect of ligand exposure on cell function	163
Figure A2.1: Microcontact printing (μ -CP) islands of self assembled monolayers (SAMs) of mixed alkanethiols (EG ₃ and EG ₆ -COOH) onto gold-coated glass substrates	181
Figure A2.2: Summary of entire optimization procedure and analysis of each major variable/condition investigated, including stamping time, stamping weight, mixed SAM ratio, and post-surface activation ligand exposure time	184
Figure A2.3: Correlation of AF488 tethered surface density between SPR and fluorescent intensity image quantification (FIIQ)	186
Figure A2.4: Control over density of tethered ligand on μ -CP islands	188
Figure A2.5: Pattern homogeneity is maintained over a range of tethered ligand density on μ -CP mixed SAM surfaces	189
Figure A2.6: Multiple ligands can be tethered in a controlled manner to μ -CP mixed alkanethiol SAM islands	191
Figure A2.7: μ -CP mixed alkanethiol SAM patterns of different sizes and shapes can be prepared by modifying the stamp design	193
Figure A3.1: Poly(OEGMA) brush synthesis schematic	200
Figure A3.2: Synthesis schematic of initiator	202
Figure A3.3: Carbonyl region of FTIR spectrum throughout formation of peptide-modified polymer brushes on titanium	202
Figure A3.4: XPS profiles of various stages of brush formation	203
Figure A3.5: Control over brush thickness	203
Figure A3.6: Poly(OEGMA) brushes on Ti resist cell adhesion	206
Figure A3.7: SPR profile of GFOGER-exposed poly(OEGMA) brushes	209
Figure A3.8: GFOGER immobilized on poly(OEGMA) brushes promotes cell adhesion	210

LIST OF SYMBOLS AND ABBREVIATIONS

ECM	extracellular matrix
FN	fibronectin
MAPK	mitogen-activated protein kinase
ERK	extracellular signal-related kinase
FAK	focal adhesion kinase
HA	hydroxyapatite
SAMs	self-assembled monolayers
COL	collagen
BSP	bone sialoprotein
RGD	arginine-glycine-aspartic acid
PHSRN	praline-histidine-serine-arginine-asparagine
DGEA	aspartic acid-glycine-glutamic acid-alanine
GFOGER	glycine-phenylalanine-hydroxyproline-glycine-glutamic acid-arginine
PLL-g-PEG	poly(L-lysine) –poly(ethelene) glycol
REDV	arginine-glutamic acid-aspartic acid-valine
FNIII ₇₋₁₀	FN fragment encompassing the 7 th through 10 th type III repeats
TI	titanium
BMP	bone morphogenic protein
BMSCs	bone marrow stromal cells
PMMA	poly methyl methacrylate
MSCs	mesenchymal stem cells
TGF	transforming growth factor
FBS	fetal bovine serum

PBS	phosphate-buffered saline
EDC	1-Ethyl-3-[3-dimethylaminopropyl]carbodiimide Hydrochloride
NHS	N-hydroxysuccinimide
BSA	bovine serum albumin
SPR	surface plasmon resonance
DTSSP	3,3'-Dithiobis[sulfosuccinimidylpropionate]
pFN	plasma fibronectin
ELISA	enzyme-linked immunosorbent assay
ADH ₅₀	half-maximal adhesion strength
OEGMA	oligo(ethylene glycol) methacrylate
XPS	x-ray spectroscopy
FTIR	fourier transform infrared spectroscopy
NPC	nitrophenyl carbamate
RT-PCR	reverse transcriptase polymerase chain reaction
SI-ATRP	surface-initiated atom transfer radical polymerization
OCN	osteocalcin
MEM	minimum essential media
ALP	alkaline phosphatase
PMSF	fetal bovine serum
LPA	Lysophosphatidic acid
GF	growth factor
SANPAH	<i>N</i> -Succinimidyl-6-(4'-azido-2'-nitrophenylamino) hexanoate
GFP	green fluorescent protein
HDT	hexadecanethiol

SUMMARY

Current orthopedic implant technologies used suffer from slow rates of osseointegration, short lifetime, and lack of mechanical integrity as a result of poorly controlled cell-surface interactions. Recent biologically-inspired surface strategies (biomimetic) have focused on mimicking the biofunctionality of the extracellular matrix (ECM) by using short, adhesive oligopeptides, such as arginine-glycine-aspartic acid (RGD) present in numerous ECM components. However, these strategies have yielded mixed results *in vivo* and marginal bone healing responses. The central goal of this dissertation project was to engineer bioactive surfaces that specifically target integrin receptors important for osteogenic functions in order to improve bone tissue repair.

In order to create integrin-specific interfaces, integrin-specific ligands reconstituting the fibronectin (FN) secondary/tertiary structure were first engineered and functionalized on material surfaces using several robust presentation schemes. We demonstrated that FN-mimetic-functionalized surfaces that directed $\alpha_5\beta_1$ binding enhanced osteoblast and stromal cell integrin binding and adhesion, osteogenic signaling, and osteoblastic differentiation compared to various other RGD-based ligand-functionalized surfaces. Next, we investigated the effect of integrin-specific biointerfaces to modulate bone healing in a rat tibia implant bone model. We demonstrated, using a robust polymer brush system, that bioactive coatings on titanium implants that conferred high $\alpha_5\beta_1$ integrin specificity *in vitro* enhanced bone formation and implant integration *in vivo*. Moreover, we showed that integrin specificity can be engineered using different immobilization schemes, including clinically-relevant ligand dip-coating, and promote

the same robust *in vivo* effect. Furthermore, we investigate the synergistic roles of integrin specificity and ligand clustering on cell response by engineering biointerfaces presenting trimeric and pentameric “heads” of FNIII₇₋₁₀ with nanoscale spacing. Integrin-specific ligand clustering supported $\alpha_5\beta_1$ -specific binding and cell adhesion and enhanced implant osseointegration *in vivo* compared to monovalent FNIII₇₋₁₀ or non-functionalized biointerfaces.

In summary, the FN-mimetic integrin-specific biointerfaces engineered in this thesis provide a clinically-relevant material surface strategy to modulate tissue healing responses. In addition, these results contribute to our greater understanding of how two specific material design parameters, integrin binding specificity and clustered ligand presentation, contribute individually and synergistically toward directing cell and tissue function.

CHAPTER 1

INTRODUCTION

Orthopedic disorders, including total joint arthroplasties, constitute a leading cause of personal and occupational disability in the U.S., incurring tremendous health care related costs. For instance, over 750,000 total joint replacements were performed in 2002 at a cost of over 15 billion dollars; by 2040, due to an aging populace, it is projected that over 500,000 total hip replacements alone will be performed [1]. The lifetime of current joint replacements depends on sufficient integration into the surrounding bone, termed osseointegration. Insufficient integration often leads to aseptic loosening, further resulting in patient pain, loss of joint function, and, ultimately, revision surgery. Unfortunately, current implants do not typically last the lifetime of the patient. For example, approximately 50% of total hip replacements will fail in the first 20 years after implantation [1]. Each revision severely diminishes the lifetime of the subsequent implant. Furthermore, the need for orthopedic implants has steadily increased among young people, making it imperative that orthopedic implant lifetime be increased to reduce the subsequent number of revisions for each patient [2]. Importantly, hip and dental implants require significant time, at least several weeks, for full recovery and bone repair [2].

Recent efforts have converged on developing implant surface technologies that promote bone osseointegration as early as possible to reduce recovery time and eventually improve implant lifetime and patient quality of life. Current orthopedic implant technologies used clinically have mainly centered on bone-bonding bioactive ceramic coatings to promote osseointegration with surrounding bone and rough/porous coatings that stimulate bone ingrowth [3]. While moderately successful, these approaches suffer from slow rates of osseointegration, short lifetime, and lack of mechanical integrity as a result of poorly controlled cell-surface interactions [4]. Recent biologically-inspired surface strategies

(biomimetic) have focused on mimicking the biofunctionality of the extracellular matrix (ECM) in order to control cell function, wound healing, and tissue remodeling – believed to be critical issues to control for successful implant-tissue integration. In particular, many approaches have concentrated on functionalizing implant surfaces with short, adhesive oligopeptides, such as arginine-glycine-aspartic acid (RGD) present in numerous ECM components, in order to control bone cell-material interactions [5-9]. However, these strategies have yielded mixed results *in vivo* and sub-optimal tissue healing responses, including bone formation and implant fixation [10-12]. The lack of consistent positive results may be attributed partly due to unregulated protein adsorption, leading to non-specific surface effects. Moreover, these surface strategies are restricted by the low activity of oligopeptides compared to the native ligand, largely due to the absence of complementary or modulatory domains involved in cell adhesion [13-15]. Controlling at a molecular level the adhesion of local cells which interact with the implant *in situ* may be a crucial step in designing biologically active osseous implants.

Cell adhesion to extracellular matrices is primarily mediated by integrin receptors, which anchor cells and trigger signals that regulate survival, cell cycle progression, and differentiation in a variety of cellular systems [16]. Many specific integrin combinations are heavily implicated in tissue-specific signaling and cell function. In particular, the $\alpha_5\beta_1$ subunit combination has been associated with robust bone-specific (osteogenic) signaling and, furthermore, is critical for bone formation in embryonic and adult cell systems. Importantly, clustering of these activated integrins into supramolecular complexes (focal adhesions) provides the physical framework that regulates integrin function and signaling. Furthermore, recent evidence suggests that integrin binding specificity also regulates the proliferation and differentiation of osteoblasts and myoblasts [17,18]. Therefore, the engineering of biomimetic surfaces that promote integrin clustering and/or specificity may be a promising biomaterial surface strategy to improve implant osseointegration.

This work aims to address implant osseointegration limitations by examining the effect of integrin specificity as a surface strategy for engineering orthopedic implants. The **overall objective** of this research project was to engineer bioactive surfaces that specifically target integrin receptors important for osteogenic functions in order to improve bone tissue repair. Our **central hypothesis** was that the controlled presentation of integrin-specific ligands reconstituting the fibronectin (FN) secondary/tertiary structure will direct cell adhesion and osteogenic signaling and protein production, and thereby enhance implant-bone integration. Moreover, we further hypothesized that controlled surface coatings of nanoscale multimeric integrin-specific ligands will modulate integrin-related binding and adhesion, and, furthermore, improve implant osseointegration compared to non-clustered ligands. The overall objective was tested with the following specific aims:

1. Engineer biomaterial surfaces presenting integrin-specific FN ligands and evaluate the *in vitro* effect on integrin binding, cell signaling, and differentiation.

Our *working hypothesis* was that a FN-mimetic protein fragment presenting the central binding domain and synergy adhesive motif in the correct structural context will support $\alpha_5\beta_1$ -mediated cell adhesion and signaling, and osteoblastic differentiation over non- $\alpha_5\beta_1$ specific substrates. We tested this hypothesis by engineering a recombinant fragment of FN (FNIII₇₋₁₀) which incorporates both the cell adhesive motif RGD as well as its synergy sequence PHSRN in the native FN secondary structure. FNIII₇₋₁₀ and other integrin ligands, including plasma FN and RGD-based oligopeptides, were functionalized on substrates using various *in vitro* ligand presentation schemes, including self-assembled monolayers and robust polymer brushes. The ability of FNIII₇₋₁₀-functionalized surfaces to direct osteoblast and stromal cell integrin binding and adhesion, osteogenic signaling, and osteoblastic differentiation was compared to various other RGD-based ligand-functionalized surfaces.

2. Evaluate the *in vivo* effect of integrin-specific biointerfaces on implant osseointegration and bone formation.

Our *working hypothesis* was that bioactive coatings of integrin-specific ligands would modulate bone repair and the extent of implant osseointegration *in vivo*. We *tested this hypothesis* by coating titanium orthopedic implants with ligands of varying integrin specificity, including FNIII₇₋₁₀, pFN, and RGD, via polymer brushes or simple dip-coating. These implants were press fit into a rat tibial cortical bone model and osseointegration was assessed at 4 weeks post-implantation via bone-implant histomorphometry and mechanical pull-out testing.

3. Investigate the effect of integrin-specific ligand multivalency on *in vitro* cell adhesive parameters and *in vivo* implant osseointegration.

The *working hypothesis* was that multivalent proteins presenting multiple FNIII₇₋₁₀ ligands will support $\alpha_5\beta_1$ -specific binding and that increasing ligand valency will enhance cell adhesive functions and implant osseointegration compared to monovalent FNIII₇₋₁₀ or non-functionalized biointerfaces. We *tested this hypothesis* by purifying multimeric constructs presenting 1,3, or 5 FNIII₇₋₁₀ heads and assessing the effect of ligand valency on integrin binding, cell adhesion strength, and osteogenic differentiation. These multimeric ligands were then used as implant coatings in a rat tibial cortical bone model and implant osseointegration evaluated via mechanical testing and histomorphometrical analysis.

This research is **significant** because it seeks to elucidate both the individual and synergistic roles of integrin specificity and ligand clustering as material surface design parameters for modulating tissue-specific cell function and promoting an effective tissue healing response. Understanding how each of these design parameters affects cell and tissue response will contribute significantly to the rational engineering of bioactive materials. The biomimetic surface strategy of using bioactive ligands to confer integrin binding specificity

is validated using several robust ligand presentation approaches, and the subsequent effect on modulating *in vitro* osteogenic function and *in vivo* implant integration is evaluated. Next, taking this technology a step further, this work evaluates the feasibility of utilizing relative spatial constraints for ligand presentation to augment integrin binding, adhesion, and implant integration.

This work is fundamentally different from current biomimetic approaches in that it concentrates on engineering integrin specificity as a rational micro-scale surface material strategy to modulate cell function and tissue repair. This research also explores the efficacy of the nano-scale strategy of ligand clustering in modulating these same functional outcomes. These studies provide new insights into the biological role of these micro-scale and nano-scale adhesion parameters and receptor-ligand interactions in controlling cell function and orthopedic tissue repair in a biomaterial context. Due to the global role of integrin binding in other tissue and organ systems, the insights gained from this project contribute significantly to our general understanding of cell adhesion mechanisms and the regulation of cell-material interactions.

CHAPTER 2

BACKGROUND AND LITERATURE REVIEW

Extracellular Matrix-derived Ligands for Selective Integrin Binding

Extracellular Matrix (ECM) : Composition and Role

The interactions of cells with their extracellular matrix (ECM) are critically involved in mediating the development, organization, and repair of numerous tissues. At the cell level, cell-matrix interactions can directly modulate cell morphology, survival, proliferation, and differentiation in multiple cell systems [19,20].

The ECM is primarily composed of a complex meshwork of fibrous proteins (fiber-forming elements) surrounded by space-filling molecules such as glycosaminoglycans (GAGs) - as well as mineral deposits in tissues such as bone. Many of these components are secreted by resident cells and primarily provide support and anchorage, but also serve important roles as tissue boundaries and in the modulation of intra- and inter-cellular communication [21]. Moreover, the ECM is not only made, but also organized and remodeled, by the cells within it. Formation and remodeling of this ECM network is vital for a number of tissue responses such as cell migration during tissue formation and repair, growth, wound healing, and fibrotic responses [22]. Many of the fibrous proteins that make up the ECM, including collagen, fibronectin, elastin, and

*Modified from

T.A. Petrie, A.J. García. *Extracellular Matrix-derived Ligands for Selective Integrin Binding to Control Cell Function*, Invited book chapter of textbook entitled “Biological Interactions on Materials Surfaces: Understanding and Controlling Protein, Cell and Tissue Responses”, *Editors: R Bizios, D Puleo; Springer Publishing, Published 2009.*

laminin, have both structural and adhesive functions, and are secreted in specific tissues by specialized cells, including fibroblasts (most connective tissue), chondroblasts (cartilage), and osteoblasts (bone).

The collagens constitute a family of abundant ECM molecules that contribute significantly to the integrity and mechanical properties of tissues such as bone, skin, cartilage, and tendon [23]. Elastin is the dominant ECM protein in elastic fibers, a major component of arteries, lungs, and skin [24]. Laminin is the major non-collagenous component of the basal lamina, playing a critical role as the “glue” that holds many body structures together [25]. Fibronectin (FN) is a complex, multifunctional protein with multiple domains, each with specific binding sites for other matrix macromolecules and for receptors on the surface of cells. FN therefore contributes to both organizing the matrix and helping cells attach to it [22,25]. These essential roles of the ECM in regulating cell and tissue structure and function are illustrated schematically in **Figure 2.1**.

Cell-ECM Adhesive Interactions: Integrins as Pivotal Linkers

Most of these structural aforementioned proteins also play fundamental roles in promoting cell adhesion and mediating intracellular signals critical to tissue function. In particular, cell adhesion to the extracellular matrix is essential for controlling such complex biological processes as embryonic development, wound healing, immune responses, and tissue organization and repair [26,27]. For example, cell-adhesive interactions with specific ECM proteins, such as FN and type I collagen, regulate bone cell survival, cell cycle progression, differentiation, and matrix formation; at a tissue

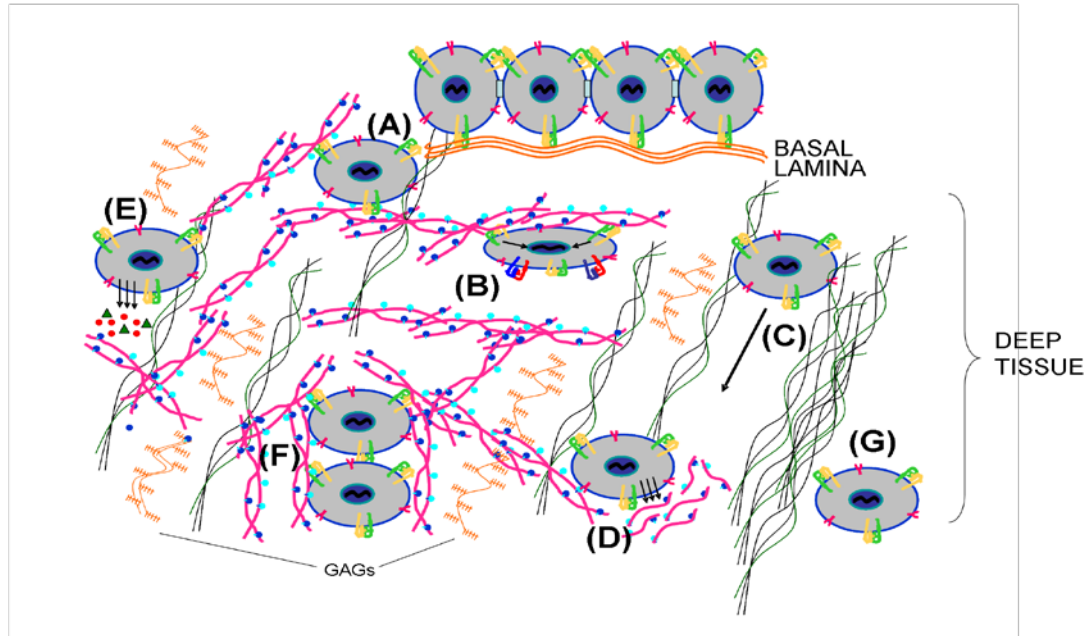


Figure 2.1. General key roles of the extracellular matrix in regulating cellular response in tissue. (A) ECM-interactions provide structure and anchorage for cells residing in tissue and modulate: (B) cell phenotype and differentiation, (C) migration of cells to specific spatial locales during development, repair, and growth, (D) matrix secretion, assembly and remodeling of the ECM environment, (E) secretion of local, soluble tissue-specific factors for degradation, repair, and migration, (F) inter-cellular communication, and (G) boundaries from one tissue to another, or within specialized regions of one tissue (GAGs = glycosaminoglycans).

level, these interactions can play crucial roles in bone remodeling, maintenance, and formation [28,29].

Moreover, ECM-mediated cell adhesion plays critical roles in animal development, as evidenced by the embryonic lethality of mice that have genetic deletions for particular ECM ligands and receptors [16,26]. Proteins such as FN are important in guiding cell movements during organism development, including migration of mesodermal cells at different embryonic stages [30]. These ECM components regulate cell behavior by interacting with cell-surface receptors to activate particular intracellular

signaling pathways, resulting in tissue-specific alterations in cell spreading, migration, cell-cell communication, and differentiation [31-33].

Although there are many types of these cell receptors that facilitate cell-ECM interactions, cells recognize and adhere to ECM ligands primarily via integrins, a widely expressed class of cell-surface receptors. Integrins are transmembrane, heterodimeric proteins consisting of a particular combination of two non-covalently associated subunits (α and β) of which 24 specific combinations have been currently identified in humans [34] (**Figure 2.2**). Integrins interact with the ECM through their extracellular domains, and are linked to cytoskeletal elements and signaling molecules through their intracellular domains, functioning as the primary bridge between the ECM environment and the cell. Different α and β subunit combinations have the capacity to bind to one or more ECM ligands, whereas many ECM proteins can act as ligands for more than one integrin. Moreover, a wide array of integrins can be expressed, typically in tissue- and development-specific patterns. For example, osteoblasts and osteoprogenitor cells express multiple integrins, including $\alpha_1\beta_1$, $\alpha_2\beta_1$, $\alpha_3\beta_1$, $\alpha_4\beta_1$, $\alpha_5\beta_1$, $\alpha_6\beta_1$, $\alpha_8\beta_1$, $\alpha_v\beta_3$, and $\alpha_v\beta_5$, that can vary in degree of expression with the stage of the osteoblast and bind to numerous extracellular matrix components [35-37].

Most integrins recognize specific binding sites, typically small peptide sequences, such as the ubiquitous arginine-glycine-aspartic acid (RGD) motif present in a variety of ECM proteins [38]. Integrin binding to ligands is a dynamic and highly regulated process that requires “activation” of the integrin and mechanical coupling to the ligand. This activation changes the conformation of the extracellular portion of the receptor into a more “high affinity” structural orientation for ligand binding, although divalent metal-

ions are also typically needed for functional binding. After integrin-ligand binding, integrins associate with the actin cytoskeleton and begin to aggregate together in clusters forming focal adhesions, distinct structures that form intracellular scaffolds of structural and signaling molecules [19,39,40] (**Figure 2.2 B, 2.3**). Focal adhesions mediate stable adhesion by providing structural links between the ECM and cell cytoskeleton to regulate force-associated cell functions such as adhesion, spreading, morphology, and migration. These adhesive structures also activate discrete signaling pathways (MAPK, JNK, ERK) through accumulation and activation of signaling mediators, such as focal adhesion kinase (FAK) and Src, that can ultimately regulate transcription factor activity and direct major cell functions such as migration, proliferation and differentiation [19,41] (**Figure 2.2 B**). For example, $\alpha_2\beta_1$ -mediated cell attachment to type I collagen stimulates the tyrosine phosphorylation of focal adhesion kinase (FAK) and, subsequently, the activation of extracellular signal-related kinase (ERK), a mitogen-activated protein kinase (MAPK) that has been implicated in the control of osteoblast-specific gene expression and matrix mineralization [42,43].

Specialized integrin-ECM ligand interactions can regulate many cell functions, including survival, proliferation, motility, morphology, and differentiation in a cell/tissue-specific and time-dependent manner. Numerous studies using antibodies that block specific integrins have underscored the importance of the FN interaction with β_1 integrins in regulating osteoblast, chondrocyte, myoblast (muscle cells), neural, and human mesenchymal stem cell survival, proliferation, gene expression, and cell fate [35,44-46]. In bone cells, blocking antibodies against collagen-specific $\alpha_2\beta_1$ impede the expression of osteoblast-specific genes, such as osteocalcin, and inhibit calcification and

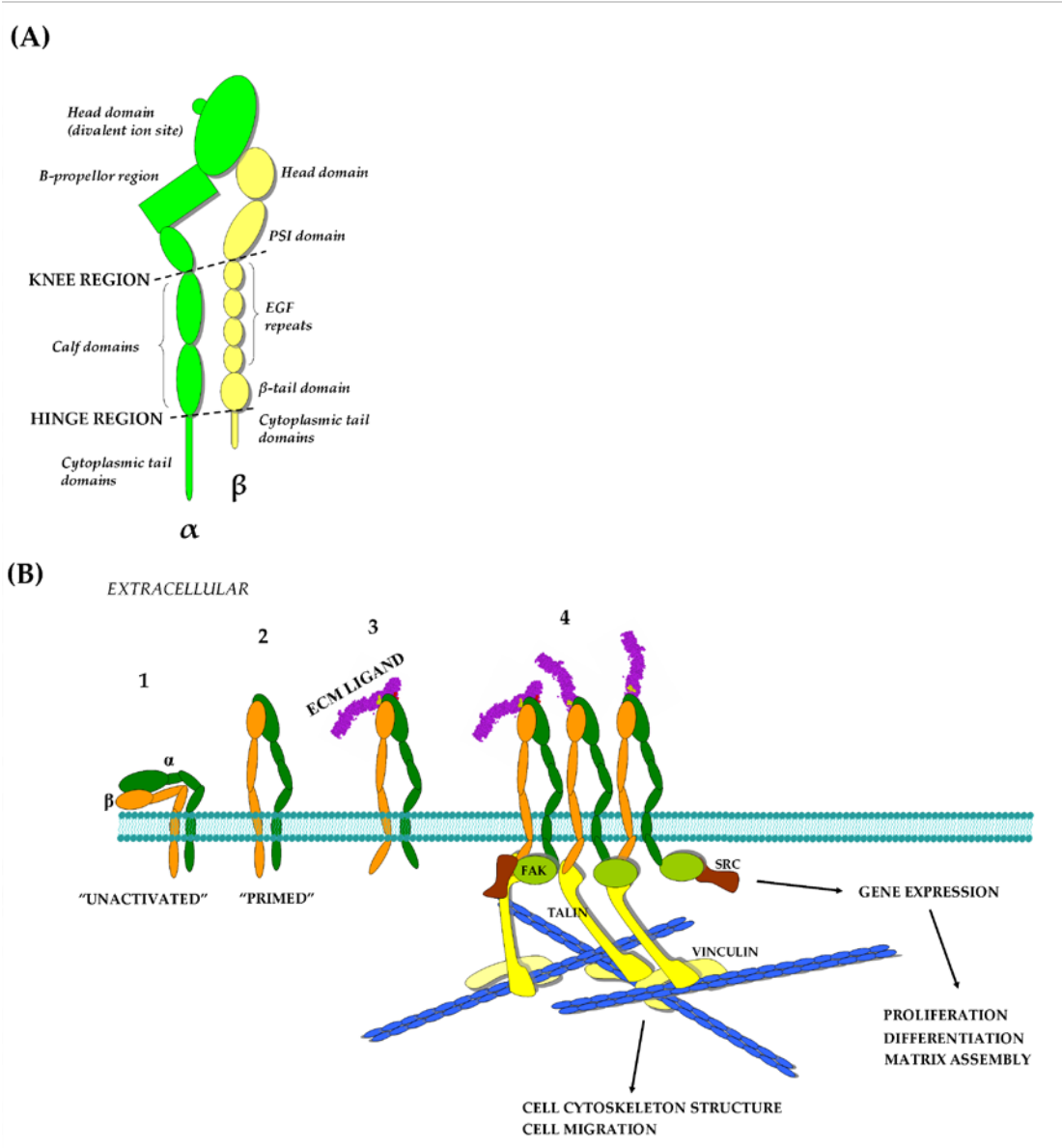


Figure 2.2. Integrins link the extracellular and intracellular environments. A) Integrin subunit structure. Each subunit (α and β) noncovalently associates with each other and contains a head (ligand binding), knee (genuflection), and hinge (at the cell membrane) region. B) Primary integrin activation and binding steps. (1) “low affinity” ligand binding unactivated integrin state demonstrating bending at knee regions, (2) “high affinity” ligand binding activated state as a result of interaction with intracellular (talin) and/or extracellular (divalent ions, ligands) factors, (3) integrin clustering into (4) focal adhesions, which also consist of large intracellular scaffolds of structural and signaling components, important in regulating functions such as cell adhesion, cell shape, migration, proliferation, and differentiation. (FAK = focal adhesion kinase, EGF = endothelial growth factor, PSI = plexin-semaphorin-integrin).

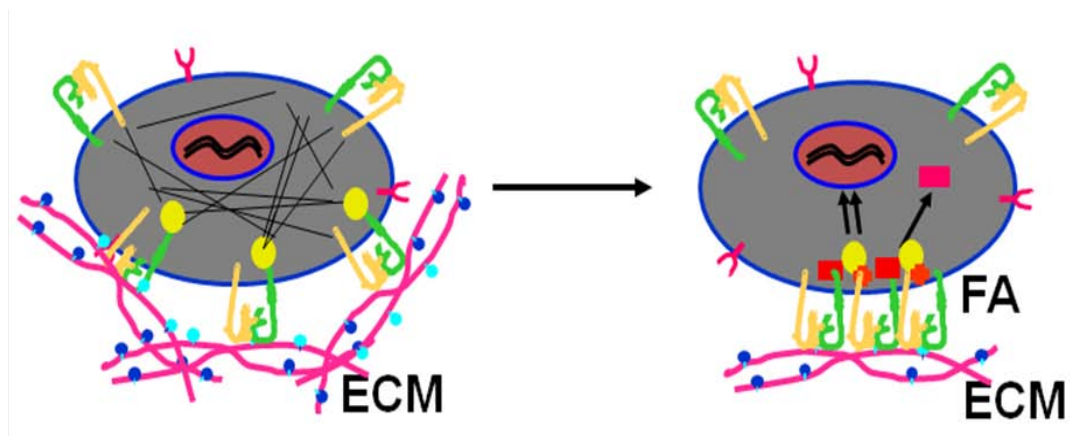


Figure 2.3. Focal adhesion (FA) formation. FAs are initiated when integrins bound to ECM are activated and subsequently “pulled” together by cytoskeletal elements.

formation of a mineralized matrix [47,48]. Engagement of distinct integrins will often direct particular cell responses which are specific to different tissues. While $\alpha_v\beta_3$ binding is pro-proliferative and aids in migration of osteoblasts, liver, and even cancer cells, activation of this same integrin will impede bone mineralization and osteoblast differentiation; these functions can be rescued by binding of $\alpha_5\beta_1$ [49-52]. Leukocyte-specific β_2 , including the Mac-1 receptor $\alpha_M\beta_2$, regulates macrophage adhesion to FN, as well as interactions with complement macromolecules and various domains of fibrinogen that may become exposed on different biomaterial surfaces [31,53,54]. A compendium of integrin subunit combinations and their demonstrated individual high-affinity recognition to various ECM proteins and their binding motifs is presented in **Figure 2.4**. These studies highlight the importance of specific integrin-ECM interactions to control tissue-specific cell function.

ECM Ligand	Integrin	Binding Motif
FN	$\alpha_4\beta_1$	IIICS (REDV, EILDV)
	$\alpha_5\beta_1$	RGD + PHSRN
	$\alpha_{IIb}\beta_3$	RGD
	$\alpha_v\beta_3$	RGD
COL-I	$\alpha_2\beta_1$	RGD, DGEA
COL-IV	$\alpha_1\beta_1$	CNBr a1(IV)2
VITRONECTIN	$\alpha_{IIb}\beta_3$	RGD
	$\alpha_v\beta_3$	RGD
FIBRINOGEN	$\alpha_{IIb}\beta_3$	RGD, KQAGD
	$\alpha_v\beta_3$	RGD
	$\alpha_M\beta_2$	P1,P2
LN	$\alpha_1\beta_1$	P1, E1-4
	$\alpha_3\beta_1$	GD6 peptide, E3
	$\alpha_6\beta_1$	E8
VON WILLENBRAND FACTOR	$\alpha_{IIb}\beta_3$	RGD
	$\alpha_v\beta_3$	RGD
OSTEOPONTIN	$\alpha_4\beta_1$	IDAPS
	$\alpha_v\beta_3$	RGD
THROMBOSPONDIN	$\alpha_3\beta_1$	TSP-768
	$\alpha_v\beta_3$	RGD
BONE SIALOPROTEIN	$\alpha_v\beta_3$	RGD
TENASCIN	$\alpha_v\beta_3$	RGD
FACTOR X	$\alpha_M\beta_2$	

Figure 2.4. List of selected native ECM proteins and known associated binding epitopes. These epitopes are noted for specific recognition of distinct integrin subunit combinations.

Engineering Biomaterial Surface Properties for Integrin Binding

Given the central roles of integrins in cellular processes, ongoing biomaterials research has focused on identifying key material surface characteristics that modulate the type, strength, and degree of ECM-integrin binding. Cell adhesion to ECM components or ECM-derived ligands on engineered surfaces governs host responses to implanted devices, integration of biomedical prostheses and tissue-engineered constructs, and the performance of biotechnological supports [55]. More specifically, integrins promote this robust cell adhesion to biomaterials by binding adhesive ligands on the material which have been (a) adsorbed from solution, (b) deposited by cells onto the surface, or (c) specifically engineered onto a surface, or a combination [56].

Several material surface properties have been identified that modulate the type, amount, strength and conformation of proteins adsorbed or immobilized on the surface, which, in turn, directly modulate the level and specificity of engaged integrins. A summary of these different adsorption states and their impact on integrin binding is illustrated in **Figure 2.5**. For example, following protein adsorption, various protein unfolding events may occur, either (a) exposing “cryptic” binding sites that promote engagement of more selective integrins or (b) “stretching” integrin-binding epitopes which may negatively affect integrin recognition and levels of binding [57,58].

Physiochemical properties of material surfaces that influence the nature of integrin binding include substrate composition, surface energy, surface charge, surface chemistry, and topography. The underlying chemical composition of a biomaterial substrate alone may regulate cell-type specific integrin expression.

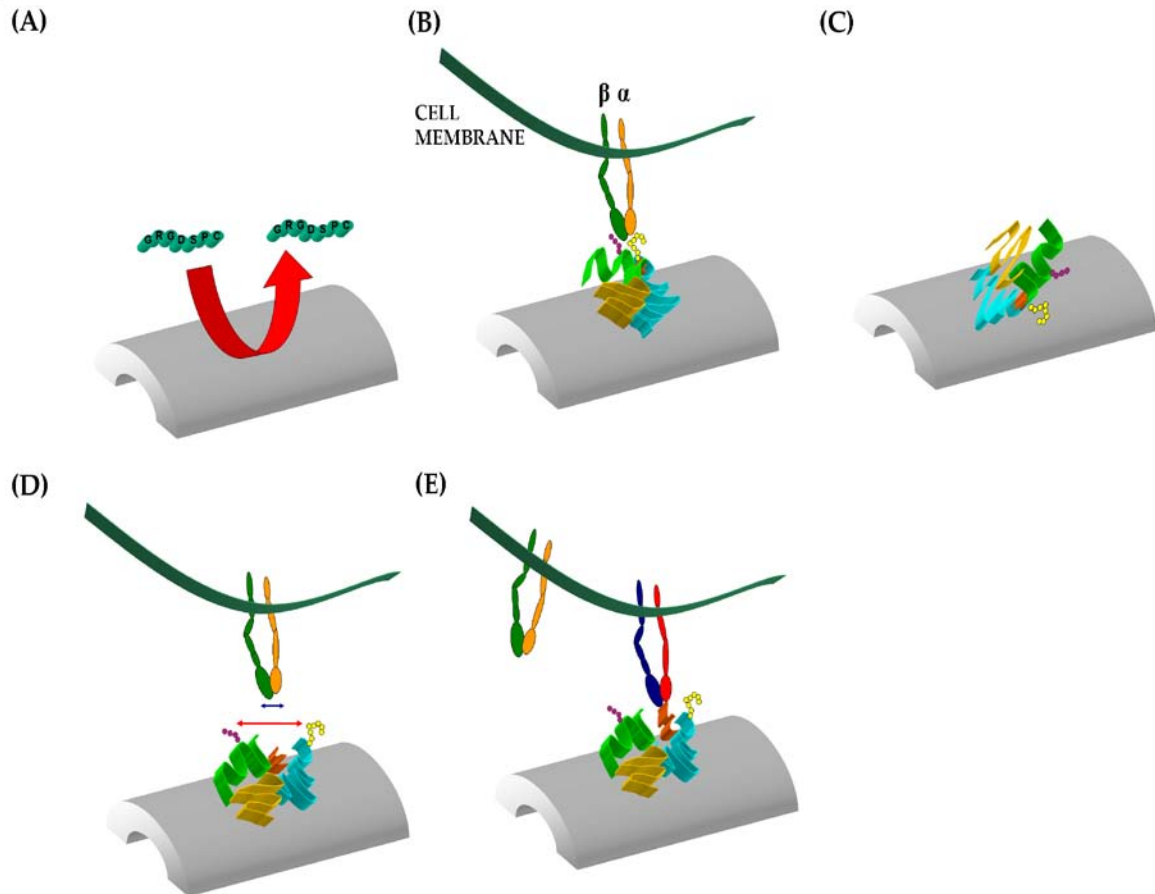


Figure 2.5. Different modes of adsorption to biomaterial surfaces for integrin binding ligands. A) Short oligopeptides typically do not physisorb well to metal and polymeric surfaces. B) favorable adsorption of larger ligands presenting adhesive epitopes in an accessible orientation promote integrin binding. C) unfavorable adsorption of ligands presenting adhesive epitopes in a non-accessible orientation reduce integrin binding. D) protein unfolding post-adsorption may “stretch” integrin-binding epitopes, resulting in sub-optimal or no integrin binding. E) protein unfolding may also expose “cryptic” epitopes that may promote interaction with different integrins.

Osteoblasts on titanium alloys express α_2 , α_3 , α_4 , α_6 , α_v , β_1 , β_3 integrin subunits; however, on CoCrMo alloys these same cells do not always express α_3 , α_6 , or β_3 [59]. Osteosarcoma and bone marrow stromal cells cultured on hydroxyapatite (HA), titanium, and CaP-coated titanium surfaces display differential trends in integrin expression [60,61]. It has been reported that HA-coated surfaces promote more robust adsorption of serum proteins compared to titanium, and that these proteins are in distinct conformations on each surface [62]. Surface energy and charge, which are closely related, also may elicit differential integrin expression profiles. Materials that are hydrophobic, including poly (methyl methacrylate) and polystyrene, typically exhibit higher levels of total protein adsorption compared to more hydrophilic surfaces, such as ceramics and metallic materials [21].

Surface strategies to utilize high charge and surface energy substrates have taken advantage of common electrostatic interactions that occur in many biomaterial interfacial events in physiological conditions. Ti implants have been engineered via glow discharge plasma (GDP) technology to exhibit altered charge density and increased surface energy [63]. It is hypothesized that this treatment enables favorable surface energy for binding serum proteins and growth factors that increase integrin expression for enhanced osteoblast differentiation compared to comparable uncharged surfaces.

Surface chemistry tailoring of material and scaffold surfaces has emerged as another strategy to regulate protein adsorption and conformation in order to better control the biological activity of adsorbed adhesive proteins [64]. Using self-assembled monolayers (SAMs) of functionalized alkanethiols on gold to present well-defined

chemistries, biomaterial-dependent differences in the total amount and conformation of adsorbed FN have been identified [45,65]. These differences in FN conformation in turn affect integrin receptor binding [66-68]. Osteoblast-like cells bound selectively with $\alpha_5\beta_1$ to OH and NH₂-presenting SAMs, but with both $\alpha_5\beta_1$ and $\alpha_v\beta_3$ to COOH-presenting surfaces [17]. This regulation of $\alpha_5\beta_1$ vs. $\alpha_v\beta_3$ binding was found to directly modulate osteoblast adhesion, signaling, proliferation, and differentiation, as well as influenced myoblast proliferation and myogenic differentiation [17,46]. Aside from demonstrating surface chemistry-dependent effects on integrin specificity, these data also underscore the importance of engaging specific integrins to achieve a directed cellular response. Nano- and micro-scale surface roughness also regulates integrin-mediated cell interactions. Human osteoblasts and bone marrow stromal cells exhibit distinct expression profiles of α_3 , α_5 and α_6 when cultured on either rough or smooth titanium substrates, ultimately influencing relative levels of adhesion and tissue-specific gene and protein expression [60]. Furthermore, MG63 human osteoblast-like cells exhibit an increase in α_2 , α_3 , α_5 , β_1 and β_3 integrin subunits on micro-scale rougher surfaces compared to smooth titanium, resulting in enhanced integrin-mediated spreading and adhesion [60]. In particular, micro-scale surface roughness modulates $\alpha_5\beta_1$ binding, correlating to a boost in FAK activation, local growth factor production, and osteoblast-specific bone markers [69-71].

ECM-mimetic Surface Modification Strategies

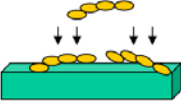
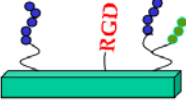
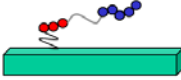
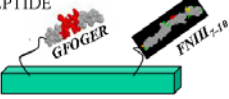
ECM Surface Modifications to Regulate Integrin-Mediated Cell Function

Cell adhesion to ECM components or ECM-derived ligands on engineered surfaces governs host response to implanted devices, the degree of integration of

biomedical prostheses and tissue-engineered constructs, and the performance of biotechnological supports [55]. While typically easy to implement, most physiochemical surface strategies alone lack the ability to consistently generate selective integrin binding and integrin-mediated cell responses. Advances in understanding the role of specific ECM biomolecules in regulating integrin expression, cell adhesion, differentiation, and tissue remodeling have led to the investigation of targeted biochemical methods of surface modification. Recent biomimetic strategies have focused on the immobilization of selected ECM matrix components, including native structural proteins, peptide sequences, or synthetic derivatives based on matrix molecules [72]. The goal of these surface strategies is to modulate integrin-matrix interactions and promote general integrin binding to direct a specific cell/tissue response. Many of these ECM-derived surface ligand modifications and their integrin-specific effect on cellular functions will be discussed in further detail in the following sections of this chapter and are summarized in **Figure 2.6**.

Coating of various biomaterial substrates with full-length ECM proteins modulates integrin binding to varying degrees. FN coatings on polystyrene increase osteoblast expression of α_3 and α_5 and reduce expression of α_2 , α_6 , and α_v subunits compared to uncoated polystyrene [59]. Stromal cell, calvarial osteoblast, and osteoblast-like cells exhibit enhanced β_1 -mediated adhesion, proliferation, and differentiation on FN- and COL I-coated surfaces compared to either uncoated glass, polystyrene, or titanium surfaces [73]. It has been postulated that FN-coated implants promote better early bone formation due to a chemotactic attraction of osteoprogenitors near the ECM-coated implant surface [74].

A)

ECM Ligand	Ligand	Targeted Integrin	Demonstrated Effect on Cell Function
 ADSORBED	FN	$\alpha_v\beta_3, \alpha_5\beta_1$	adhesion, migration, proliferation, differentiation
	COL-1	$\alpha_2\beta_1$	
	COL-IV	$\alpha_1\beta_1, \alpha_2\beta_1, \alpha_3\beta_1$	adhesion
	BSP	$\alpha_v\beta_3$	adhesion, osteoconductivity
	VN	$\alpha_v\beta_3, \alpha_v\beta_5$	adhesion
 SHORT OLIGOPEPTIDE	EILDV, REDV	$\alpha_4\beta_1$	adhesion
	IDAPS, KQAGD	$\alpha_{5b}\beta_3$	adhesion
	RGD	$\alpha_v\beta_3$	adhesion, proliferation, migration, differentiation
	DGEA	$\alpha_2\beta_1$	adhesion, differentiation
	GFOGER	$\alpha_2\beta_1$	adhesion, differentiation
	KGGGAHEEICTTNEGVM (FN13)	$\alpha_2\beta_1$	matrix assembly, proliferation
 MULTI-MOTIF PEPTIDE/AMPHIPHILE	RGD-PHSRN amphiphile	$\alpha_v\beta_3$	adhesion, differentiation
	RGD-PHSRN phospholipid	$\alpha_v\beta_3, \alpha_2\beta_1$	adhesion
	RGD with elastin-like repeats	$\alpha_v\beta_3$	adhesion
	GFOGER-SPARC	$\alpha_2\beta_1$	adhesion, proliferation
 ECM FRAGMENT/ENGINEERED PEPTIDE	FNIII ₁₀	$\alpha_v\beta_3$	adhesion
	FNIII ₉₋₁₀	$\alpha_2\beta_1$	adhesion, differentiation
	FNIII ₇₋₁₀	$\alpha_5\beta_1$	adhesion, proliferation, differentiation
	V25/CS-1	$\alpha_4\beta_1$	adhesion, matrix assembly
	GFOGER (triple-helical)	$\alpha_2\beta_1$	adhesion, proliferation, differentiation

B)

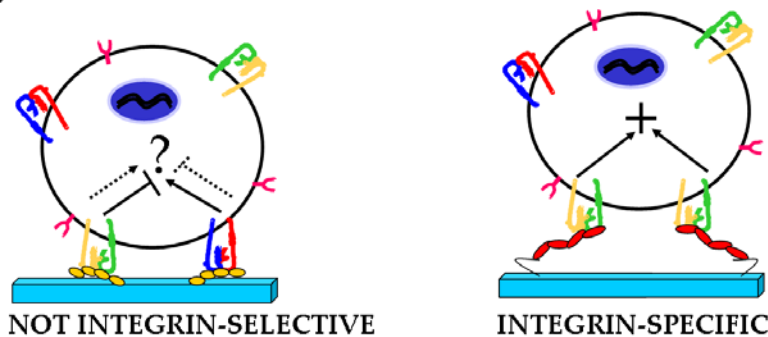


Figure 2.6. ECM-derived surfaces to direct integrin specificity to direct a focused cell response. A) Major ligand surface modification schemes utilizing full and modified ECM ligands to design integrin-selective interfaces. B) Substrates which do not discriminate between integrin binding and activation often may produce antagonistic signaling pathways. Integrin-specific surfaces facilitate single integrin-mediated adhesive and signaling pathways to produce a more-directed and robust cell response.

Although there are conflicting data regarding the functional effects of collagen-coating on polystyrene and titanium for various cell types, there is evidence of cell type-specific distinct integrin expression profiles on collagen vs. non-collagen-coated surfaces [75,76]. Osteoblasts upregulate α_3 expression over α_6 on collagen type I-coated polystyrene, whereas collagen type IV coatings mediate greater α_1 , α_2 , α_3 , and β_1 expression and activation [59]. Other bone-specific matrix proteins, including bone sialoprotein and osteopontin, have also been explored as bioactive surface coatings to control β_3 -mediated binding and signaling for human osteoblasts and stromal cells. Bone sialoprotein (BSP) is an acidic, noncollagenous glycoprotein abundantly expressed in mineralized tissues. BSP bound to collagen type I was found to orient in a bioactive orientation that augments β_3 binding and subsequent osteoblast adhesion and differentiation over unmodified interfaces [77]. Implants coated with BSP were found to be fairly osteoconductive yet supported only sub-optimal functional integration and mechanical fixation [78]. Vitronectin is another ECM protein that dominates serum-exposed adsorption to polystyrene [56]. Interestingly, coating vitronectin on polystyrene enhances mouse osteoblast expression of $\alpha_v\beta_3$, but also has been shown to weaken adhesion of murine cells compared to uncoated polystyrene [36]. However, for human osteoblasts, adhesion to vitronectin was found to be primarily $\alpha_v\beta_5$ -mediated and more robust over uncoated surfaces [79]. These studies highlight cell-type dependent effect on integrin binding and cell function that surface modifications using natural ECM proteins may elicit.

Although promoting functional effects, the functionalization of biomaterials with natural matrix proteins has several drawbacks. Since many full-length matrix proteins

contain multiple integrin and other biomolecule binding sites, it is likely that these proteins may induce significant binding of more than one integrin, and hence, do not truly support an “integrin-specific” surface. Moreover, immunogenic and pathogen transmission concerns across species limit widespread use of these ligands as bioactive coatings for implants in humans. Furthermore, processing issues including scale-up difficulties and long-term stability may reduce the wide-spread application of these matrix functionalized surfaces.

Small Peptide Biomimetic Surface Strategies

Synthetic biomimetic strategies to promote cell adhesion have primarily focused on presenting short bioadhesive motifs derived from ECM components onto biomaterial or implant surfaces [80]. A number of adhesion motifs from ECM components have been identified that can be subsequently incorporated in a small synthetic peptide. These motifs consist of a short linear sequence of amino acids, typically no more than a dozen amino acids in length, that one or more integrin receptors can recognize and bind [81]. These short sequences can be easily incorporated into adhesive oligopeptides that can be strategically immobilized in numerous ways on a biomaterial support to promote integrin-mediated adhesive and functional responses. These immobilization schemes include covalent tethering directly onto a biomaterial substrate, using plasma-treating to increase the functional groups on the substrate, or tethering onto polymer coatings functionalized on an underlying substrate. Non-fouling supports (polyethylene glycol or alginate) are often used to better isolate the activity of these motifs by utilizing a background with minimal non-specific protein adsorption [82].

Many of these adhesive sequences are specifically associated with ECM components from a particular tissue environment. For example, BSP- and collagen-derived sequences have been identified that remain functional only with bone-associated cell types. Multiple integrin-binding sequences have also been identified on single ECM proteins. For instance, the EILDV and REDV sequences on FN mediate $\alpha_4\beta_1$ -binding of endothelial cells, while the RGD and PHSRN sequences, when presented together correctly, promote $\alpha_5\beta_1$ -mediated osteogenic differentiation [83,84]. The adhesion motifs DGEA and GFOGER from collagen type I both mediate $\alpha_2\beta_1$ -mediated function - although in separate cell systems, i.e., neurite migration for DGEA and osteoblast differentiation for GFOGER [85,86]. Other ECM-specific integrin-binding sequences identified include the IDAPS sequence in osteopontin, which promotes $\alpha_4\beta_1$ -mediated adhesion of lymphocytes and the KQAGD sequence in fibrinogen, which itself controls $\alpha_{IIb}\beta_3$ -adhesion of osteoclasts [87,88]. Hydrogels functionalized with adhesive peptides incorporating IKLLI, IKVAV, LRE, PDSGR, RGD, or YIGSR, and the collagen type I sequence, DGEA, differentially regulated pancreatic cell survival [89]. Many of these synthetic oligopeptide-based strategies have been successfully used in vivo for tissue repair and regeneration. For example, GFOGER-coated implants promote extensive bone formation and implant integration in orthopedic applications [48].

The most common oligopeptide strategy to control integrin binding relies on the surface presentation of the arginine-glycine-aspartic acid (RGD) adhesive sequence, which mediates cell attachment to several matrix proteins, including fibronectin, vitronectin, osteopontin, and bone sialoprotein [90]. Since the RGD sequence is an ubiquitous adhesive motif in most ECM components, biomaterial substrates and tissue-

engineered constructs coated with RGD-peptides have been employed to control *in vitro* adhesion, migration, and differentiation in numerous cellular systems, including neural, endothelial, and bone cells [91-93]. For example, synthetic ECM proteins incorporating the GRGDSP cell-binding domain as well as elastin-like repeats (for more robust mechanical strength) enhance adhesion and spreading of endothelial cells over similar adhesive peptides [94]. The density and presentation of RGD peptides can have a profound effect on their overall influence on cell function for certain cell types. The degree of osteoblast proliferation, bone-specific gene expression, and differentiation varies directly with RGD-ligand density [95]. However, relatively high RGD densities can also negatively affect neurite extension and outgrowth in 3-D gel scaffolds [96]. Although RGD-immobilized peptides typically mediate osteoblast cell function through the $\alpha_v\beta_3$ integrin, altering the structural presentation of this motif can mediate other cell type functions via non- α_v and/or β_3 integrins [97]. For example, immobilized synthetic alkyl amphiphiles of RGD promote $\alpha_3\beta_1$ -mediated adhesion and migration of melanoma cells [98]. Grafting implant materials with either cyclic or oligomeric peptides presenting multiple RGD arms increases human osteoblast adhesion and spreading in a primarily $\alpha_v\beta_5$ -dependent mechanism, depending on alterations to the RGD structure and the exact flanking sequence surrounding the tripeptide [99,100]. Although it has been shown that RGD presented in cyclic, or “constrained”, conformations exhibit enhanced integrin affinity to many α_v or β_3 integrins compared to linear RGD, due to the conformation of RGD and its flanking regions, these peptides still retain minimal $\alpha_5\beta_1$ selectivity [95,99].

Nonetheless, while many studies have demonstrated that RGD-functionalized materials support integrin-mediated adhesion, proliferation, and differentiation *in vitro*,

mounting evidence suggests that this biomimetic surface strategy does not enhance biomedical implant integration in more rigorous animal models. A number of studies have concluded that RGD-immobilized titanium implant coatings do not improve peri-implant new bone formation and yield only marginal increases in implant integration and mechanical fixation [10,12,100-104]; in contrast, very few studies demonstrate a significant *in vivo* enhancement in osseointegration [105,106]. Furthermore, when RGD peptides were immobilized onto hydroxyapatite-discs in conjunction with serum proteins such as FN and vitronectin, there was a detrimental effect on mesenchymal stem cell survival as well as new bone formation [100]. Even the benefits of this biomimetic surface treatment *in vitro* are unclear. Osteoblasts cultured on RGD functionalized PLL-g-PEG surfaces exhibit reduced bone-specific markers and osteogenic differentiation compared to unmodified surfaces [107]. Even RGD peptides of varying flanking sequences tethered on SAMs all displayed sub-standard adhesive capacity compared to full-length FN surfaces [108,109]. Although the stability, relative cost-effectiveness, ease of immobilization, and reduced immunogenicity are all advantages of using these small adhesive motifs, there are several limitations that reduce their efficacy for more directed tissue repair and regeneration. First, the biological activity of these peptides is substantially lower than that of the whole protein due to the absence of modulatory integrin-binding domains. Second, this lack of essential modulatory domains limits surface selectivity for integrins. Because RGD is recognized by a large number of integrins in numerous cell types, this lack of integrin specificity may result in non-discriminatory attachment of cells to the RGD-coated surfaces. For example, in order to achieve high affinity $\alpha_5\beta_1$ -binding, both the RGD sequence in the 10th type III repeat of

FN as well as its synergy site, the PHSRN sequence in the 9th type III repeat, are required to be presented together [110]. Since $\alpha_5\beta_1$ is especially critical for induction of various osteoblastic signaling pathways and activities, this lack of integrin binding may be detrimental for orthopedic applications. Third, these small peptides may lack the ability to bind specific receptors due to conformational differences among adhesive sequences compared to the native ECM ligand. As a consequence of these collective limitations, newer generations of bio-inspired surfaces have focused on more effectively mimicking the structure and make-up of natural ECM integrin-binding epitopes.

Multi-Motif Integrin-Specific Ligands

An advanced biomimetic surface strategy that has been recently explored to obtain more directed cell/tissue response is the engineering of surfaces to engage specific integrin receptors among RGD-binding integrins [28]. Recent studies suggest that the marginal healing responses of RGD-functionalized implants might arise from the lack of selectivity of this adhesive ligand for specific integrin receptors [49,111]. Since activation and signaling by more than one type of integrin receptor on the same cell may induce antagonistic cellular responses, as evidenced by the aforementioned effect of $\alpha_5\beta_1$ vs. $\alpha_v\beta_3$ binding on osteoblast function, a more selective integrin binding surface may achieve a more controlled cellular response [17]. Unfortunately, full-length matrix proteins possess multiple integrin binding sites, whereas short RGD peptides can also bind multiple integrins without a high degree of specificity. Therefore, several recent approaches have utilized ligands presenting this RGD motif with additional modulatory domains to selectively target particular integrin receptors, while excluding other non-essential biological domains.

Although cyclic-RGD peptides improve ligand specificity for several integrins, including $\alpha_v\beta_3$ and $\alpha_3\beta_1$, the ability of these constrained peptides to achieve levels of high affinity $\alpha_5\beta_1$ binding comparable to full-length FN is limited. As previously mentioned, RGD and its PHSRN synergy sequence in FN individually contribute little to high affinity $\alpha_5\beta_1$ binding, but, when presented together, promote $\alpha_5\beta_1$ -mediated cell adhesion [94]. The synergistic effects of the RGD and PHSRN sites is strongly dependent in the molecular structure as slight alterations in the nanoscale spacing (30-40 nm), relative angle, mechanical tension, and flanking sequences between these two sites result in significant losses in biological activity and integrin binding behavior [113-115]. Because of this tight dependence of receptor binding on the structural context of the ligand, the ability to mimic the integrin binding and functional abilities of the native ligand is especially challenging with single RGD peptides. FN-mimetic peptide-amphiphiles and multi-motifed peptides presenting both the RGD and PHSRN site have been engineered to address some of these structural limitations and to study at different molecular levels the ligand binding properties of $\alpha_5\beta_1$ [116]. Surfaces of PEG molecules attached to phospholipids presenting the GRGDSP and PHSRN sites were used to demonstrate that $\alpha_5\beta_1$ binding to peptide-amphiphiles is dependent on membrane composition, temperature, and density [117]. Bioartificial membranes constructed from GRDGSP and PHSRN have led to insights on binding/unbinding events with $\alpha_5\beta_1$ down to a single molecular level. The results of research with these FN-mimetic peptide-amphiphiles suggest that accessibility and relative spatial orientation is crucial for FN-like robust $\alpha_5\beta_1$ binding [118]. An RGD-PHSRN amphiphile which presented the RGD motif in structurally distinct variations exhibited enhanced $\alpha_v\beta_3$ specificity when the RGD was

looped rather than linear [119]. Another RGD-PHSRN amphiphile consisting of the two adhesive motifs, a spacer, and a linker (designed to mimic the distance and hydrophobicity of the two motifs in FN) was reported to enhance endothelial cell adhesion over FN, although a direct comparison of the two surfaces on an equimolar basis was not performed [120,121]. Moreover, another similar RGD-PHSRN amphiphile that was connected by a linker recapitulating the native spacing of fibronectin enhanced osteoblast differentiation over surfaces immobilized with RGD alone [122]. Linear and cyclic lipid-linked RGD ligands also seem to enhance integrin-mediated adhesion, even at low surface densities [123].

Although several studies have indicated that FN-mimetic peptide-amphiphiles enhance integrin binding and cell function over RGD alone, the relative biological activity of these second-generation peptides, compared to the native protein and even simple RGD peptides, remains poorly characterized. Recently, a study in which both RGD and an RGD-PSRHN peptide, mimicking the natural spacing of FN, were tethered on a mixed SAM at equimolar levels revealed no significant differences in adhesion or integrin binding specificity among the two ligands [108]. Comprehensive analyses, including antibody blocking, varying ligand surface densities, and signaling evaluations are necessary to more fully establish the adhesive and functional potential of these engineered interfaces. Hence, although these adhesive interfaces do promote integrin-mediated adhesion, mimicking the full biological activity of the native protein (FN) using these synthetic short adhesive motifs remains challenging.

FN-Derived Integrin-Selective Ligands

As an alternative strategy, the engineering of high molecular weight ligands recapitulating the primary, secondary, and tertiary structure of the native protein has been very recently pursued to reconstitute full biological activity and convey integrin binding specificity. In particular, recombinant fragments of FN incorporating specific integrin-binding domains of FN have been designed. For example, FN-ligands that incorporate the 10th type III repeat (RGD) or the 9th type II repeat (PHSRN) have been recently engineered [124]. These protein fragments present the aforementioned adhesive motifs or flanking sequences in the correct structural conformation and spatial orientation as native FN. These recombinant FN fragments were prepared using DNA recombinant technology, which affords flexibility in designing unique ligand characteristics to study structure/function, control immobilization and orientation, and enhance bioactivity. Using fragments of FN limits antigenicity (compared to full-length FN) and eliminates other modulatory domains which may either interfere with specific integrin binding or elicit undesired inflammatory responses. FN10, a FN fragment comprising the 10th type III FN repeat and engineered to present a modified RGDWXE motif, exhibited more robust binding to human $\alpha_v\beta_3$ compared to normal RGD-containing FN10 fragments [125]. This finding highlights the utility of using recombinant protein technology to correlate structural adhesive motif characteristics with receptor binding activity and cell function. Specific binding to $\alpha_4\beta_1$ has been linked to an alternatively spliced V (residues 1-25 of the IIICS) region of FN distant from the central cell-binding domain (V25/CS-1) [126]. FNIII(del1-7), a recombinant FN ligand that incorporates this V25/CS-1 region and the

tetrapeptide Arg-Glu-Asp-Val (REDV) motif (recognized by $\alpha_4\beta_1$), display $\alpha_4\beta_1$ -mediated function for neural crest cells, including adhesion and matrix assembly [127].

Collagen-Mimetic Integrin-Specific Ligands

Although much surface engineering work has centered on RGD-binding receptors, other integrin receptors play critical roles in cell and tissue responses. $\alpha_1\beta_1$ and $\alpha_2\beta_1$ integrins are the major collagen-binding integrins, with $\alpha_2\beta_1$ dominating osteoblast integrin-mediated adhesion to type I collagen, the major ECM constituent of bone [23]. The $\alpha_2\beta_1$ -collagen interaction promotes osteoblast-specific signaling, gene expression, and differentiation, even in multipotent bone marrow stromal cells [47,128]. Adhesion sequences have been identified that regulate collagen-integrin interactions, including the collagen-binding motif DGEA and the hexapeptide sequence GFOGER (residues 502-507 of the $\alpha_1(I)$ chain in type I collagen) [86]. However, linear peptides using these sequences lack the full binding specificity for $\alpha_2\beta_1$ *in vitro* compared to full-length collagen in multiple cell types [129]. Not surprisingly, molecular binding studies found that full $\alpha_2\beta_1$ recognition and high affinity binding of this GFOGER sequence is critically dependent on the tertiary structure of collagen, which resembles a triple-helix [130-132]. To engineer a stable, biomimetic ligand that reconstitutes this crucial tertiary collagen structure, a 4 kDa peptide was engineered that incorporates this $\alpha_2\beta_1$ -specific GFOGER sequence surrounded by GPP triplet repeats that provide structural motifs for the formation of a stable, right-handed triple-helical structure mimicking native collagen [133]. When this GFOGER peptide was adsorbed on a polystyrene surface, this peptide specifically targeted the $\alpha_2\beta_1$ integrin receptor on osteoblasts, and supported FAK activation, osteoblast-specific gene expression, and matrix mineralization at levels

comparable to adsorbed collagen type I surfaces [86]. Integrin-subunit blocking-antibody studies confirmed $\alpha_2\beta_1$ -mediated adhesion for GFOGER coatings on orthopedic-relevant titanium substrates. In addition, studies using rat bone marrow stromal cells verified that GFOGER-coated titanium surfaces induced higher levels of osteoblast-specific gene expression, enzyme activity, and matrix calcification compared to serum-exposed titanium substrates [49]. Notably, GFOGER peptide coatings also significantly improved peri-implant new bone formation, implant integration, and functional osseointegration compared to the current clinical standard, unmodified titanium [49]. Given the ubiquitous role of collagen in other tissue types, these studies may point toward a significant clinical role for this GFOGER biomolecular strategy to control even non-orthopedic implant-tissue responses.

In fact, similar triple-helical GFOGER peptides have indeed been employed fairly successfully in other tissue systems to promote *in vitro* $\alpha_2\beta_1$ -mediated adhesion and function [133]. Peptides incorporating slight alterations in the flanking sequence to GFOGER, resulting in variable differences in helix stability, mediated liver cell and mouse fibroblast adhesion and spreading to varying degrees [134-137]. The collagen-mimetic peptides, which demonstrated greater relative stability than others, afforded higher levels of adhesion for these cell types. Mixed ligand surfaces presenting this triple-helical GFOGER peptide with other ECM-derived adhesion motifs on the same surface have also been explored in various tissue systems. A triple-helical peptide utilizing the collagen residues 496-507 (incorporating the GFOGER motif as well as 6 other amino acids) presented with a second ligand, an endothelial proliferating motif from the ECM protein SPARC, mediated $\alpha_2\beta_1$ -dependent activation of endothelial cells, although

presentation with the second ligand had no significant effect compared to the GFOGER peptide alone [138,139]. Interestingly, compared to single ligands, incorporation of this triple-helical GFOGER peptide in an amphiphile, which also incorporated this SPARC motif as well as a pseudolipid (monoalkyl hydrocarbon chain) for flexible interaction, showed the greatest activity in the activation and adhesion of endothelial cells [140]. These conflicting results may be explained by differences in ligand density as well as presentation of the two motifs to modulate optimal cell interactions.

Finally, non-fouling surfaces presenting both this $\alpha_2\beta_1$ -specific triple-helical GFOGER peptide as well as the $\alpha_5\beta_1$ -specific ligands were engineered in order to evaluate the effects of integrin crosstalk on adhesive responses. Mixed ligand surfaces synergistically enhanced cell adhesion strength, focal adhesion assembly, FAK activation, and proliferation rate compared to single FN and COL-I mimetic ligand surfaces [141]. Given the crucial and overlapping roles multiple integrins play in various cell signaling and functional pathways, engineering interfaces to present multiple integrin-specific ligands may be a successful strategy to achieve more robust and/or complex, directed cell/tissue responses. Collectively, these studies suggest that creating biointerfaces with highly directed integrin selectivity may be a clinically applicable surface strategy to obtain a directed tissue healing response, and, moreover, may be a facile approach for more robust tissue integration of other biomedical devices.

FN-Derived Integrin Ligands to Direct Matrix Assembly

A key property of the ECM environment is its tightly regulated, supramolecular 3-D structure that provides positional and environmental information essential for tissue function. In particular, the fibrillar architecture of FN is a major ECM network that

modulates cell cycle progression, migration, differentiation, and even assembly of other matrix proteins in tissues at all stages of development [142-144]. FN matrix assembly is a multi-step process which involves integrin interactions with specific regions of FN, that, in coordination with the actin cytoskeleton, expose “self-association” sites on FN (initiation) and mediate subsequent fibril assembly steps [145]. In addition, these specific integrin-FN interactions regulate cell-mediated FN secretion that is integral in normal matrix assembly and remodeling [145]. Unfortunately, although cells will organize assembled matrices on biomaterials, most synthetic materials do not directly recapitulate this essential function of the ECM, limiting the use of these materials in tissue engineering and regenerative medicine. Development of FN-derived ligands that interact with specific integrin receptors have afforded more precise control over FN matrix assembly on biointerfaces. FN10, a recombinant fragment of FN incorporating the adhesive RGD motif, is an essential requirement for initiation of $\alpha_5\beta_1$ -mediated FN matrix assembly. Presentation of FN10 with FN9, incorporating the synergy site PHSRN of $\alpha_5\beta_1$, augmented assembly over FN10 alone [146]. Interestingly, when mice were mutated so that the RGD motif became RGE on all cellular FN, the FN matrix assembly was not compromised, although embryonic development was stunted [147]. Studies using other recombinant fragments of FN containing various deletions of type III repeats verified that the RGD sequence is essential for the initiation step, but fibrils can form independently of the FNIII₁₋₇ modules [148]. It is noteworthy that deletion of the 1st through 7th type III repeats did alter the rate of FN assembly, suggesting a role for non-essential epitopes such as these to modulate different stages of matrix formation. Although the RGD-dependent $\alpha_5\beta_1$ -mediated assembly pathway is perhaps the most

studied, other integrins and FN regions have also been identified that are actively involved in matrix assembly. FNIII(del1-7), a recombinant FN ligand that incorporates the V25/CS-1 region and the tetrapeptide Arg-Glu-Asp-Val (REDV) motif recognized by $\alpha_4\beta_1$, was found to promote $\alpha_4\beta_1$ -mediated FN matrix assembly, although actin filament morphology was altered compared to $\alpha_5\beta_1$ -mediated assembly and cell proliferation rate was unaffected [148].

A 13 amino acid sequence localized between the type II2 and I7 repeats of FN, the self-assembly domain, was found to induce the assembly of fibrillar ECM; this sequence also exhibits collagen binding activity in tumorigenic cells [139]. Applying this knowledge, a synthetic oligopeptide FN13 (KGGGAHEEICTTNEGVM) incorporating this sequence was covalently tethered to a non-fouling mixed SAM surface to nucleate the assembly of fibrillar FN matrix networks [149]. A specific surface threshold of tethered FN13 not only nucleated robust FN fibril matrices, but also served as a template for collagen fibril assembly, along with increasing osteoblast cell proliferation rate over scrambled FN13, RGD-tethered, and unmodified surfaces. This synthetic matrix-nucleating ligand offers the distinct advantage of spatial control over matrix assembly, although reproduction of these results in a 3-D system may be more challenging. These synthetic matrix assembly-directing ligands may be of practical use in bottom-up organ building and other longer-term *in vivo* biotechnological applications, as well as fundamental studies on cell-matrix interactions.

Advanced ECM-Mimetic Surface Strategies: Multivalent, Clustered Ligands

After integrin binding to a ligand, clustering of integrins facilitates assembly of multiple cytoplasmic regulatory and structural proteins into important supramolecular

structures, termed “focal adhesions”. These structures activate various intracellular signaling pathways that regulate gene and protein expression, migration, and differentiation and mediate strong adhesive forces (**Figure 2.7**) [150]. Multivalent integrin-binding ECM ligands have been developed to promote integrin aggregation by presenting nanoscale clusters of adhesion ligands, in particular, RGD peptide-based motifs. These ligands have been immobilized on either 2-D surfaces or beads to study the effect of integrin aggregation/clustering on cell responses. Key multi-clustered integrin ligands and the underlying bases of ligand clustering are shown schematically in **Figure 2.7**. For example, the adhesion ligand GRGDSPK was presented in nanoscale synthetic polymer clusters of varying size on non-fouling substrates [151]. At higher cluster sizes (>3.6 ligands/cluster) an adhesion strengthening response was observed in which greater fractions of cells remained adherent as the detachment force was increased up to a force threshold. A similar polymeric RGD-dendrimer system correlated larger cluster sizes with an increase in cell migration behavior [152]. Alpha-helical coiled coil peptides fused with an RGD-containing fragment were over 100-fold more efficient than linear RGD peptides in blocking $\alpha_v\beta_3$ -mediated adhesion and, once immobilized on a surface, significantly more efficient in promoting cell adhesion and spreading [153]. Taking advantage of the robust recognition of $\alpha_v\beta_3$ for the RGD sequence, template assembled cyclopeptides of RGD were used to successfully target *in vitro* $\alpha_v\beta_3$ -expressing cells for drug delivery and detection applications [154,155]. Possible explanations for the augmented efficacy of $\alpha_v\beta_3$ selectivity and related adhesive activities may be the relatively close RGD spacing, higher localized density, and constrained tripeptide and flanking sequence conformations. More rigorous studies must be conducted to ascertain

the effect of these multimeric RGD ligands on integrin clustering and higher-order cell functions compared to native matrix proteins and single ECM-mimetic ligands.

However, given the lack of integrin selectivity of RGD peptides for one specific integrin, such as $\alpha_5\beta_1$, multimeric ligands presenting more integrin-specific components may be useful in examining functional effects of single integrin clustering. Moreover, these clustered ligand schemes rely mainly on “statistical averages” for valency values, rather than absolute ligand cluster sizes. Multimers presenting 1,2,3, and 5 heads of FNIII₇₋₁₀, an $\alpha_5\beta_1$ -specific FN-mimetic ligand, have been developed to investigate the role of $\alpha_5\beta_1$ clustering on integrin-cytoskeleton interactions in fibroblasts [156]. Beads of these FNIII₇₋₁₀ multimers localized to actin filaments and the higher valency (N=>3) multimer beads translocated along the cell periphery on actin highways, describing a link between ligand clustering and cytoskeletal pathways. The overall efficacy of these multimeric integrin-specific ligands in coordinating a variety of cell adhesive responses allude to the potential of these next generation ligands for use on biointerfaces for more controlled cell responses and therapeutic detection applications.

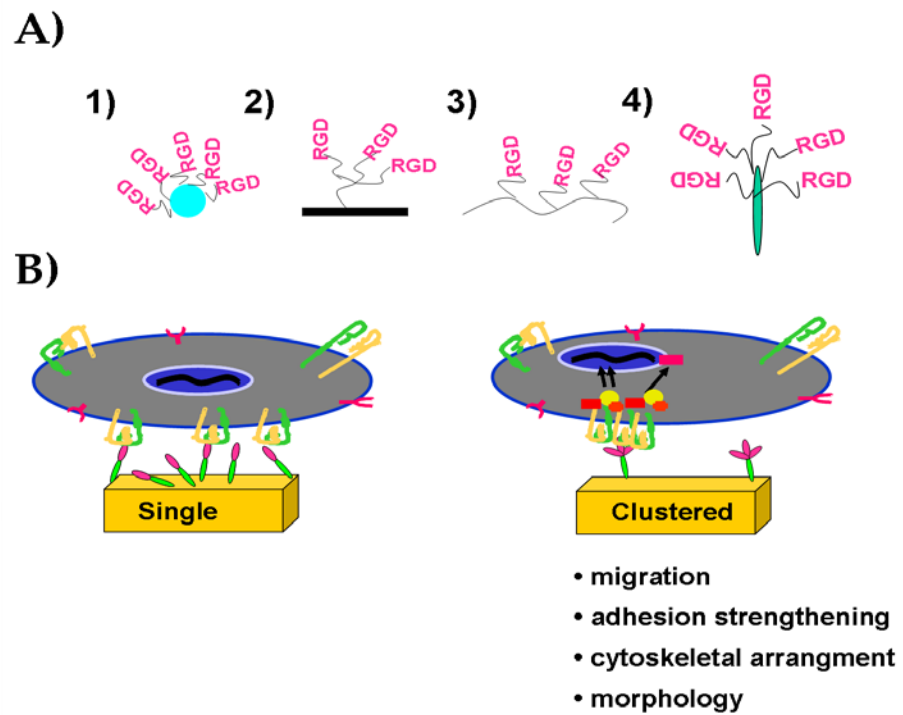


Figure 2.7. Integrin-specific ligand clustering may augment integrin-mediated cell functions. A) Schematic of various clustered ligand schemes that have been developed recently including: 1) nano-spaced ligands covalently tethered to micro-scale beads, 2) ligands functionalized on “star polymer” systems on substrate surfaces, 3) ligands tethered to the backbone of polymer gels/coatings in 2-D/3-D, and 4) “multi-headed” ligands which present individual integrin ligands nano-scale spacing apart. B) Various cell functions which appear to be modulated partly by ligand clustering effects.

Orthopedic Implant Surface Technologies

Bone Function and Formation

Bone is a composite material consisting of an organic component, primarily type I collagen for tensile strength, and an inorganic component, primarily mineral which contributes to resistance to compression [157]. Bone has several roles in the body, including a mechanical role as the structural support for tissues and organs, a central calcium reservoir for the body, and storage within the marrow cavities of mesenchymal and hematopoietic stem cells as well as immune cells.

Bone formation initially involves undifferentiated mesenchymal cells or preosteoblasts developing into osteoblasts, which promote bone formation by regulating deposition of osteoid and mineral nucleation [158]. Subsequent matrix mineralization around these osteoblasts eventually transforms these cells into osteocytes. Osteoclasts are later recruited to initiate the remodeling process through the secretion of hydrogen ions and acid proteases, converting immature woven bone into structurally mature and solid lamellar bone [159]. Following the initial ossification of the skeleton, osteoclasts and osteoblasts begin the dynamic and highly regulated process of modeling and remodeling bone.

Cortical and trabecular bone contain the same fundamental constituents: bone resorbing cells (osteoclasts), heterogeneous populations of bone forming cells (osteoprogenitors, osteoblasts, osteocytes, and periosteal lining cells), and a highly organized ECM, which consists of a poorly organized hydroxyapatite mineral phase and a mixture of collagenous and noncollagenous proteins (including osteopontin, bone sialoprotein, osteocalcin, fibronectin, and collagen I) which are expressed during

different stages of maturation [160]. Skeletal development involves two main mechanisms: intramembranous ossification and endochondral ossification. In intramembranous ossification, mesenchymal precursors differentiate into an osteoblastic phenotype. Endochondral ossification, occurring during fracture healing, involves the formation of an intermediate avascular cartilaginous matrix phase from mature hypertrophic chondrocytes. This cartilaginous matrix then becomes vascularized, calcified, and remodeled by osteoblasts/osteoclasts into mineralized matrix, and, ultimately, lamellar trabecular bone [161].

Bone Growth and Differentiation Factors

Stromal cells (BMSCs) are a heterogeneous population of connective tissue cells that reside generally in the bone marrow and retain a robust multipotency, similar to MSCs, which are often used interchangeably. Differentiation of BMSCs into an osteoblastic phenotype is regulated by a spatiotemporal cascade of growth, transcription, and differentiation factors, and ECM protein remodeling and secretion [162]. Osteoinductive factors, including BMPs, bind to transmembrane receptors and initiate specific signaling cascades that often converge to activate one or more osteogenic transcription factors [162]. In particular, the bone-related transcription factors Runx2/Cbaf1 have been heavily studied in their temporal role in commitment of multipotent stem-like cells into the osteoblastic lineage [163,164]. Forced expression of Runx2 upregulates osteoblast-specific gene expression and induces mineralization in a cell-dependent type format. Steroids, including the vitamin D group of molecules, have been linked as transcriptional regulators of bone matrix proteins, stimulating the

expression of osteocalcin and osteoclast differentiation. Moreover, vitamin D has been shown to affect the surface roughness-dependent differentiation of osteoblasts via an integrin-linked pathway. Detection of various secreted ECM proteins, including bone sialoprotein, osteocalcin, and osteopontin, has been widely used as temporal indicators of osteoblastic differentiation. More long-term differentiation. Levels of bone-specific alkaline phosphatase activity are valid biochemical indicators of early bone turnover and osteoblastic differentiation. Since the initial protein matrix of bone consists partly of calcium salts, assaying for calcium levels in cultures is another indicator of more advanced osteoblastic differentiation.

Osseointegration of Bone-Anchored Implants

The goal of current orthopedic implantology is the engineering of devices that induce controlled, guided, and rapid healing and proper osseointegration, defined as the strong anchorage between newly differentiated bone and the implant [6]. Bioactive porous coatings, including bone cement (PMMA), have been partially successful in augmenting initial bone fixation to the implant, although are prone to brittle fracture over time[7]. Implants that support faster osseointegration allow for quicker and more complete patient recovery, and reduced osteoatrophy of the surrounding bone. Nonetheless, in order to design effective surface strategies to achieve these goals, it is crucial to understand as completely as possible the process of tissue healing and the various host and material responses to implanted biomedical orthopedic devices.

Host and Material Response at the Bone-Implant Interface

After several days following implantation of Ti implants, mesenchymal stem cells housed in the bone marrow will migrate toward the defect site and osteoblasts begin

producing osteoid near the surface [8,9]. In addition, bone has also been observed to form away from the implant surface near the intramedullary canal, suggesting new bone formation occurring in two directions, towards and away from the bone-implant interface [10].

Ideally, an orthopedic implant will be anchored and fixed to bone and present a strong bone-implant interface. Variables that influence the quality of this fixation include material factors, such as implant composition, shape, surface topography and chemistry, as well as non-material issues, including surgical technique, patient lifestyle and bone quality [11-14]. Strategies to improve both early and overall osseointegration of bone-anchored implants have focused primarily on the material variables that have been shown to impact the local healing response. These separate factors include implant shape, material, and, most significantly, surface properties [12,14,15].

The first event that occurs near the defect site upon implantation of biomaterial implants is the adsorption, within seconds, of proteins, lipids, and ions from blood at or near the implantation site [16-18]. In particular, proteins can denature, desorb, or remain in native conformation on the device surface over time. These adsorbed proteins play a critical role in regulating cell-biomaterial interactions mainly because cell membrane receptors, specifically integrins, directly associate and interact with them [11]. It is the surface properties of the implant that dictate the quantity, nature, and type of proteins that are initially present. Surface parameters including composition, topography, roughness, surface energy, and chemistry have individually and collectively been shown to affect the in vivo biological nature of the implant surface shortly after implantation [11,14]. In turn,

the nature of the implant surface directly has an influence on the subsequent type and adhesion of cells on the surface, and, further, the function of these adherent cells.

Orthopedic Surface Strategies

Since cells mainly interact with the surface of an implant via integrins as previously discussed, current efforts to engineer a more integrated bone-implant interface have largely concentrated on surface modification strategies in order to obtain the desired biological response. Orthopedic titanium alloy has been the most extensively used metal for bone-integrated implants due to its excellent fatigue properties and the dense, passive oxide layer which renders it one of the most highly corrosion-resistant metals in existence [30,31]. Titanium alloys display high biocompatibility and “gold standard” osseointegration properties for bulk orthopedic implant materials [32]. Most current surface modification approaches focus on modifying the surface of titanium implants in three separate manners: morphologically, physicochemically, and biochemically.

Morphological parameters, such as surface roughness and porosity of implant coatings, have been modified to generally satisfactory clinical results. Macroporous coatings have displayed significant mechanical interlocking during the initial time period post-implantation [33], but evidence of porous-surface delamination and femoral atrophy at longer time points, as well as low overall bone mineral ingrowth relative to total pore volume, may collectively limit the longer-term applicability [34]. In vitro studies reveal that surfaces with microrough topographies promote the formation of an osteogenic environment [35], reduce osteoclast activity [36,37], improve the osteoblast-like cell phenotype [38,39], and enhance differentiation [40,41]. In vivo studies have demonstrated greater mechanical interlocking, and higher levels of bone formation and

apposition compared to smooth surfaces [14]. Nevertheless, these strategies alone do not perform well in challenging cases, including inferior patient bone quality and quantity, as evidenced by poor mechanical fixation and slow rates of osseointegration [42].

Physiochemical strategies take advantage of the theory that the initial type, amount, and conformation of proteins on the surface can have significant downstream effects on integrin binding, cell adhesion and, ultimately, tissue response, as previously discussed [43]. Titanium surfaces of increased energy and charge have been proposed to multiply the common electrostatic interactions that occur in many early biological-implant interfacial events. These surfaces have shown improved osteoblast differentiation in vitro compared to unmodified titanium surfaces [44]. Bone cement coatings, which display favorable surface energy for binding bone growth factors and proteins, have been used clinically for decades successfully to improve implant osseointegration and lifetime [45]. Finally, tailoring the implant surface chemistry has recently emerged as a strategy to elicit specific protein conformation and adsorption in order to elicit favorable bone cell adhesion and function. Our lab and others have demonstrated that surface chemistry-dependent differences in adhesive interactions modulate osteoblast differentiation [46,47]. Nonetheless, purely physiochemical surface strategies are inherently limited by lack of control of surface protein and cell specificity, making it difficult to direct precise cellular function and downstream pathways.

Recent advances in our understanding of the importance of distinct adhesion-influenced cellular pathways in promoting proper osseointegration have led to the investigation of biochemical implant surface modification methods as a potent strategy to target bone formation. These strategies involve delivering bioactive proteins, peptides,

enzymes, and/or growth factors to the implant surface to elicit a specific cellular response. As discussed in great detail in the beginning of this chapter, engineering orthopedic surfaces with immobilized biomimetic ligands, including integrin-binding peptide sequences such as RGD, remains one of the most promising surface strategies to improve implant osseointegration.

Biomolecule Delivery Approaches to Engineer Bioactive Surfaces

The surface delivery method for these biomolecules is critical for the overall functional efficacy of the implant. The biomolecule must be at or above a threshold density and it must also remain on the surface for a long enough time to elicit the desired cellular response. Since many biomolecule-functionalized surfaces have displayed in vitro density-dependent effects on cell adhesion, it is important to be able to control biomolecule surface density [48,49]. The simplest way of immobilizing biomolecules on a tissue-material interface is via adsorption from a protein solution prior implantation. Studies have shown that adsorbing TGF- β on porous coatings and alkaline-phosphatase on titanium can each enhance bone growth at the implant-tissue interface[50]. The clear advantage of the adsorption method is the clinical simplicity of the approach and easy maintenance of sterile surfaces. However, this method provides minimal control over the orientation, conformation, and retention time of the biomolecule, limiting its potential in directing specific cellular pathways and function.

In order to create a biointerface with more control over the presentation and retention of biomolecules, covalent tethering is a more optimal method of delivery. In vitro creation of well-defined, stable surfaces on gold substrates for covalent tethering of biomolecules has been performed using self-assembled monolayers (SAMs). Stable

SAMs formed by depositing alkanethiols with different terminal functional groups on gold have been used as model surfaces to control the tethering of ligands in a protein-adsorption resistant background [51]. Furthermore, the type and quantity of functional groups can be easily chemically tailored, offering versatility for protein tethering [52,53]. However, studies exploring the use of SAMs in physiological settings demonstrate minimal stability of these surfaces in an in vivo-like environment, restricting the use of this immobilization system as model in vitro surfaces [54]. In response to creating a more in vivo-relevant ligand presentation system, functionalizable polymer brushes on non-titanium metals have been developed. Nonetheless, few of these surfaces have demonstrated enhanced osseointegration or bone formation. Moreover, there are currently no functionalizable brush systems on titanium in the literature that offer retained, long-term stability in vivo, further limiting the ability to explore in detail the osseointegration capability of biomimetic ligand-inspired surface strategies.

Summary

As we continue to accumulate greater understanding of how integrins regulate robust cell functions in distinct pathways and, in turn, how biointerfaces regulate integrin-mediated activities, new biomaterial surface modification strategies geared toward engineering integrin selectivity have been recently explored to take advantage of integrin function. Since integrins direct signaling pathways, cytoskeletal arrangements, and phenotype, and are major mediators of how cells detect and respond to their outside environment, it has become apparent that the better we control material-integrin interactions, the more directed cell and tissue response we might be able to achieve, particularly in orthopedic applications. These integrin-specific strategies utilize a multi-

disciplinary approach, incorporating synthetic and organic chemistry, material science, knowledge of biological pathways, and genetic engineering, to design ligands functionalized on biointerfaces that direct selective integrin binding and activation.

Although by no means inclusive, this chapter sought to highlight the major engineered ligand strategies and ligand presentation approaches used, and relative successes achieved, directed at this integrin-specific paradigm. Promising future approaches include targeting spatial, temporal, and multi-integrin components of integrin binding and signaling. These strategies include engineering multi-clustered integrin ligands, mixed integrin ligand surfaces geared to synergistically utilize multiple integrins for a direct cell effect, and alternatively, reversible ligand presentation schemes to control temporal activation.

CHAPTER 3

INTEGRIN SPECIFICITY AND ENHANCED CELLULAR ACTIVITIES ASSOCIATED WITH SURFACES PRESENTING A RECOMBINANT FIBRONECTIN FRAGMENT COMPARED TO RGD SUPPORTS

Introduction

Extracellular matrices (ECMs) play central roles in tissue morphogenesis, homeostasis, and repair by providing structural and signaling scaffolds that organize, coordinate, and regulate cellular activities [22,26]. Therefore, ECMs provide attractive characteristics worthy of mimicking to convey biofunctionality to synthetic materials in order to control cell functions, tissue structure, and regeneration [31]. In particular, biomimetic strategies focusing on presenting short bioadhesive oligopeptides, including the arginine-glycine-aspartic (RGD) motif present in numerous ECM components, on a non-fouling support to target integrin adhesion receptors have demonstrated in vitro control of cell adhesion and differentiation, and, more importantly, enhancements in tissue healing responses in vivo, including bone formation [5,6,10], nerve regeneration [8,9], and corneal tissue repair [7]. Nevertheless, these bio-inspired strategies are limited

*Modified from

T.A. Petrie, J.R. Capadona, C.D. Reyes, A.J. García. *Biointerfaces Presenting a Recombinant Fibronectin Fragment Exhibit Integrin-Specificity and Enhanced Cellular Activities Compared to RGD Supports*. *Biomaterials* 2006; 27(31):5459-70.

by low activity of the oligopeptides compared to the native ligand due to the absence of complementary or modulatory domains [13-15]. For example, binding of integrin $\alpha_5\beta_1$ requires both the PHSRN sequence in the 9th type III repeat and RGD motif in the 10th type III repeat of fibronectin (FN) [13]. Each domain independently contributes little to binding, but, in combination, they synergistically bind to $\alpha_5\beta_1$ to provide stable adhesion [15,165]. Moreover, linear RGD peptides exhibit limited specificity among particular integrin receptors [28]. This limitation is particularly important as recent evidence suggests that integrin binding specificity regulates cell proliferation and differentiation [17,45,50].

To address limitations associated with short oligopeptides, conformation-constrained peptides (e.g., cyclic RGD) [166], simple mixtures of adhesive motifs [73,117,120,167], and linear molecules incorporating several binding sequences are being pursued [122,168]. However, because of the exquisite dependence of receptor binding on the structural context of the ligand, the ability to reconstitute activities mimicking the native ligand via these methods is extremely challenging. For instance, alterations in the nanoscale spacing, relative angle, and flanking sequences between the 9th and 10th type III repeats in FN result in significant losses in biological activity [92,113,114]. As an alternative strategy, we have focused on engineering high molecular weight ligands that recapitulate the primary, secondary, and tertiary structure of the native protein to reconstitute full biological activity as well as convey integrin binding specificity. For example, we have synthesized a triple helical peptide incorporating the GFOGER (O=hydroxyproline) integrin binding sequence of type I collagen that promotes $\alpha_2\beta_1$ -mediated cell adhesion, signaling, and differentiation [86,133]. In the case of FN, we

have engineered a recombinant fragment of FN encompassing the 7th-10th type III repeats (FNIII₇₋₁₀) to present the PHSRN and RGD sequences in the correct structural orientation [124]. This recombinant fragment exhibited equivalent adhesive activities as plasma FN. It is important to note that, while all these surface engineering approaches have demonstrated integrin-mediated adhesive activities, the relative potency of these different ligands as biomaterial modification strategies remains poorly understood.

The present analysis was undertaken to directly compare the cell adhesive activity, in terms of adhesion strength, integrin binding specificity, and signaling, of three adhesive ligands: short linear RGD, RGD-PHSRN peptide presenting the RGD and PHSRN motifs joined by a polyglycine sequence designed to mimic the spacing of the domains in FN, and recombinant FNIII₇₋₁₀. Adhesive ligands were tethered on model supports presenting anchoring groups within a non-fouling background in order to engineer well-defined, stable biointerfaces. We demonstrate that biointerfaces presenting ligands reconstituting FN secondary structure display enhanced cell adhesion activity, signaling, and integrin binding specificity.

Materials and Methods

Reagents, Antibodies, and Cells

Bacterial and mammalian cell culture reagents, Dulbecco's phosphate buffered saline (DPBS) and human plasma fibronectin (pFN) were obtained from Invitrogen (Carlsbad, CA). Fetal bovine serum (FBS) was acquired from Hyclone (Logan, UT). RGD peptide (GRGDSPC) was purchased from BACHEM (San Diego, CA), and GRGDG₁₃PHSRN peptide was synthesized by the Emory University Microchemical Facility (Atlanta, GA). Peptide tethering reagents, *N*-hydroxysuccinimide (NHS) and *N*-

(3-dimethylaminopropyl)-N'-ethylcarbodiimide hydrochloride (EDC), lysozyme and DNase were obtained from Sigma-Aldrich (St. Louis, MO). DH5 α and JM109 bacterial cells were purchased from Invitrogen and Promega (Madison, WI), respectively. The XA3 Pinpoint Vector biotinylation expression system and ECF substrate were obtained from Promega and Amersham Pharmacia Biotech (Piscataway, NJ), respectively.

Monoclonal HFN7.1 anti-human fibronectin antibody was obtained from the Developmental Studies Hybridoma Bank (Iowa City, IA). Rabbit antibodies against α_v (AB1930) and α_5 (AB1921) integrin subunits were purchased from Chemicon (Temecula, CA), and anti-vinculin antibody (V284) was acquired from Upstate Biotechnology (Lake Placid, NY). Function-perturbing hamster anti-rat β_1 integrin (Ha2/5), anti-mouse β_3 (2C9.G2), and anti-BrdU antibodies were purchased from BD Pharmingen. Alkaline phosphatase-conjugated donkey anti-mouse IgG (Jackson ImmunoResearch, West Grove, PA) was used in ELISA. AlexaFluor488-conjugated goat anti-mouse and anti-rabbit IgG antibodies, calcein-AM, and Hoechst 33258 dye were from Molecular Probes (Eugene, OR). Monoclonal antibodies against total FAK (Upstate Biotechnology) and specific phosphotyrosine residues in FAK (pY397, pY576) (BioSource International, Camarillo, CA) were used for FAK analysis. Biotinylated anti-rabbit IgG (Jackson ImmunoResearch) and alkaline phosphatase-conjugated anti-biotin antibodies (BN-34, Sigma-Aldrich) were used for Western blotting.

MC3T3-E1 murine immature osteoblast-like cells (Riken Cell Bank, Hirosawa, Japan) were used for all experiments because of their expression of multiple integrins, including $\alpha_v\beta_3$ and $\alpha_5\beta_1$. Cells were maintained at 37 °C in α -MEM supplemented with

10% FBS and 1% penicillin-streptomycin and passaged every 2-3 days via standard culture techniques.

Recombinant FNIII₇₋₁₀ Production

A monobiotinylated FN fragment spanning the 7-10th type III repeats of FN, FNIII₇₋₁₀, was produced using standard recombinant DNA techniques. cDNA encoding for human FNIII₇₋₁₀ was ligated into the XA3 plasmid (Pinpoint System, Promega). The resulting construct, encoding for FNIII₇₋₁₀ with a biotin tagging sequence at the amine terminus, was amplified in DH5 α cells, purified, and sequenced. JM109 bacterial cells were transformed the plasmid and streaked onto LB agar plates containing 100 μ g/mL ampicillin and incubated overnight. Colonies were isolated and dynamically cultured in LB broth (100 μ g/mL ampicillin; 2 μ m d-biotin). At 6 h, 100 μ M IPTG was added to augment protein production. The cell broth was spun down at 8000g for 10 min at 4C, and the cell pellet was resuspended at 10 mL/g of cell paste in lysis buffer (50 mM Tris-HCl pH 7.5, 50 mM NaCl, 5 % glycerol). Lysozyme (1 mg/mL) was added at 4C to the cell suspension and stirred for 20 min, then sodium deoxycholate (1 mg/mL) for 5 minutes, and finally DNAase I (40 μ g/mL) for another 10 min. The lysate was centrifuged (10,000g) for 20 min. The protein supernatant was sterile-filtered, and purified by affinity chromatography using a 5 mL column of Ultralink Immobilized Monomeric Avidin (Pierce) connected to a gradient pump, UV monitor, and fraction collector (BioRad, Hercules, CA). Briefly, after sequential column washes with regeneration and elution buffers, the protein solution was allowed to bind to the column for 1 h at a 0.4 mL/min flow rate. After washing with DPBS, elution buffer (0.5 mg/mL d-biotin in DPBS) was flowed through (1 mL/min) and the eluted fractions monitored for

protein. Protein fractions were filtered using 30 kDa Microcon centrifugal filter devices (Millipore, Bedford, MA) to remove d-biotin, and verified as > 98% pure FNIII₇₋₁₀ by Western blotting and SDS-PAGE. Purified samples were flash frozen for storage (-80°C).

Model Biomaterial Surfaces

Self-assembled monolayers (SAMs) on alkanethiols on gold were used to present well-defined, ordered surfaces with anchoring groups within a non-fouling background. Tri(ethylene glycol)-terminated alkanethiol (HS-(CH₂)₁₁-(OCH₂CH₂)₃-OH; EG₃) and carboxylic acid-terminated alkanethiol (HS-(CH₂)₁₁-(OCH₂CH₂)₆-OCH₂COOH; EG₆-COOH) were previously synthesized and characterized [149]. Gold-coated substrates were prepared by sequential deposition of titanium (100 Å) and gold (200 Å) films via an electron beam evaporator (Thermionics Laboratories, Hayward, CA, 2 x 10⁻⁶ Torr, 1 Å/s) onto clean 6-well plate lids or glass coverslips. Mixed SAM surfaces were prepared on substrates by immersing in a 1.0 mM mixed solution of EG₃/EG₆-COOH thiols (4 h). Peptide ligands were tethered using standard peptide chemistry [169]. Briefly, following washing in ethanol and ultrapure H₂O, SAMs were incubated in 2.0 mM EDC and 5.0 mM NHS in 0.1 M 2-(*N*-morpho)-ethanesulfonic acid and 0.5 M NaCl (pH 6.0), and subsequently immersed in a 20 mM solution of 2-mercaptoethanol in deionized H₂O. Adhesive ligands in PBS were then incubated on the activated supports for 30 min and unreacted surface NHS esters then quenched in 20 mM glycine. Finally, surfaces were blocked in 1% heat-denatured bovine serum albumin (BSA) and then incubated overnight in DPBS to reduce non-specific protein adsorption [170].

Enzyme Linked Immunosorbent Assay (ELISA) and Surface Density Measurements

An ELISA was used to probe for the biological activity of the FNIII₇₋₁₀ fragment compared to pFN. FNIII₇₋₁₀ or pFN was adsorbed onto either uncoated or Neutravidin-coated (100 µg/mL) 96-well black U-well Dynex plates at various concentrations for 30 min. Following incubation in blocking buffer (0.25% BSA, 0.1 M EDTA, 2.5% Tween-20, 0.00125% NaN₃), HFN7.1 antibody (0.6 µg/mL in blocking buffer) was added for 1 h at 37 °C, and, after washing with blocking buffer, surfaces were incubated in alkaline phosphatase-conjugated anti-mouse IgG (0.6 µg/mL) for 1 h at 37 °C. Washed surfaces were exposed to 4-methylumbelliferyl phosphate (25 mg/mL in 10 mM diethanolamine, pH 9.5). The resulting fluorescence was quantified using an HTS 7000 Plus plate reader (Perkin Elmer, Foster City, CA) at 360 nm excitation and 465 nm emission.

Surface density measurements were obtained via surface plasmon resonance (SPR) using a Biacore X instrument (Biacore, Piscataway, NJ). Mixed SAM surfaces were prepared as described above on Au-coated SIA chips (Biacore), primed with sterile DPBS, and the baseline allowed to stabilize at a flow rate of 15 µl/min in DPBS. Ligands were tethered by activating the surface with EDC/NHS for 10 min at a 10 µl/min flow rate, and ligand solutions were subsequently injected at a flow rate of 4 µl/min for 30 min. Finally, surfaces were washed with 20 mM glycine at 10 µl/min and the signal allowed to stabilize for 2 min thereafter to measure tethered peptide levels. To assay for relative degree of biotinylation, a solution of FNIII₇₋₁₀ was flowed over a streptavidin chip at 20 µl/min for 4 min. Resonance units (R.U.) were converted to surface density values (10 R.U. = 1 ng/cm²).

Centrifugation Cell Adhesion Assay

A modification of a centrifugation assay [171] was used to apply controlled detachment forces to cells adhering to engineered surfaces. Multi-wells of engineered surfaces were created on gold-coated polystyrene plate lids using silicone gaskets (Grace Bio-Labs, Bend, OR). Mixed SAMs were assembled and ligands tethered at varying densities. MC3T3-E1 cells were labeled with 4 mM calcein-AM, a membrane-permeable green fluorescent dye, in 2 mM dextrose-DPBS for 30 min and resuspended in α -MEM with 10% fetal bovine serum. Cells were seeded onto the surfaces at 200 cells/mm², and allowed to attach for 1 h at 37 °C. For blocking antibody experiments, cells were incubated in the presence of function-perturbing antibodies (10 μ g/mL) for 10 min with gentle agitation prior to cell seeding. Before centrifugation, cell images were taken using a Nikon TE-300 fluorescence microscope and Spot RT digital camera. Wells were then filled completely with dextrose-PBS, sealed, inverted, and centrifuged for 5 min at a prescribed speed on a Beckman Allegra 6 centrifuge (GH 3.8 rotor) to apply normal detachment forces. Media was then gently aspirated from the wells, and wells were refilled for post-spin image collection. Post/pre-spin cell ratios were determined by image analysis, and this adhesive fraction was plotted against ligand surface density to obtain cell adhesion profiles.

Immunofluorescence Staining for Integrins and Focal Adhesions

Surfaces were prepared on either 6 well plate lids or 35 mm tissue culture dishes, and cells seeded at 75 cells/mm² in serum-containing media for 4 h at 37 °C. For integrin staining, a cross-linking/extraction biochemical method that selectively isolates bound

integrins was employed [172]. Cells were washed, and 1.0 mM DTSSP (Pierce) was added for 15 min to cross-link ligated integrins. After quenching with 50 mM Tris, uncrosslinked cellular components were extracted in 0.1% SDS supplemented with protease inhibitors (350 µg/mL PMSF). Samples were then blocked in 5% FBS for 1 h and incubated with integrin-specific antibodies for 1 h at 37 °C. Fluorochrome-labeled secondary antibodies were then incubated for 1 h at 37 °C. Following washing, samples were mounted on slides with Gel/Mount mounting media (Biomed, Foster City, CA). For staining of focal adhesions, cells were extracted in 0.5% Triton X-100 in ice-cold cytoskeleton buffer (50 mM NaCl, 3 mM MgCl₂, 150 mM sucrose, 20 µg/mL aprotinin, 1 µg/mL leupeptin, 1 mM PMSF, 50 mM Tris, pH 6.8) for 2 min and fixed in cold 3.7% formaldehyde in DPBS for 5 min. Cultures were blocked, subsequently incubated in anti-vinculin monoclonal antibody (1:70 in 5% FBS) and fluorochrome-labeled secondary antibodies for 1 h, and samples mounted on slides.

FAK Phosphorylation Assay

Cells were detached and gently agitated in serum-free suspension for 45 min to reduce background. Cells were then seeded at 200 cells/mm² serum-free for 1 h. Cells were lysed in RIA buffer (1% Triton X-100, 1% sodium deoxycholate, 0.1% SDS, 150 mM NaCl, 150 mM Tris-HCl (pH 7.2), 350 µg/mL PMSF, 10 µg/mL leupeptin, and 10 µg/mL aprotinin) for 20 min on ice. Samples were pipetted up and down 20 times and centrifuged at 8000g for 10 min to shear DNA and isolate protein contents. Total protein was quantified using micro-BCA (Pierce). Equal amounts of protein were boiled for 10 min in Laemmli buffer and separated by SDS-PAGE on a 7% gel, transferred to nitrocellulose membranes, and blocked with Blotto (5% nonfat dry milk, 0.2% Tween 20)

overnight at 4°C. Membranes were gently rocked in antibodies against FAK and specific phosphorylated FAK tyrosine residues (anti-total FAK at 1 µg/mL, anti-FAK pY397 at 0.35 µg/mL, anti-FAK pY576 at 0.5 µg/mL) for 1 h. After washing with TBS-Tween (20 mM Tris HCl pH 7.6, 137 mM NaCl, 0.1% Tween-20), secondary antibody (biotin-conjugated anti-rabbit IgG; 1:20,000) was added for 1 h, followed by alkaline phosphatase-conjugated anti-biotin antibody (1:10,000) in Blotto. Immunoreactivity was assessed by ECF fluorescent substrate. FAK bands were visualized by a Fuji Image Analyzer and phosphorylation levels normalized to total FAK.

Cell Proliferation Rate

Cells were seeded on surfaces in 10% serum for 16 h, and BrdU (3.1 µg/mL) was added for the last 4 h. After washing with DPBS, samples were fixed in 70% cold ethanol for 10 min, denatured in 4 M HCl for 20 min, neutralized in 50 mM NaCl in 100 mM Tris-HCl (pH 7.4), washed, and blocked with 5% FBS + 1% heat-denatured BSA. Cultures were incubated in anti-BrdU antibody (1:1000) and AlexaFluor488-conjugated anti-mouse IgG (1:200). Nuclei were counter-stained with Hoechst dye (1:10,000). Fluorescent images were used to quantify the number of cells positive for BrdU relative to total cell nuclei using an in-house image analysis routine. Ten representative fields were analyzed per well with multiple wells for each surface condition.

Statistics

Data represent characteristic results from a particular experimental run, although at least three independent runs were conducted. Data are reported as mean ± standard error. Results were analyzed by one-way ANOVA using SYSTAT 11.0 (SPSS). If

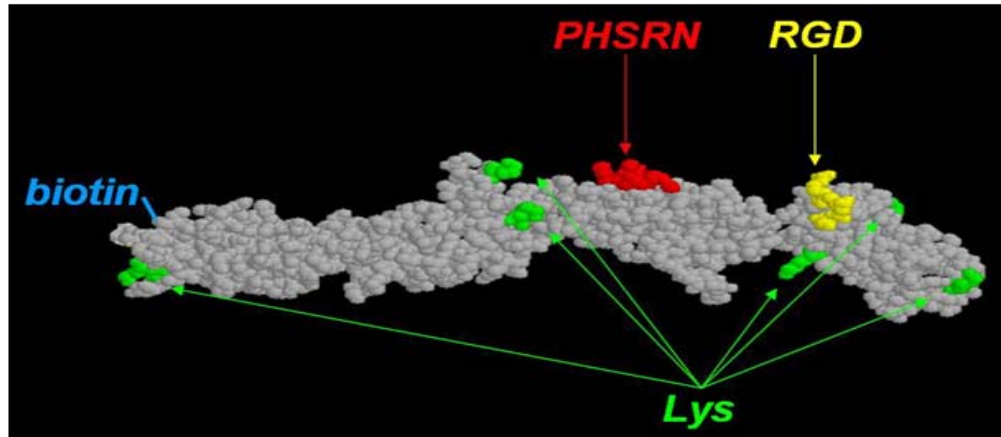
treatment level differences were determined significant, pair-wise comparisons were performed using a Tukey post-hoc test. A 95% confidence level was considered significant.

Results

Recombinant FNIII₇₋₁₀ has Equivalent Biological Activity as Plasma FN

We previously developed a recombinant FN fragment (FNIII₇₋₁₀), presenting both the RGD and the synergy PHSRN domain in the correct native structure and orientation, in order to target the $\alpha_5\beta_1$ integrin [124]. Recombinant DNA technology allows for production of FN-mimetic ligands that reconstitute the secondary structure of the native ligand and affords the ability to engineer enhanced or new functionality. In the present work, we engineered a monobiotinylated FNIII₇₋₁₀ by encoding a biotinylation sequence at the amine terminus of the protein. The crystal structure for FNIII₇₋₁₀ is presented (**Figure 3.1 A**) with relevant residues highlighted and a schematic biotin tag added [173]. This fibronectin fragment represents an enhanced version of the previously described fragment with a single biotin tag introduced at a specific site [124]. In addition to providing a simple system to generate large quantities of purified protein via affinity chromatography (2-10 mg from 1 L culture, >98% purity, **Figure 3.1 B**), this strategy incorporates a well-defined tag for tethering onto avidin supports as well as a tracking marker for future in vitro and in vivo studies.

A)



B)

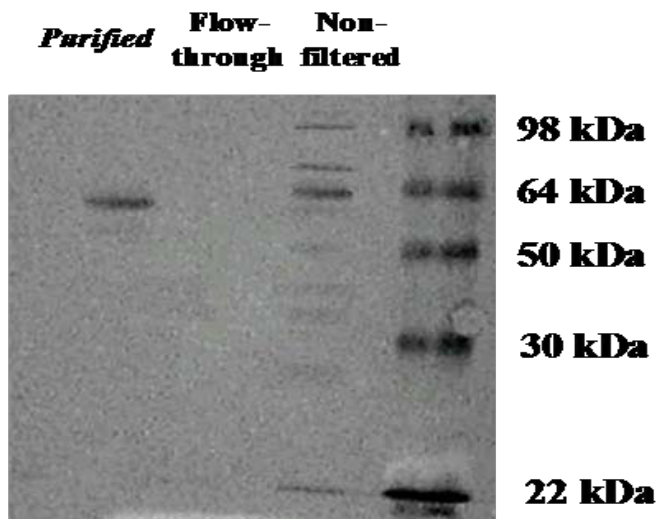


Figure 3.1. Monobiotinylated FNIII₇₋₁₀. (a) Crystal structure of FNIII₇₋₁₀ displaying both the RGD and PHSRN binding site in the native structural orientation (PDB file 1FNF). Also shown are lysine residues available for tethering and single biotin tag encoded at the amine terminus of the 7th type III repeat. (b) Purification of FNIII₇₋₁₀ from bacterial cell lysate using avidin-affinity chromatography. Ponceau stain showing lysate, wash, column-bound, and post-wash pooled protein fractions.

The biological activity of FNIII₇₋₁₀ was evaluated by ELISA using the HFN7.1 monoclonal antibody which is specific for the central cell-binding domain in the 9th to 10th type III repeats of FN [174]. Furthermore, we have shown that HFN7.1 binding efficiency correlates closely with the binding affinity of the integrin $\alpha_5\beta_1$ for FN [65]. For passively adsorbed ligands, HFN7.1 binding increased with protein coating concentration for both pFN and FNIII₇₋₁₀, and there were no significant differences in either the hyperbolic shape or magnitude for the binding curves (see **Figure 3.2 A**), indicating equivalent functional activity between monobiotinylated FNIII₇₋₁₀ and pFN.

To demonstrate biotinylation of the fragment, both ELISA on Neutravidin-coated polystyrene and surface plasmon resonance (SPR) on streptavidin-coated gold chips were performed (see **Figure 3.2 B**). High levels of HFN7.1 antibody bound to FNIII₇₋₁₀ incubated on Neutravidin-coated surfaces, whereas background levels of HFN7.1 binding were observed on Neutravidin supports exposed to pFN (no biotin tag). This result is expected since only biotinylated ligand (FNIII₇₋₁₀) would be tethered on Neutravidin. Similarly, SPR measurements revealed high levels of immobilized FNIII₇₋₁₀ on streptavidin-coated chips.

FNIII₇₋₁₀ Displays Enhanced Cell Adhesive Activity Compared to RGD Peptides

Mixed alkanethiol SAMs were used as model surfaces presenting well-defined anchoring groups (-COOH) for controlled tethering of ligands in a protein adsorption-resistant background (tri(ethylene glycol groups): EG₃). Peptides were tethered via free amines using EDC/NHS coupling chemistry [169,170]. The percentage of anchoring groups within the SAM is expected to be an important design parameter; densities of anchoring groups must be optimized to afford for a wide range of ligand densities while

preventing non-specific ligand adsorption. We examined FNIII₇₋₁₀ tethering/adsorption onto activated/unactivated SAMs with EG₆-COOH:EG₃ solution ratios ranging from 0.0001 to 0.1 via ELISA (data not shown). We determined that an EG₆-COOH:EG₃ solution ratio of 0.02 yielded the highest tethered ligand density while maintaining background levels of non-specific adsorption. This model system presents a well-defined surface with a single adhesive ligand that allows direct functional comparison on a molar basis among different adhesive ligands.

Three adhesive ligands were examined: (i) RGD peptide (GRGDSPC); (ii) RGD-PHSRN peptide (GRGDG₁₃PHSRN) presenting the RGD and PHSRN motifs joined by a polyglycine sequence designed to mimic the spacing of the domains in FN but not interfere with the adhesion characteristics of the two linked sequences [24]; and (iii) FNIII₇₋₁₀. Quantification of ligand tethering onto SAMs was conducted via SPR. Tethered ligand surface density increased hyperbolically with coating concentration, reaching saturation levels at higher concentrations (**Figure 3.3 A**). The measured surface densities are in good agreement with previous results [169,170], and are below the theoretical limits based on the calculated surface density of the EG₆-COOH thiols. Although these surfaces were prepared in situ in the SPR, as opposed to the surfaces prepared on the benchtop used for the cell culture work, ELISA-based measurements indicated no significant differences in tethered profile shape or relative densities (data not shown), supporting the validity of these quantitative density values.

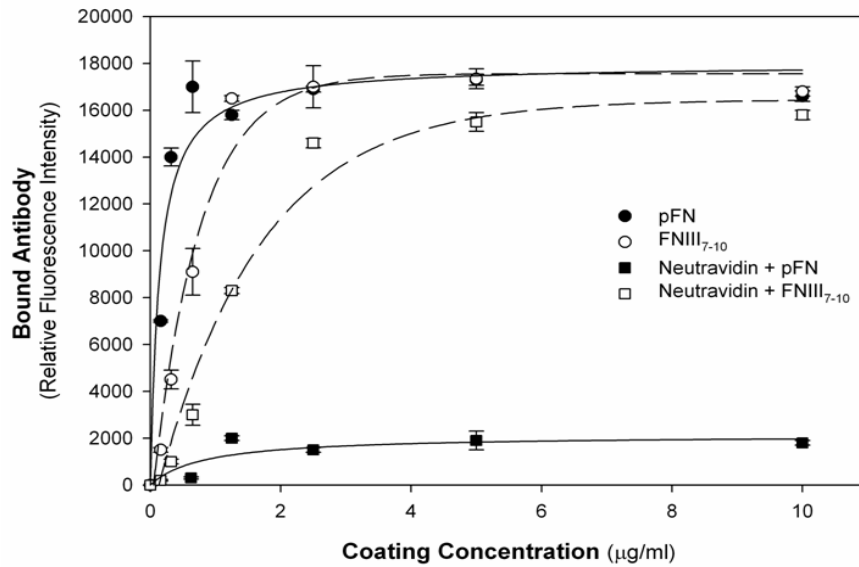
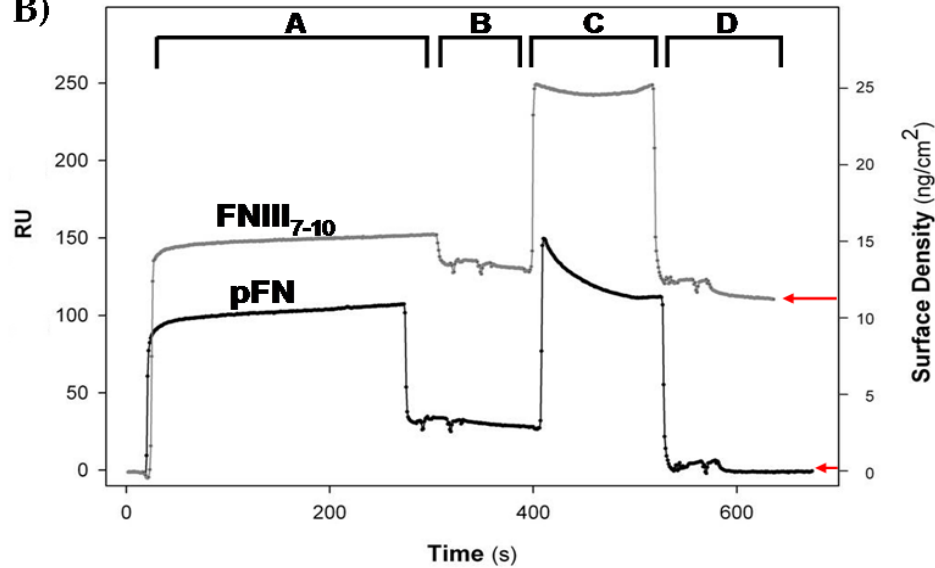
A)**B)**

Figure 3.2. Monobiotinylated FNIII₇₋₁₀ exhibits equivalent biological activity as pFN. (a) HFN 7.1 antibody binding follows hyperbolic profile vs. protein coating concentration for passively adsorbed pFN and FNIII₇₋₁₀. In contrast, antibody binding to FNIII₇₋₁₀ is 10-fold higher than pFN on Neutravidin-coated surfaces. (b) SPR measurements on streptavidin-coated chips highlight successful biotinylation of FNIII₇₋₁₀. SPR steps were: (A) 4 min protein injection, 10 µL/min, 10 µg/mL, (B) 1 minute PBS wash, (C) 2 min 0.01% SDS wash, (D) 2 min PBS wash. Arrows indicate immobilized protein density.

These data indicate that control over tethered peptide density can be achieved by varying coating concentration accordingly. Although the tethering curves exhibited similar hyperbolic profiles, RGD and RGD-PHSRN tethered at >10-fold higher molar densities than FNIII₇₋₁₀ (see **Figure 3.3 A**). Tethering efficiencies for RGD and RGD-PHSRN were identical. This result is not unexpected given the significant differences in size as well as availability of anchoring groups on FNIII₇₋₁₀ compared to the linear RGD peptides. Tethered ligands were biologically active as determined by cell spreading. At saturated surface densities, all engineered surfaces exhibited equivalent levels of cell spreading, while very few cells attached to EG₃ or unactivated EG₆-COOH: EG₃ surfaces (see **Figure 3.3 B**).

To further characterize the adhesive activities of these engineered biointerfaces, we measured the adhesion strength of MC3T3-E1 cells using a centrifugation assay that applies controlled detachment forces to adherent cells [172]. For all surfaces, the fraction of adherent cells increased sigmoidally with adhesive ligand surface density (see **Figure 3.4**), and adhesion strength was characterized as the ligand density required for half-maximal adhesion (ADH₅₀). Adhesion strength is inversely related to ADH₅₀, as a shift of the curve left (decreasing ADH₅₀) represents an increase in adhesion strength since less ligand is needed for cell adhesion. Cell adhesion profiles for RGD- and RGD-PHSRN-tethered surfaces were almost identical, and ADH₅₀ values were 2300 and 1950 fmol/cm², respectively, indicating similar adhesive activity for these two peptides (see **Figure 3.4**). FNIII₇₋₁₀-tethered surfaces displayed a pronounced leftward shifted adhesion profile compared to the other two peptide tethered-surfaces, reflected in the relatively low ADH₅₀ value of 70 fmol/cm² (see **Figure 3.4**).

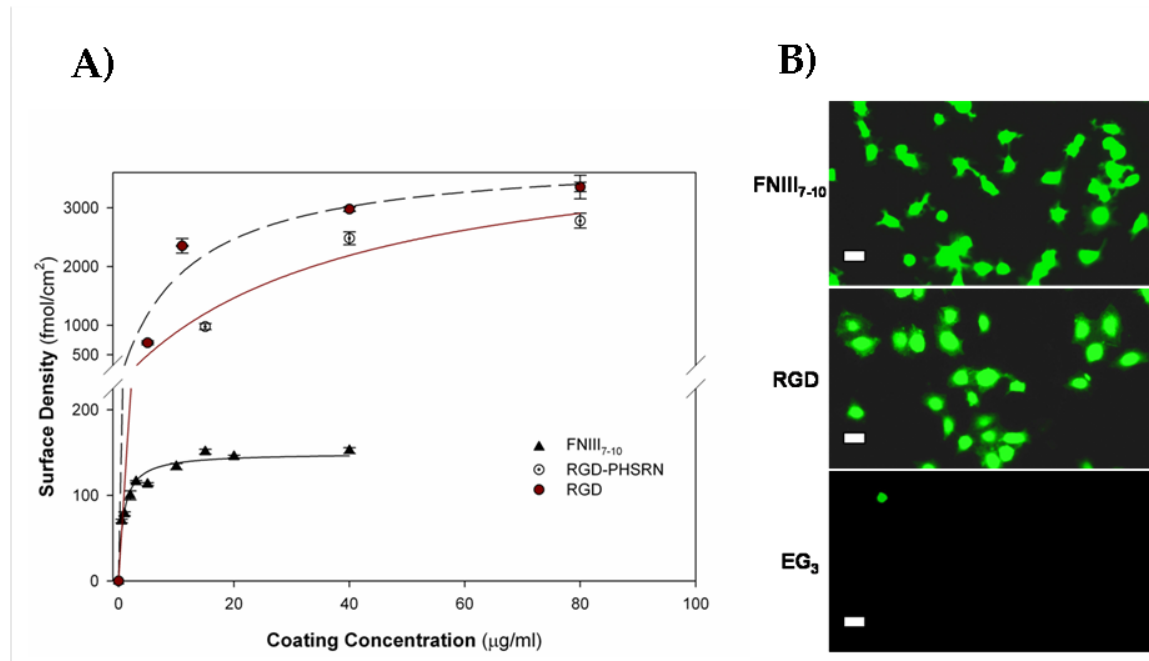


Figure 3.3. Bioadhesive ligand tethering to mixed SAMs. (a) Surface density of FNIII₇₋₁₀, RGD, and RGD-PHSRN tethered to 2% EG₆-COOH:EG₃ SAM surfaces as a function of coating concentration as determined by SPR (mean \pm standard deviation; hyperbolic curve fit: RGD, $R^2 = 0.95$; RGD-PHSRN, $R^2 = 0.95$, FNIII₇₋₁₀, $R^2 = 0.97$); (b) Images of calcein-labeled MC3T3-E1 cells adhering to peptide-tethered SAM surfaces for 1 h. Overall spreading and adhesion were similar on each peptide-tethered surface whereas few cells attached to EG₃-terminated controls (Scale bars = 20 μm).

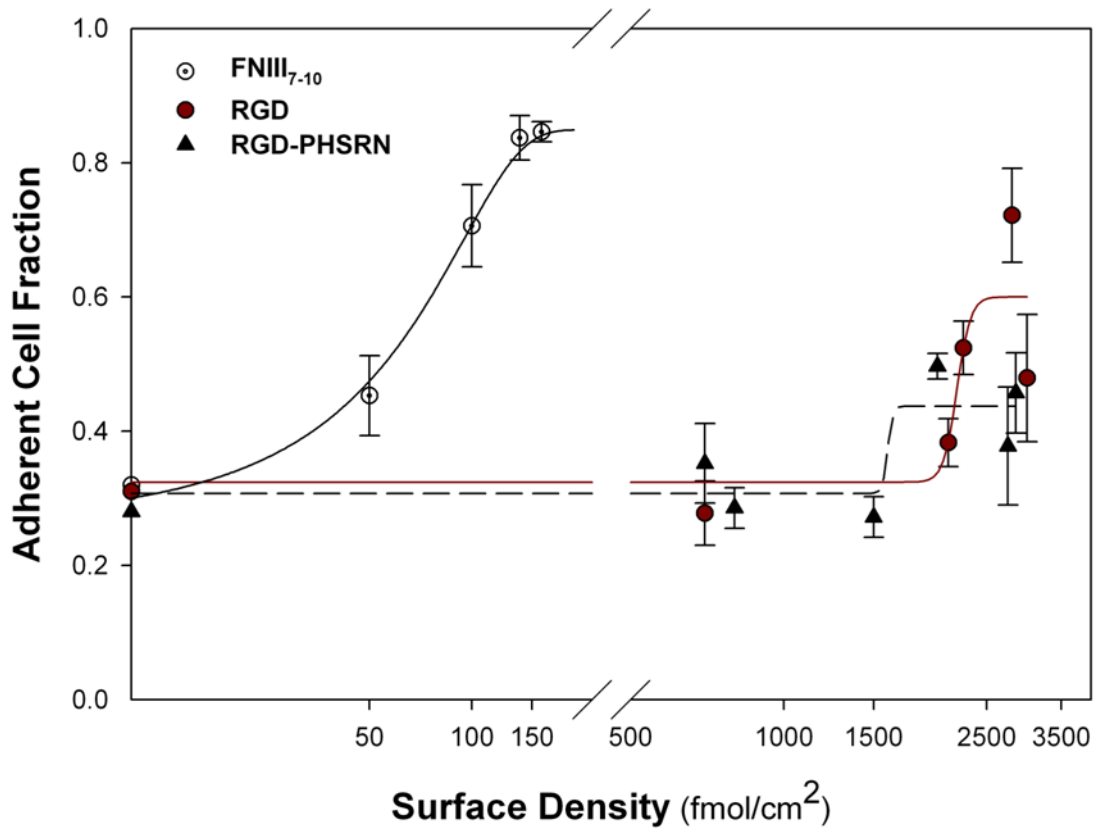


Figure 3.4. MC3T3-E1 cell adhesion strength to SAMs presenting controlled densities of bioadhesive ligands (1 h adhesion, centrifugation at 57 g for 5 min). FNIII₇₋₁₀ cell adhesion strength profile is shifted upward and leftward, indicating an increase in adhesion strength over RGD and RGD-PHSRN-tethered surfaces (mean \pm standard error, 4 independent experiments with $n = 5$; sigmoidal curve fits: RGD, $R^2 = 0.80$; RGD-PHSRN, $R^2 = 0.79$; FNIII₇₋₁₀, $R^2 = 0.96$).

These data indicate that the FNIII₇₋₁₀-tethered surface displays higher cell adhesive activity compared to RGD or RGD-PHSRN-tethered surfaces.

FNIII₇₋₁₀ Surfaces Exhibit Different Integrin Specificity than RGD Supports

We then examined whether these different adhesive surfaces supported cell adhesion by binding different integrin receptors. Function-perturbing antibodies directed against different integrin subunits were used to block adhesion to the engineered interfaces. Since integrins $\alpha_5\beta_1$ and $\alpha_v\beta_3$ represent the dominant adhesion receptors for FN in MC3T3-E1 cells [17], we analyzed the contributions of these receptors to adhesion strength on the peptide-functionalized SAMs. Surfaces were tethered with maximum density of ligand, and the relative cell adhesion was normalized to unblocked controls. Blocking antibodies directed against $\alpha_5\beta_1$ integrin reduced adhesion to background levels (EG₃) for the FNIII₇₋₁₀-tethered surface, but only slightly reduced adhesion on the RGD and RGD-PHSRN surfaces (see **Figure 3.5**). In contrast, antibodies against the β_3 integrin subunit did not alter adhesion significantly for FNIII₇₋₁₀-tethered surfaces, but reduced adhesion over 75% for both the RGD and RGD-PHSRN surfaces (see **Figure 3.5**). These results demonstrate that the FNIII₇₋₁₀-tethered surface primarily supports $\alpha_5\beta_1$ -mediated adhesion, whereas the RGD- and RGD-PHSRN-functionalized surfaces promote $\alpha_v\beta_3$ -mediated cell adhesion.

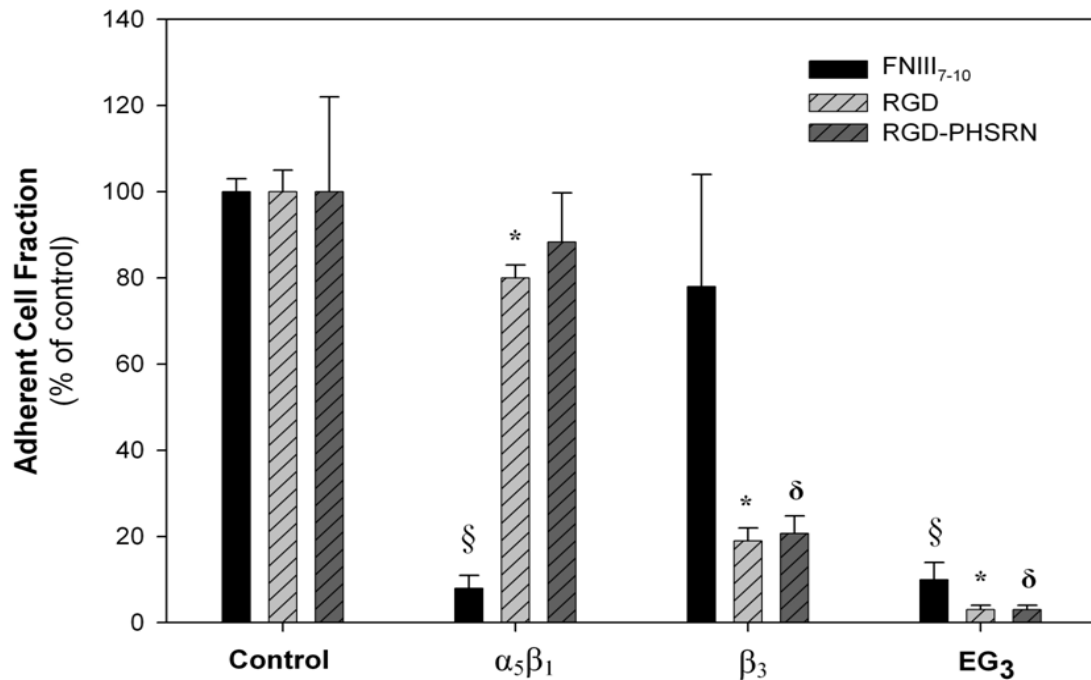


Figure 3.5. Surfaces presenting FNIII₇₋₁₀ display integrin binding specificity compared to RGD supports. Blocking antibodies against integrin $\alpha_5\beta_1$ completely inhibited cell adhesion to FNIII₇₋₁₀ surfaces (§ vs. control, $p < 0.0009$) and, to a much lesser extent, the RGD surface (* vs. RGD control, $p < 0.01$). In contrast, blocking β_3 blocked cell adhesion only to the RGD (* vs. control, $p < 0.0009$) and RGD-PHSRN (δ vs. control, $p < 0.0009$) surfaces. Adhesion to peptide-incubated EG₃ control surfaces was minimal. Results are expressed as percent inhibition compared to unblocked cell control (mean \pm standard error, 3 independent experiments with $n = 8$).

Since MC3T3-E1 cells assemble robust focal adhesions containing clustered integrins and intracellular structural and signaling proteins, we examined integrin binding and focal adhesion assembly on the engineered interfaces by staining for different integrin subunits and vinculin, which localizes to focal adhesions [175]. MC3T3-E1 cells were allowed to adhere on each saturated ligand-functionalized support for 2 h and integrin binding was evaluated via a crosslinking/extraction and immunostaining protocol which isolates integrins ligated to the ligand [172]. Cells adhering to FNIII₇₋₁₀-tethered surfaces displayed robust, well-defined adhesive structures containing $\alpha_5\beta_1$ integrins but minimal $\alpha_v\beta_3$ binding (see **Figure 3.6**). Cells on RGD-tethered surfaces exhibited clustering of $\alpha_v\beta_3$ and little staining for $\alpha_5\beta_1$ (see **Figure 3.6**). We note that the crosslinking and extraction technique relies in coupling free amines on both the receptor and ligand. Since the tethered RGD has no free amine, we attribute the $\alpha_v\beta_3$ staining in the RGD surfaces to focal adhesions that were not completely extracted. These results are further supported by the integrin antibody blocking adhesion data. Both surfaces assembled focal adhesions containing vinculin (see **Figure 3.6**). These results further demonstrate that surfaces presenting FNIII₇₋₁₀ primarily support $\alpha_5\beta_1$ -mediated adhesion, while RGD-functionalized SAMs mediate adhesion via $\alpha_v\beta_3$.

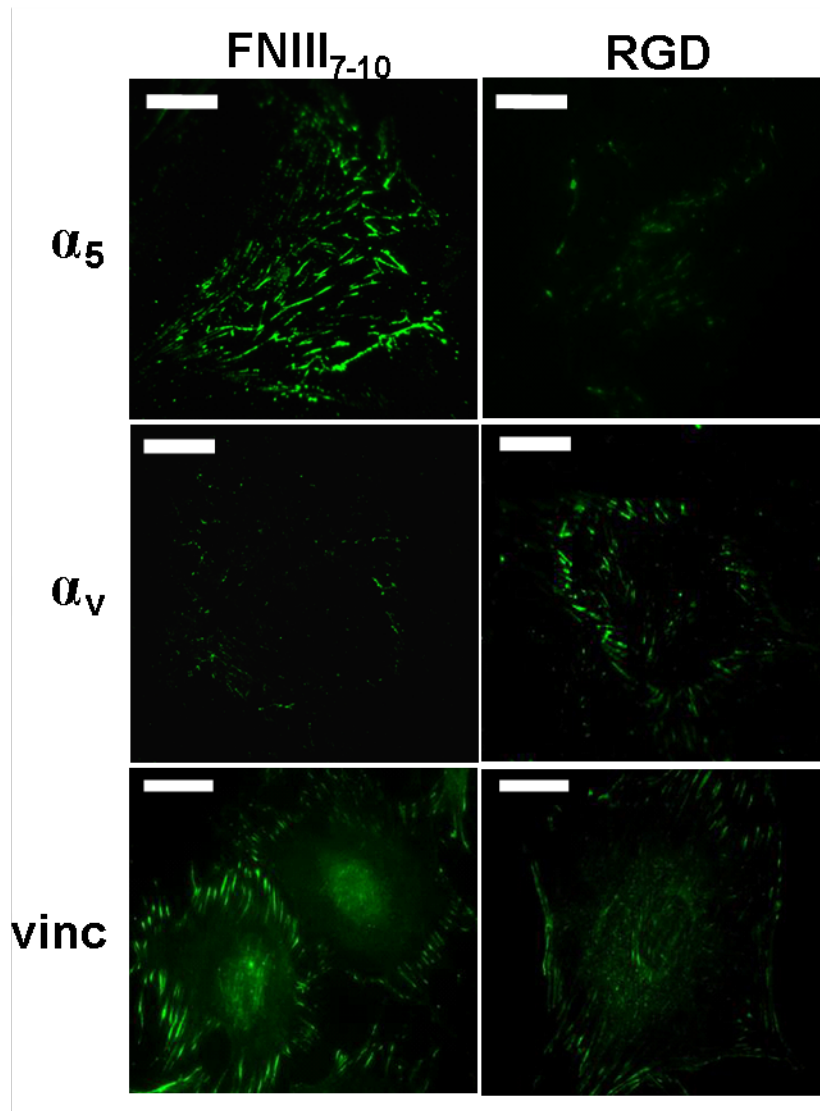


Figure 3.6. Immunofluorescence staining for bound integrins and vinculin in MC3T3-E1 cells seeded for 4 h on FNIII₇₋₁₀ and RGD-tethered SAMs. Cells on FNIII₇₋₁₀ surfaces display intense clusters of $\alpha_5\beta_1$ integrin and minimal α_v staining, while RGD-tethered surfaces exhibit peripheral clusters of α_v and sparse $\alpha_5\beta_1$ staining. Vinculin recruitment to focal adhesions was observed on both surfaces, although in more abundance and intensity on FNIII₇₋₁₀ surfaces compared to RGD (Scale bars = 10 μm).

FNIII₇₋₁₀ Interfaces Trigger Enhanced Signaling and Cell Proliferation

We next determined whether these bioadhesive interfaces modulated intracellular signaling and high-order cell activities. We analyzed levels of focal adhesion kinase (FAK) phosphorylation as a marker of integrin-mediated signaling. FAK localizes to focal adhesions and activates various signaling cascades regulating cell survival, proliferation and differentiation [176]. We probed for phosphorylation of important tyrosine residues using site-specific antibodies in Western blotting. Phosphorylation of tyrosine-397, the autophosphorylation site on FAK which also binds to the p85 subunit of PI3-kinase, was increased almost threefold on the FNIII₇₋₁₀ surface compared to the RGD-tethered surface at maximum peptide densities (**Figure 3.7**). Similarly, phosphorylation of tyrosine-576, located in the FAK catalytic loop and responsible for maximal FAK kinase activity, was significantly higher on the FNIII₇₋₁₀-tethered surface compared to the RGD-functionalized support (**Figure 3.7**). Tyrosine-861, a major Src phosphorylation site, was phosphorylated at similar levels among both peptide-tethered surfaces (data not shown). These results demonstrate differential activation of FAK on these engineered interfaces, suggesting that different integrins trigger different signaling pathways on biomimetic surfaces.

Because integrin-mediated activation of FAK has been linked to upregulation of cell proliferation [178,179], we investigated whether adhesion to the different biointerfaces would modulate MC3T3-E1 proliferation. The proliferation rate of cells seeded for 16 h on each ligand-tethered surface was probed by BrdU incorporation.

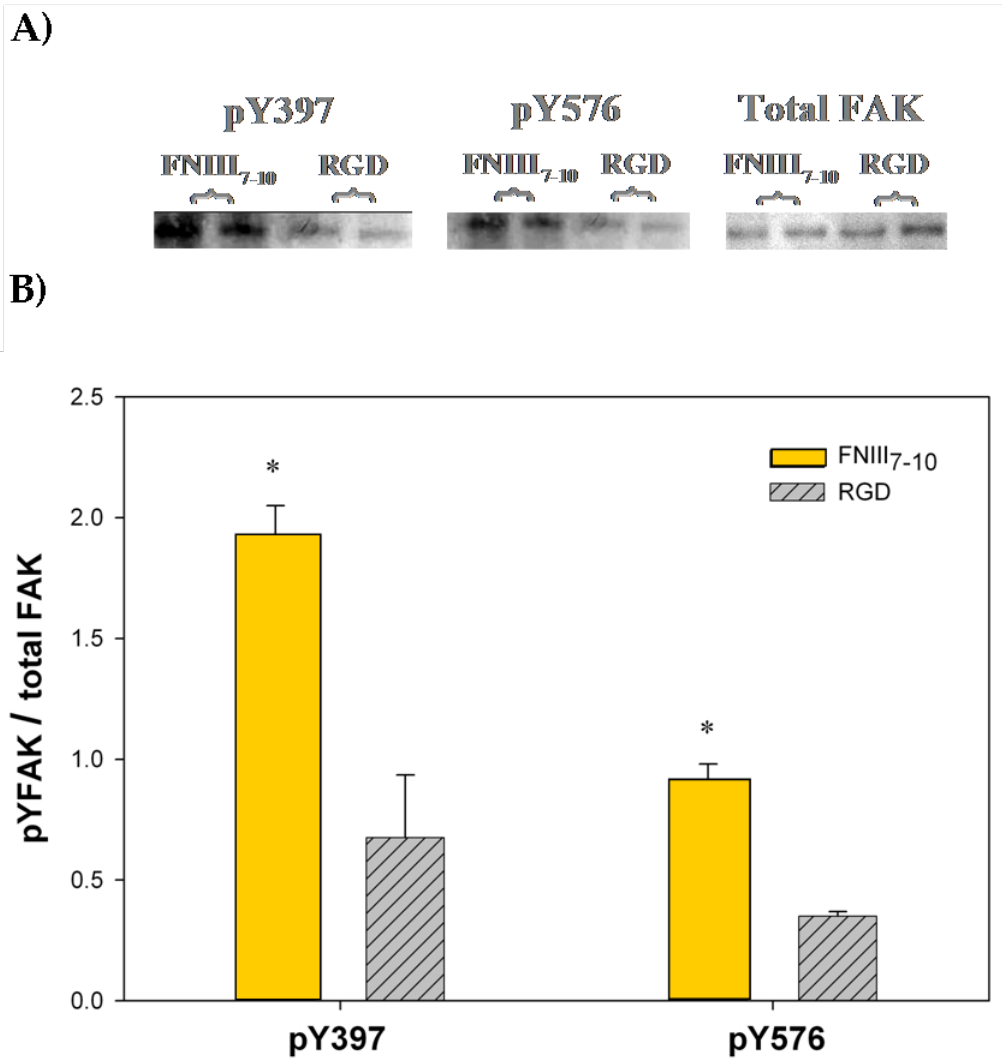


Figure 3.7. Phosphorylation of site-specific tyrosine residues of focal adhesion kinase (FAK) in MC3T3-E1 seeded cells on saturated density RGD and FNIII₇₋₁₀-tethered surfaces (3000 and 150 fmol/cm², respectively). (a) Representative Western blots for phosphorylated Tyr-397 and Tyr-576 residues and total FAK for cells seeded for 1 h on peptide-tethered SAMs. (b) Quantification of Western blot band intensity demonstrating higher phosphorylation of Tyr-397 ($p < 0.006$) and Tyr-576 ($p < 0.001$) on FNIII₇₋₁₀ over RGD-tethered surfaces (Mean \pm standard error, 3 separate experiments in duplicate). Intensities for phosphorylated FAK were normalized to total FAK.

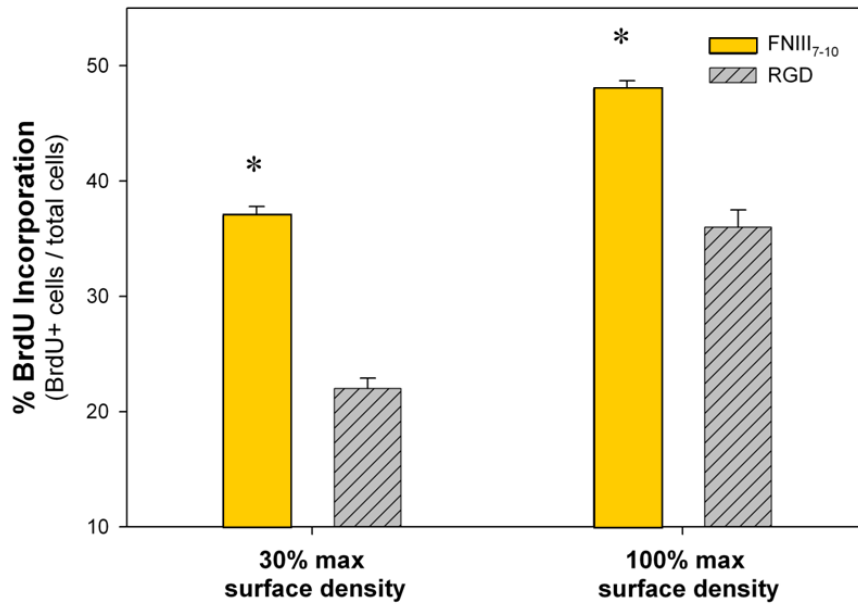


Figure 3.8. Proliferation rate (% BrdU+ cells, mean \pm standard error) for MC3T3-E1 cells cultured for 20 h on RGD and FNIII₇₋₁₀-tethered surfaces for two different peptide densities. BrdU was added at 16 h adhesion for 4 h and percentage of BrdU+ cells was determined via microscopy. FNIII₇₋₁₀-tethered surfaces display higher proliferation rate compared to RGD supports for both saturated (150 and 3000 fmol/cm²; p<0.01) and sub-saturated (45 and 1150 fmol/cm²; p<0.001) surface densities.

Cells seeded on FNIII₇₋₁₀ surfaces displayed a two-fold increase in cell proliferation rate compared to RGD-tethered surfaces at low and high relative peptide surface densities (Figure 3.8).

Discussion

We generated well-defined biointerfaces presenting different adhesive ligands to directly compare their biological activities in terms of cell adhesion strength, integrin binding, and signaling. Mixed SAMs of COOH-EG₆- and EG₃-terminated alkanethiols were optimized to engineer robust supports that present anchoring groups for ligand tethering within a non-fouling, protein adsorption-resistant background. Controlled bioadhesive interfaces were generated by tethering adhesive ligands via standard EDC/NHS chemistry, and the resulting tethered surface density could be easily modulated by altering the ligand concentration in solution during tethering. The ability to precisely control tethered ligand densities is an important design parameter as cell adhesion, focal adhesion assembly, spreading and migration, neurite extension, and cell differentiation exhibit peptide density-dependent effects [73,96,152,179,180-182]. We examined the adhesive activities of three FN-mimetic ligands of increasing complexity: (i) linear RGD peptide presenting the minimal cell adhesive motif of FN; (ii) RGD-PHSRN peptide presenting the RGD and PHSRN motifs joined by a polyglycine sequence designed to mimic the spacing of these domains in FN, and (iii) recombinant FNIII₇₋₁₀ reconstituting the primary and secondary structure of the central cell binding domain of FN. Since we have previously shown that cyclic RGD peptide confers no additional integrin-specific mechanical adhesion strength or integrin specificity for $\alpha_5\beta_1$, linear RGD peptide was used in this study. Furthermore, current biomimetic surfaces mainly focus on linear RGD, making the use of linear RGD in this study more relevant to current strategies. On a molar basis, biointerfaces presenting FNIII₇₋₁₀ exhibited significantly higher adhesion strength, FAK activation, and cell proliferation rate than

supports presenting RGD or RGD-PHSRN. Moreover, FNIII₇₋₁₀-functionalized surfaces displayed specificity for $\alpha_5\beta_1$ integrin, while cell adhesion to SAMs presenting RGD or RGD-PHSRN was primarily mediated by $\alpha_v\beta_3$ integrin. These results are significant to the rational engineering of bioactive materials that promote cell adhesion and function. Importantly, recent evidence indicates that integrin binding specificity, particularly $\alpha_5\beta_1$ vs. $\alpha_v\beta_3$, regulates osteoblast and myoblast differentiation in response to biomaterial surface chemistry [17,18]. Therefore, biomolecular engineering strategies that convey integrin binding specificity to bio-inspired materials may provide a facile route to elicit desired cellular responses. Finally, DNA recombinant technology provides a versatile platform to engineer bioactive ligands mimicking the structure of the native ligand as well as a system to incorporate new functionality. For example, Tirrell and colleagues have synthesized artificial proteins presenting different adhesive sites from FN as a bioartificial matrix [94,117,183]. This technology may provide a time and cost efficient alternative to chemical synthesis methods to engineer complex biologically active peptide ligands.

The improved adhesive activities of FNIII₇₋₁₀-engineered surfaces compared to RGD- and RGD-PHSRN-functionalized supports can be attributed to enhanced binding of integrin $\alpha_5\beta_1$. Simple RGD linear peptides, even those co-presenting the PHSRN motif in the appropriate spacing as in the native FN molecule, cannot support binding of integrin $\alpha_5\beta_1$, but instead promote binding of $\alpha_v\beta_3$. We attribute the integrin specificity for $\alpha_5\beta_1$ of FNIII₇₋₁₀-tethered surfaces to the presentation of PHSRN and RGD in the same structural context as the native FN ligand, while the RGD peptides either lack the PHSRN site (RGD peptide) or present it in a suboptimal orientation (RGD-PHSRN). This result underscores the exquisite sensitivity of the integrin $\alpha_5\beta_1$ -FN interaction on the specific molecular structure of the ligand. Notably, in addition to presenting PHSRN and RGD in a specific structural conformation, FNIII₇₋₁₀ has the RGD motif constrained to a

loop extending from the backbone of the molecule [173]. While this RGD constrained conformation probably improves receptor binding affinity, we cannot attribute the improved specificity of FNIII₇₋₁₀ for $\alpha_5\beta_1$ integrin to the constrained RGD loop. We previously showed using FN mutants that the PHSRN site is absolutely required for $\alpha_5\beta_1$ integrin binding, and this receptor cannot bind the RGD loop by itself [84]. The $\alpha_5\beta_1$ -mediated enhancements in adhesion strength, FAK activation, and cell proliferation rate on FNIII₇₋₁₀-engineered interfaces may reflect increases in the number of integrin-ligand bonds and/or $\alpha_5\beta_1$ -specific activities.

Surfaces presenting RGD-PHSRN exhibited identical adhesive activities as RGD-functionalized supports, suggesting that the PHSRN motif in this peptide provides no additional effects. This result contrasts a previous study from Anseth et al. reporting enhanced activities of RGD-PHSRN compared to RGD when presented within a hydrogel [122], although no antibody blocking experiments were performed. Possible explanations for this discrepancy include differences in peptide presentation/accessibility and cell type-specific activities. Furthermore, previous analyses with simple RGD and PHSRN peptide mixtures also documented increases in cell adhesion compared to pure RGD [117,120,167]. It is important to point out that two of these studies employed peptide-amphiphile supports which exhibit significant peptide mobility. Reconfiguration of the interface may allow for rearrangement of ligands to approximate the structural context in FN and “fit” the integrin. Moreover, these studies used extremely high surface densities of peptides (compared to physiological densities of FN) that could give rise to non-physiological effects. Comprehensive analyses, including antibody blocking, varying peptide surface densities, and signaling evaluations, are necessary to fully establish the adhesive activities of these engineered surfaces.

This study provides an experimental platform to engineer integrin-specific biointerfaces to manipulate cell and host responses to biotechnological/biomedical supports and implanted devices. We hypothesize that integrin binding specificity

($\alpha_5\beta_1$ vs. $\alpha_v\beta_3$) will regulate cellular activities, including cell cycle progression and expression of differentiated phenotypes, as well as tissue healing responses. This approach of conveying integrin binding specificity may provide a robust biomolecular strategy to elicit directed biological responses. In addition, integrin-specific biomimetic surfaces utilizing recombinant peptides of matrix molecules, such as FNIII₇₋₁₀, often exhibit lower immunogenicity and higher stability than the whole proteins, as well as lack binding sites for other ligands which may impede in a more directed cellular response. In particular, this surface strategy may present a clinically relevant approach to improving bone formation and integration in biomedical devices and tissue-engineered scaffolds.

Summary

Using a model system to present controlled ligand densities within a non-fouling background, we demonstrate that biointerfaces functionalized with the FNIII₇₋₁₀ recombinant fragment presenting the RGD and PHSRN motifs in the correct structural context exhibited significantly higher adhesion strength, FAK activation, and cell proliferation rate than supports presenting RGD or RGD-PHSRN oligopeptides. Moreover, FNIII₇₋₁₀-functionalized surfaces displayed specificity for $\alpha_5\beta_1$ integrin, while cell adhesion to SAMs presenting RGD or RGD-PHSRN was primarily mediated by $\alpha_v\beta_3$ integrin. These results are significant to the rational engineering of bioactive materials that promote cell adhesion and function.

CHAPTER 4

THE EFFECT OF INTEGRIN-SPECIFIC BIOACTIVE COATINGS ON TISSUE HEALING AND IMPLANT OSSEOINTEGRATION

Introduction

Over 713,000 joint arthroplasties, mostly hip and knee procedures in arthritic patients, at a cost of \$15 billion were performed in the U.S. in 2000 [1]. Even though artificial joint replacements can function properly for a decade, the long-term success of arthroplasties is limited by implant loosening and wear, often resulting in patient discomfort and pain and requiring revision surgery [184]. More importantly, the lifetime of these implants must increase as the number of younger patients needing joint replacements continues to steadily increase [2]. Considerable efforts have focused on implant surface technologies, particularly macro- and micro-porous coatings for bone ingrowth and bone-bonding ceramic coatings, to promote early integration into the surrounding bone [3]. However, inadequate cell-material interactions leading to slow rates of osseointegration and poor mechanical properties currently restrict these approaches [4].

Cell-biomaterial interactions govern host responses to implanted devices, integration of biomedical prostheses and tissue-engineered constructs, and the

*Modified from

T.A. Petrie, J. Raynor, K.L. Burns, D.M. Collard, A.J. García, *Integrin-Specific Bioactive Coatings Enhance Tissue Healing and Implant Osseointegration*. *Biomaterials* 2008; 29:2849-57.

performance of biotechnological supports [31,32,185]. In most instances, cells recognize and adhere via integrin receptors to biomacromolecules that adsorb non-specifically onto synthetic surfaces [186]. Integrins are a widely expressed family of heterodimeric ($\alpha\beta$) transmembrane receptors that provide anchorage forces and trigger signals regulating cell survival, proliferation, and differentiation, often overlapping with other receptor pathways [16]. For example, α_v -containing integrins are essential for steroid hormone and growth factor induction of osteoblast differentiation [80,187]. Because of the central roles of integrin-mediated adhesion in tissue formation, maintenance, and repair, recent bio-inspired biomaterial strategies have focused on presenting integrin ligands such as extracellular matrix proteins and short bioadhesive motifs derived from these components on implant surfaces [81]. The most common approach relies on the presentation of the arginine-glycine-aspartic acid (RGD) adhesive sequence derived from FN. While synthetic and natural materials functionalized with RGD oligopeptides support integrin-mediated adhesion, proliferation, and differentiation *in vitro*, mounting evidence indicates that this biomaterial surface engineering strategy does not enhance biomedical implant integration or function in rigorous animal models [12,104,105]. Based on previous *in vitro* work demonstrating that integrin binding specificity ($\alpha_5\beta_1$ vs. $\alpha_v\beta_3$) regulates osteoblastic differentiation [17], we hypothesized that the marginal healing responses to RGD-functionalized implants arise from the lack of selectivity of this ligand for specific integrins. In the present study, we used a novel polymer brush system to analyze mechanistically the effect on *in vitro* osteogenic stromal cell differentiation and bone tissue healing for clinical-grade titanium functionalized with ligands with varying specificity for target integrin receptors. We demonstrate that biomaterial coatings specific

for integrin adhesion receptors regulate osteoblastic differentiation of marrow-derived progenitor cells and enhance bone tissue healing and the functional integration of clinically-relevant biomedical implants.

Materials and Methods

Poly(OEGMA) Polymer Brush Preparation and Peptide Tethering on Titanium

Polymeric brushes, which are arrays of polymer chains attached at one end to a surface, on titanium substrates were synthesized by surface-initiated atom-transfer radical polymerization of poly(oligo(ethylene glycol) methacrylate) (poly(OEGMA)) [128]. Titanium-coated glass slides or custom-made commercially pure titanium implants were incubated in a 1:1 solution of chlorodimethyl(11-(2-bromo-2-methylpropionyloxy)undecyl)silane and dodecyldimethylchlorosilane in anhydrous hexane. Poly(OEGMA) brushes were polymerized by immersion into a solution of OEGMA (28.3 mmol), CuBr (1.6 mmol), 2,2'-dipyridyl (2.8 mmol) in a 1:4 mixture of MeOH and H₂O for 4 h. The resulting polymer brushes were 135 Å as determined by ellipsometry. For ligand tethering, brushes were first incubated in 4-nitrophenyl chloroformate (1.4 mmol in THF), which “activates” the brushes for subsequent ligand tethering by replacing a portion of the hydroxyl groups situated at the end of the polymer brushes with nitrophenyl chloroformate (NPC). The “activated” NPC-terminated brushes are then susceptible to attack and replacement by primary amine groups on bioadhesive peptides or proteins. Likewise, the activated brushes are then incubated in FNIII₇₋₁₀ or RGD in PBS for 30 min to allow ligand tethering, and residual activated NPC sites were quenched in 20 mM glycine in PBS. FNIII₇₋₁₀ was expressed in *E. coli* and purified [108],

and the linear RGD oligopeptide (GRGDSPC) was purchased from BACHEM. Brush synthesis and functionalization reactions were verified by XPS (X-ray spectroscopy) and FTIR (Fourier Transform infrared spectroscopy). Ligand surface density measurements were obtained via surface plasmon resonance using a Biacore X instrument.. Antibody-based bioactivity assay was performed by ELISA using HFN7.1 antibody.

Cell Adhesion and Integrin Binding Assays

Rat bone marrow stromal cells were isolated from male Sprague-Dawley rats and cultured under IACUC-approved procedures [49]. Cell adhesion to engineered surfaces under serum-free conditions was measured at 1 h at 37 °C using a centrifugation assay [133]. For integrin blocking, cells (passage 3 or less) were incubated in blocking antibodies (anti-rat CD49e [HM α 5-1] or anti-rat CD51, BD Biosciences) for 20 min prior to cell seeding. Integrin binding was quantified using a crosslinking/extraction/reversal procedure using DTSSP crosslinker [172]. For FAK activation assays, cells were plated in the presence or absence of integrin-blocking antibodies on engineered substrates for 2 h at 37 °C under serum-free conditions. Cells were lysed in RIPA buffer (1% Triton X-100, 1% sodium deoxycholate, 0.1% SDS, 150 mM NaCl, 150 mM Tris-HCl (pH 7.2), 350 μ g/mL PMSF, 10 μ g/mL leupeptin, and 10 μ g/mL aprotinin), equal amounts of total protein loaded on 8% SDS-PAGE gels, separated by SDS-PAGE, and transferred to nitrocellulose membranes. FAK activation was assessed by subsequent western blotting using antibodies specific for FAK phosphotyrosines and normalized to total FAK.

Osteogenic Differentiation Assays

Rat bone marrow stromal cells at low passage (3 or less) were seeded on appropriate surfaces at 100 cells/mm² in growth medium. After 24 h, cultures were maintained in osteogenic medium consisting of growth medium supplemented with 50 µg/mL L-ascorbic acid and 3 mM sodium β-glycerophosphate. Total RNA was isolated at 7 days after initial cell seeding, and gene expression was analyzed by RT-PCR using osteoblast-specific primers and normalized to a standard curve [49]. Alkaline phosphatase activity was quantified at 7 days after cell seeding using a fluorescence-based enzymatic assay [49]. Calcium content was determined using a commercial arsenazo III-containing Calcium Reagent kit (Diagnostic Services Ltd).

Implantation Procedure and Analysis

Implantations into the tibiae of mature Sprague-Dawley male rats were conducted in accordance with an IACUC-approved protocol as described previously [49]. Animals were euthanized after 4 weeks, and proximal tibiae were fixed in neutral buffered formalin for histology or recovered without fixation and maintained in PBS-moistened gauze for immediate mechanical testing. For histology, fixed tibiae were embedded in poly(methyl methacrylate), ground (50-80 µm), and stained with Sanderson's Rapid Bone Stain™ and a van Gieson counter stain. This stained mineralized bone (yellow-orange) and soft tissue and osteoid (blue-green). Bone implant contact was measured as the percentage of implant's circumference that was in direct contact with bone tissue. Implant mechanical fixation to the bone was measured with a pull-out force test using an EnduraTEC Bose ELF 3200 biomechanical testing apparatus [49]. Tests were performed

at a constant force rate of 0.2 N/sec parallel to the long axis of the implant. The pull-out force was the maximum load achieved before failure.

Statistics

Data are reported as mean \pm standard error. Results were analyzed by one-way ANOVA using SYSTAT 8.0 (SPSS). If treatment level differences were determined to be significant, pair-wise comparisons were performed using a Tukey post-hoc test. A 95% confidence level was considered significant.

Results

Bio-Functionalized Implant Coatings to Convey Integrin Binding Specificity

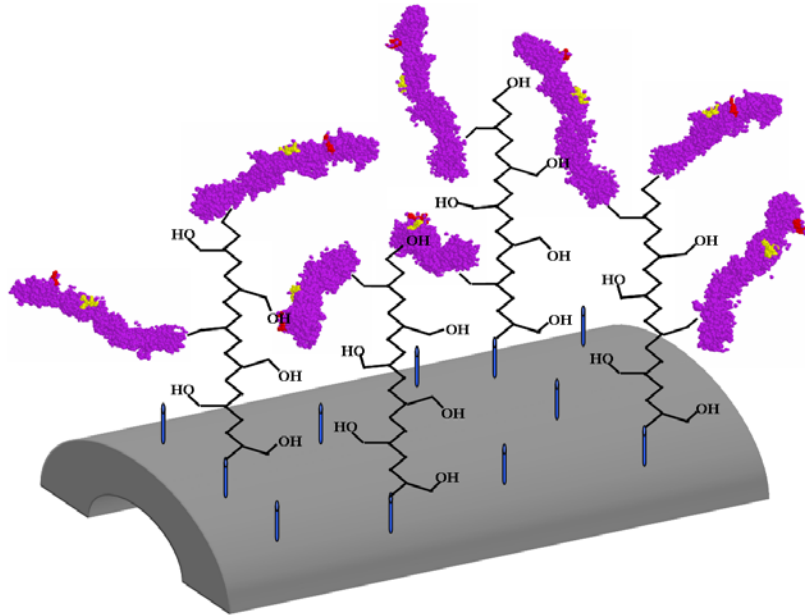
In order to develop a robust coating for tunable presentation of bioactive factors on a clinically-relevant material, we designed and synthesized a polymer brush system incorporating a physiologically stable, non-fouling (resists protein adsorption) oligo(ethylene glycol)-substituted polymer brushes on clinical-grade titanium supports and functionalized the polymer coating with controlled densities of bioadhesive ligands.

We employed a “grafting from” approach based on surface-initiated atom-transfer radical polymerization (SI-ATRP) of poly(OEGMA) brushes on titanium [128] (**Figure 4.1 A**). Briefly, a 1:1 mixed self-assembled monolayer (SAM) of bromine-terminated initiator and unreactive, methyl-terminated co-adsorbate was formed on a clean titanium surface. The terminal bromine served as the radical initiator for the subsequent SI-ATRP of oligo(ethylene glycol) monomer to form thick, dense poly(OEGMA) brushes (**Figure 4.1 B-1,2**). The hydroxyl groups at the termini of the oligo(ethylene glycol) side chains were converted to 4-nitrophenyl carbonate by treatment with 4-nitrophenyl chloroformate

(NPC) and functionalized with bioadhesive ligands via a urethane linkage (**Figure 4.1 B-3,4**). The progress of the synthesis and ligand tethering was validated by spectra from X-ray photoelectron spectroscopy (XPS) and glancing angle Fourier transform infrared (FTIR) spectroscopy [18]. Brush thickness was easily modulated by polymerization time as previously shown [18]. All poly(OEGMA) brushes used in this study were grown to a thickness of 135 Å.

Two bioadhesive ligands with different integrin specificities were examined: (i) the recombinant fragment FNIII₇₋₁₀, which presents the RGD motif in the 10th type III repeat and the PHSRN synergy sequence in the 9th type III repeat of FN in the correct structural context and exhibits high selectivity for integrin $\alpha_5\beta_1$ [19]; and (ii) a linear RGD oligopeptide (GRGDSPC) that primarily supports $\alpha_v\beta_3$ -mediated adhesion and is considered the “gold” standard in the field [108]. Controlled surface densities of tethered ligands were obtained by treating the NPC-modified polymer brushes with varying concentrations of peptide (**Figure 4.2 A**). The differences in tethering efficiency between FNIII₇₋₁₀ and RGD can be attributed to significant differences in ligand size. Importantly, ligand densities adsorbed on control surfaces presenting unmodified poly(OEGMA) brushes were <5% of the density immobilized on the functionalized surfaces, demonstrating the non-fouling nature of the unmodified poly(OEGMA) brush.

A)



B)

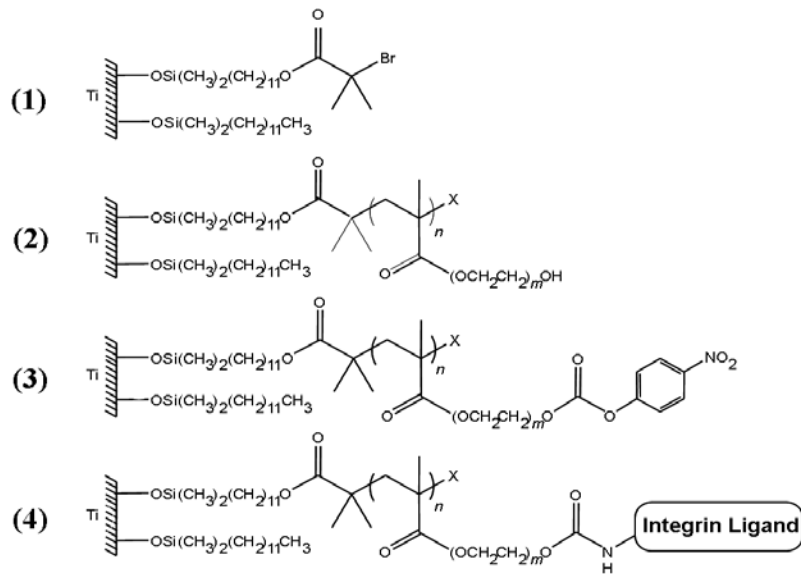


Figure 4.1. Poly(OEGMA) brushes with ligand tethered on titanium. (A) Schematic of FNIII₇₋₁₀-tethered poly(OEGMA) brush system on titanium. Both linear RGD peptide and a fibronectin fragment FNIII₇₋₁₀ (purple) containing both the RGD (red) and PHSRN (yellow) sequence in the native ECM structural conformation were tethered to poly(OEGMA) brushes via NPC chemistry. Unactivated hydroxyl groups provided the non-fouling nature of the brushes. (B)

Tethering scheme of integrin ligands to “activated” poly(OEGMA) brushes on titanium.

We next assessed the *in vitro* bioresistance and adhesive capacity of unmodified poly(OEGMA) brushes and brushes with peptide tethered on titanium. Surfaces were incubated in serum-containing media for various times and subsequently challenged with osteoblastic cells for 1 h. In contrast to control unmodified titanium which supported high levels of cell adhesion and spreading, unmodified poly(OEGMA) brushes resisted cell adhesion for over 56 days (Fig. 2B). The unfunctionalized poly(OEGMA) brushes exhibited excellent bioresistance compared to commonly-used model self-assembled monolayers of tri(ethylene glycol)-functionalized alkanethiols on gold, which displayed loss of bioresistance by the 10-day time point in serum-containing media. Moreover, poly(OEGMA) brushes presenting either FNIII₇₋₁₀ or RGD supported levels of cell adhesion comparable to the unmodified titanium (**Figure 4.2 B**), demonstrating that the tethered ligand is in a bioactive form that supports adhesive activities. Furthermore, NPC-activated brushes which were quenched with glycine, and to which no ligand was added, supported minimal cell adhesion, verifying that surface activation does not affect the brush non-fouling nature (**Figure 4.2 B**). In addition, this data indicates that, after glycine quenching, effectively no NPC groups are available for tethering of serum proteins, which could have potentially reduced the specificity of the surface. Finally, we demonstrated surface density-dependent increases in available FNIII₇₋₁₀ ligand using a receptor-mimetic antibody-based assay (**Figure 4.2 C**). Taken together, these results demonstrate a robust approach to coat clinical-grade titanium with non-fouling/bioresistant oligo(ethylene glycol)-substituted polymer brushes which can be functionalized with controlled densities of bioadhesive ligands.

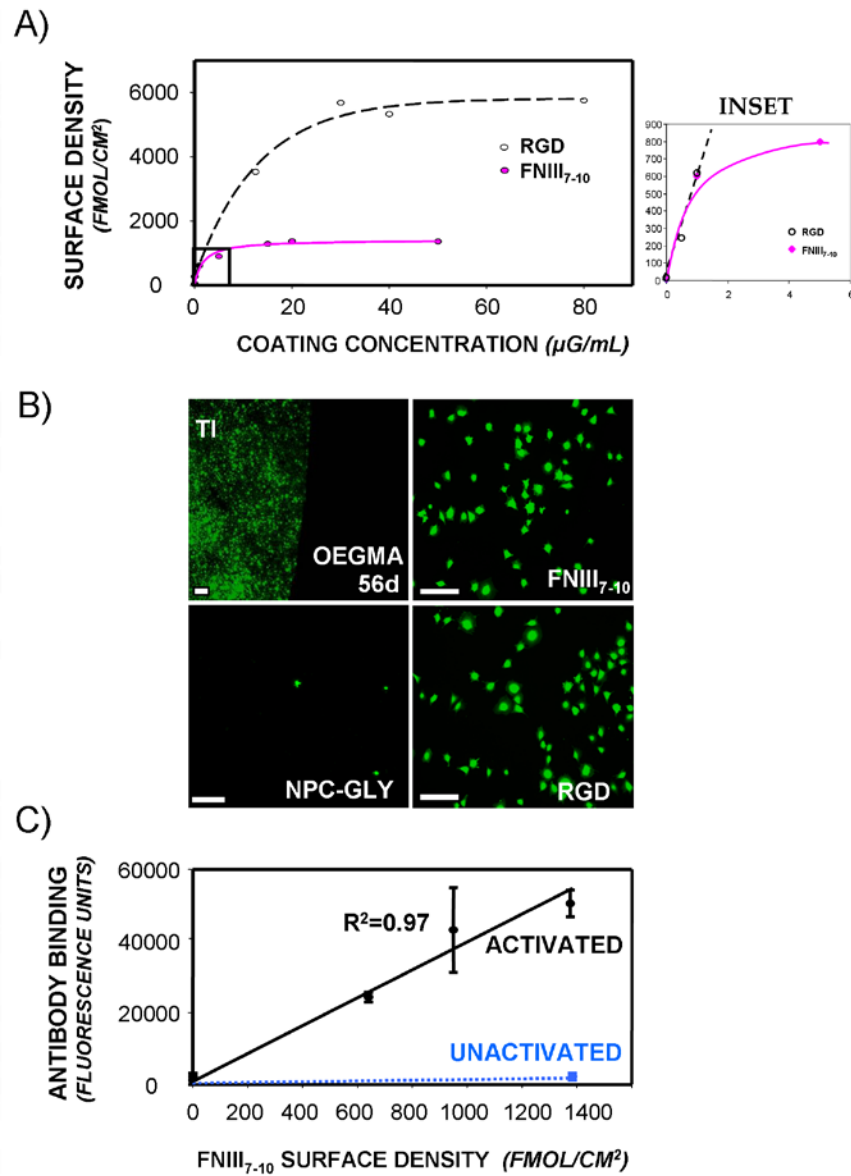


Figure 4.2. Bioresistance and ligand tethering on poly(OEGMA) brushes on titanium (Ti). (A) Tethered densities of RGD and FNIII₇₋₁₀ on poly(OEGMA) brushes on Ti (hyperbolic curve fit, $R^2=0.95$). (B) *In vitro* bioresistance of poly(OEGMA) brushes on Ti to cell adhesion in serum-containing media. Cells were stained with green-colored calcein-AM (scale bar 100 μm). EG₃ SAMs were cell-resistant until day 10, while poly(OEGMA) brushes remained cell adhesion-resistant for at least 56 days. Cells adhered (1 h) and spread in serum-free conditions on FNIII₇₋₁₀- and RGD-tethered brushes (0.9 pmol/cm²) to the same extent as on serum-treated unmodified Ti. Cells did not adhere or spread in serum on NPC-activated brush surfaces quenched with glycine to which no bioadhesive ligand was added. (C) Bioactivity and accessibility of FNIII₇₋₁₀

tethered to poly(OEGMA) brushes as determined by a receptor-mimetic antibody assay. FNIII₇₋₁₀ activity was detected on the NPC-modified poly(OEGMA) brushes (but not the unmodified brushes).

In vitro evaluation of these engineered titanium surfaces was performed using primary rat bone marrow stromal cells since this heterogeneous population contains osteoprogenitors, and human bone marrow stromal cells are currently used in clinical applications. Cell adhesion was examined using a centrifugation assay that applies a controlled detachment force. To allow direct comparisons between ligand-tethered surfaces, an equimolar ligand density of 0.9 pmol/cm² was used; this value represents the highest ligand density that could be ascribed for both surfaces to be equimolar. Upon exposure to serum, high levels of cell adhesion were observed for polymer brushes modified with either FNIII₇₋₁₀ or RGD brushes, as well as unmodified titanium (which adsorbs RGD-containing adhesive proteins from serum) (**Figure 4.3 A**). Unmodified poly(OEGMA) brushes displayed background levels of adhesion, further illustrating the bioresistance of this system. Importantly, a blocking anti- α_5 antibody completely eliminated cell adhesion to FNIII₇₋₁₀-tethered surfaces ($p < 0.005$), whereas an anti- α_v antibody had no effect, verifying the specificity of this surface for $\alpha_5\beta_1$ integrin. Conversely, a function-perturbing anti- α_v antibody eliminated adhesion to both RGD-tethered surfaces and serum-exposed unmodified titanium ($p < 0.01$; **Figure 4.3 A**), indicating that adhesion to these surfaces is primarily mediated by the $\alpha_v\beta_3$ integrin. As a complementary test of integrin specificity, we quantified integrin binding using a biochemical cross-linking/extraction/reversal technique [172]. Consistent with the antibody blocking experiments, FNIII₇₋₁₀-tethered brushes supported significantly higher levels of bound $\alpha_5\beta_1$ integrin compared to RGD-tethered brushes and serum-exposed titanium ($p < 0.01$; **Figure 4.3 B**). On the other hand, the RGD-tethered brushes and

serum-exposed titanium supported higher levels of bound $\alpha_v\beta_3$ than the FNIII₇₋₁₀ support ($p < 0.006$). We note that the crosslinking/extraction technique has been validated for integrin binding to extracellular matrix proteins and relies on crosslinking free amines on both the receptor and ligand. Because the tethered RGD has no free amine, we attribute the $\alpha_v\beta_3$ signal on the RGD surfaces to crosslinking of clustered integrin-RGD bonds that were not completely extracted. This observation is consistent with previous results for cells adhering to RGD-presenting self-assembled monolayers [108]. The possibility that RGD tethering altered the non-fouling character of the brushes to result in non-specific protein adsorption from serum is highly unlikely as SPR measurements demonstrated background protein adsorption to RGD-functionalized supports. Furthermore, minimal cell adhesion under serum conditions to NPC-activated, glycine-quenched brush surfaces verified that brushes presenting a non-adhesive amino acid residue retain their non-fouling nature (**Figure 4.2 B**). More importantly, the integrin-specific character of each specific surface treatment was demonstrated by the integrin-blocking adhesion results. Collectively, these data demonstrate that FNIII₇₋₁₀-functionalized titanium selectively supports $\alpha_5\beta_1$ -mediated cell adhesion, whereas the RGD-tethered surface primarily binds $\alpha_v\beta_3$ integrin.

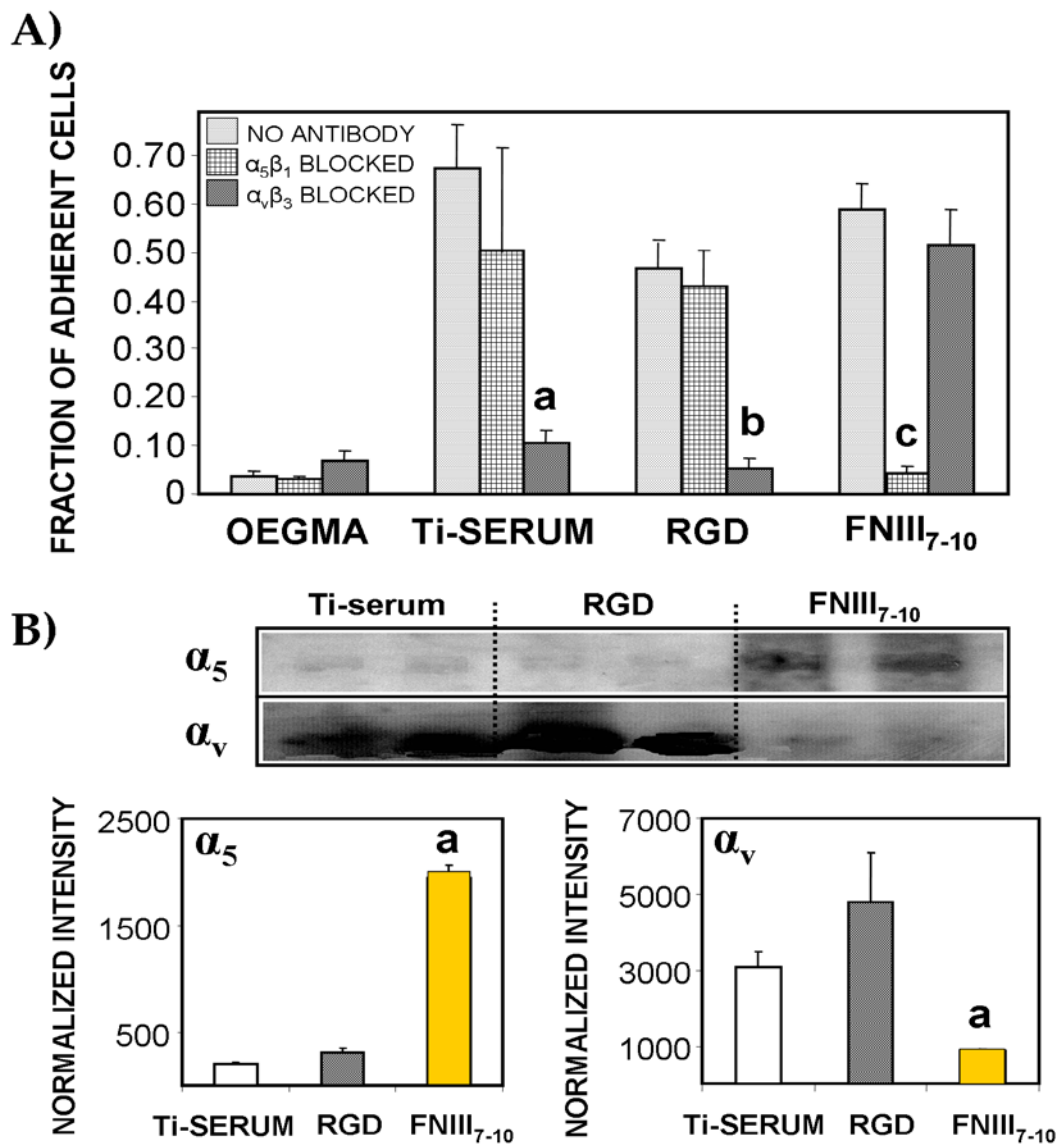


Figure 4.3. Poly(OEGMA) brushes on Ti functionalized with integrin ligands display integrin specificity. (A) Bone marrow stromal cell adhesion to engineered surfaces is mediated by different integrin receptors as demonstrated by blocking antibodies. Ti-serum: a vs. no antibody control ($p < 0.01$); RGD: b vs. no antibody control ($p < 0.01$); FNIII₇₋₁₀: c vs. no antibody control ($p < 0.005$). (B) Integrin binding analysis using a crosslinking/extraction/reversal procedure for stromal cells plated on ligand-tethered brush surfaces of equimolar density. α_5 : a vs. RGD, Ti-serum ($p < 0.01$); α_V : a vs. Ti-serum ($p < 0.006$).

As a final demonstration of the integrin-specific nature of these engineered supports, we assessed FAK phosphorylation in the presence of integrin blocking antibodies. FAK is an intracellular signaling molecule involved in integrin-mediated signal transduction and the osteogenic differentiation pathway [175,188]. We used phosphotyrosine-specific antibodies to examine the activation state of three important tyrosines in FAK: Y397 (autophosphorylation site), Y576 (essential for maximal kinase activity), and Y861 (major Src phosphorylation site) (**Figure 4.4**). FAK Y397 and Y576 exhibited higher phosphorylation levels on FNIII₇₋₁₀-engineered surfaces compared to RGD-functionalized brushes and serum-exposed titanium ($p < 0.01$), whereas Y861 phosphorylation was elevated for the RGD-functionalized and serum-exposed titanium relative to the FNIII₇₋₁₀-tethered surface ($p < 0.03$). Moreover, blocking antibodies against α_5 , but not β_3 , reduced the levels of phospho-Y397 and Y576 on the FNIII₇₋₁₀-presenting titanium ($p < 0.04$). For the RGD-functionalized poly(OEGMA) brushes, only the anti- β_3 antibody reduced FAK phosphorylation ($p < 0.05$). We postulate that these differences in integrin binding specificity and FAK activation modulate cell signaling pathways and higher order cellular activities.

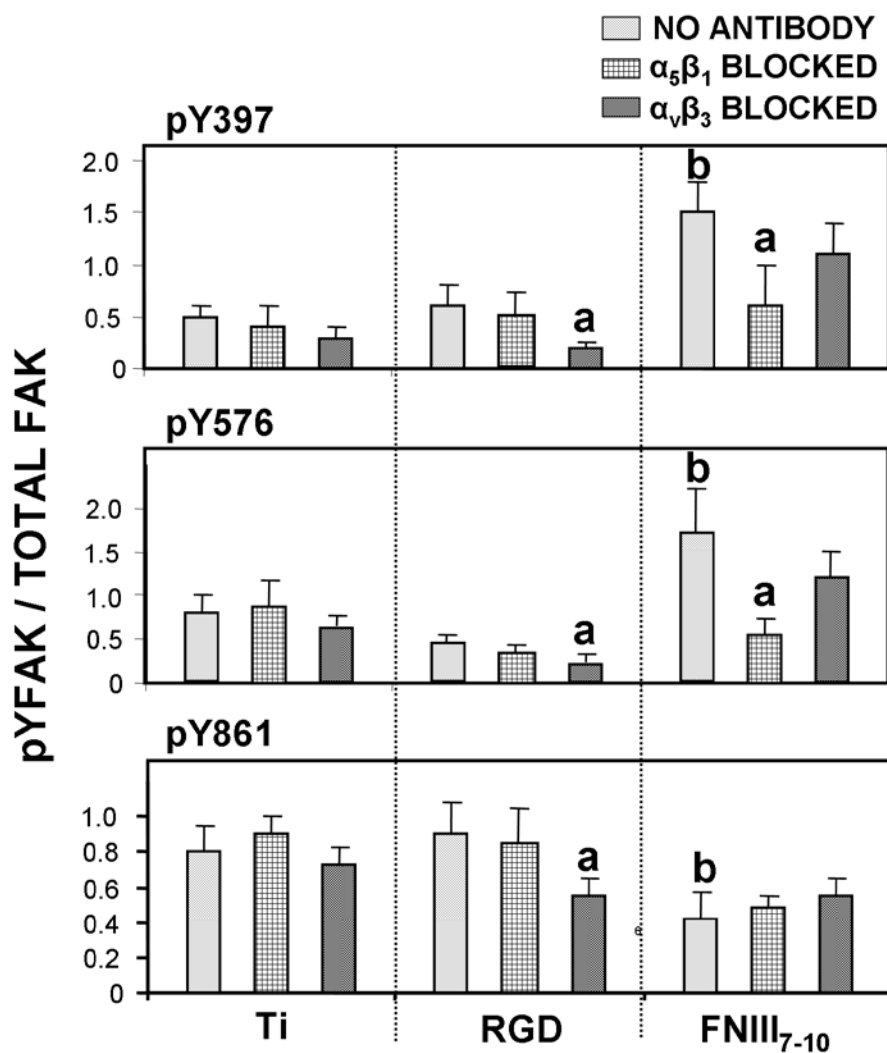


Figure 4.4. FAK activation on equimolar ligand-tethered brush surfaces and serum-treated titanium is integrin-dependent. Relative levels of phospho-Y in FAK in the presence or absence of integrin blocking antibodies. Activation levels for Y397 and Y576 were higher on FNIII₇₋₁₀-tethered brushes than RGD-functionalized and Ti-serum supports (b; $p < 0.01$). Y861 phosphorylation levels were reduced in FNIII₇₋₁₀-functionalized titanium relative to the other surfaces (b; $p < 0.03$). Integrin blocking antibodies selectively reduced FAK phosphorylation. Y397: a vs. no antibody control ($p < 0.04$); Y576: a vs. no ab control ($p < 0.05$); Y861: a vs. no ab control ($p < 0.05$).

Effects of Integrin-Specific Implant Surfaces in Modulating Osteoblastic Differentiation and Mineralization

We used quantitative RT-PCR to probe osteoblastic gene expression in 7-day cultures of bone marrow stromal cells cultured in osteogenic media to investigate effects of integrin binding specificity on osteoblastic differentiation. Expression levels of Runx2/Cbfa1, a transcription factor essential for osteoblastic differentiation and bone formation [163], were elevated on the FNIII₇₋₁₀-functionalized surface compared to brushes functionalized with equimolar densities of RGD ($p < 0.03$; **Figure 4.5 A**). The late osteoblastic markers osteocalcin (OCN) and bone sialoprotein (BSP) also exhibited increased transcript levels on FNIII₇₋₁₀-tethered brushes relative to RGD-functionalized supports ($p < 0.003$). Consistent with the gene expression results, FNIII₇₋₁₀-tethered surfaces displayed higher alkaline phosphatase activity than RGD-functionalized surfaces ($p < 0.03$; **Figure 4.5 B**). Finally, matrix mineralization, as determined by calcium incorporation, was used as an end-point functional marker. FNIII₇₋₁₀-engineered titanium displayed a 2-fold enhancement in mineralization relative to the RGD-tethered supports ($p < 0.01$; **Figure 4.5 C**). No differences were observed between RGD-functionalized brushes and serum-exposed unmodified titanium for any differentiation marker. Collectively, these results demonstrate that non-fouling brush surfaces presenting FNIII₇₋₁₀ to target $\alpha_5\beta_1$ integrin trigger enhance osteoblastic differentiation and mineralization in primary bone marrow stromal cells compared to RGD-tethered brushes and serum-treated titanium surfaces that support $\alpha_v\beta_3$ binding.

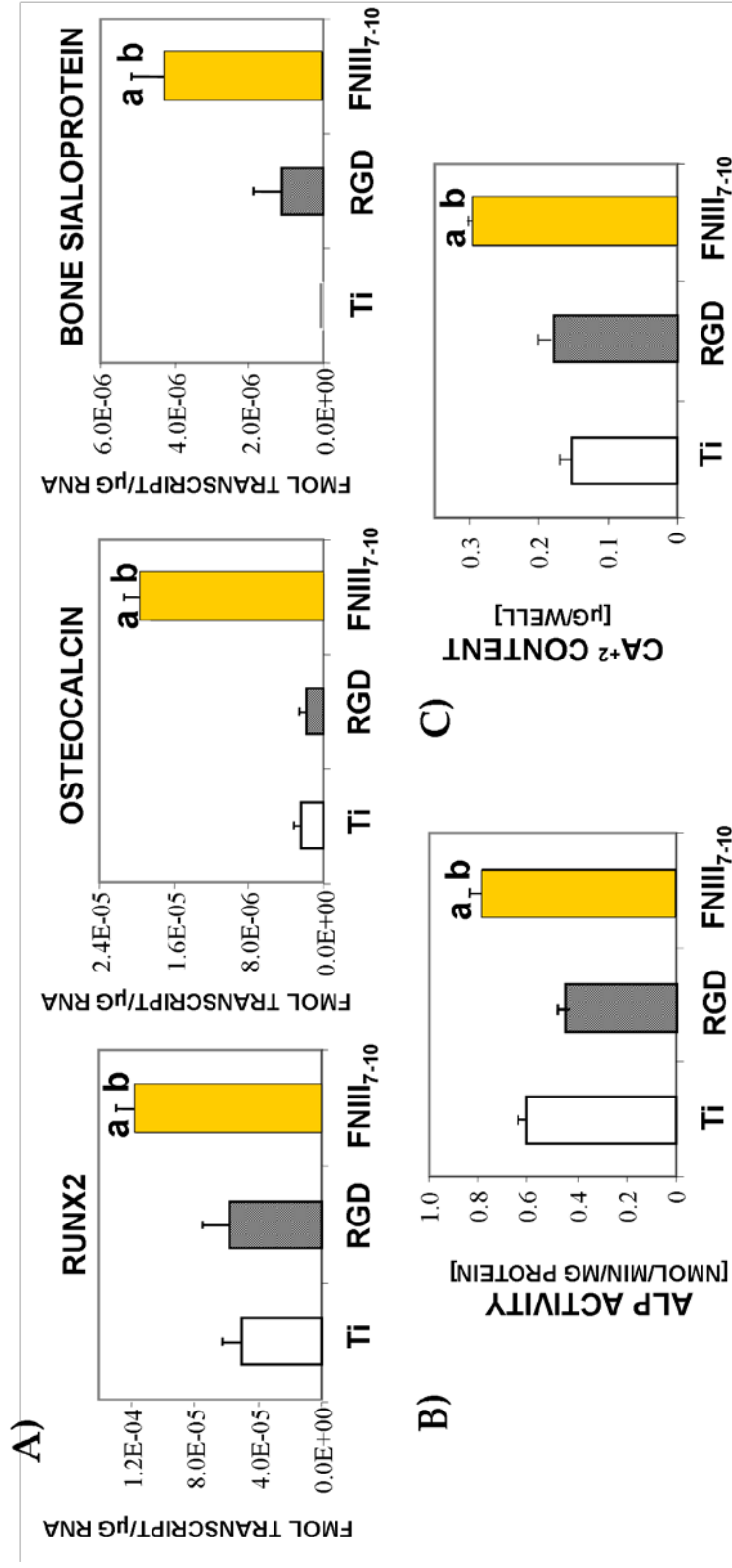


Figure 4.5. FNIII₇₋₁₀-functionalized surfaces enhance osteoblastic differentiation and mineralization in bone marrow stromal cultures at 7 days. (A) Gene expression levels for Runx2 transcription factor, osteocalcin, and bone sialoprotein. a vs. RGD ($p < 0.02$); b vs. Ti-serum ($p < 0.02$). (B) Alkaline phosphatase activity. a vs. RGD ($p < 0.01$); b vs. Ti-serum ($p < 0.03$). (C) Calcium content. a vs. RGD ($p < 0.01$); b vs. Ti-serum ($p < 0.008$).

Integrin Specificity Modulates Functional Implant Osseointegration In Vivo

We quantified osseointegration of implants in a rat tibia cortical bone model [49] to evaluate the *in vivo* performance of the engineered titanium surfaces in bone healing. Importantly, this *in vivo* model provides a rigorous platform to evaluate implant coating function in a relevant orthopedic setting. Two 2.0-mm diameter defects were drilled into the medial aspect of the proximal tibial metaphysis using a saline cooled drill. Tapered cylindrical implants (**Figure 4.6 A**) of clinical-grade titanium were press-fit into the cortical defects (**Figure 4.6 B**). Implants were machined with a tapered stop collar to ensure equivalent initial bone contact across all samples, and each implant had a small channel spanning the head to permit subsequent pull-out testing following explantation. Biomaterial surface treatments evaluated were (i) unmodified poly(OEGMA) brushes, (ii) unmodified titanium (as a reference to the current clinical treatment), and brushes modified with either (iii) FNIII₇₋₁₀ or (iv) RGD at equimolar ligand densities (0.9 pmol/cm²). In addition, a small number of implants with varying densities of FNIII₇₋₁₀ were analyzed. All implants were well-tolerated, and no complications were encountered during the course of the study. Following four weeks of implantation, the rat tibiae were harvested and analyzed for bone-implant contact by histomorphometry and implant mechanical fixation by pull-out testing.

Histological sections revealed extensive and contiguous bone matrix around FNIII₇₋₁₀-functionalized titanium implants (**Figure 4.6 C**). Less bone tissue was observed around the unmodified poly(OEGMA) brushes, poly(OEGMA) brushes with RGD tethered, and reference unmodified titanium implants, and the tissue present displayed a more porous morphology (**Figure 4.6 C**). Histomorphometric analysis of

histological sections demonstrated a 70% enhancement in bone-implant contact area for FNIII₇₋₁₀-functionalized implants compared to the RGD-tethered or unfunctionalized poly(OEGMA) brushes ($p < 0.02$; **Figure 4.6 D**). Notably, the bone-implant contact area for the FNIII₇₋₁₀ group was significantly higher than that for the unmodified clinical-grade titanium implant ($p < 0.02$). No evidence of multi-nucleated cells, foreign body giant cells, or fibrous capsule was observed in any of the sections. These findings demonstrate that controlled presentation of the integrin-specific ligand FNIII₇₋₁₀ using our polymer brush strategy significantly enhances implant integration into the host bone compared to implants presenting RGD-functionalized poly(OEGMA) brushes and the current clinical standard (unmodified titanium).

Mechanical fixation was used as an outcome measure of functional osseointegration. Pull-out mechanical testing revealed significantly higher mechanical fixation of the FNIII₇₋₁₀-functionalized implants over all other groups ($p < 0.03$; **Figure 4.6 E**). Implants coated with unmodified poly(OEGMA) brushes generated the lowest amount of bone apposition and mechanical fixation, suggesting that the polymer brushes retain their non-fouling/bioresistant character *in vivo*. FNIII₇₋₁₀-functionalized implants exhibited a 3.0-fold enhancement in fixation over RGD-tethered implants ($p < 0.009$) and approximately a 4-fold improvement compared to the unmodified poly(OEGMA) brush coating ($p < 0.001$). Notably, there were no differences in bone apposition or mechanical fixation between RGD-functionalized and unmodified poly(OEGMA) implants, demonstrating that presentation of the linear RGD sequence has no effects on implant osseointegration. Unmodified titanium displayed higher fixation than the unfunctionalized poly(OEGMA) brush ($p < 0.01$), but the pull-out force was not

statistically different from the RGD-tethered surface. Remarkably, FNIII₇₋₁₀-functionalized titanium exhibited higher mechanical fixation than the unmodified titanium ($p < 0.05$), indicating that this biomolecular engineering strategy outperforms the current clinical standard.

A major advantage of the poly(OEGMA) brush system described in this work is the ability to precisely control the presentation of tethered ligands. Increases in the density of tethered FNIII₇₋₁₀ yielded linearly proportional increases in available bioactive ligand *in vitro* (**Figure 4.2 D**). We examined whether the density of tethered bioadhesive ligand modulated *in vivo* bone healing by implanting samples with varying tethered densities of FNIII₇₋₁₀. Mechanical fixation increased with FNIII₇₋₁₀ surface density, displaying linear increases at low surface densities and reaching a saturation limit at high densities (Fig. 5F). These results are accurately described by a simple hyperbolic relationship ($R^2 = 0.87$). This functional dependence is consistent with *in vitro* results for simple receptor-mediated phenomena such as adhesion strength [150]. To our knowledge, this is the first experimental study demonstrating finely tuned *in vivo* healing in response to engineered bioadhesive cues on material surfaces.

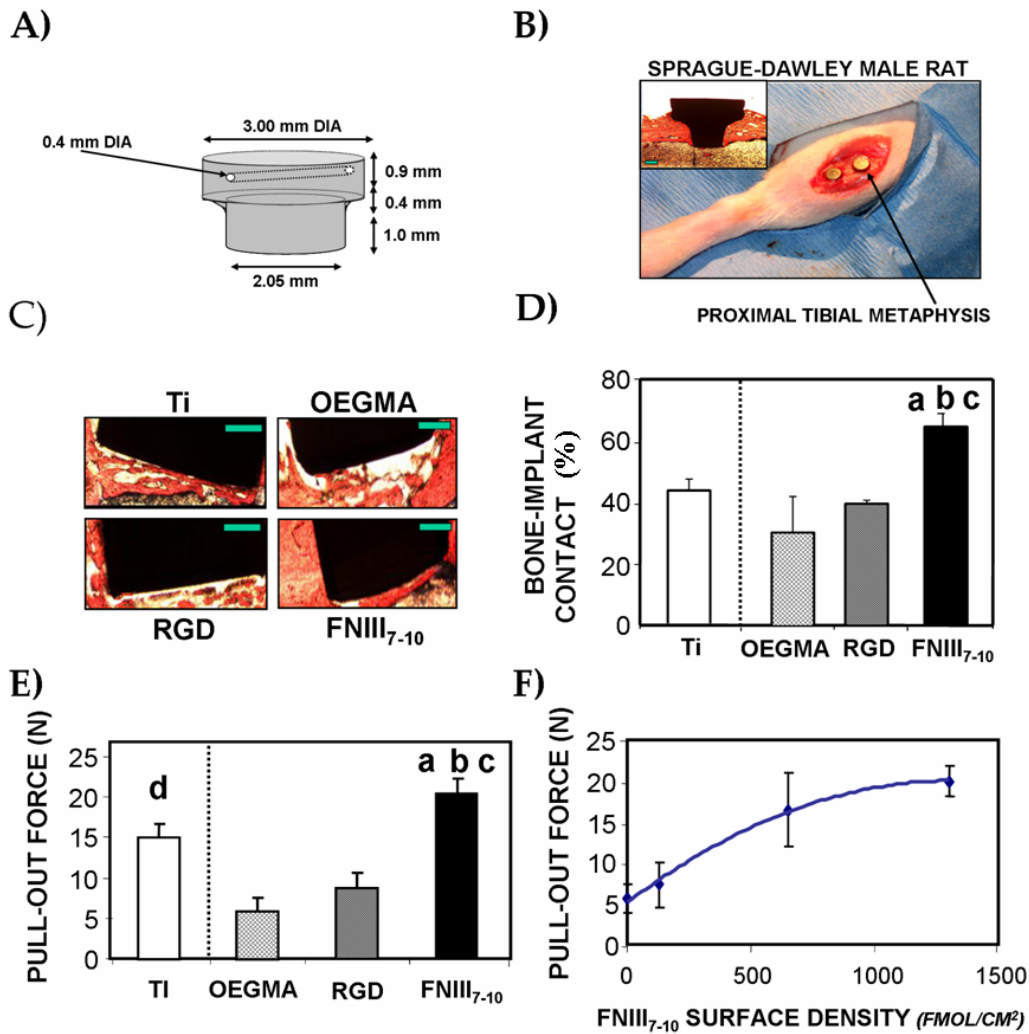


Figure 4.6. Integrin specificity modulates *in vivo* implant osseointegration. (A) Schematic of tapered titanium implant used in rat tibia implant model. (B) Photograph showing placement of implants in rat tibia. Two implants were placed in each tibia. Inset micrograph is of longitudinal section of entrenched implant after 4 wk implantation, stained with Sanderson's Rapid Bone Stain™ and van Gieson counterstain. (C) Histological sections at 4 weeks post-implantation showing mineralized bone (orange)-implant (black) contact (scale bar 0.5 mm). FNIII₇₋₁₀-tethered implant surfaces displayed greater bone tissue formation and connectivity compared to other surface treatments. (D) Bone-implant contact area. a vs. RGD ($p < 0.02$); b vs. Ti-serum ($p < 0.02$); c vs. poly(OEGMA) ($p < 0.02$). (E) Functional osseointegration as determined by pull-out force. a vs. RGD ($p < 0.009$); b vs. Ti-serum ($p < 0.05$); c vs. poly(OEGMA) ($p < 0.001$); d vs. poly(OEGMA) ($p < 0.01$). (F) Functional osseointegration increases with FNIII₇₋₁₀ tethered density (hyperbolic fit, $R^2 = 0.87$).

Discussion

The presentation of biological active factors on the surface of biomedical devices has emerged as a promising strategy to enhance host healing responses to implanted devices [31,187]. Nonetheless, these biomimetic approaches have elicited marginal improvements in *in vivo* functional performance [10-12]. We hypothesized that these marginal healing responses result from uncontrolled signaling responses at the tissue-implant interface arising from unregulated or sub-optimal integrin binding. While model biomaterial surfaces to control ligand presentation (e.g., self-assembled monolayers on gold or silicon) have been extensively studied, the development of robust coating technologies for tunable presentation of bioactive factors on materials approved for biomedical implantation has been particularly challenging. Recent bioactive implant surface treatments on Ti, including porous hydroxyapatite, collagen I, and calcium phosphate co-precipitated with various other biological ligands, have augmented aspects of bone healing compared to unmodified Ti in various animal models [189-191]. However, these strategies lack control over protein adsorption, ligand presentation and density, and surface stability. The utility of this brush system in this study is the level of precise control over bioactive ligand density and presentation and cellular integrin interaction in a physiological environment.

In the present work, we grafted clinical-grade titanium implants with a robust non-fouling polymer coating functionalized with controlled densities of ligands of varying integrin specificity to examine the role of integrin binding specificity on tissue responses to implanted devices. Our results demonstrate that conferring integrin binding

specificity to biomedical implants regulates the osteoblastic differentiation of bone marrow-derived progenitor cells and significantly enhances *in vivo* bone healing and implant functional osseointegration. This work provides the first experimental demonstration that *in vivo* healing response can be finely tuned by engineering bioadhesive cues on synthetic biomedical material surfaces, and provides novel insights into the role of integrin receptors in directing specific signaling pathways and osteogenic cell functions. Importantly, this biomolecular strategy is based on surface engineering a robust non-fouling polymer coating on clinical-grade titanium, and therefore is applicable to existing biomedical implants. The integrin-specific biomaterial surfaces significantly enhanced *in vivo* implant integration and fixation compared to the current clinical standard (unmodified titanium) as well as biomimetic RGD-based surface treatments. This integrin-specific enhancement of functional integration may be potentially even greater since the FNIII₇₋₁₀ surface density tethered to the polymer coating was below saturation. Given the central role of integrin receptors in the maintenance and repair of numerous tissues, we expect that this strategy of conveying integrin specificity will enhance healing responses and integration of other biomedical implanted devices.

We attribute the enhanced bone tissue formation and functional osseointegration of the $\alpha_5\beta_1$ -specific titanium implants to increased recruitment of osteoprogenitor cells and differentiation into osteoblasts at the tissue-implant interface. As demonstrated in the *in vitro* analyses (Fig. 3), $\alpha_5\beta_1$ -mediated adhesion upregulated osteoblastic gene and protein expression and matrix mineralization in marrow-derived progenitor cells. The $\alpha_5\beta_1$ integrin is the central fibronectin receptor, and its expression has been associated with increased mineralization of osteosarcoma and calvarial osteoblast cells [189]. This

study provides further evidence for directed $\alpha_5\beta_1$ -mediated osteogenic differentiation as well as additional associated signaling through specific residues of FAK. In addition to cells directly interacting with the bioadhesive ligands on the implant surface, paracrine factors secreted at the tissue-interface could contribute to the pro-osteogenic healing response by recruiting additional osteoprogenitors and/or promoting osteoblastic differentiation in neighboring cells.

No differences in bone-implant contact or functional osseointegration were observed between RGD-tethered and unmodified titanium implants. We attribute the suboptimal host healing responses to these implants to reduced osteoblastic differentiation and bone formation. These two surfaces present adhesive ligands that primarily bind $\alpha_v\beta_3$. Osteogenic cell adhesion to the short synthetic RGD is primarily mediated by this integrin (Fig. 2). Similarly, cell adhesion to the unmodified titanium is mediated by RGD-containing proteins (e.g., fibrinogen, vitronectin [192]) that adsorb non-specifically to titanium and support $\alpha_v\beta_3$ -mediated adhesion. As demonstrated in the *in vitro* analyses (Fig. 3) and previous work (15), binding of $\alpha_v\beta_3$ suppresses osteoblastic differentiation. Moreover, $\alpha_v\beta_3$ -overexpressing osteoblasts exhibited impeded mineralization capacity due to suboptimal integrin-matrix interactions, JNK activity, and matrix protein expression [50]. In addition to reduced osteoblastic differentiation, it is possible that presentation of $\alpha_v\beta_3$ -selective ligands reduces overall bone formation by enhancing osteoclastic activity. Integrin $\alpha_v\beta_3$ is a major component of podosomes in the sealing zones of resorptive pits [193], and $\alpha_v\beta_3$ antagonists reduce bone resorption by reducing osteoclast activity [194-196]. However, we did not observe accumulation of

multi-nucleated cells at the bone tissue-implant interface, suggesting that osteoclastic responses were not the dominant mechanism. Using the unique integrin-specific ligand presentation system in this study, we have obtained mechanistic insights into the functional roles of integrins in directing osteogenic behavior of stem-like stromal cells both *in vitro*, and, for the first time, *in vivo*.

A major contribution of the present study is the application of a stable non-fouling polymer coating that can be precisely engineered to present bioactive factors as a general strategy to convey biofunctionality to existing clinical devices. This approach is directly translatable to metal oxides and ceramic materials, and the tethering scheme is amenable to other protein ligands, including growth factors, antibodies, and enzymes, as well as aminated nucleic acids, carbohydrates, and lipids. Moreover, we have established the high physiological stability of this polymer brush system, affording long-term direct *in vivo* functional comparison of bioactive ligands. Consequently, we have been able to demonstrate in this study an integrin-specific mechanism for the regulation of progenitor cell differentiation into osteoblasts and *in vivo* enhancement of bone healing and implant osseointegration.

Summary

Clinical-grade titanium implants were grafted with a non-fouling oligo(ethylene glycol)-substituted polymer coating functionalized with equimolar densities of either RGD peptide or $\alpha_5\beta_1$ -integrin-specific FN fragment FNIII₇₋₁₀. Biomaterials presenting FNIII₇₋₁₀ supported enhanced $\alpha_5\beta_1$ integrin binding and osteoblastic differentiation in bone marrow stromal cells compared to unmodified titanium and RGD-presenting surfaces, which promoted primarily $\alpha_v\beta_3$ binding. Importantly, FNIII₇₋₁₀-functionalized

titanium significantly improved functional implant osseointegration compared to RGD-functionalized and unmodified titanium *in vivo*. This work identifies a robust strategy that may be applicable to improve the biological performance of other biomedical devices and constructs for regenerative medicine.

CHAPTER 5

SIMPLE APPLICATION OF FIBRONECTIN-MIMETIC COATING TO ENHANCE OSSEOINTEGRATION OF TITANIUM IMPLANTS

Introduction

Current orthopedic implant surface technologies, including porous coatings and calcium phosphate overcoats, seek to promote bone cell ingrowth and mineral formation [3,197,198]. Although these approaches are successful in many cases, they can be restricted by slow rates of osseointegration and poor mechanical anchorage, especially in challenging clinical cases, such as those associated with large bone loss and poor bone quality [4]. In addition, these surface modification approaches rely on costly and manufacturing-intensive processes. As an alternative to these surface technologies, emerging biomimetic strategies have focused on the presentation of biological motifs, including extracellular matrix sequences and growth factors [117,199-209]. The general paradigm of these bio-inspired approaches is the covalent immobilization (tethering) of the biological entities onto the underlying material support, which often involves multi-step procedures to render the support suitable for biofunctionalization [31,81]. In contrast, we recently described a simple, one-step coating procedure that relies on the

*Modified from

T.A. Petrie, C.D. Reyes, K.L. Burns, A.J. García, *Simple Application of Fibronectin-Mimetic Coating Enhances Osseointegration of Titanium Implants*. Journal of Cellular and Molecular Medicine 2008, *In Press*.

passive adsorption of a synthetic collagen-based peptide onto biomedical grade titanium to enhance osseointegration [49].

Integrins are a large family of heterodimeric ($\alpha\beta$) transmembrane receptors that mediate cell-matrix and cell-cell adhesion and trigger signals regulating cell survival, proliferation, and differentiation [16,28,210-212]. Osteoprogenitor cells and osteoblasts express a wide panel of integrins, including $\alpha_5\beta_1$, $\alpha_v\beta_3$, $\alpha_3\beta_1$, $\alpha_8\beta_1$ and $\alpha_2\beta_1$, that mediate interactions with collagens [213,214], fibronectin [36,215], laminins [216] and other matrix components [37,80]. Specific integrin-ECM adhesive interactions regulate osteoblast function and mineralization [17,217-220]. Importantly, osteoblast integrin-ECM interactions are dynamic, and the extent of early and late mineralization is dependent on the particular integrin-matrix protein interactions engaged [36,221-222].

Because of the central roles of integrin-ECM interactions in osteoblast activities, integrins represent an attractive target in the design of biofunctionalized orthopedic implants [81]. The large majority of these efforts have centered on presenting short binding motifs incorporating the arginine-glycine-aspartic acid (RGD) minimal binding sequence from FN, bone sialoprotein and osteopontin [105,106,223]. Despite improved adhesion and differentiation *in vitro*, implant surfaces presenting RGD motifs do not consistently enhance osseointegration and bone formation in animal models [10,12,104,105]. In the present work, we evaluated the ability of different fibronectin-inspired biomolecular coatings to promote *in vitro* osteoblastic differentiation and implant osseointegration in a rat cortical bone model. Notably, these biomolecular coatings rely on simple physisorption of FN-based ligands onto biomedical-grade titanium as a simple, clinically-translatable, implant biofunctionalization strategy.

Materials and Methods

Bioadhesive Ligands and Preparation of Surfaces

The bioadhesive ligands examined in this study were: (i) a recombinant fragment spanning the 7th-10th type III repeats of human fibronectin (FNIII₇₋₁₀), (ii) human plasma fibronectin (pFN), and (iii) a linear RGD peptide (GRGDSPC). FNIII₇₋₁₀ was expressed in *E. coli* and purified as previously described [108]. Briefly, JM109 cells were transformed with plasmid encoding for biotinylated FNIII₇₋₁₀, streaked onto agar plates, colonies isolated, and cultures grown overnight in standard LB Broth. Cells were lysed via lysozyme/sonication and the FNIII₇₋₁₀ was purified by affinity chromatography on a monomeric avidin column by elution with d-biotin (Pierce, Rockford, Ill.). Purity was > 95% as assessed by SDS-PAGE and Ponceau solution staining. After further filtering with 30 kDa Microcon centrifugal filter devices (Millipore, Bedford, MA) to remove excess d-biotin, purity was determined to be > 98%. FNIII₇₋₁₀ was maintained in a stock solution of Dulbecco's phosphate buffered saline at 2 mg/mL (PBS; Invitrogen, Carlsbad, CA). Human pFN was purchased from Invitrogen (catalog #33016) and reconstituted in aliquots of sterile distilled water. Purity was assessed by SDS-Page by Invitrogen Quality Control at > 95%. The RGD peptide was obtained from BACHEM (Torrance, CA, catalog #H-7245), reconstituted in 0.1% TFA (trifluoroacetic acid) and assessed as > 98% pure.

Titanium (Ti) metal was obtained from Kurt J. Lesker Company Part #EVMTI137EXE (Clairton, PA) as pellets of 99.97% pure titanium. For *in vitro* assays, thin films (300 Å) of this titanium were deposited onto clean glass coverslips using an electron beam evaporator (2×10^{-6} Torr) at a deposition rate of 1 Å/s. Slides were then

immersed in a FNIII₇₋₁₀, pFN, or RGD peptide solution at various coating concentrations in PBS for 30 min. Surfaces were subsequently blocked with 1% heat denatured bovine serum albumin (BSA). For the *in vivo* experiments, implants were machined from commercially pure, clinical-grade (grade 4) titanium rods (Titanium Industries, Inc., Cleveland OH). Ligand surface density measurements were obtained via surface plasmon resonance (SPR) using a Biacore X instrument. For subsequent cell-based experiments, FNIII₇₋₁₀ and pFN were coated on Ti surfaces at equimolar (RGD binding site) surface densities as determined by SPR. Other surfaces were either exposed to serum or RGD peptide (50 µg/mL) for 30 min.

Cell Adhesion, Integrin Binding, and Signaling Assays

Primary rat bone marrow stromal cells (rBMSCs), a heterogeneous cell population containing osteoprogenitors and which represents an analogous cell source to human bone marrow stromal cells currently used in clinical applications [224,225], were selected as the cell model to examine this biomimetic coating technology. rBMSCs were isolated and cultured under IACUC-approved procedures [49]. Cells were passaged no more than three times post-rat isolation in growth medium (α -MEM + 10% fetal bovine serum + 1% penicillin-streptomycin) before usage in all *in vitro* experiments. During culture, cells were split prior to 90% confluence, typically every 3 days. Cell adhesion to ligand-adsorbed Ti surfaces under serum-free conditions was measured at 1 h adhesion time at 37 °C using a centrifugation assay [171]. For integrin blocking experiments, cells were incubated in the presence of 20 µg/mL anti-rat α_5 integrin (CD49e, clone HM α 5-1, BD Biosciences) or anti-rat α_v (CD51, clone 21, BD Biosciences) blocking antibodies for 20 min prior to cell seeding, and seeded for 1 h adhesion time.

Integrin binding levels (post 30 min adhesion) were assessed using a crosslinking/extraction/reversal procedure [172]. This procedure uses DTSSP to specifically crosslink integrins bound to their ligand. Cellular components are then extracted using detergent and protease inhibitors, and crosslinks are reversed and the once bound integrins are collected. Integrin levels were quantified by Western blotting using primary antibodies against α_5 integrin (AB1928, Chemicon; 0.5 $\mu\text{g}/\text{mL}$), and α_v integrin (AB1930, Chemicon; 0.5 $\mu\text{g}/\text{mL}$). Membranes were washed in TBS-Tween (20 mM Tris HCl pH 7.6, 137 mM NaCl, 0.1% Tween 20) for 45 min and incubated in secondary antibody (biotin-conjugated anti-rabbit IgG, 1:20,000 dilution in Blotto) for 1 h at room temperature while rocking. Membranes were washed again in TBS-Tween for 45 min and incubated in a tertiary antibody (alkaline phosphatase-conjugated anti-biotin IgG, 1:10,000 dilution in Blotto) for 1 h at room temperature while rocking. After antibody incubation, membranes were washed in TBS-Tween for 45 min and immunoreactivity was detected using an ECF fluorescent substrate for 5-10 min. Bands were visualized using a Fuji Image Analyzer and further quantified and analyzed using Adobe Photoshop software.

For FAK activation experiments, rBMSCs were incubated in serum-free suspension ($\alpha\text{MEM} + 5\% \text{BSA}$) for 30 min to reduce FAK background activation and then in the presence or absence of integrin blocking antibodies for 20 min prior to cell seeding for 2 h at 37 °C. Cells were lysed in cold RIPA buffer (1% Triton X-100, 1% sodium deoxycholate, 0.1% SDS, 150 mM NaCl, 150 mM Tris-HCl (pH 7.2), 350 $\mu\text{g}/\text{mL}$ PMSF, 10 $\mu\text{g}/\text{mL}$ leupeptin, 10 $\mu\text{g}/\text{mL}$ aprotinin) on ice for 15 minutes. FAK activation was subsequently quantified via Western blotting using primary antibodies against

specific phosphorylated FAK tyrosine residues (pY397, pY576, pY861 in Blotto for 1 h) and total FAK (anti-FAK). Bands were visualized and quantified in the same manner as the integrin binding procedure. FAK phosphorylation levels were normalized to the amount of total FAK for each experimental condition.

Proliferation Assay

After plating for 16 h in 10% serum, cells were incubated in BrdU (3.1 µg/mL) for 4 h. Samples were fixed in 70% ethanol, denatured in 4 M HCl, neutralized in 100 mM Tris-HCl + 50 mM NaCl, and blocked with 5% fetal bovine serum. Samples were then incubated with anti-BrdU (1:1000) and AF488 anti-mouse IgG (1:200) as well as Hoechst dye (1:10,000) to stain nuclei. Using in-house image analysis, the number of cells positive for BrdU relative to total cell nuclei was quantified.

Osteoblast-Specific Gene Expression

rBMSCs at low passage were seeded on appropriate surfaces at 200 cells/mm² in growth medium (α -MEM + 10% fetal bovine serum + 1% penicillin-streptomycin). After 24 h, cultures were switched to osteogenic medium consisting of growth medium supplemented with 50 µg/mL L-ascorbic acid and 3 mM sodium β -glycerophosphate. Total RNA was isolated at day 7 using Qiagen RNEasy kits. cDNA synthesis was performed on DNAase I-treated (25 Kunitz units) RNA by oligo(dT) priming via SuperScript II preamplification system (Invitrogen). Reverse-transcriptase PCR was performed with an Applied Biosystems ABI Prism 7700 using osteoblast-specific primers and SYBR green intercalating dye [20]. Transcript concentration was quantified from a

linear curve of standards, which were amplified from cDNA via oligonucleotide primers for each gene assayed (Runx2, BSP, and OCN).

Alkaline Phosphate (ALP) Activity and Matrix Mineralization Assays

ALP activity was quantified biochemically at 7 days post-seeding. Protein was isolated from cell cultures and equal amounts (2.5 µg) were added to 5-methyl umbelliferyl phosphate fluorescent substrate (60 µg/mL) for 60 min. Fluorescence was measured (360 nm/465 nm) and enzymatic activity normalized to total amount of protein. Calcium content was analyzed at 7 days in culture by dissolving mineralized deposits overnight in 1.0 N acetic acid and using a calcium-detecting reagent (Diagnostic Services Ltd.). Mineralization analyses were conducted by von Kossa staining 14-day cultures, and percent mineralization was quantified by image analysis.

Implantation Procedure and Functional Analysis

Implantations into the tibiae of mature Sprague-Dawley male rats were conducted in accordance with an IACUC-approved protocol as described previously [49]. A day before implantation, Ti implants were soaked in de-ionized water for 30 minutes, and subsequently stripped of the existing oxide layer by submersion in 4% HF for 30 s. A new oxide layer was formed by incubation of implants in 35% HNO₃. This cleaning and re-growth of the oxide layer can be performed days before implantation as long as samples are subsequently kept clean. This stripping and re-growth of the titanium oxide layer was done to generate relatively clean surfaces free of organic debris and have surfaces equivalent to what is used in clinical implants. This cleaning step is not required for adsorption of bioactive peptides. At the time of surgery, implants were coated with

ligand by incubating in ligand solutions in PBS for 30 min. Tapered Ti implants treated with FNIII₇₋₁₀ or pFN at equimolar RGD-coating density (0.8 pmol/cm²) or unmodified Ti were press fit into the cortical defects. Two 2-mm diameter defects were drilled into the medial aspect of the proximal tibial metaphysis of each leg to achieve a total of four implants per animal (**Figure 5.6 A,B**). Implant locations (R/L leg, proximal/distal location) were randomized for each surface condition (pFN, FNIII₇₋₁₀, unmodified Ti) and a total of 11 rats were used. After four weeks of implantation [49], the rat tibiae were harvested and assessed for bone apposition and implant mechanical fixation. Proximal tibiae were explanted and either fixed in neutral buffered formalin for histology or wrapped in PBS to maintain moisture for immediate mechanical testing. Formalin-fixed tibiae were embedded in poly(methyl methacrylate), dehydrated, and stained with Sanderson's Rapid Bone StainTM and a van Gieson counterstain. This stained mineralized bone (yellow-orange) and soft tissue and osteoid (blue-green). Bone apposition was quantified as the percentage of the implant's surface in contact with the bone, and 8 fields/implant were quantified (N=4 implants per condition). Pull-out testing was performed to quantify implant mechanical fixation to surrounding bone tissue using an EnduraTEC Bose ELF 3200. The ends of each excised tibia were secured using a customized holding apparatus and the exposed head of the implant attached to a load cell via a customized grip apparatus. Pre-loaded samples (< 2 N) were then subjected to a constant pull rate of 0.2 N/sec. The pull-out force (N), parallel to the long axis of implant, was the maximum load achieved before implant detachment or failure.

Statistics

Results are presented as mean \pm standard error. Quantification of *in vitro* and *in vivo* experiments was performed on all samples used in each experiment. Results were analyzed by ANOVA in SYSTAT 8.0 (SPSS). If deemed significant, pairwise comparisons were performed using Tukey's post hoc test and a confidence level of 95% was considered significant. *In vitro* assays were conducted in at least triplicate and replicated in two separate experiments.

Results

FN-mimetic Ligand Coatings

Ti surfaces were either exposed to serum or passively coated with one of three biomimetic ligands: (1) FNIII₇₋₁₀, a recombinant fragment of FN spanning the central cell binding domain that promotes $\alpha_5\beta_1$ -mediated cell adhesion and signaling [108]. This domain contains the central integrin-binding domain comprising the RGD and PHSRN synergy motifs that are essential for high affinity $\alpha_5\beta_1$ binding; (2) full-length human plasma fibronectin (pFN), which is a dimer comprising multiple cell receptor binding sites; and (3) a linear RGD-containing peptide. Importantly, the FNIII₇₋₁₀ fragment reconstitutes the 3-D presentation of both the RGD and PHSRN sequences found in pFN, excluding most of the additional adhesion and binding domains also present in pFN [108]. Adsorbed densities were measured by SPR. As expected, adsorbed ligand density increased with ligand coating concentration exhibiting linear increases at low coating concentrations and reaching saturation values at high coating concentrations, described accurately by hyperbolic curve fits (**Figure 5.1 A**). For all subsequent experiments,

ligand coating concentrations were adjusted to yield equimolar surface densities (0.8 pmol/cm^2) of adhesive (RGD) sites in order to directly compare FNIII₇₋₁₀ (45 ng/cm^2) to pFN (125 ng/cm^2). The linear RGD peptide was also considered for comparison as a ligand coating but exhibited poor adsorption efficiency. Minimal RGD peptide densities (below the SPR detection limit $0.1 \pm 0.07 \text{ ng/cm}^2$ corresponding to 0.08 pmol/cm^2) were measured ($50 \text{ }\mu\text{g/mL}$ coating concentration). The density of adsorbed biomolecules for serum-exposed surfaces was 195 ng/cm^2 .

An enzyme-linked immunoabsorbent assay (ELISA) using the HFN 7.1 antibody, a mimetic of $\alpha_5\beta_1$ binding to FN [52], verified that both FNIII₇₋₁₀ and pFN adsorbed in a bioactive orientation which is highly accessible to integrin binding (**Figure 5.1 B**). Moreover, the antibody binding curve for adsorbed FNIII₇₋₁₀ on Ti was shifted upward and to the left compared to the pFN curve, indicating that the average FNIII₇₋₁₀ orientation is more accessible to $\alpha_5\beta_1$ binding than adsorbed pFN. We did not perform ELISA measurements for serum-treated Ti because various RGD-containing proteins adsorb onto Ti from serum [226].

FN-Mimetic Ligand Surfaces Promote Integrin-Specific Cell Adhesion and Signaling

To probe for the main integrin receptors actively engaged during adhesion, a centrifugation cell adhesion assay was performed in the presence and absence of integrin-specific blocking antibodies. rBMSCs displayed greater levels of adhesion to FNIII₇₋₁₀-coated surfaces compared to Ti surfaces exposed to RGD or serum-treated Ti ($p < 0.008$), and adhesion levels were equivalent to pFN-adsorbed surfaces (**Figure 5.2 A**). Because the *in vitro* adhesion assay is performed under serum-free conditions, the serum-exposed titanium surface was included to correspond to the untreated titanium surfaces in

subsequent *in vitro* assays performed in the presence of serum. Control experiments demonstrated no differences in adhesion between cells plated under serum-free conditions on surfaces pre-exposed to 10% serum and cells seeded on untreated titanium in the presence of serum. Hence, the untreated (in the presence of serum) and serum-exposed surfaces are equivalent in terms of cell adhesion. Cell adhesion on RGD-exposed surfaces was not different from background levels, corroborating the SPR results that this short peptide cannot stably adsorb to titanium. Importantly, a blocking anti- α_5 antibody effectively eliminated cell adhesion to FNIII₇₋₁₀ surfaces ($p < 0.008$), verifying the specificity of this surface for $\alpha_5\beta_1$ integrin, but did not significantly reduce adhesion to pFN-coated or serum-treated surfaces. Conversely, a blocking anti- α_v antibody significantly reduced adhesion to the serum-exposed Ti surface ($p < 0.02$), indicating that adhesion to this surface is mediated primarily by α_v -containing integrins. This data also reflects the ability of titanium to adsorb many RGD-containing serum proteins, including vitronectin, which is recognized mainly by the $\alpha_v\beta_3$ integrin.

We next examined integrin binding to further characterize the adhesion mechanism to ligand-coated implant surfaces. Bound levels of α_5 and α_v integrins (after 45 min adhesion) were quantified using a biochemical crosslinking/extraction/reversal technique. This robust technique utilizes a water-soluble crosslinker that isolates bound integrin-ligand pairs, and allows direct quantification of the total bound number of integrins. Consistent with the integrin blocking antibody experiments, cells displayed higher levels of bound α_5 on FNIII₇₋₁₀ surfaces over pFN ($p < 0.03$) or Ti-serum ($p < 0.005$) surfaces, whereas higher levels of α_v integrin were engaged on pFN ($p < 0.03$) and serum-treated Ti surfaces ($p < 0.001$) compared to FNIII₇₋₁₀-coated Ti (**Figure 5.2 B**). Taken

together, these data establish that the FNIII₇₋₁₀-adsorbed surfaces mainly support $\alpha_5\beta_1$ -mediated adhesion, whereas the serum-treated and pFN surfaces engage α_v -containing integrins, most likely $\alpha_v\beta_3$.

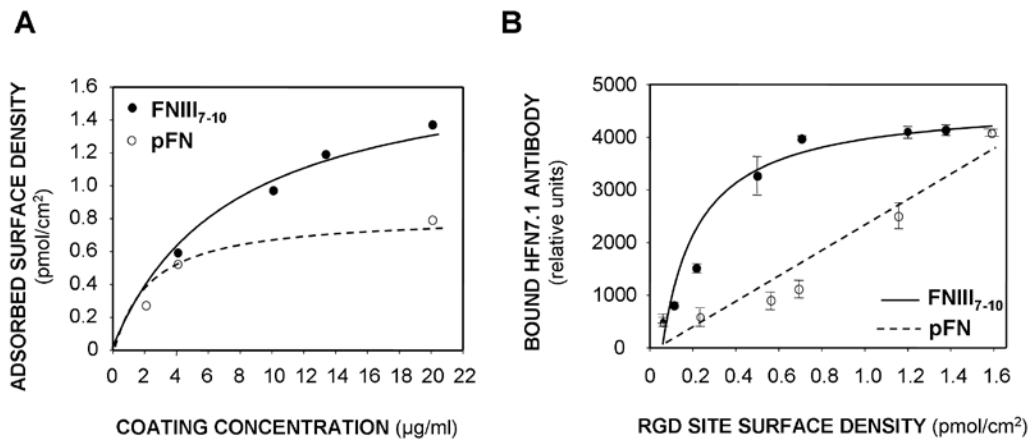


Figure 5.1. Surface density and accessibility of bioactive integrin ligands adsorbed on titanium surfaces. (A) Adsorbed surface densities of pFN and FNIII₇₋₁₀ to Ti surfaces as measured by surface plasmon resonance. A total of at least 8 independent measurements for each peptide was performed. The tethering profile was fit to a simple hyperbolic curve (FNIII₇₋₁₀ curve: $R^2=0.94$; pFN curve: $R^2=0.96$). (B) ELISA using $\alpha_5\beta_1$ -mimetic HFN 7.1 antibody demonstrating accessibility differences on FNIII₇₋₁₀ and pFN-adsorbed Ti surfaces (hyperbolic curve fit, FNIII₇₋₁₀ curve: $R^2=0.97$; pFN curve: $R^2=0.95$).

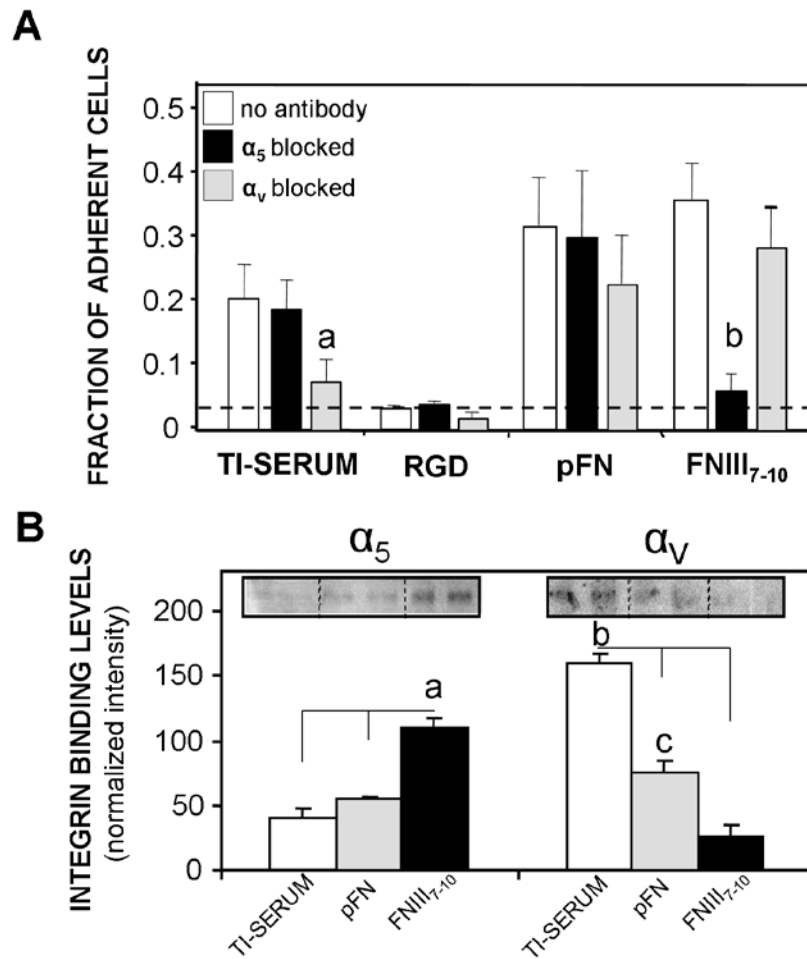


Figure 5.2. Titanium surfaces functionalized with bioactive integrin ligands display integrin specificity. (A) Bone marrow stromal cell adhesion (30 min) to adsorbed ligand surfaces is mediated by different integrin receptors as demonstrated by blocking antibodies in a cell centrifugation assay. Hashed line represents adhesion levels of cells on Blotto-blocked surfaces and no ligand (N=4). Ti-serum: * $p < 0.02$ vs. no antibody control; FNIII₇₋₁₀: * $p < 0.008$ vs. no antibody control. (B) Integrin binding analysis using a crosslinking/extraction/reversal procedure for stromal cells plated on ligand-treated titanium surfaces of equimolar density (N=5). α_5 : ** $p < 0.03$ vs. pFN, ** $p < 0.005$ vs. Ti-serum; α_V : ** $p < 0.01$ vs. pFN, ** $p < 0.001$ vs. FNIII₇₋₁₀; # $p < 0.03$ vs. FNIII₇₋₁₀.

To examine early integrin-mediated signaling on these supports, we analyzed phosphorylation levels of important FAK tyrosines. FAK is an intracellular signaling molecule implicated in integrin-mediated signal transduction and is directly involved in the osteogenic differentiation pathway [188]. We assessed the phosphorylation of two important residues in FAK: tyrosine 397 (the autophosphorylation site of FAK) and tyrosine 576 (essential for maximal kinase activity) for cells plated on implant surfaces in the presence of integrin blocking antibodies. FAK phosphorylation levels for Y397 and Y576 were enhanced on FNIII₇₋₁₀ surfaces compared to pFN-coated ($p < 0.01$) or Ti-serum surfaces ($p < 0.01$) (**Figure 5.3 A,B**). Furthermore, when rBMSCs were pre-incubated with blocking antibodies against β_3 , phosphorylation levels of Y397 and Y576 were significantly reduced compared to unblocked controls for cells adhering to either pFN-coated or serum-coated Ti surfaces. Importantly, blocking antibodies against α_5 reduced phosphorylation of FAK tyrosine 397 and 576 residues for cells only on FNIII₇₋₁₀-coated surfaces; blocking α_5 did not produce a significant effect for the other surfaces. This data indicates that the specific integrins engaged during early adhesive events, primarily $\alpha_5\beta_1$ for FNIII₇₋₁₀-coated surfaces and $\alpha_v\beta_3$ for pFN- and serum-coated surfaces, differentially modulate downstream signaling pathways (such as FAK activation) that may be a prerequisite for bone cell differentiation.

Integrin-Specific Ti Coatings Modulate In Vitro Osteogenic Activities

We postulated that differences in integrin binding specificity and FAK activation modulate particular cell responses, including proliferation and expression of osteogenic markers. Indeed, a short-term (16 h) proliferation assay based on BrdU incorporation

demonstrated that cells on FNIII₇₋₁₀-treated Ti surfaces exhibited increased proliferation rates compared to pFN-coated ($p < 0.05$) or serum-treated Ti surfaces ($p < 0.004$) (**Figure 5.3 C**). In addition, cells displayed a significantly higher proliferation rate on pFN-coated surfaces over serum-treated Ti ($p < 0.009$).

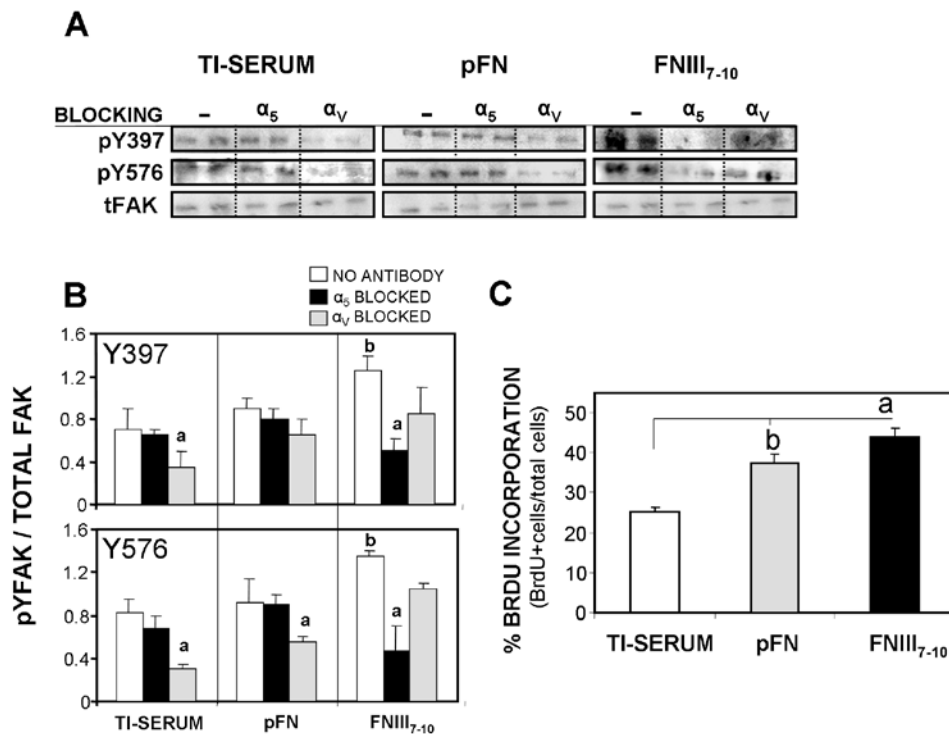


Figure 6.3. Initial cell signaling (FAK activation) and proliferation on equimolar ligand-treated and serum-treated Ti surfaces is integrin-dependent. (A) Relative levels of phospho-Y in FAK were quantified, in the presence or absence of integrin blocking antibodies prior to cell seeding (2 h), by Western blotting of cell lysates. Representative blots of each surface condition are shown (N=4). (B) Activation levels for Y397 and Y576 (normalized to total FAK) were higher on FNIII₇₋₁₀-coated surfaces than pFN-treated and Ti-serum supports after 2 h cell adhesion (Y397: #p<0.01; Y576: #p<0.01). Integrin blocking antibodies selectively reduced FAK phosphorylation. Y397: *p<0.05 vs. no antibody control (Ti-serum), *p<0.01 vs. no antibody control (FNIII₇₋₁₀); Y576: *p<0.02 vs. no antibody control (Ti-serum), *p<0.05 vs. no antibody control (pFN), *p<0.03 vs. no antibody control (FNIII₇₋₁₀). (C) FNIII₇₋₁₀-treated surfaces display higher proliferation rate (%BrdU + cells/total cells) than pFN-coated or Ti-serum surfaces (16 h adhesion) (FNIII₇₋₁₀: **p<0.05 vs. pFN, **p<0.004 vs. Ti-serum). pFN-treated surfaces also enhanced proliferation rate over serum-treated Ti (#p<0.009) (N=5).

To examine if these integrin-specific adhesive and signaling cues influence osteoblastic differentiation, we used quantitative RT-PCR to monitor osteoblast-specific gene expression in 7 day rBMSC cultures. Expression levels of Runx2/Cbfa1, a transcription factor involved in early osteoblastic differentiation [163], were significantly elevated on FNIII₇₋₁₀-treated surfaces compared to pFN ($p < 0.006$) or serum-treated Ti ($p < 0.03$) (**Figure 5.4 A**). Moreover, RT-PCR for late differentiation markers of osteoblastic differentiation, namely osteocalcin (OCN) and bone sialoprotein (BSP), revealed greater levels of gene expression on FNIII₇₋₁₀ surfaces compared with either other surface (**Figure 5.4 B**). Notably, transcript levels were not statistically different between pFN- and serum-treated Ti surfaces for any of the three genes examined.

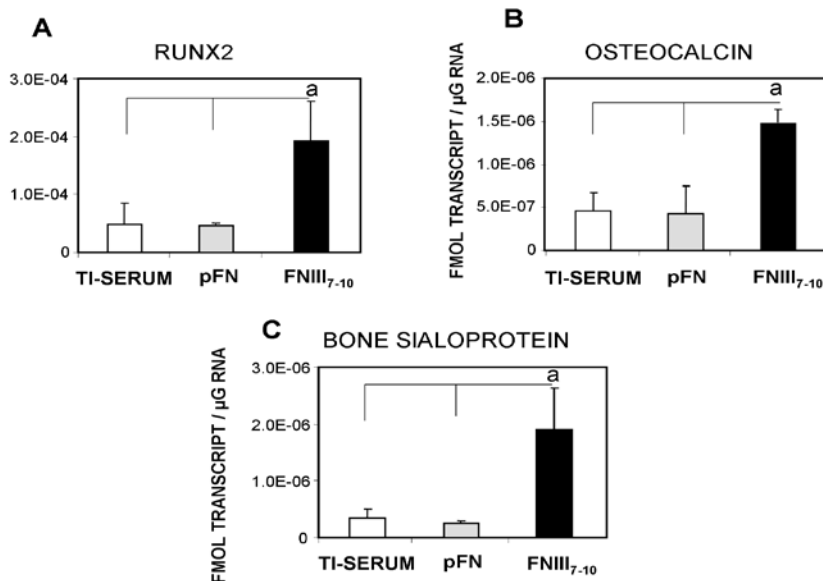


Figure 5.4. FNIII₇₋₁₀-treated surfaces enhance expression of osteoblast-specific genes in bone marrow stromal cultures at 7 days post-seeding. Gene expression levels for: **(A)** Runx2 transcription factor (FNIII₇₋₁₀: ** $p < 0.006$ vs. pFN, ** $p < 0.03$ vs. Ti-serum), **(B)** osteocalcin (FNIII₇₋₁₀: ** $p < 0.02$ vs. pFN, ** $p < 0.01$

vs. Ti-serum), and **(C)** bone sialoprotein (FNIII₇₋₁₀: **p<0.01 vs. pFN, **p<0.02 vs. Ti-serum) (N=4).

We next examined alkaline phosphatase (ALP) activity and calcium deposition as markers of osteoblastic differentiation. Cells on FNIII₇₋₁₀-surfaces displayed a roughly two-fold increase in levels of both ALP activity and calcium-based mineral deposition compared to pFN-coated or serum-treated Ti (**Figure 5.5 A,B**). No differences were observed between pFN-treated titanium and serum-exposed Ti for ALP, but levels of calcium mineral levels were significantly higher on pFN surfaces compared to the serum-treated Ti (p<0.04). Moreover, when the mineralized nodules were visualized and quantified after 14 days post-cell seeding via von Kossa staining, FNIII₇₋₁₀ surfaces supported the highest levels of nodule formation (p<0.04 vs. pFN; p<0.005 vs. Ti-serum), followed by pFN surfaces (p<0.03 vs. Ti-serum), and finally serum-treated Ti surfaces (**Figure 5.5 C**). In addition, RGD peptide-incubated Ti surfaces displayed no significant differences in calcium incorporation or von Kossa staining (data not shown) from serum-treated Ti surfaces; we attribute these results to the inadequate adsorption behavior of the RGD peptide on Ti. Taken together, these results indicate that various biomolecular coatings of different integrin specificity elicit distinct osteoblastic responses *in vitro*.

Integrin $\alpha_5\beta_1$ -Specific Bioactive Coatings Enhance Implant Osseointegration

To evaluate the performance of these integrin-specific coatings *in vivo*, we quantified osseointegration of implants in a rat tibial cortical bone model using quantitative histomorphometry and pull-out mechanical testing (**Figure 5.6 A,B**) [49]. Extensive, adjoining bone matrix was visible in histological sections around FNIII₇₋₁₀-

treated Ti implants, while less substantial and more scattered areas of mineral were present around the pFN-treated and, especially, the uncoated Ti implants (**Figure 5.6 C**).

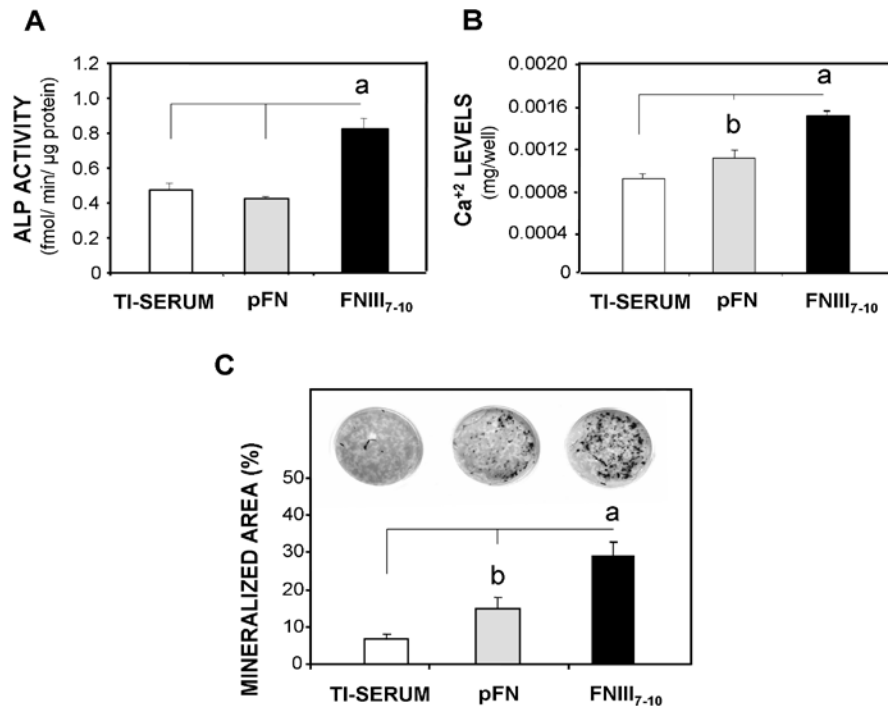


Figure 5.5. Bone marrow stromal cells on FNIII₇₋₁₀-treated surfaces exhibit higher levels of markers for osteoblastic differentiation after 7 days in culture and more advanced matrix mineralization than pFN-treated or serum-treated Ti (14d). (A) FNIII₇₋₁₀-treated surfaces enhance alkaline phosphatase activity (N=4) at 7 days over pFN-treated or serum-treated Ti (FNIII₇₋₁₀: **p<0.0001 vs. pFN, **p<0.0001 vs. Ti-serum), (B) Calcium content was increased at 14 days (N=4) on FNIII₇₋₁₀-treated surfaces over pFN or serum-treated Ti (FNIII₇₋₁₀: **p<0.008 vs. pFN, **p<0.0001 vs. Ti-serum). In addition, cells on pFN-treated surfaces also exhibited a significant increase in Ca²⁺ content over unmodified, serum-treated Ti (#p<0.04), (C) Quantification (percent mineralized area) of von Kossa staining for mineral nodule formation (black) on ligand-treated

surfaces at 14 days. (FNIII₇₋₁₀: **p<0.04 vs. pFN, **p<0.005 vs. Ti-serum; pFN: #p<0.03 vs. Ti-serum).

Moreover, image quantification (8 fields/implant; N=4 implants per surface condition) to determine the level of bone-implant apposition demonstrated > 50% enhancement in bone apposition on FNIII₇₋₁₀-treated implants compared to unmodified Ti (p<0.01) and over 25% compared to the pFN-treated Ti implants (p<0.03) (**Figure 5.6 D**). In addition, pFN-coated implants exhibited increased bone apposition over unmodified Ti (p<0.05).

The overall quality and degree of osseointegration can be most directly assessed by measuring the mechanical strength of implant-bone interaction. Accordingly, functional mechanical testing may be a vital functional predictor of long-term implant success and lifetime [56]. Pull-out mechanical testing (N=7-9 implants per surface condition) revealed significantly higher mechanical fixation of the FNIII₇₋₁₀-treated implants over both pFN-treated (85%, p<0.05) and unmodified Ti (290%, p<0.001), the current clinical standard. (**Figure 5.6 E**). Notably, implants coated with pFN also displayed higher fixation than the unmodified Ti implants (66%, p<0.04), although to a much lower extent than FNIII₇₋₁₀-coated implants. Collectively, these data corroborate *in vitro* results and demonstrate that a simple-to-apply bioactive coating using this $\alpha_5\beta_1$ integrin-specific ligand FNIII₇₋₁₀ can significantly enhance implant integration into the host bone to a greater degree over coatings of incorporating native full-length pFN and even more potently over the current clinical standard (unmodified Ti).

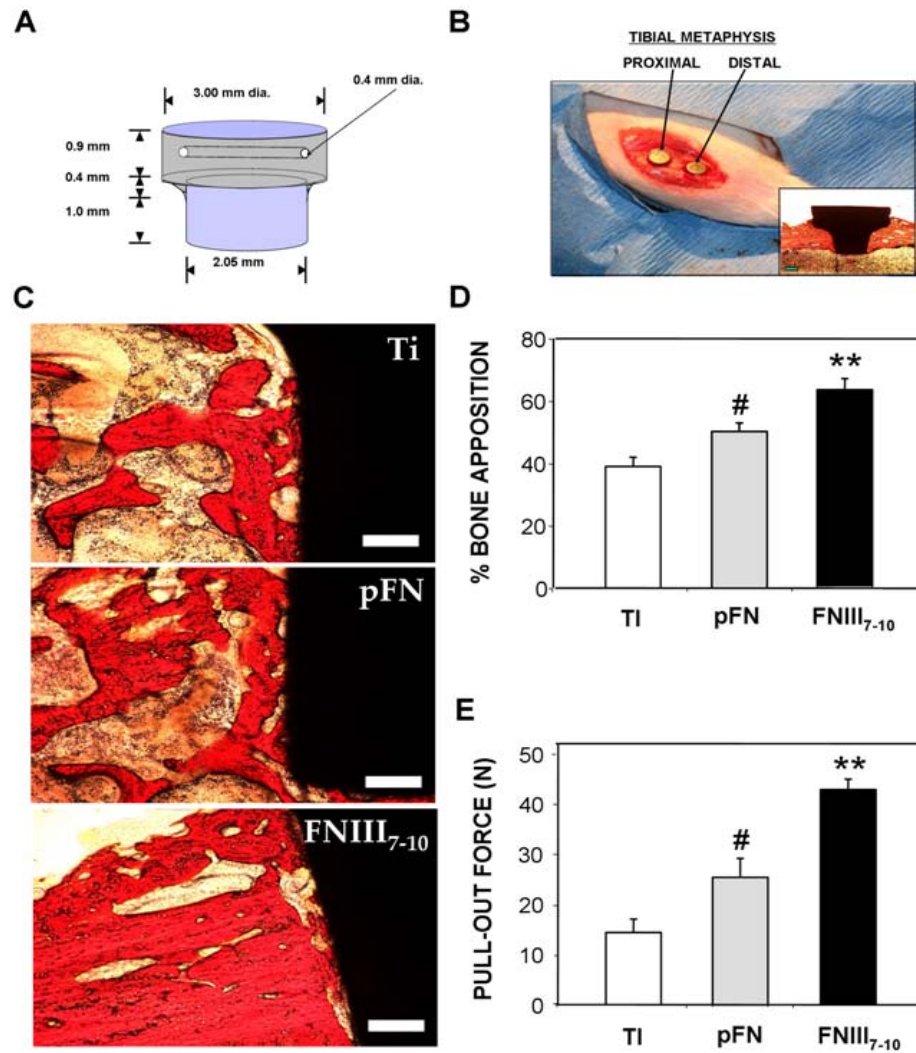


Figure 5.6. Biomimetic ligand coatings targeting specific integrin receptors modulate *in vivo* implant osseointegration. (A) Schematic of titanium (clinical grade) implant design and dimensions. (B) Image of implants press fit into rat tibial metaphysis. Inset is a histological image of a slice of full implant and surrounding tissue (28 d post-implantation). (C) Representative histological sections at 4 weeks post-implantation showing bone (orange)-implant (black) contact (scale bar 0.2 mm). FNIII₇₋₁₀-treated implant surfaces exhibited more contiguous bone tissue formation and connectivity compared to other surface treatment conditions. (D) Quantification of bone-implant contact area. Bone apposition was quantified from histological sections as the percentage of the implant's circumference in direct contact with bone tissue. For each implant, 8 fields were quantified, and multiple slices of the same implant were averaged (N=4 implants per surface condition) (FNIII₇₋₁₀: ^{**}p<0.03 vs. pFN, ^{**}p<0.01 vs. Ti-serum;

pFN: # $p < 0.05$ vs. Ti-serum). (E) Functional osseointegration as determined by pull-out force. There were 7-9 different implants for each surface condition (FNIII₇₋₁₀: ** $p < 0.05$ vs. pFN, ** $p < 0.0001$ vs. Ti-serum; pFN: # $p < 0.04$ vs. Ti-serum.

Discussion

This study examined the ability of a clinically-translatable and simple biomolecular implant coating strategy to promote bone tissue healing and implant osseointegration. These coatings rely on the physisorption of FN-based ligands onto biomedical-grade titanium substrates. Given the functional importance of integrin receptors in modulating a variety of osteogenic pathways *in vitro*, promising surface coating strategies have sought to specifically promote integrin-mediated adhesion and signaling in a bone defect site. These strategies often employ functionalizing implant surfaces with adhesive ligands consisting of matrix proteins (e.g., FN, collagen) or peptides derived from important bone matrix molecules (e.g., RGD motif from FN). However, these approaches have only marginally improved bone formation. Possible explanations for the corresponding lack of improvement in *in vivo* bone formation include non-specific responses to biological macromolecules with multiple bioactive motifs that may provide antagonistic signals (e.g., fibrinogen- and complement-binding activities in pFN) and insufficient pro-healing signaling due to lack of integrin specificity. Here, we demonstrate that an integrin-specific biomolecular surface strategy, using simple passive adsorption on titanium substrates of a fragment of FN that primarily engages integrin $\alpha_5\beta_1$, represents an effective approach for functional bone healing. This FN-mimetic orthopedic implant coating confers integrin-specific cues to stem-like cells that enhance *in vitro* adhesion, proliferation, and osteogenic signaling compared to the current clinical standard (unmodified Ti) as well as full-length FN-based coatings. These findings are consistent with results from an *in vitro* long-term differentiation study

conducted with function-perturbing β_1 and β_3 antibodies on osteoblast-like cells [17]. Moreover, this biomimetic treatment also promoted elevated expression of osteoblast-specific genes, alkaline phosphatase activity, and matrix mineralization and calcification, indicative of a surface-dependent pro-osteoblastic differentiation effect. Finally, as a clinical validation of this surface strategy, cortical bone implantation studies revealed greater contiguous bone contact area around FNIII₇₋₁₀-treated titanium implants compared to plasma FN and uncoated titanium implants. Most importantly, these *in vivo* studies also demonstrated significant improvements in mechanical fixation and functional osseointegration of this FN-mimetic surface coating over full-length pFN-treated titanium implants (2-fold greater) and, notably, unmodified Ti implants (3-fold greater). Notably, this FNIII₇₋₁₀-mediated enhancement of functional osseointegration may be potentially even greater since the FNIII₇₋₁₀ implant surface density was below the saturation level demonstrated by SPR.

We attribute the enhanced functional integration of the $\alpha_5\beta_1$ -specific FNIII₇₋₁₀-implant coatings to increased cell recruitment and osteoblastic differentiation at the cell-material interface. Indeed, recent *in vivo* work suggests that extracellular matrix-coated implants may promote implant integration at early time points by modulating endogenous stromal cell chemotaxis to the implant surface very early (<3 days) after implantation [75]. Since endogenous bone cells can quickly remodel their underlying adherent surface [227], potentially masking these integrin-specific surface cues, these surface cues may act very early to differentiate cells in the bone remodeling process post-implantation. In addition, surface-contacted cells may pass along osteogenic signals to more distant cell

populations via cell-cell contact or secreted soluble biological factors, further influencing the tissue healing over a more extensive spatial and temporal range.

The differences in *in vitro* osteoblastic activities and *in vivo* bone formation between implants coated with FNIII₇₋₁₀ and pFN were unexpected because these two ligands present the 7th-10th type III repeats of FN. The recombinant FNIII₇₋₁₀ fragment, however, isolates the biological activity to this integrin binding site, while the full pFN molecule contains additional sites that may affect the osteoblastic differentiation and bone healing responses. In addition, our *in vitro* results with a receptor-mimetic antibody and integrin binding analyses suggest that the passively adsorbed recombinant fragment is more active than the full native protein (Fig 1). This difference in biological activity could arise from difference in the structure/orientation of the adsorbed protein. Finally, it is worthwhile to note that the recombinant fragment lacks significant post-translational modifications (e.g., glycosylation) compared to the native protein which could influence its biological activity.

Importantly, this biomimetic surface approach utilizes a simple, point-of-care dip-coating of FNIII₇₋₁₀ to pre-sterilized Ti implants, a quick and versatile surface application conducted under physiological conditions that the surgeon can employ seconds before implantation. This single-step procedure, in turn, minimizes the chance of infection, reduces implant surface treatment variability, and minimizes cytotoxicity concerns inherent with covalent immobilization schemes, while maintaining the surgeon's dexterity. The more robust osseointegration demonstrated for FNIII₇₋₁₀-treated implants is expected to improve implant function and lifetime. Moreover, this straightforward coating protocol can be applied to virtually any dental and orthopedic implant

application. This FNIII₇₋₁₀ coating retains its bioactivity when dip-coated on a variety of other non-titanium material surfaces with different surface topographies, including other metals, polymers, and ceramics. Furthermore, it may be advantageous to employ this biomimetic coating in conjunction with other implant surface technologies such as surface topography/roughness, calcium phosphate coatings, bone morphogenetic proteins, and anti-inflammatory agents, in order to potentiate healing responses [228,229].

Summary

$\alpha_5\beta_1$ -specific FNIII₇₋₁₀ biomolecular coatings significantly enhance *in vitro* osteoblastic differentiation and implant osseointegration in a rat cortical bone model over full-length fibronectin coatings and the clinical orthopedic “gold standard”. Importantly, this biomolecular coating relies on simple physisorption of bioactive ligands onto biomedical-grade titanium as a simple, clinically-translatable, implant biofunctionalization strategy to enhance tissue healing responses.

CHAPTER 6

NANOSCALE CLUSTERING OF INTEGRIN-SPECIFIC LIGANDS MODULATES ADHESIVE ACTIVITIES AND IMPLANT OSSEOINTEGRATION

Introduction

Cell-biomaterial interactions are governed by cell adhesion via integrin receptors to surface ECM biomacromolecules [28,56,217,226]. Integrins are a widely expressed family of heterodimeric ($\alpha\beta$) transmembrane receptors that provide anchorage forces and trigger signals regulating cell survival, proliferation, and differentiation [16]. Integrin clustering is a critical step in the adhesive process by facilitating assembly of multiple cytoplasmic regulatory and structural proteins into critical supramolecular structures, termed focal adhesions [19,39,40]. These structures activate various intracellular signaling pathways that regulate gene and protein expression, migration, and differentiation and mediate strong adhesive forces [150]. Yamada and colleagues demonstrated that integrin binding (occupancy) and clustering can synergistically affect integrin-mediated cell function [230,231]. Monovalent ligand-integrin binding induced receptor redistribution but no cytoskeletal/signaling recruitment, whereas antibody-induced integrin aggregation in turn only promoted FAK recruitment – both occupancy and aggregation together were required for robust focal adhesion formation and signaling.

In order to investigate the effects of ligand clustering on adhesive processes and cell responses, studies have developed synthetic polymers presenting nanoscale clusters

of RGD ligands, albumin-RGD conjugates, and RGD-dendrimer systems [151-155]. Overall, these studies have demonstrated that ligand clustering at the nanoscale can play a large role in directing global cell migration, adhesion strengthening, spreading, and signaling. Furthermore, the relative nano-spacing of integrin-ligand interactions may be a critical element in this robust clustering effect on adhesive responses. Recently, Spatz precisely patterned RGD ligands and showed that focal adhesion formation, cell adhesion, and migration required close integrin spacing (<73 nm) [233]. Moreover, Erickson used beads coated with oligomeric constructs presenting multiple copies of the cell adhesive domain of FN to demonstrate that only trimers and pentamers (as opposed to monomers and dimers) of FN promote rearward cell movement and functional cytoskeletal-integrin connections [156].

While these studies have shed light on the importance of integrin clustering for adhesive processes, the application of these insights to designing functional biomaterials to control cell function and tissue responses has been thoroughly unexplored. Recent bio-inspired biomaterial strategies have focused on functionalizing biomaterials with full-length extracellular matrix proteins or short bioadhesive motifs, such as RGD – all with marginal success in promoting *in vivo* tissue healing [104-106]. Recent *in vitro* and *in vivo* work has demonstrated that integrin binding specificity ($\alpha_5\beta_1$ vs. $\alpha_v\beta_3$) regulates osteoblastic and myoblastic differentiation [17]. We've recently used multiple ligand presentation platforms to demonstrate that biomaterial coatings specific for integrin receptors regulate *in vitro* progenitor differentiation, and *in vivo* bone issue healing and implant integration [103,108,111,233]. Engineering of biomaterials using clustered ligands, including cyclic RGD dendrimers and polyvalent ligands, have been successfully

applied for drug targeting and therapeutics, as well as imaging applications [234-237]. However, critical limitations of these strategies include: 1) these clustered ligands lack precise control over valency (rely on “statistical averages”) , and 2) suboptimal integrin specificity with these primarily RGD-based systems. Given the importance of integrin specificity and integrin clustering individually to modulate key initial adhesive responses, we hypothesized that engineering materials that promote both of these parameters together may enhance integrin-mediated adhesive processes and, further, promote better implant osseointegration. In this study, we engineered biomaterial surfaces presenting well-defined densities of nano-clustered integrin-specific ligands, using the constructs designed by Erickson et al. that present one, three, or five copies of the $\alpha 5\beta 1$ -specific FNIII₇₋₁₀ ligand [156]. We demonstrate that ligand clustering and integrin specificity synergistically modulate integrin binding, adhesion strength, and implant fixation in bone tissue.

Materials and Methods

Multimer Preparation and Ligand Characterization

Recombinant multimeric FNIII₇₋₁₀ proteins (monomer, trimer, pentamer) presenting the central cell-binding domain of FN, were expressed as previously described [156]. Briefly, constructs of each multimer type were transformed into E.Coli BL21(DE3), and protein expressed by addition of 0.4 M IPTG at 6 hours. Cells were lysed with 0.1% TritonX-100 and 10mg/mL lysozyme. Lysate was centrifuged at 20,000 *g* for 15 minutes and the protein precipitated from the bacterial supernatant (40% for monomer, 30% for trimer, 20% for pentamer). Ammonium sulfate pellets were

suspended in column buffer (0.02 TRIS, 0.1 NaCl). Protein solutions were run over a Sephacryl 500 column (Amersham-Pharmacia), and peak fractions were run over a resource Q column (Amersham-Pharmacia). Proteins eluted at 0.22 M NaCl (pentamer, trimer) through 0.27 M NaCl (monomer). FNIII₇₋₁₀ was expressed in *E. coli* and purified as previously described [108]. Purified proteins were run on SDS-Page gels (non-reducing) showing a mixture of oligomers (trimer, pentamer). Bioactivity was assessed by ELISA with adsorbed multimer surfaces via an HFN 7.1 antibody, cell adhesion experiments, and integrin SPR experiments.

Titanium (Ti) and gold (Au) metal was obtained from Kurt J. Lesker Company Part #EVMTH137EXE (Clairton, PA) as pellets of 99.97% pure titanium. For *in vitro* assays, thin films of this titanium (100 Å) and gold (200 Å) were deposited onto clean glass coverslips using an electron beam evaporator (2×10^{-6} Torr) at a deposition rate of 1 Å/s. Slides were then immersed in a FNIII₇₋₁₀, monomer, trimer, or pentamer protein solution at various coating concentrations in PBS for 30 min for SPR adsorption and cell adhesion experiments. Surfaces were subsequently blocked with 1% heat denatured bovine serum albumin (BSA).

For the *in vivo* experiments, implants were machined from commercially pure, clinical-grade (grade 4) titanium rods (Titanium Industries, Inc., Cleveland OH) and poly(OEGMA) brushes grafted onto the surface as previously described [128]. Poly(OEGMA) brushes were polymerized by immersion into a solution of OEGMA (28.3 mmol), CuBr (1.6 mmol), 2,2'-dipyridyl (2.8 mmol) in a 1:4 mixture of MeOH and H₂O for 4 h. The resulting polymer brushes were 135 Å as determined by ellipsometry. For ligand tethering, brushes were first incubated in 4-nitrophenyl chloroformate (1.4 mmol

in THF), which “activates” the brushes for subsequent ligand tethering by replacing a portion of the hydroxyl groups situated at the end of the polymer brushes with nitrophenyl chloroformate (NPC). The activated brushes were then incubated in multimer or FNIII₇₋₁₀ solutions in PBS for 60 min to allow ligand tethering, and residual activated NPC sites were quenched in 20 mM glycine in PBS. Brush synthesis and functionalization reactions were verified by XPS (X-ray spectroscopy) and FTIR (Fourier Transform infrared spectroscopy). Ligand surface density measurements were obtained via surface plasmon resonance (SPR) using a Biacore X instrument.

Cell Source and Culture

NIH3T3 fibroblasts were used for initial bioactivity characterization and patterning experiments. MC3T3-E1 murine immature osteoblast-like cells (Riken Cell Bank, Hirosawa, Japan) were used principally for integrin binding and cell adhesion experiments because of their expression of multiple integrins, including $\alpha_v\beta_3$ and $\alpha_5\beta_1$. MC3T3-E1 cells were maintained at 37 °C in α -MEM supplemented with 10% FBS and 1% penicillin-streptomycin and passaged every 2-3 days via standard culture techniques prior to passage 8. Cells were split prior to 90% confluence, typically every 3 days.

Binding Site Accessibility and Integrin Binding Assays

To assess ligand accessibility to multimer-adsorbed surfaces, surface plasmon resonance measurements were conducted with soluble human $\alpha_5\beta_1$ integrin using a Biacore X instrument (Biacore, Piscataway, NJ). Briefly, Au-coated SIA chips (Biacore), were primed with sterile DPBS, and the baseline allowed to stabilize at a flow rate of 15

$\mu\text{l}/\text{min}$ in DPBS. Ligands were adsorbed for 30 min at a $8 \mu\text{l}/\text{min}$ flow rate, blocked with 1% heat-denatured BSA for 10 min, and then were washed with PBS at $10 \mu\text{l}/\text{min}$ and the signal allowed to stabilize for 5 min thereafter to measure adsorbed protein levels. Equimolar multimer surface densities were used for all integrin binding SPR experiments. A $200 \mu\text{g}/\text{mL}$ solution of soluble $\alpha_5\beta_1$ was flowed over the multimer-coated chips at $20 \mu\text{l}/\text{min}$ for 10 min in integrin-activating conditions (PBS + 1mM Mn^{+2}), the chips washed 3 times with PBS, and the baseline allowed to stabilize for 10 minutes. Resonance units (R.U.) were converted to surface density values ($10 \text{R.U.} = 1 \text{ng}/\text{cm}^2$).

Integrin binding levels (post 30 and 60 min adhesion) were assessed using a crosslinking/extraction/reversal procedure [172] on multimer-coated surfaces of equimolar densities of the FNIII₇₋₁₀ binding site. Surfaces were prepared by incubating gold-coated wafers (100 \AA Ti, 200 \AA Au) with an alkanethiol SAM solution of 1 mM hexadecanethiol ($\text{CH}_3[\text{CH}_2]_{15}\text{SH}$) (4 h). Adhesive ligands in PBS were then incubated on the activated supports for 30 min and 1% heat-denatured BSA for 30 min. MC3T3-E1 cells were incubated on surfaces in serum-free conditions (2mM Dextrose in PBS) for 30 or 60 minutes. The integrin binding procedure uses DTSSP to specifically crosslink integrins bound to their ligand. Cellular components are then extracted using detergent and protease inhibitors, and crosslinks are reversed and the once bound integrins are collected. Integrin levels were quantified by Western blotting using primary antibodies against α_5 integrin (AB1928, Chemicon; $0.5 \mu\text{g}/\text{mL}$), and α_v integrin (AB1930, Chemicon; $0.5 \mu\text{g}/\text{mL}$). Membranes were washed in TBS-Tween (20 mM Tris HCl pH 7.6, 137 mM NaCl, 0.1% Tween 20) for 45 min and incubated in secondary antibody (biotin-conjugated anti-rabbit IgG, 1:20,000 dilution in Blotto) for 1 h at room

temperature while rocking. Membranes were washed again in TBS-Tween for 45 min and incubated in a tertiary antibody (alkaline phosphatase-conjugated anti-biotin IgG, 1:10,000 dilution in Blotto) for 1 h at room temperature while rocking. After antibody incubation, membranes were washed in TBS-Tween for 45 min and immunoreactivity was detected using an ECF fluorescent substrate for 5-10 min. Bands were visualized using a Fuji Image Analyzer and further quantified and analyzed using Adobe Photoshop software.

Spinning Disk Adhesion Strength Assay

Micropatterned surfaces of 10 μm diameter circular adsorbed-multimer islands were created for a cell adhesion strength assay as previously described [150]. PDMS stamps were inked with a 1.0 mM hexadecanethiol (HDT) (in ethanol) solution, dried under nitrogen briefly, and brought into contact with clean gold-coated wafers for 15 seconds (100 g weight). The unstamped, bare gold areas on the substrate were “backfilled” with a 1.0 mM solution of EG₃ alkanethiol for at least 2 h. Substrates were then immersed in multimer protein solutions for 30 min at equal FNIII₇₋₁₀ surface densities as previously measured by SPR measurements, blocked with 1% heat-denatured BSA, and incubated in PBS for 1 hr. MC3T3-E1 cells were seeded on micropatterned substrates in D-MEM at 200 cells/mm² supplemented with 1% FBS (serum conditions) or 1% BSA (serum-free conditions) for 2 hrs.

Cell adhesion strength was measured with a spinning disk apparatus [Garcia, 97,98]. Cell-seeded substrates after 2 hrs were mounted on the device and spun for 5 minutes at various spinning speeds in 2mM Dextrose in PBS. Cells were then fixed in

3.7% formaldehyde, 1% Triton X-100, and stained with ethidium homodimer. Cells were then counted with an in-house imaging analysis at various radial positions using a Nike TE300 with a motorized stage. Sixty fields/sample were analyzed and counts normalized to number of cells present in the center of the wafer disks. The fraction (f) of adherent cells was fit to a sigmoid curve [$f=1/(1 + \exp[b(\tau - \tau_{50})])$] where τ_{50} is the shear stress for 50% detachment and a direct measure of adhesion strength and “ b ” is the inflection slope.

Implantation Procedure and Functional Analysis

Implantations into the tibiae of mature Sprague-Dawley male rats were conducted in accordance with an IACUC-approved protocol as described previously [49]. A day before implantation, Ti implants were soaked in de-ionized water for 30 minutes, and subsequently stripped of the existing oxide layer by submersion in 4% HF for 30 s. A new oxide layer was formed by incubation of implants in 35% HNO₃. This cleaning and re-growth of the oxide layer can be performed days before implantation as long as samples are subsequently kept clean. Poly(OEGMA) brushes were then grafted on clean Ti implants, and tethering of monomer, trimer, pentamer, or FNIII₇₋₁₀ was conducted on brush-grafted implants as previously described. Equimolar FNIII₇₋₁₀ densities were used (0.6 pmol/cm²) for all implantation studies. Prior to surgery, implants were incubated in a 0.1% azide solution to sterilize implants. Tapered Ti implants treated with FNIII₇₋₁₀ or the various multimers or unmodified Ti were press fit into the cortical defects. Two 2-mm diameter defects were drilled into the medial aspect of the proximal tibial metaphysis of each leg to achieve a total of four implants per animal. Implant locations (R/L leg, proximal/distal location) were randomized for each surface condition and a total of 27 rats were used. Three distinct post-implantation timepoints were assessed for implant

function: 10 days, 28 days (4 wks), and 3 months. 10 day and 4 wk timepoints were assessed for bone apposition via histological analysis. 4 wk and 3 month timepoints were assessed for implant fixation via mechanical pull-out testing. Proximal rat tibiae were explanted and either fixed in neutral buffered formalin for histology or wrapped in PBS to maintain moisture for immediate mechanical testing. Formalin-fixed tibiae were embedded in poly(methyl methacrylate), dehydrated, and stained with Sanderson's Rapid Bone Stain™ and a van Gieson counterstain. This stained mineralized bone (yellow-orange) and soft tissue and osteoid (blue-green). Bone apposition was quantified as the percentage of the implant's surface in contact with the bone, and 8 fields/implant were quantified (N=3,4 implants per condition). Pull-out testing was performed to quantify implant mechanical fixation to surrounding bone tissue using an EnduraTEC Bose ELF 3200. The ends of each excised tibia were secured using a customized holding apparatus and the exposed head of the implant attached to a load cell via a customized grip apparatus. Pre-loaded samples (< 2 N) were then subjected to a constant pull rate of 0.2 N/sec. The pull-out force (N), parallel to the long axis of implant, was the maximum load achieved before implant detachment or failure.

Statistics

Results are presented as mean \pm standard error. Quantification of *in vitro* and *in vivo* experiments was performed on all samples used in each experiment. Results were analyzed by ANOVA in SYSTAT 8.0 (SPSS). If deemed significant, pairwise comparisons were performed using Tukey's post hoc test and a confidence level of 95% was considered significant. *In vitro* assays were conducted in at least triplicate and replicated in two separate experiments.

Results

FNIII₇₋₁₀ Multimeric Ligand Purification and Assembly

Recombinant integrin proteins presenting one, three, or five “heads” of FNIII₇₋₁₀ were expressed from multimeric constructs originally developed by Erickson et al [156]. Three DNA multimeric constructs were developed to encode for three distinct protein elements, each assembling post-expression into a specific multimeric supramolecular protein presenting one (monomer), three (trimer), or five (pentamer) FNIII₇₋₁₀ ligands in a nano-clustered format. These recombinant constructs are schematically shown in **Figure 6.1 A**. Each construct encodes for a single FNIII₇₋₁₀ element at the N-terminus which is 14 nm in length, separated by a TN 3-8 spacer element (21 nm in length, 6 domains from tenascin FNIII 3-8). For the trimer and pentamer constructs, a short coiled-coil segment is placed at the C-terminus end to promote self-assembly with protein strands with like coiled-coil regions. Specifically, the trimer constructs use a short segment from the cartilage matrix protein (CMP) that forms a three-stranded coiled-coil [239], while the pentamer constructs incorporate a segment from cartilage oligomeric matrix protein (COMP), which forms a five-stranded coil. Monomer constructs contained no coiled-coil region. A schematic of the fully-assembled pentamer protein is shown in **Figure 6.1 B**. The TN spacer arms are linked to the other elements via short amino acid segments which afford flexibility in movement. These flexible linkers allow cells to control to a large extent the spacing between integrin-multimer interactions in order to promote ideal spacing. In addition, these TN spacers were optimized to remain non-adhesive, in effect conferring the only adhesive activity on each multimer to the FNIII₇₋₁₀ element. Once these constructs were transformed and protein strands expressed in *E.Coli*, multivalent

proteins were purified using anion-exchange chromatography as previously described [156]. Purified multimers were run on non-reducing SDS-Page gels, stained for HFM 7.1, and proper multimer assembly assessed. Gels showed three bands for the pentamer samples (intense band at the expected assembly MW, weaker band at $3/5$ the expected MW, and a weak band at $1/5$ the expected MW), two bands for the trimers (at the expected MW, and $1/3$ the MW), and one band for the monomers (data not shown). Although these gels demonstrate incomplete assembly for the trimer and pentamer, the most intense bands were present at the expected MW. Image quantification of these bands in ponceau stains showed $>80\%$ of the total band intensity were for the expected MW, and less than 20% for the “incomplete assembly” bands (data not shown). Moreover, previous characterization by electron microscopy demonstrated anywhere from 66% to nearly 100% of multimers possess the full complement of ligand “arms” and proper valency. Therefore, these results verify the large majority of multimers assembled correctly and with proper valency of ligand “arms”.

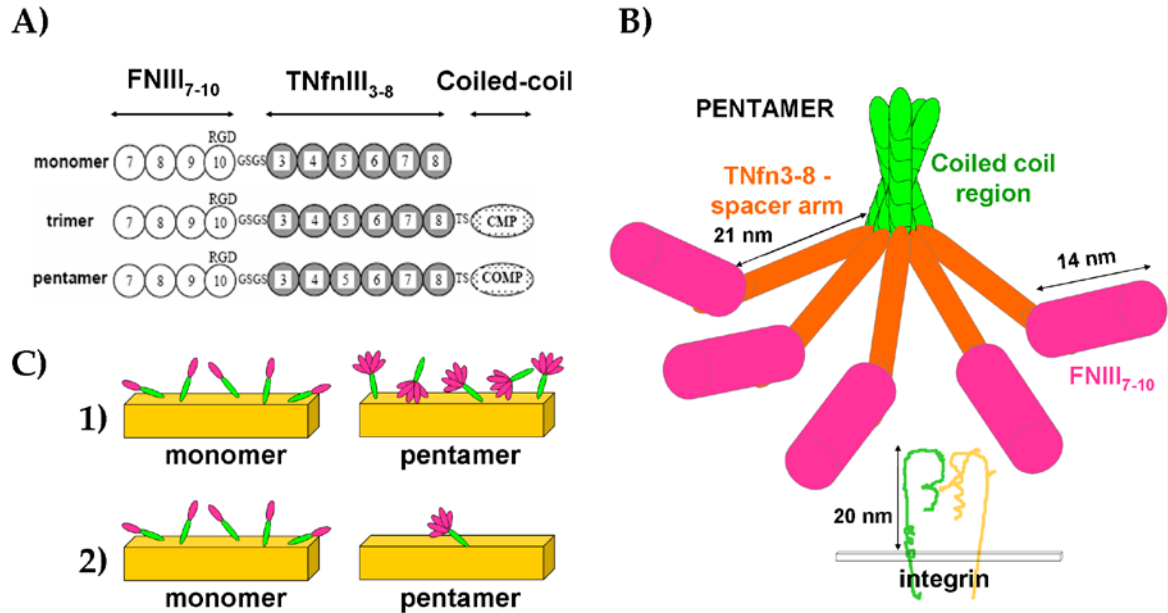


Figure 6.1. Multimeric integrin ligands with varying FNIII₇₋₁₀ valency. (A) Multimeric constructs consisting of FNIII₇₋₁₀ “head” at N-terminus, a “spacer arm” comprising the FN-III domains 3-8 from tenascin, and a distinct oligomerization sequence at the C-terminus (CMP for trimer, COMP for pentamer), (B) Schematic of 5-“headed” multimeric ligand (pentamer) interacting with integrins with key lengths highlighted, (C) **1)** Equimolar Multimer surface density, **2)** Equimolar FNIII₇₋₁₀ “Head” surface density.

Multivalent FN-mimetic Ligands Enhance Integrin-Specific Binding and Adhesion

To initially assess multimer bioactivity, an ELISA was performed on adsorbed multimer surfaces (gold-coated polystyrene) using a $\alpha_5\beta_1$ receptor-mimetic antibody (HFN 7.1). Antibody binding levels were > 50x higher than background controls for each multimer surface, verifying that expressed multimers display bioactivity. In order to more stringently assess integrin binding behavior and ligand accessibility, surface plasmon

resonance measurements were conducted whereby soluble human $\alpha_5\beta_1$ was flowed over passively adsorbed multimeric ligand SPR chip surfaces. An equimolar multimer surface density was used for each sample condition (**Figure 6.1C-1**) – therefore it was expected that trimer surfaces would bind three times the total integrin as monomer, etc. Total amount of $\alpha_5\beta_1$ mass bound to each multimer-adsorbed surface was quantified in integrin-activating conditions (PBS + 1mM Mn^{+2}) after several washes to remove loosely bound, non-specifically adsorbed integrins. We observed linear increases in soluble receptor binding with valency of multimers (**Figure 6.2 B**), indicating that binding sites in the multimeric proteins were accessible and, moreover, that the inter-ligand spacing was sufficient to support integrin binding without steric inhibition.

Next, we examined cell adhesive responses for surfaces coated with non-clustered monomers or nano-clustered pentamer ligands. For these subsequent experiments, we used equimolar FNIII₇₋₁₀ surface densities, in order to isolate the effect of increasing the nano-clustering of integrin-specific ligands, rather than overall ligand density, on cell activities. This equimolar FNIII₇₋₁₀ density (0.6 pmol/cm²) results in the total density of FNIII₇₋₁₀ remaining constant, but the spacing between ligands is theoretically different (**Figure 6.1C-2**). We chose this density as it was close to the saturation for adsorbed monomer and about half saturation for the pentamer surface (**Figure 6.2 A**). This density value represents a maximum of roughly 20% of the total surface area taken up by monomer assuming a full footprint – most likely these ligands do not adsorb at maximum possible footprint area, and so the total surface area adsorbed is probably much less than 20% at this molar density, i.e. not nearly a monolayer. Therefore, the total surface area taken up by monomer and pentamer at this molar density should be significantly less than

20%, and the ligand-ligand distance on each surface should be reasonable enough to uphold spatial clustering differences of each multimer surface. Integrin binding analyses were conducted on multimer-adsorbed SAMs of adhesive hexadecanethiol for MC3T3-E1 cells. Total $\alpha_5\beta_1$ binding was quantified at 30 min and 60 min post-seeding using an extraction/crosslinking/reversal technique [172]. This assay revealed that the pentameric construct enhanced $\alpha_5\beta_1$ binding by 2.5x ($p<0.003$) after 30 min and 2x ($p<0.05$) after 60 min compared to monomer-coated surfaces (**Figure 6.2 C**).

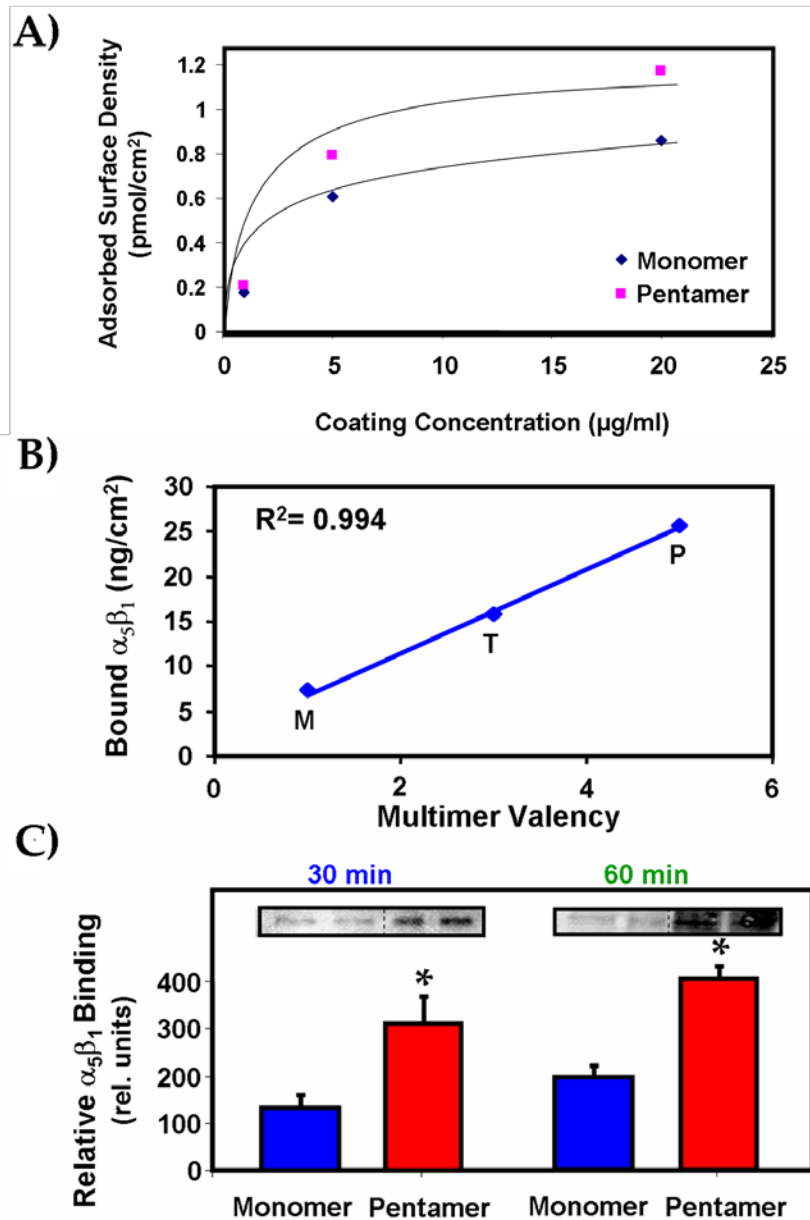


Figure 6.2. Nanoclustering integrin ligands augments integrin-specific binding. (A) Adsorbed surface densities as assessed by SPR of multimers on hexadecanethiol SAMs. (B) Integrin binding sites of multimers remain highly accessible and bioactive when randomly adsorbed on metal substrates. Soluble human $\alpha_5\beta_1$ was flowed over gold substrates adsorbed with multimeric ligands at equimolar multimer density in an SPR, washed, and amount of adsorbed integrin quantified, (C) Greater FNIII₇₋₁₀ “head” valency promotes more robust early integrin binding. MC3T3-E1 cells were seeded onto a SAM of hexadecanethiols adsorbed with equimolar FNIII₇₋₁₀ surface densities (0.6 pmol/cm²) of multimers for 30 or 60 min, then relative bound $\alpha_5\beta_1$ quantified using a crosslinking/extraction/reversal technique (Pentamer: 30 min, $p < 0.03$ vs. Monomer; 60 min, $p < 0.005$ vs. Monomer, N=4).

We next measured the adhesive force of cells to the multimeric ligands using a hydrodynamic spinning disk assay [150]. Multimers were adsorbed to hexadecanethiol alkanethiols on gold using microcontact printing. This technique afforded control over adhesive area while maintaining a consistent cell shape. For the circular island configuration used, cells at the center experience negligible force, while increasing centripetal force is applied as the radial position increases outward from the center towards the edge of the sample. A detachment profile of fraction adhered vs. radial position for each sample was made, from which a robust measure of adhesion strength was quantified called τ_{50} , or the shear stress which 50% of cells detach (**Figure 6.3 A**). Equimolar FNIII₇₋₁₀ surface densities were used for monomer and pentamer surfaces, and MC3T3-E1 cells were allowed to adhere in serum-free (-LPA) and serum (+LPA) conditions for 2 hrs before detachment via spinning disk. Cells adhered to pentamer FNIII₇₋₁₀ ligand surfaces exhibited a 30% enhancement in adhesion strength in serum-free conditions compared to the monomeric ligand surfaces (**Figure 6.3 B**). This enhancement was increased to 50% in serum conditions which contained LPA and soluble growth factors (**Figure 6.3 B**). Taken together, these *in vitro* results demonstrate our ability to engineer multimeric integrin-specific ligands that retain a specific multivalency and indicates that ligand clustering modulates integrin binding and adhesive force.

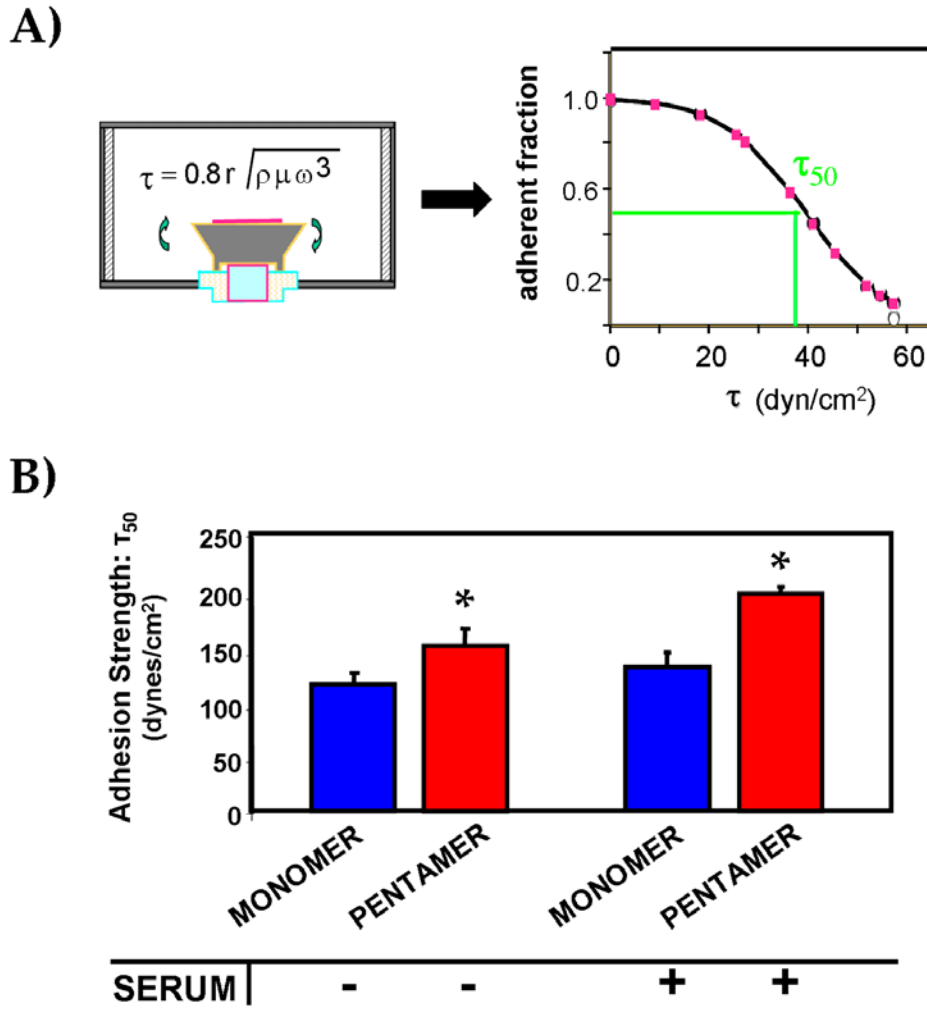


Figure 6.3. Nano-clustered integrin-specific ligands enhance cell adhesive strength. (A) To investigate the effect of integrin ligand clustering on cell adhesive strength, a spinning disk assay was employed which applies a linear range of detachment forces on each sample to obtain a measure of adhesion strength for the entire cell population on the sample, the τ_{50} . MC3T3-E1 cells were seeded on patterned adsorbed-multimer SAM substrates (equimolar FNIII₇₋₁₀ density) and allowed to adhere for 2 hours in serum-free (-LPA) and serum (+LPA) conditions. Samples were spun in a spinning disk apparatus for 5 minutes, and adherent fraction quantified, (B) Nano-clustered integrin-specific ligands enhance adhesive strength in both serum-free and serum conditions over non-clustered ligands. (Pentamer: Serum-free, * $p < 0.04$ vs. monomer; Serum, * $p < 0.002$ vs. monomer, N=7).

Multivalent FN-mimetic Ligand Coatings Enhance Early and Longer-Term Implant Osseointegration

We quantified osseointegration of implants in a rat tibia cortical bone model [49] to evaluate the *in vivo* effect of ligand clustering/spacing on tissue (bone) healing. This *in vivo* model provides a rigorous platform to evaluate implant coating function in a relevant orthopedic setting and has been used extensively in past studies [49,103]. Bioactive ligands were tethered to poly(OEGMA) brushes grafted onto clinical-grade titanium (Ti) to provide a robust, physiologically stable coating as previously verified (**Figure 6.4 A**) [103,111,128]. A major advantage of the poly(OEGMA) brush system described in this work is the ability to precisely control the presentation of tethered ligands. Increases in the density of tethered multimer on brushes on Ti yielded increases in available bioactive ligand *in vitro* (**Figure 6.4 B**). Implant coatings examined were (i) unmodified poly(OEGMA) brushes, (ii) unmodified titanium (as a reference to the current clinical treatment), and brushes modified with either (iii) FNIII₇₋₁₀, (iv) monomer, (v) trimer, or (vi) pentamer at equimolar FNIII₇₋₁₀ surface densities (0.6 pmol/cm²) (**Figure 6.4 B**). Equimolar FNIII₇₋₁₀ densities were used to afford direct comparison of ligand cluster size/organization on implant osseointegration. All implants were well-tolerated, and no complications were encountered during the course of the study. Following 10 days, four weeks, and 12 weeks of implantation, the rat tibiae were harvested and analyzed for bone-implant contact (10d, 4 wks) by histomorphometry and implant mechanical fixation (4 wks, 12 wks) by pull-out testing.

At 10 days post-implantation, a number of samples were harvested for histomorphometrical analysis, but many implants were dislodged from the bone during the

explantation process. Of those that survived, histological sections revealed few samples with extensive and contiguous bone matrix around the periphery of the titanium implants (**Figure 6.4 C**). However, the greatest amount of bone matrix was observed around pentamer-treated implants; less bone tissue was observed around the unmodified poly(OEGMA) brushes, and intermediate amounts around poly(OEGMA) brushes with tethered monomer and trimer ligands (**Figure 6.4 C**). The tissue present around all implants displayed a porous morphology (**Figure 6.4 C**). Histomorphometric analysis of histological sections demonstrated no statistically significant differences in bone-implant contact area among all implant surface conditions due to small number of intact implants. Nonetheless, pentamer and trimer-coated implants displayed the greatest quantified bone-implant contact area for than that for the unmodified poly(OEGMA) brushes and monomer (**Figure 6.4 D**). It is likely that, at this early timepoint, the full cycle for tissue healing, bone remodeling, and new bone formation may not be completed enough to manifest in significant differences in observable new peri-implant mineral. Moreover, the experimental forces that occur during tibial explantation may significantly disrupt the peri-implant architecture at this early timepoint.

However, at 4 wks, extensive and contiguous bone matrix was observed around trimer and pentamer-functionalized implants; noticeably less matrix was found around unmodified Ti and unmodified poly(OEGMA) brush implants (**Figure 6.5 A**). Monomer-treated implants also displayed fairly extensive matrix around the implant periphery, although not to the same extent as the trimer or pentamer, and the surrounding tissue was more porous. Histomorphometric analysis of histological sections demonstrated at least a

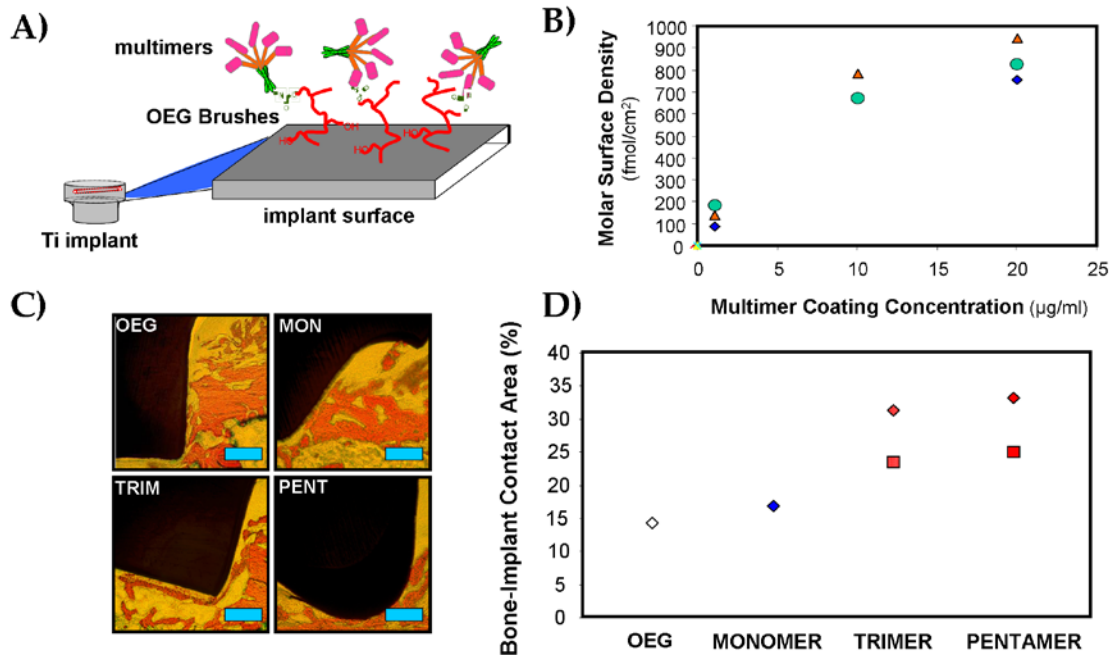


Figure 6.4. Nano-clustered ligand coatings targeting specific integrin receptors modulate early time-point (10 d) *in vivo* implant osseointegration. (A) Schematic of titanium (clinical grade) implant surface showing multimer-tethered OEG brushes. (B) Tethered densities of monomer, trimer, and pentamer on poly(OEGMA) brushes on Ti. Surface density on brushes was controlled by varying coating concentration and equimolar FNIII₇₋₁₀ density (0.6 pmol/cm^2) was used for implantation studies, (C) Representative histological sections at 10 d post-implantation showing bone (orange)-implant (black) contact (scale bar = 0.2 mm). Although most samples did not exhibit extensive peripheral bone formation at this timepoint, pentamer and trimer-treated implant surfaces exhibited more contiguous bone tissue formation and connectivity compared to other surface treatment conditions, (D) Quantification of bone-implant contact area showing individual sample values. Bone apposition was quantified from histological sections as the percentage of the implant's circumference in direct contact with bone tissue. Multiple slices of the same implant were averaged.

2.5-fold enhancement in bone-implant contact area for multimer-functionalized implants compared to the unmodified poly(OEGMA) brushes ($p < 0.009$); **Figure 6.5 B**). Notably, the bone-implant contact area for the pentamer group was significantly higher than that of the monomer-modified group ($p < 0.04$). Importantly, the bone-implant contact area for the monomer and FNIII₇₋₁₀-treated implants were nearly identical, indicating no loss of *in vivo* function for FNIII₇₋₁₀ presented in this TN spacer format. No evidence of multi-nucleated cells, foreign body giant cells, or fibrous capsule was observed in any of the sections. These findings demonstrate that nano-clustered presentation of integrin-specific ligands enhances implant integration compared to non-clustered ligand coatings.

Mechanical fixation was used as an outcome measure of functional osseointegration. Pull-out mechanical testing at 4 wks revealed significantly higher mechanical fixation of the multimer-functionalized implants over unmodified poly(OEGMA) brushes ($p < 0.01$; **Figure 6.5 C**), verifying the stability of the brush system used in this study. Increasing ligand clustering was a statistically significant trend resulting in increased mechanical fixation. Remarkably, at 12 wks, pentamer-functionalized implants exhibited an even greater 2.4-fold enhancement in fixation over monomer-tethered implants ($p < 0.002$) and approximately a 4-fold improvement compared to the unmodified poly(OEGMA) brush coating ($p < 0.001$; **Figure 6.5 C**). While not statistically significant, trimer-functionalized implants displayed a 2-fold enhancement in fixation compared to monomer-treated as well as unmodified titanium implants. Taken together, these results indicate that control over ligand spacing, in conjunction with integrin specificity, can modulate bone healing and *in vivo* tissue healing responses.

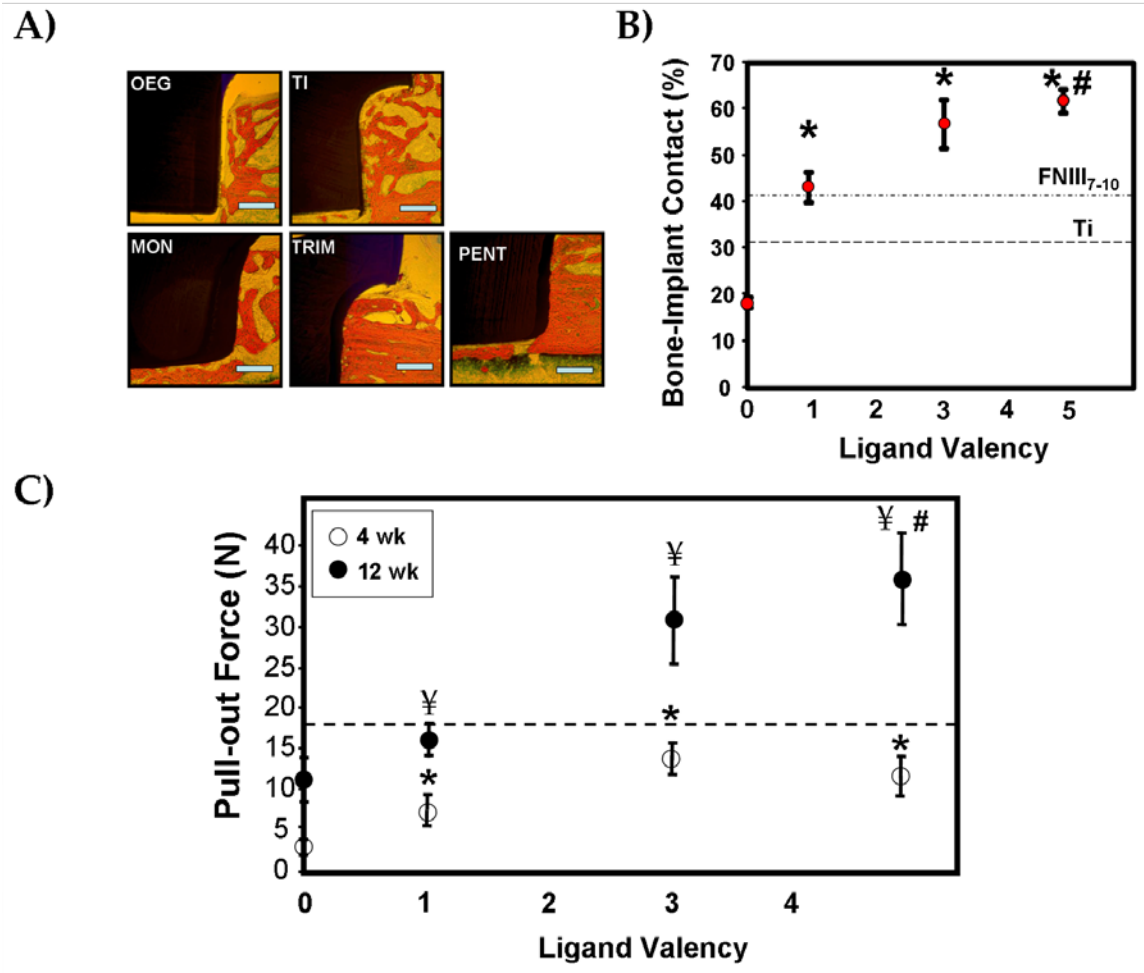


Figure 6.5. Nano-clustered ligand coatings targeting specific integrin receptors enhance functional *in vivo* implant osseointegration at 4 and 12 wks. (A) Representative histological sections at 4 weeks post-implantation showing bone (orange)-implant (black) contact (scale bar = 0.2 mm). (B) Quantification of bone-implant contact area. Pentamer-treated coatings enhanced bone-implant contact at 4 wks significantly over monomer and non-treated brush coatings (Pentamer: # $p < 0.04$ vs. Monomer, * $p < 0.0001$ vs. OEG; Trimer: * $p < 0.0001$ vs. OEG; Monomer: * $p < 0.009$ vs. OEG) (N=3,4 each condition). (C) Functional osseointegration as determined by pull-out force. Equivalent density of total FNIII₇₋₁₀ binding sites were used. Dotted line is 12 wk Ti-serum condition. There were 4-8 different implants for each surface condition (Pentamer: # $p < 0.002$ vs. Monomer, P/T/M: ¥ $p < 0.01$ vs. OEG; P/T/M: * $p < 0.01$ vs. OEG).

Discussion

The development of novel biomaterials presenting biomimetic bioactive ligands for implantable devices is an emerging field that has yielded various success *in vitro*, but elicited marginal improvements *in vivo*. Recently, we demonstrated that bioactive coatings conferring high integrin specificity for $\alpha_5\beta_1$ significantly enhance osteoblast differentiation and implant osseointegration and bone healing [103,108,111,233]. This macroscale parameter may be critical as activation and binding of specific integrin combinations can promote signaling pathways affecting a specific downstream cell phenotype. Aside from receptor specificity for ligands, many recent experimental *in vitro* studies using nanoscale clusters of RGD ligands on multifunctional polymers, microspheres, and dendrimers have shown that ligand organization clearly has a role in integrin clustering and initial cell adhesive responses, including migration, adhesion, and even cell growth [151-155]. Moreover, many natural ECM ligands *in vivo* exist as multivalent structures, including tenascin-C, polymerized fibers of FN and collagen, which drive strong integrin aggregation [16,240]. In the present work, we developed material surfaces functionalized with controlled densities of multivalent constructs presenting exactly one, three, or five copies of the $\alpha_5\beta_1$ -specific FN fragment, FNIII₇₋₁₀, in order to examine the nanoscale role of ligand clustering on integrin-specific binding, adhesion, and *in vivo* tissue responses to implanted devices. Past nano-clustered ligand designs relied on imprecise ligand cluster sizes and non-specific integrin ligands. A major strength of these multimeric constructs is the exclusive control over ligand valency (number of ligands in a cluster) and the directed targeting of a specific, osteogenic integrin receptor. Moreover, for *in vivo* experiments, the robust polymer brush strategy

employed offered stringent control in a physiological environment over ligand density and presentation [128]. Importantly, presentation of these precise multivalent integrin-specific ligands on robust, physiologically stable brush coatings on titanium implants afforded an accurate *in vivo* comparison between ligands of different valency. Our results demonstrate that the nanospatial organization of bioadhesive ligands on material surfaces can directly modulate *in vivo* tissue healing, and provides mechanistic insights into how ligand organization at a nanoscale directs specific integrin-mediated adhesive responses. Indeed, bioactive surfaces presenting clusters of at least 5 integrin-specific ligands significantly enhanced *in vivo* implant integration after both 4 weeks and, even greater, after 12 weeks post-implantation. This functional effect may be partially resultant from enhanced adhesive responses of endogeneous progenitor cells at initial adhesion times on clustered ligand (N=5) surfaces, perhaps reflected in the *in vitro* increase of overall $\alpha_5\beta_1$ binding and adhesion strength for multiclustered ligands in this study.

Previously, we attributed the enhanced bone formation of the $\alpha_5\beta_1$ -specific monovalent titanium coatings to increased osteoprogenitor cell recruitment and subsequent integrin-mediated differentiation. In this study, the considerable improvement in implant integration of the multivalent integrin-specific surface over the previously used monovalent integrin-specific FNIII₇₋₁₀ surface is a unique and exciting finding; however, the molecular mechanisms underlying this functional effect are not presently fully clear, although many theoretical models and experimental studies offer relevant explanations. Maheshwari et al. showed that, for equivalent total density surfaces, RGD clusters of 9 ligands increased fibroblast adhesion by twofold [152]. In this study, we demonstrated that constructs presenting 5 integrin-specific ligands in close nanospacing

(pentamer) increased adhesion strength by 50% over unclustered, randomly spaced ligands. This experimental result is supported very closely by a number of force simulations and computational adhesive models simulating ligand/integrin clustering effects. Gallant et al. predicted using a simple force simulation based on spinning disk experimental data and a mechanical equilibrium analysis that integrin clustering could provide a 60% enhancement of adhesive force compared with uniformly distributed bonds [150]. Brinkerhoff developed a 2-D Monte Carlo model of the cell-surface interface and predicted a 35% increase in adhesive strength for 2-fold greater ligand cluster sizes due mainly to increases in integrin binding [241,242]. Two proposed mechanisms ascribing an increase in adhesion strength are increasing the affinity of receptor for ligand (affinity modulation) and an overall increase of integrin-ligand bonds. In a mathematical model of affinity modulation, receptors in clusters were assigned a greater affinity for ligands, so as ligand cluster size increased, receptors that randomly diffuse next to the cluster receive this higher affinity and bound tighter to ligands [243]. This effect was proposed to be due to integrin dimerization, or “partner switching” – the switching of bonds between neighboring integrins due to weak dimerization. The separate simulations by Brinkerhoff et al. and Dinner et al. show that the amount of ligand binding and integrin clustering are increased significantly when ligands are organized in clusters, mainly due to integrin dimerization, which is believed to occur in vivo as well [242,244,245]. Likewise, using a two-state binding energy model, Irvine concluded that small changes in the binding energy due to localize integrin interactions caused by dimerization or initial clustering can significantly increase overall receptor binding to ligands. Our experimental results demonstrate an over 2-fold increase in $\alpha_5\beta_1$ binding for

clustered (pentameric) ligands over monovalent ligands, which, according to adhesion models of avidity modulation, could easily manifest in the corresponding increase in adhesion strength. Hence, our results support several aspects of these aforementioned theoretical models and simulations. Furthermore, we've utilized a well-controlled experimental platform to test the functional significance of these theories *in vivo* through use of this precisely tailored multivalent integrin-specific construct and robust OEGMA brush presentation system – demonstrating a robust role of ligand clustering in regulating *in vivo* bone healing.

A major finding of this study is the direct correlation of ligand valency with adhesive responses and *in vivo* healing, which may be of significance for bioactive material engineering. However, before directly applying these results towards design of novel biomimetic materials, a further discussion of two important design parameters - spacing between ligands within a cluster and cluster size - of ligand clustering is required. Most previous studies using nano-clustered ligands involve such large ranges of intracluster ligand spacings, few conclusions can be taken from them regarding optimal spacing range. Interestingly, Spatz alluded to a top spatial ceiling of 73 nm for optimal focal adhesion formation and adhesive function [232]. Brinkerhoff et al. simulated that ligand spacing less than 9 nm would result in negative steric effects, while ligand spacings over 21 nm would decrease the pro-clustering dimerization and binding energy effect previously discussed [242]. Notably, in this study, the multivalent constructs employ flexible linkers that allow the ligands to move within a compliant range of 10-48 nm, yet the lengths of FNIII₇₋₁₀ arms restricts the upper spacing ceiling toward an optimal range, according to these aforementioned experimental and simulation studies. Hence,

these bioactive constructs may afford the ideal theoretical spacing necessary for optimal integrin binding, clustering, and adhesion strength. Notably, our results justify that this particular range of ligand spacing can result in functional increases in adhesive responses and local tissue healing *in vivo*, further contributing to our understanding of important design parameters which affect the rational design of biomimetic materials for directed cell and tissue response. Finally, Brinkerhoff et al. proposed an optimal cluster size of ~ 9-16 ligands, while Irvine proposed an ideal cluster domain of 10 ligands to optimize steric and energy considerations [242,243]. Since this study used constructs from 1- 5 ligands/cluster, and since 5 ligands/cluster provided the maximum functional effect, it may be prudent in future studies to design ligands that assemble even large cluster sizes. Again, the modular construct design used here lends ease to this process through simple replacement of the coiled-coil region with a coil peptide of increased valence via recombinant protein engineering. Recently, several small oligomerization sequences have been identified that bind 7 and even 9 other members, creating the distinct possibility of studying even larger cluster sizes with the same precise valency and ligand presentation schemes used in this study.

Summary

Using these multivalent integrin-specific constructs and a robust polymer brush system, we have provided an experimental link to further elucidate our knowledge of the roles of integrins and nanoscale ligand organization on initial and long-term cell and tissue responses. We have been able to demonstrate that nanoscale ligand organization can regulate osteoblast adhesive processes and modulate *in vivo* bone healing and implant osseointegration. This study identifies a robust material parameter, ligand nanoscale

organization, that may be particularly relevant for designing biomedical devices and tissue constructs for directed tissue responses and regenerative medicine applications.

CHAPTER 7

SUMMARY AND FUTURE CONSIDERATIONS

Introduction

This study utilized integrin-specific ligands derived from the major ECM protein fibronectin to direct osteogenic differentiation of osteoblast-like cells and stromal cells, as demonstrated in Aim 1. Using robust ligand presentation systems that afforded control over ligand density and minimized non-specific protein adsorption, the functional effects of this integrin-specific ligand compared to RGD, FN, and RGD-based peptides were assessed. This study investigated not only the macroscale design parameter of ligand specificity for integrin receptors, but also the functional effects of nano-scale ligand spacing in unison with integrin specificity. Multimers of FNIII₇₋₁₀ functionalized material surfaces directed mainly $\alpha_5\beta_1$ -mediated adhesion and promoted greater osteogenic signaling, gene expression, and mineralized matrix over FN-derived ligands which directed less robust $\alpha_5\beta_1$ binding. This study investigated not only the macroscale design parameter of ligand specificity for integrin receptors, but also the adhesive and *in vivo* osteogenic effects of nano-scale ligand spacing in unison with integrin specificity. Multimers of these integrin-specific FNIII₇₋₁₀ ligands promoted greater integrin-mediated adhesion strength and implant osseointegration than monovalent ligands. This study is significant because it examines both this macro-scale (integrin specificity) design parameter individually as well as in unison with this nano-scale parameter (ligand spacing) both *in vitro* and *in vivo*.

Discussion

Fine-Tuning Integrin Specificity

Since this research demonstrates that ECM-derived ligands that direct integrin binding may be a robust strategy to direct in vitro cell response, it may be relevant to apply this strategy to non-orthopedic tissues to explore possible ligands that direct binding of non-bone integrin combinations. There are many examples of integrins uniquely involved in healing and development of specific tissues and cell systems. For example, $\alpha_M\beta_2$ has been shown to mediate adhesion of macrophages on various surfaces [53,54]. Controlling the body's response to foreign materials while promoting a specific tissue healing response is the "holy grail" of biomedical engineering research. Material coatings functionalized with multiple integrin ligands that target two or more biological pathways may improve the ultimate in vivo efficacy of biomaterials. For instance, functionalizing implants with both osteogenic integrin-specific ligands and macrophage-specific ligands that direct adhesion of a pro-healing population of macrophages may synergistically create a more powerful healing microenvironment. The research in Aim 1 establishes a number of ligand presentation platforms that effectively allow accurate comparison of functional effects between different integrin ligand-functionalized surfaces for virtually any cell system. Growth factor receptors have also been demonstrated to actively associate with activated integrins to partially direct integrin-mediated signaling, cytoskeletal arrangement, and cell proliferation [246]. Previous studies have focused solely on engineering RGD (non-integrin specific) and GF ligands in order to direct cell response [152]. Engineering controlled mixed ligand surfaces of particular growth factor receptors and integrin-specific ligands would not only contribute to our understanding of

receptor-driven function, but may augment directed cell and tissue healing over single ligand surfaces.

Moreover, improving the integrin specificity of biomimetic ligands may be an effective way to improve the benefits of this material strategy. Currently, scale-up, immunogenic, and non-specific binding concerns limit the widespread clinical applicability of this integrin-specific surface strategy. This study demonstrated several processing and purification advantages of using a recombinant approach to engineering these ligands. One important advantage not thoroughly utilized in this research is the ability to conduct structure-function studies to improve integrin-affinity and specificity, reduce ligand size (and hence afford greater surface density), and allow other tethering schemes, as well as contribute to fundamental research on ligand-receptor binding mechanisms. Using site-directed mutagenesis to alter various residues on the FN9 and FN10 portion of the FNIII₇₋₁₀, including flanking sequences to the PHSRN and RGD sites would give us more precise insight into $\alpha_v\beta_3$ and $\alpha_5\beta_1$ -ligand binding and cellular effects of varying binding specificity and affinity.

As recent studies have also indicated that physical surface properties may affect integrin-mediated adhesion and signaling, further studies implementing this integrin specific strategy in unison with surfaces of varying roughness and nanotopographies may be beneficial. Keselowsky et al. recently demonstrated that surfaces of increasing micro-scale roughness promoted greater $\alpha_5\beta_1$ binding and FAK phosphorylation in osteoblasts on FN-adsorbed surfaces [70]. We showed in this study that, on relatively smooth titanium surfaces, physisorbed FN promoted reduced $\alpha_5\beta_1$ binding, signaling, and osteogenic differentiation than FNIII₇₋₁₀ adsorbed surfaces at equimolar ligand densities.

Moreover, since saturated surfaces of adsorbed FNIII₇₋₁₀ result in greater molar densities than adsorbed FN, there may be a robust synergistic effect between surface roughness and integrin-specific ligands given that rougher surfaces have greater surface areas than smooth surfaces. Surfaces of varying linear nanotopographies (FN-adsorbed) have also been recently exhibited to directly modulate myoblast differentiation [247]. It is not a stretch to hypothesize that using FNIII₇₋₁₀ and other integrin-specific ligands on these surfaces may produce an even more enhanced cellular effect.

Exploring Clustered Ligand Presentation

In addition to examining integrin specificity, this research demonstrates that ligand clustering can modulate both in vitro and in vivo cell and bone tissue responses. However, the molecular mechanisms behind these global responses are unknown. Careful examination at the protein and even molecular level of why this ligand clustering effect is so robust is necessary for our fundamental understanding of material-cell interactions as well as to potentially improve the efficacy of these surfaces in the future. Functionalizing OEG brushes with these multimers would afford in vitro characterization of the functional cellular effects of integrin-specific ligand clustering. Integrin subunit-blocking antibodies and integrin immunostaining would be necessary to determine the extent of integrin-mediated adhesion and downstream cell function as a result of ligand valency. Extent of integrin clustering, which is believed to be the main mechanism responsible for the enhanced functional effect, could be estimated by conducting integrin binding analysis and focal adhesion immunostaining side-by-side, and counting FA number and size for each surface. It would have to be assumed that most bound integrins at later

timepoints are involved in these FA clusters and the staining would have to clearly indicate individual FAs. Analyzing the integrin clustering and subsequent signaling effects of multimer-functionalized substrates is critical to our understanding of how these material design parameters can be exploited for directed cell and tissue responses.

Elucidating *In Vivo* and *In Vitro* Mechanisms

Importantly, this study demonstrates that these integrin-specific coatings significantly enhance implant osseointegration and peri-implant bone formation, and this effect can be further heightened by introducing clustered ligand presentation, and finally that the density of ligand itself is an important design parameter affecting tissue healing response (Aim 2 + 3). While this is a clinically exciting result and relevant to biomaterial engineering for directed tissue response, the exact *in vivo* mechanism governing these results is unclear. In fact, few biomaterial-related studies have revealed any great insight into how ECM-inspired materials affect physiological both the cellular response and overall tissue-level healing and remodeling. An experimentally supported mechanism is that mesenchymal cells adhere and proliferate on integrin-specific surfaces, and attract distinct populations of osteoprogenitors to the area by secreting chemotactic factors, or creating a favorable osteogenic microenvironment [75]. This mechanism has been partially supported through FN-adsorbed implant studies showing a chemoattractive *in vivo* effect at early times post-implantation (< 3 days) [75]. Furthermore, a potent chemoattractive protein for mouse calvaria, but not monocytes (osteoclast precursors) was found in demineralized bone matrix [249]. Exploring the *in vivo* mechanism of these integrin-specific surfaces is critical to our understanding of how designed materials affect

tissue function, at both a cellular and tissue level. Elucidating these mechanisms is not an easy task, but can be accomplished through various imaging, material, genetic, and in vitro experiments.

Preliminary in vitro experiments examining possible osteogenic/chemoattractive soluble factors secreted by cells on distinct integrin-specific surfaces provide initial insight into this mechanism. Stromal cells were seeded on separate surfaces of equimolar FNIII₇₋₁₀ and RGD on mixed SAMs, and, after a 3d incubation, media was transferred to dishes of the different surface for 3 more days before quantification of alkaline phosphatase activity. Cells on RGD surfaces supplemented at 3d by FNIII₇₋₁₀-incubated media displayed higher 7d activity than RGD surfaces incubated in the same media for the entire 7 days, indicating that factors in the FNIII₇₋₁₀ cell media may promote a more robust osteogenic response than RGD cell media (unpublished) (**Figure 7.1**).

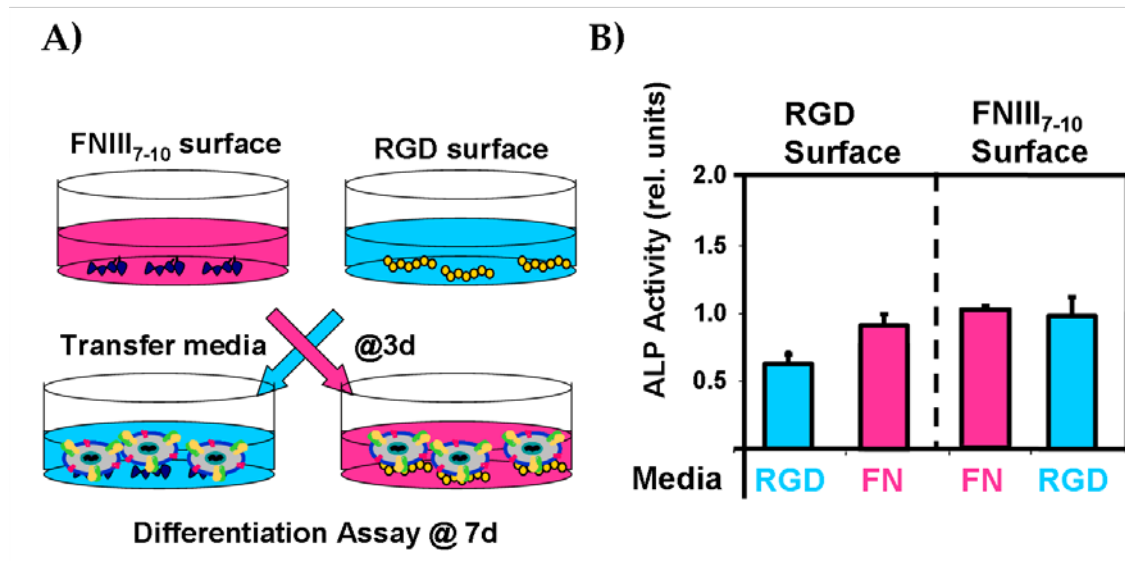


Figure 7.1. Preliminary paracrine experiment examining osteogenic role of media soluble factors of cells on different integrin-specific surfaces. A) Stromal cells on equimolar (0.2 pmol/cm^2) densities of FNIII₇₋₁₀ or RGD (mixed SAMs) were seeded for 3 days, media exchanged, and alkaline phosphatase activity assessed at 7 d. B) Media from cells on FNIII₇₋₁₀ surfaces promoted greater activity for cells on RGD surfaces than no media exchange.

This initial experiment lays the groundwork for more detailed experiments that could examine various surface densities, mixed ligands, time points, and cell densities that may all contribute to this potential soluble osteogenic effect from cells adhered on integrin-specific substrates. Further experiments would also need to examine co-culture effects (migration, differentiation) using Boyden chamber assays and subsequent testing of media for chemotactic and osteogenic factors via protein chips and mass spectrometry. Integrin subunit-blocking experiments would demonstrate if any significant soluble effect detected is integrin-mediated. It would be interesting to see if the factors found in

abundance could be formulated into an artificial media, or if FNIII₇₋₁₀ cell media alone could promote differentiation of cells on normally non-orthopedic materials, such as polystyrene, in order to isolate the relative roles of physical adhesion and soluble factor environment on maintaining directed cell function. The time-dependence of any functional effects would also need to be closely examined. Furthermore, the impact of cell-cell communication may be studied using micro- and nano-patterning techniques that afford control over cellular contact with other cells. It is possible to even pattern islands of different ligands on the same surface to investigate cell-cell, and paracrine factor effects while controlling cell shape and area [238,249].

The idea of “memory” in cell adhesion is a pertinent but thoroughly uninvestigated notion that may be particularly relevant to the *in vivo* success of this surface strategy. The time-dependent exposure of cells to different integrin-specific ligand and densities may be a critical part of the *in vivo* mechanism, since most serum and blood-borne proteins that adsorb to implant surfaces are primarily $\alpha_v\beta_3$ -specific (VN, FN, etc.) and may replace or degrade $\alpha_5\beta_1$ -specific ligands on implants soon after placement in the body [3,4]. Studying the time-dependent effect of distinct ligand exposure on the same cell population *in vitro* may be important to understanding *in vivo* ligand-cell interactions. Recently, del Campo et al. designed a caged cyclo(RGD) peptide which is UV-phototriggerable and non-bioactive in the dark [250]. However, exposure to 365 nm light cleaves the cage and renders the peptide bioactive. We have engineered mixed SAM surfaces with this caged RGD peptide in controlled densities, and demonstrated our ability to control cell adhesion, ligand density at different post-cell seeding time points, and a functional effect of time-dependent exposure of RGD density

(“adhesive temporal threshold”) on myoblast proliferation and differentiation (**Figure 7.2**). We can further use this caged ligand system to study time-dependent effects of integrin specificity on cells to model potential *in vivo* mechanisms in a controlled *in vitro* setting. Mixed ligand surfaces of FNIII₇₋₁₀ and caged RGD would be prepared, and stromal cells seeded initially exposed to FNIII₇₋₁₀, but at various timepoints exposed to uncaged RGD as well. Further experiments could include density-dependent effects on signaling and differentiation (high FNIII₇₋₁₀, low RGD; low FNIII₇₋₁₀, high RGD, etc.). This system could possibly be further applied *in vivo* in a hydrogel-like subcutaneous mouse model, with varying time-dependent exposures to RGD on mixed ligand FNIII₇₋₁₀ gels.

Many of these fundamental *in vitro* experiments cannot be recapitulated *in vivo*, but alternate experiments can be performed to further illuminate implant-tissue mechanisms. Tissue-specific integrin knockout mice have been proposed using the Cre-Lox promoter system that may be able to reduce or eliminate β_1 or β_3 only in isolated bone tissue. Integrin-specific ligand implants can be placed in these mice and the *in vivo* role of integrin-mediated tissue healing on these surfaces can be more closely examined via pull-out testing and histomorphometric analysis.

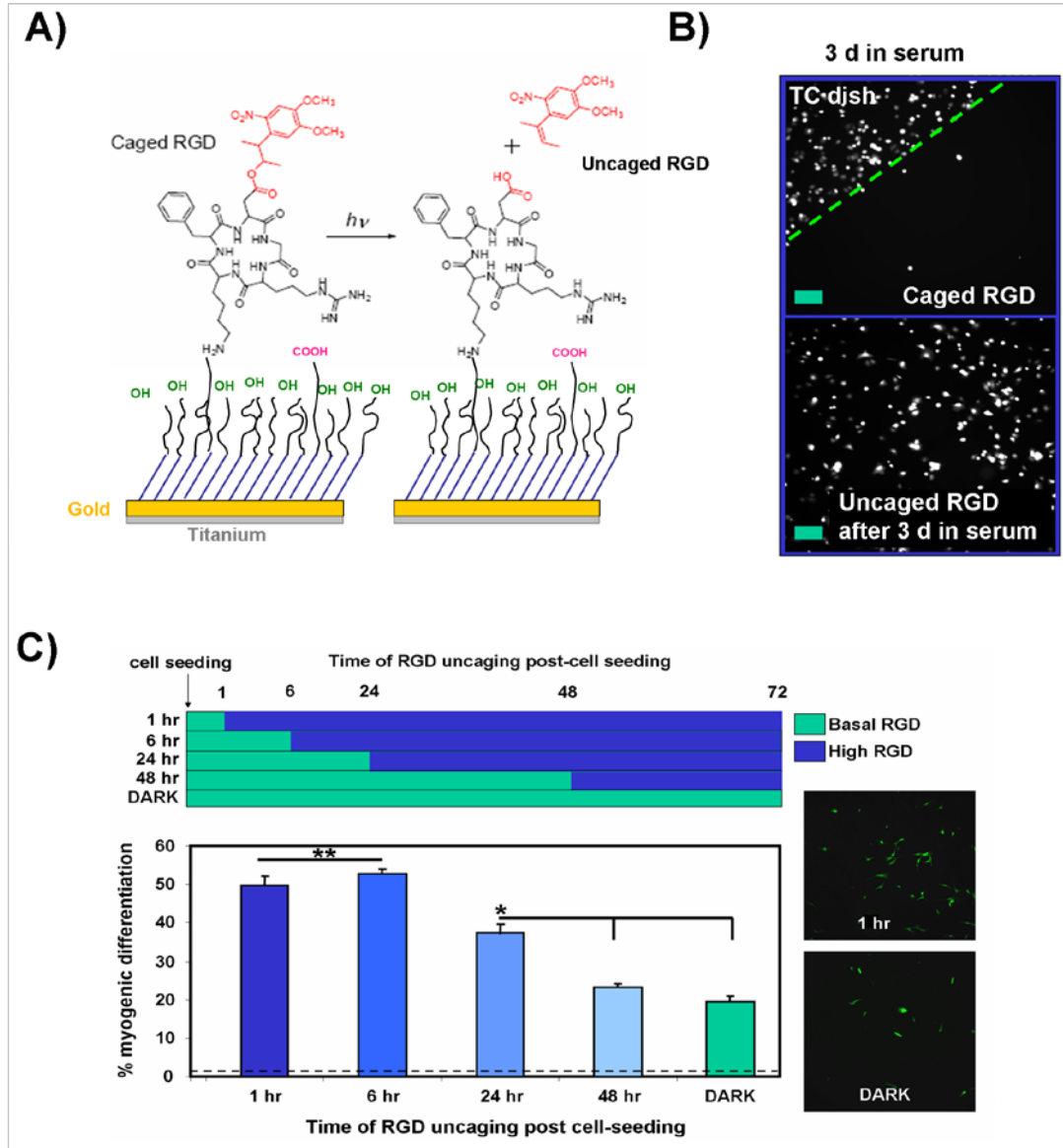


Figure 7.2. Caged cyclo(RGD) peptide system for assessing time-dependent effect of ligand exposure on cell function. A) Schematic of caged cyclo(RGD) on mixed SAMs for controlled peptide density and presentation, B) Caged RGD surfaces remain non-adhesive after 3d incubation in serum, and exposure to UV light renders surface adhesive, C) Time-dependent uncaging and exposure to high RGD density modulates myoblast differentiation, as assessed by sarcomeric myosin staining. Each surface contains a “basal” level of tethered linear RGD (0.8 pmol/cm^2) to maintain adhesion throughout the experiment. “Uncaged” surfaces exhibit “high” density of approximately 3.6 pmol/cm^2 RGD.

Expanding Beyond 2D: Three-Dimensional Cell-Material Interactions

Although 2-D coatings have been primarily used in this study, an abundance of clinical applications rely on 3-D scaffolds and porous coatings for orthopedic healing and regeneration. Recent studies have suggested that cells behave quite differently in 3-D environments than 2-D [251]. Examination of these integrin-specific surfaces in 3-D physical environments would be an important initial step toward application of this integrin-specific strategy for these tissue regenerative purposes. These ligands could be tethered in 3-D hydrogels using standard peptide tethering chemistries (such as EDC/NHS) or SANPAH, or even 'click' chemistries. The examination of the osteoinductive effect of functionalizing these gels with ligands of varying integrin specificity could be tested fairly easily *in vitro* with migration studies and confocal immunostaining. Implanting into subcutaneous animal models would be a controlled and effective way of examining the *in vivo* impact of 3-D presentation of these ligands. Moreover, as BMP has been shown to augment osteoinductivity, fashioning these gels with soluble BMP either in drug-eluting microcarriers or bioactively tethered may improve the overall efficacy of this material strategy [252]. Utilizing these integrin-specific ligands in unison with other osteogenic factors may indeed be a useful strategy to study the fundamental interaction between different signaling pathways both *in vitro* and *in vivo*. Another reasonable direction is the creation of even more long-lasting and effective tissue interfaces. Recently, Phillips et al. formed *in vitro* fibrous-bone interfaces by seeding scaffolds with a spatial density gradient of Runx2-encoding retrovirus [253]. It may be possible to use dip-coating of FNIII₇₋₁₀-related ligands to create reverse gradients on virus-gradient surfaces to encourage more precisely graded bone-cartilage

interfaces. Since we demonstrated that bone formation *in vivo* was related to ligand density, coating in different concentrations of FNIII₇₋₁₀ may produce an even more precisely graded interfaces.

Assessing Clinical Coating Stability

Finally, elucidating how stable these integrin-specific ligand surfaces actually are in the body is another critical fundamental question that remains unanswered. The OEG brushes used in this study are very robust *in vitro* in physiological environmental conditions, but the time-dependent *in vivo* stability is unknown. Moreover, all cells will begin remodeling their surfaces very quickly (within 48 hours) *in vitro*. Therefore, how long endogeneous cells actually interact with these ligand-functionalized surfaces, and how long these surfaces remain integrin-specific, are important issues that would contribute greatly to our mechanistic insight. To investigate, FNIII₇₋₁₀ ligands can be either genetically modified via protein cloning to express physiologically stable fluorescent markers (GFP), or chemically altered to tether imaging markers, possible even including quantum dots. The degradation of surfaces and ligands can be visualized and monitored *in vivo* to obtain a greater idea of the time-dependent stability of these surfaces. Biotin-tethered ligands can only be quantified after explantation, which may shear off much of the protein layer and give inaccurate measurements.

Notably, this integrin-directed response was still elevated on adsorbed integrin ligand substrates, which implies that this integrin-mediated mechanism may be less dependent on the specific presentation and orientation of exposed ligands. Moreover, the robust nature of this integrin-central surface strategy is further emphasized by the success

of simple dip-coated FNIII₇₋₁₀ implants in promoting bone formation and implant osseointegration in a relevant animal model, as shown previously. This thesis highlights the robust effect of both integrin specificity and ligand clustering on *in vitro* cellular adhesion, signaling, differentiation, and, more relevant to clinical applications, bone healing. However, as mentioned in this chapter, much work needs to be performed to elucidate the molecular mechanisms *in vivo* that lead to this functional effect.

Summary

These studies would contribute greatly to our fundamental understanding of how materials can be engineered via biomimetic strategies to direct cell and tissue responses including osteogenic differentiation and bone remodeling and healing. Moreover, this thesis lays out the groundwork for studies that may ultimately be able to apply these unique biomimetic surface strategies to non-orthopedic applications and varied material constructs.

APPENDIX A

PROTOCOLS

Biotinylated Protein Purification Protocol

A. Cell Lysis

Cell Lysis Buffer (CLB)

- i.) 50 mM Tris-HCl (pH=7.5)
 - ii.) 50 mM NaCl
 - iii.) 5% glycerol
 - iv.) all in water
 - v.) example:
 - i. 785 MG TRIS-HCL
 - ii. 290 MG NACL
 - iii. 5 ML GLYCEROL
 - iv. 95 ML WATER
2. Resuspend cells fully in CLB @ 10 mL/mg cell paste @ 4 C.
 3. Add lysozyme @ 1 mg/mL at 4 C or room temp if protein is stable ~ stir for 20 min
 4. Add sodium deoxycholate @ 1 mg/mL ~ 10 minutes stirring (solution may begin to get more viscous).
 5. Add DNAase I to reduce viscosity @ 1 mg/50 mL ~ 15 minutes mixing.

6. Centrifuge lysate @ 10000 g ~ 20 minutes. Save supernatant, could be slightly brownish but should be fairly transparent.

B. Affinity-Chromatography Purification (Biotin)

- a. We use Bio-Rad pump system, but you can use a simple protein purification pump system: just a pump by which the flow rate can be controlled (from 0.3 mL/min to about 10 mL/min is really all you need)
- b. For biotinylated proteins we use the Ultralink immobilized monomeric avidin (prod# 53146) from Pierce (5 mL). It is in a slurry form. You also need some type of plastic column, preferably around 10-15 mL or so. These are available everywhere, and they are cheap and come in all sizes. The slurry just needs to be poured carefully into the column a little at a time and drained (maintaining a bit of liquid of course – don't let column ever dry out, even in fridge) so that few air bubbles occur in the packed column of avidin gel.

c. PROTOCOL:

1. Force protein solution through 0.45 um filter to get rid of residual cell sludge and bacteria.
2. Following “Ultralink Immobilized Avidin” protocol pretty closely (should be online on the product page).
 1. Make buffers:
 - i.) ELUTION: 100 mL PBS + 50 mg D-biotin
 - ii.) REGEN: 100 mL DiH₂O + 750 mg glycine
 2. Equilibrate column to room temp (normally store in 4 C)

3. Hook up column to tubing and pump system.
4. Flow PBS @ 1.5 mL/min through the system ~ 10 minutes.
5. Wash system with ELUTION buffer @ 1.5 mL/min ~ 10 minutes. Will elute any residue biotin from last time you used column
6. Wash system with REGEN buffer @ 1.5 mL/min ~ 10 minutes. Regenerates column.
7. Wash system with PBS @ 3 mL/min ~ 10 minutes. Zero spec at this point.
8. Flow protein solution through system at 0.5 mL/min until all the way through. Spec should read very high throughout this process as protein solution should be pretty concentrated. Flow rate is low because you want the column to catch as much of your protein as possible.
9. After all protein through, wash system with PBS @ 3 mL/min and monitor spec until goes to baseline or near baseline.
10. Apply elution buffer (concentrated biotin will outcompete biotinylated protein for avidin and make the protein “fall off” the column @ 2 mL/min and collect fractions as spec reading rises. Readings should peak well above baseline, not as high as when the protein solution was flowing

through most likely, but dramatically higher. Collect fraction until the readings return close to baseline.

11. Wash column with REGEN buffer @ 2 mL/min – this also will release all the rest of the column clung biotinylated protein, but will be less pure than the ELUTION buffer.
12. Was column with PBS + 0.01% azide for 20 minutes and wrap column in parafilm with liquid still in the column and store in 4 C.
13. You can spec the collected fractions, and/or concentrate them more in 30 kDA Microcon centrifuge filters.
14. Run a ponceau and western blot to ascertain purity and quality of product and to make sure you actually got what you wanted. We also do an ELISA because it is easy to do as well (with just adsorbed protein and an anti-biotin and anti-FN antibody).

Make sure little leakage occurs in the system, and that the tubing is hooked up tight so that the flow rate is stable. If input is 300 mg of protein solution (3mg/mL, maybe 100 mL) from cell lysate ~ expect to get out about 3-4 mg of protein. Purity should be above 95% .

Integrin Blocking FAK Phosphorylation

1. Incubate cells in serum-free 2mM PBS-Dextrose for 35 minutes, while adding integrin blocking antibodies (α_5 , α_5 @ 30:1).
2. Seed cells at 90,000 cells/well (optimal 200,000 cells/well) for 6-well plate.
3. Adhere for 2 hrs.
4. Wash cells 1X PBS gently, and incubate for 20 min in cold RIPA buffer (w/ 350 $\mu\text{g}/\text{mL}$ PMSF, 10 $\mu\text{g}/\text{mL}$ leupeptin and aprotonin) – 200-300 $\mu\text{L}/\text{well}$.
5. Scrape cells and pipette up/down 25 times with needle.
6. Run BCA assay.
7. Boil samples with 6X sample buffer for 10 minutes.
8. Run western blot.
9. Antibodies: anti-FAK (1 $\mu\text{g}/\text{mL}$); anti-FAK397 (0.35 $\mu\text{g}/\text{mL}$); anti-FAK 576 (0.5 $\mu\text{g}/\text{mL}$); anti-FAK 861 (1 $\mu\text{g}/\text{mL}$).

Peptide Tethering to OEG/NPC Brushes

1. Place slides in individual wells (6-well plate for 22X22 slides).
2. Place OEG brushes in PBS for 30-45 minutes to form water layer.
3. Make peptide solution in PBS (20 $\mu\text{g}/\text{mL}$ for GFOGER) – meaning 1 mg/20 mL PBS, etc.
4. Incubate NPC slides in peptide solution (in PBS) for 30 minutes. Put 800 μl of solution into each well and place each slide upside down so floating in solution.
5. After 30 minutes, turn over NPC slides to right side up.
6. Aspirate PBS and peptide solution from wells.
7. Rinse all wells with PBS – 2X.
8. Incubate all wells in 20 mM Glycine in PBS for 5 minutes (2 mL/well).
9. Aspirate BSA and add PBS (3-4 mL/well).
10. Rinse all wells with PBS – 2X.
11. PURELY OPTIONAL: Add 1% heat-denatured BSA in PBS to all wells (2 mL/well)
12. Aspirate BSA and add PBS (3-4 mL/well).
13. Incubate in PBS at room temp overnight to dislodge non-specifically adsorbed peptide.

APPENDIX B

MICROPATTERNED SURFACES WITH CONTROLLED LIGAND TETHERING

Introduction

Patterning of ligands with high degrees of density and spatial control has become a powerful approach for applications in tissue engineering [254-256], studying cell-surface interactions [257-259], cell-culture analogues and substrates [260,261], and both cell-based and ligand-based biosensors [262-264]. For example, precise spatial control of cell position on 2-D biosensors is vital to the performance of the living circuitry [264]. Furthermore, effective manipulation of ligand and cell placement may greatly assist in basic studies of cell function on biomaterials. Recent studies suggest that spatial extracellular matrix cues, including size, geometry, and surface ligand density of adhesive regions, significantly regulate downstream cell responses [258,265-269]. Moreover, creation of controlled gradients of different ligands and cell types may assist in the design of cell culture substrates to direct specific cell function, biomaterials for assembly of multifunctional tissues, or even interfaces to enhance *in vivo* tissue healing [270,271].

*Modified from
T.A. Petrie, B.T. Stanley, A.J. García, *Micropatterned Surfaces with Controlled Ligand Tethering*. J Biomed Mater Res A; 2008, In Press.

In order to pattern ligand islands of prescribed shape, size, and spatial position on substrates on the cellular scale, a variety of direct and soft lithographic techniques have recently been employed – the most widely used being microcontact printing [259,264,272-274]. Microcontact printing (μ -CP) is an easily reproducible, cost effective, simple, and versatile technique to create 2-dimensional patterns of ligand “islands” of specific shape, size, and substrate spatial locale [275-279]. Current strategies have utilized μ -CP patterns of “adhesive” hydrophobic self-assembled monolayers (SAMs) of alkanethiolates, typically methyl-terminated, on gold substrates, backfilled with “nonadhesive” SAMs of ethylene-glycol (EG₃)-terminated alkanethiolates [275,280,281]. For cell adhesion applications, these islands can adsorb adhesive proteins to promote cell adhesion. Moreover, the size and geometry of these adhesive islands will determine the spatial pattern of adhered cells on the surface. Alternatively, other strategies have focused on using μ -CP to pattern proteins directly onto substrates, relying on protein physisorption to synthetic materials to create localized adhesive regions on a substrate [282,283].

Nonetheless, there are significant limitations associated with using this μ -CP technique with ligand adsorption-dependent alkanethiol SAMs. Since ligands are not covalently immobilized on patterns, but rather passively adsorbed, the ability to implement large ranges of well-controlled ligand density on each pattern is considerably limited. Recently, mixed SAMs of alkanethiolates on gold, consisting of a mixture of reactive carboxylic acid-terminated (EG₆-COOH) and nonfouling tri(ethylene glycol)-terminated (EG₃) alkanethiolates, have exhibited the ability to immobilize controlled surface densities of tethered ligands within a protein-adsorption resistant background

[170,281,284]. The ligand is immobilized to the surface by peptide bond-forming reactions between the active esters on the alkanethiol and the terminal amino group of the ligand, promoting a stable covalent tethering to the SAM surface.

Here, we have optimized a technique that combines the advantages of mixed alkanethiol SAMs with the patterning utility of μ -CP to afford controlled immobilization of one or more ligands to specific, well-defined patterns of prescribed size, shape, and spatial location. We demonstrate that this easily reproducible μ -CP protocol with mixed SAMs of alkanethiolates generates micropatterns with controlled immobilized ligand densities.

Materials and Methods

Materials

Two alkanethiols were used to produce self-assembled monolayers (SAMs): tri(ethylene glycol)-terminated alkanethiol (HS-(CH₂)₁₁-(OCH₂CH₂)₃-OH; EG₃) and carboxylic acid-terminated alkanethiol (HS-(CH₂)₁₁-(OCH₂CH₂)₆-OCH₂COOH; EG₆-COOH), obtained from Prochimia (Sopot, Poland). AlexaFluor350-conjugated goat anti-mouse (AF350) and AlexaFluor488-conjugated goat anti-mouse (AF488) antibodies were obtained from Invitrogen (Carlsbad, CA). Different size (9mm x 9mm squares, 25 mm diameter circles, No. 1.5) glass slides were used as the underlying substrates for subsequent Ti/Au deposition and SAM assembly. Dulbecco's phosphate buffered saline (DPBS) was purchased from Invitrogen. Peptide tethering reagents, N-hydroxysuccinimide (NHS) and N-(3-dimethylaminopropyl)-N'-ethylcarbodiimide hydrochloride (EDC) were obtained from Sigma-Aldrich (St. Louis, MO). Glycine and 2-mercaptoethanol were also

acquired from Sigma-Aldrich. Gel Mount used for fluorescent slide placement was purchased from Biomedica (Foster City, CA). PDMS stamps were made from Sylgard 184 and 186 obtained from Dow Corning (Midland, MI).

Stamp and Substrate Preparation

Master molds of microarrays of different shapes (rectangles, ovals, circles, squares), sizes (including 20 μm diameter circles, 8 μm diameter ovals, rectangular patterns [64, 100, 1000 μm^2 area], and squares [64, 100, 1000 μm^2 area]), and island spacings (55 μm center-to-center spacing for circles, 10 – 50 μm for other shapes) were fabricated on Silicon wafers using standard photolithography methods. Following photoresist spin coating (5 μm thick) and exposure to UV light through an optical mask (consisting of “holes” comprising of the negative stamp pattern desired), exposed patterns were etched away to leave recessed areas of the pre-determined stamp pattern. Poly(dimethylsiloxane) (PDMS) stamps were created using standard methods^{22,19}. Briefly, Silicon molds were rendered hydrophobic to prevent elastomer-Silicon adhesion by adding 200-300 μl of (tridecafluoro-1,1,2,2-tetrahydrooctyl)-1-trichlorosilane onto the mold surface. PDMS precursors and curing agents (Sylgard 184 and 186) were mixed (5:1 for precursor elastomers; 10:1 for curing agents), poured onto the microfabricated molds, and placed under vacuum to eliminate bubbles. Following casting on molds, the PDMS was cured overnight at 60°C. After curing, the PDMS stamp was carefully pried off the mold and washed with 70% ethanol. Stamp features were confirmed by microscopy and image analysis. The dimensions of the PDMS stamps used in this study were 30 mm x 30 mm x 5 mm.

Gold-coated substrates were created by cleaning glass slides in a custom-made tabletop etcher for 4 min, followed by sequential deposition of titanium (100 Å) and gold (200 Å) films at a deposition rate of 2 Å/sec onto clean glass slides (9 x 9 mm or 25 mm diameter circles) via an electron beam evaporator (Thermionics Laboratories, Hayward, CA) at a pressure of 2×10^{-6} Torr. The gold-coated glass substrates were stored in a dessicator under vacuum for a maximum of 3 weeks.

μ-CP of Mixed Alkanethiol SAMs

Before μ-CP, all PDMS stamps and Au-coated substrates were sonicated in 70% ethanol and dried under a stream of nitrogen. Self-assembled monolayers (SAMs) of mixed alkanethiols on Au-coated substrates were used to present well-defined and ordered domains for subsequent ligand tethering. PDMS stamps were “inked” with a specific mixed alkanethiol ratio of EG₆-COOH:EG₃ (1.0 mM total thiol concentration; 0.001 to 0.1 ratios EG₆-COOH:EG₃) and allowed to dry for 10 seconds under a stream of nitrogen to permit excess solution to run off the stamp. Inked stamps were then brought into contact with the Au-coated substrates under various weights (50 – 200 g) and for a range of time periods (15 – 300 s). Only the raised patterns on the stamp contacted the substrates and, therefore, the mixed alkanethiols only transferred to the substrate at these points. After the various stamping times, the PDMS stamp was carefully removed using thin tweezers, and the unstamped, bare gold areas on the substrate were “backfilled” with a 1.0 mM solution of EG₃ alkanethiol for at least 2 h. Model ligands (AF350- or AF488-conjugated antibodies) were tethered onto the mixed alkanethiol SAM islands using standard peptide chemistry [169]. Briefly, patterned substrates were washed in 70%

ethanol and rinsed multiple times in ultrapure H₂O for at least 15 min. Next, the substrates were incubated in 2.0 mM EDC and 5.0 mM NHS in 0.1 M 2-(N-morpho)-ethanesulfonic acid and 0.5 NaCl (pH 6.0) to “activate” the EG₆-COOH SAMs for subsequent ligand tethering. After 30 min, the activated surfaces were immersed in a 20 mM solution of 2-mercaptoethanol in dH₂O. For single ligand patterns, antibody ligand (either AF488 or AF350) solution at particular concentrations was incubated on the activated supports for various exposure times (15-60 min). For multi-ligand patterns, antibody ligands were sequentially added to activated patterns. This procedure entailed adding the first ligand to activated substrates for a specific length of time, followed by addition of the second ligand to the activated surfaces for another precise time period. Following ligand incubation, unreacted NHS esters were quenched in 20 mM glycine and patterned surfaces were incubated overnight in DPBS to minimize non-specific protein adsorption [170].

Surface Plasmon Resonance Surface Density Measurements

Tethered-antibody surface density measurements on μ -CP mixed SAMs were obtained using a Biacore X instrument (Biacore, Piscataway, NJ) [108]. μ -CP surfaces were prepared as described as above on in-house glass SPR chips coated with Ti (57 Å) and Au (338 Å). Surfaces were primed in the SPR with sterile DPBS, and the baseline allowed to stabilize for 5-10 min. Surfaces were activated by flowing a 5.0 mM NHS/2.0 mM EDC solution at 4 μ l/min for 10 min. Antibody was subsequently tethered by injection of AF488 at varying solution concentrations at a flow rate of 4 μ l/min for 15 min. Finally, surfaces were washed for 3 min with 0.1% sodium dodecyl sulfate detergent

in DPBS to eliminate untethered ligand, and the baseline allowed to stabilize for 2 min thereafter before tethered antibody levels measured. Resonance units (RU) were converted to surface density values ($10 \text{ RU} = 1 \text{ ng/cm}^2$). We previously showed that tethered densities determined in situ in the SPR were equivalent to those generated via conventional bench-top incubation methods [108].

Image Quantification and Analysis

Following overnight incubation in PBS, samples were washed in ultrapure water and mounted on slides with Gel/Mount mounting media. Fluorescence images were taken using a Nikon TE-300 fluorescence microscope and Spot RT digital camera. Different objective lenses (4-100 X) were used. All images for all samples and patterning conditions at each magnification were acquired at the same camera settings to allow direct comparison of fluorescence intensity among all samples. In order to assess relative density of tethered antibody on each sample/condition, the total fluorescence intensity (minus background intensity) was quantified on multiple 10X images from the same sample using ImagePro (Version 6.0, MediaCybernetics). Fluorescence intensity line profiles were also prepared from representative images of various magnifications also using ImagePro. Profiles were normalized to background intensity (reference line).

Statistical Analysis

Fluorescence images of patterns presented represent characteristic results from those particular experimental conditions and ligands. Quantified fluorescence intensity and ligand density are reported as mean \pm standard error. All experimental conditions

involved at least an $N = 5$, except mixed antibody tethered patterned surfaces, which involved $N = 4$ samples/condition, and at least three independent runs were conducted.

RESULTS

Micropatterning with Mixed Alkanethiol Solutions

In order to develop micropatterned substrates with tethered ligand islands of controlled sizes and shapes, we developed a microcontact printing protocol implementing a mixed ratio of specific alkanethiols to covalently immobilize ligands to specific patterned areas. We and others have shown previously that a homogeneous (unpatterned) surface presenting a SAM of a ratio of EG_6 -COOH and EG_3 - terminated alkanethiols on gold-coated substrates affords controlled tethering of amine-presenting ligands, while preventing significant non-specific adsorption of non-tethered ligands (**Figure A2.1 A**) [108,149]. The carboxyl-terminated alkanethiols can be modified through standard EDC/NHS tethering chemistry to present an NHS ester intermediate, which is readily displaced by freely-presented amine groups, typically on peptides or protein ligands, to form a peptide bond [284]. The EG_3 alkanethiols provide for biofouling resistance.

Our protocol for μ -CP mixed ratios of alkanethiols entailed “inking” the cleaned PDMS stamp with a mixed solution of these alkanethiols (**Figure A2.1 B-1**), bringing it in contact with the substrate (the standard μ -CP technique) (**Figure A2.1 B-2**), and subsequently backfilling with EG_3 to preserve non-fouling behavior on the unpatterned areas (**Figure A2.1 B-3**). Patterns were then “activated” via EDC/NHS chemistry (**Figure A2.1 B-4**) and ligands were tethered (**Figure A2.1 B-5**).

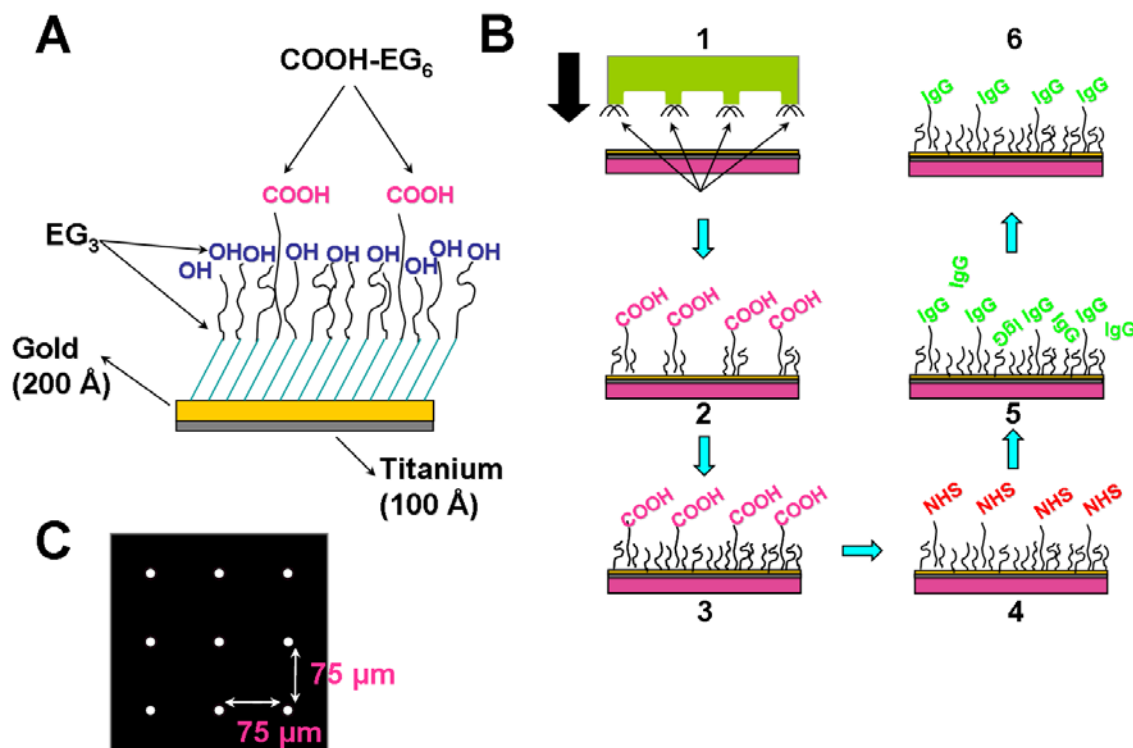


Figure A2.1. Microcontact printing (μ -CP) islands of self assembled monolayers (SAMs) of mixed alkanethiols (EG_3 and EG_6 -COOH) onto gold-coated glass substrates. (A) Schematic of mixed alkanethiol SAM (95:5 EG_3 : EG_6 -COOH). (B) Microcontact printing procedure for mixed SAMs: 1) SAMs “inked” onto PDMS stamp, 2) SAMs stamped and subsequently transferred to substrate, 3) unstamped area backfilled with EG_3 to generate non-fouling background, 4) mixed alkanethiol islands “activated” through conversion of COOH groups into NHS esters via EDC/NHS chemistry, 5) tethering of amine-presenting IgG to ester-converted SAMs, 6) Rinsing of mixed alkanethiol SAM surface overnight to eliminate weakly bound, non-specific ligand (IgG) adsorption to surface. (C) Schematic of patterned tethered islands of IgG (white circles) in a non adhesive background (black). Circular islands used in this study were $20\ \mu\text{m}$ diameter, $55\ \mu\text{m}$ spacing apart.

After quenching unreacted "activated" surface groups, patterned substrates were rinsed overnight in a buffered solution to eliminate non-specific ligand adsorption (**Figure A2.1 B-6**). For this study, the optimal resulting μ -CP surface resembles circular islands of tethered fluorescent antibody amid a minimally fluorescent background (**Figure A2.1 C**).

Optimizing the μ -CP Protocol for Mixed Alkanethiols

A central goal of this study was to systematically optimize this μ -CP protocol using an evaluation-based approach. We used two fluorescent antibodies, AF488 (green) and AF350 (blue), as model ligands because of the widespread use of antibodies in biotechnological applications and the ability to easily visualize patterns and eliminate the need for immunostaining of proteins. Early μ -CP patterns were extremely variable, inconsistent, and faint. Therefore, we identified several key experimental design variables/parameters that potentially influence the fidelity of these patterns and qualitatively assessed their impact on pattern quality. These variables included: (1) stamping weight, (2) total stamping time, (3) ratio of alkanethiols used for inking, and (4) ligand (antibody) exposure time post-activation of the stamped substrate, which can have a profound effect for adsorbed or covalently bound ligands³⁶. We qualitatively evaluated the relative parameter effect on 4 quality-control outcomes:

1. **surface homogeneity** (corresponding to the overall conformity and consistency of the intensity/shape of all islands over the entire patterned substrate);
2. **pattern homogeneity** (corresponding to the conformity and consistency of the intensity/shape of each individual island from one edge to the other);

3. **pattern integrity** (fidelity of each pattern shape to the original stamp design over the entire substrate);
4. **fluorescence intensity** (ratio of fluorescence intensity, corresponding directly to antibody surface density, of ligand-tethered patterns to background).

The qualitative results for all conditions tested are summarized in **Figure A2.2**. One specific stamp dimension was used for this assessment (30 mm x 30 mm x 5 mm). The best performing condition of each variable was: 90-second stamping time, 5% mixed SAM ratio, and 45-min antibody exposure time. The chosen stamping weight was 150 g, since it exhibited better pattern integrity than the 200 g weight.

OUTCOME		Surface Homogeneity	Pattern Homogeneity	Pattern Integrity	Fluorescence Intensity	
Stamping time	15s	+	++	+++	+	
	30s	++	++	++++	++	
	1 m	+++	++++	++++	+++	
	1.5 m	++++	++++	++++	++++	
	2 m	++++	++++	+++	++++	
	5 m	+++	++++	+	++++	
Stamp weight	50g	+	+++	+++	+	
	100g	++	++++	+++	+++	
	150g	+++	++++	++++	++++	
	200g	++++	++++	+++	++++	
Mixed SAM ratio (EG ₆ -COOH:EG ₃)	1%	+++	++	++++	+++	
	5%	++++	+++	++++	++++	
	10%	++++	++++	++	++++	
Ab exposure time	Single-Ab	10 m	+	+++	++++	+
		30 m	+++	++++	++++	+++
		45 m	++++	++++	++++	++++
		60 m	++++	++++	++++	++++
		20m-30m	++	+++	++++	++/+++
	Mixed-Ab (1 ST Ab-2 ND Ab)	40m-30m	++++	++++	++++	++++/+++
		60m-30m	++++	++++	++++	++++/++
		20m-60m	+++	+++	++++	++/++++
		40m-60m	++++	++++	++++	++++/++++
		60m-60m	++++	++++	++++	++++/+++

Figure A2.2. Summary of entire optimization procedure and analysis of each major variable/condition investigated, including stamping time, stamping weight, mixed SAM ratio, and post-surface activation ligand exposure time. Each variable was scored on the relative success of 4 different functional outcomes on a qualitative scale of 1 (poor) to 4 (worked perfectly) “pluses”. The overall best working condition of each variable set is bolded and the corresponding relative scores highlighted in red. (N3 was performed for each condition).

Controlling Single Antibody Tethering to μ -CP Mixed Alkanethiol Circular Patterns

Relative tethered surface densities were determined by quantifying the fluorescence intensity of patterns from their corresponding fluorescent images (a quantification process we term FIIQ). This FIIQ method entailed quantifying total

fluorescence intensity on each image of each sample, using an in-house imaging macros, and normalizing to background fluorescence. To validate this method and compare to absolute measurements of tethered density, we conducted parallel measurements using surface plasmon resonance (SPR). We quantified tethered AF488 antibody densities at two different coating concentrations on both unpatterned (homogeneous 5% COOH SAM surface) and patterned (5% COOH SAM patterns backfilled with EG₃) gold-coated SPR chips (**Figure A2.3 A**). SPR quantitative antibody densities are in excellent agreement with FIIQ relative density results (Fig 2b,c). For example, the predicted ratio of AF488 (at 100 µg/mL) surface density on µ-CP compared to unpatterned surfaces (10.3%, based on area) correlates well with the ratio from the SPR runs (11.2%) and the FIIQ analysis (7.8%) (**Figure A2.3 C**, 1st panel). In addition, AF488 surface density ratios between 100 µg/mL and 25 µg/mL coating concentrations for patterned (36.6%) and unpatterned (30.2%) surfaces were similar to the relative density values obtained by FIIQ (32.2%) (**Figure A2.3 C**, 2nd panel). Taken together, this data validates the FIIQ method for quantifying relative AF488/AF350 surface density and provides evidence for control of ligand surface density on µ-CP mixed SAM surfaces.

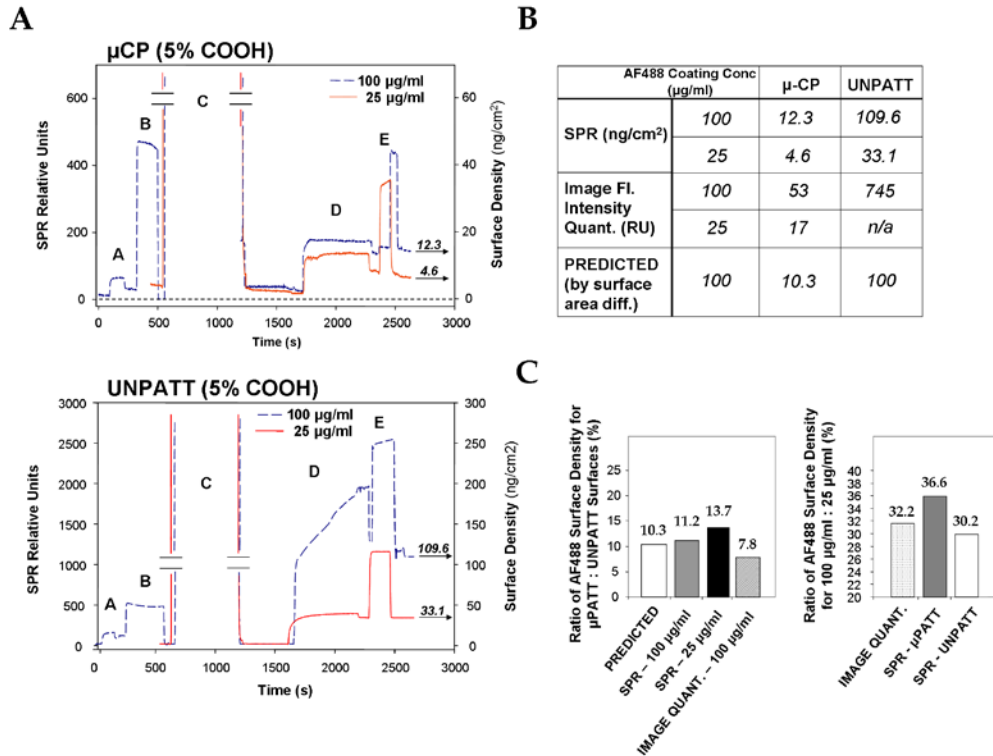


Figure A2.3. Correlation of AF488 tethered surface density between SPR and fluorescent intensity image quantification (FIIQ). (A) SPR measurement profiles on μ -CP or unpatterned slides using a 5% COOH-EG₆:EG₃ SAM. AF488 coating concentrations of either 100 μ g/mL or 25 μ g/mL were flowed over activated surfaces. SPR steps were: (a) AF488 adsorption on unactivated surfaces, (b) 0.1% SDS wash, (c) EDC/NHS surface activation, (d) AF488 tethering to activated surfaces, (e) 0.1% SDS wash. (B) Table summarizing quantitative AF488 surface density results from SPR experiments, FIIQ, and predicted relative density based on ratio of island:background surface area. (C) Graphs highlighting close correlation between SPR and FIIQ techniques for quantifying tethered IgG ligand surface density.

To assess the ability to vary the density of tethered ligand on activated patterns in greater detail, FIIQ was used to quantify AF488 (green) or AF350 (blue) surface density on μ -CP mixed SAM patterns using a range of antibody coating concentrations (**Figure A2.4**). For antibody coating concentrations above 50 $\mu\text{g/mL}$ for AF488 and 75 $\mu\text{g/mL}$ for AF350, patterns were well-formed and consistent throughout the entire substrate (**Figure A2.4 A**). However, for lower coating concentrations of 25 and 37 $\mu\text{g/mL}$ for AF488 and AF350 respectively, pattern fidelity began to degrade both across the substrate and within each pattern (**Figure A2.4**). At these low concentrations, tethered antibodies seemed to localize either in clumps or along the periphery of each sample (**Figure A2.5 D,H**). At high magnification, overall pattern fidelity, as evidenced by line profiles of intensity across representative images, was relatively high using either antibody. At lower magnifications, the intensity line profiles demonstrated patterns of homogeneous intensity across the substrate, even at lower coating concentrations (**Figure A2.5 A,B**). Moreover, background intensity for all coating concentrations was minimal, indicative of minimal unspecific antibody adsorption to EG_3 backfilled areas. For both AF488 and AF350, tethered antibody surface density increased hyperbolically with antibody coating concentration on activated μ -CP mixed alkanethiol surfaces (**Figure A2.4 B,C**). This functional dependence of tethered density on coating concentration is in excellent agreement with measurements for tethering onto unpatterned substrates [108]. Taken together, this data validates control over tethered single ligand density using this μ -CP mixed alkanethiol protocol.

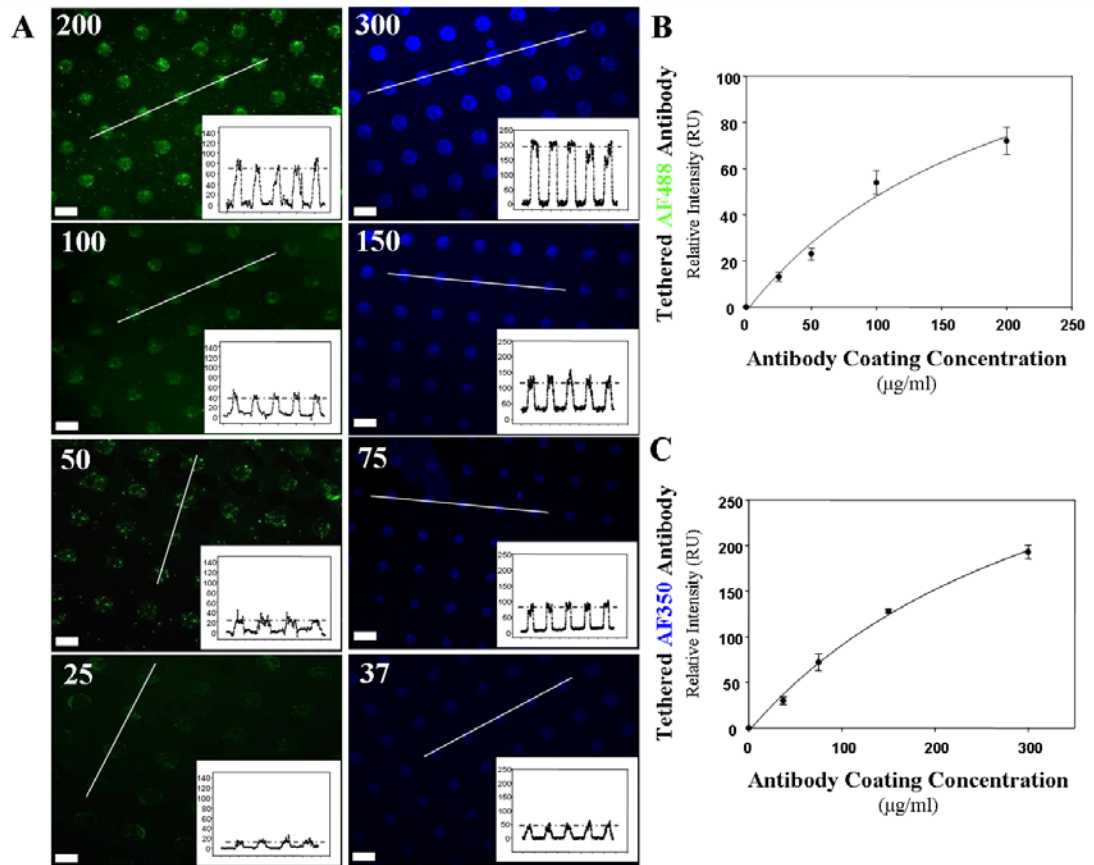


Figure A2.4. Control over density of tethered ligand on μ -CP islands. (A) Fluorescence images of AF488 (green) and AF350 (blue) tethered-antibody on μ -CP circular islands. AF488-tethered island images were at 200, 100, 50, 25 $\mu\text{g}/\text{mL}$ coating concentration, while images of AF350 were at 300, 150, 75, 37 $\mu\text{g}/\text{mL}$ dilutions. Inset graphs are line intensity profiles at the prescribed linear path indicated on each image. Scale bar is 25 μm . (B) Demonstration of control over tethered antibody density via graph of normalized total fluorescence intensity on each sample at varying coating concentrations of AF488. (C) Graph of normalized total intensity on each sample at varying coating concentrations of AF350.

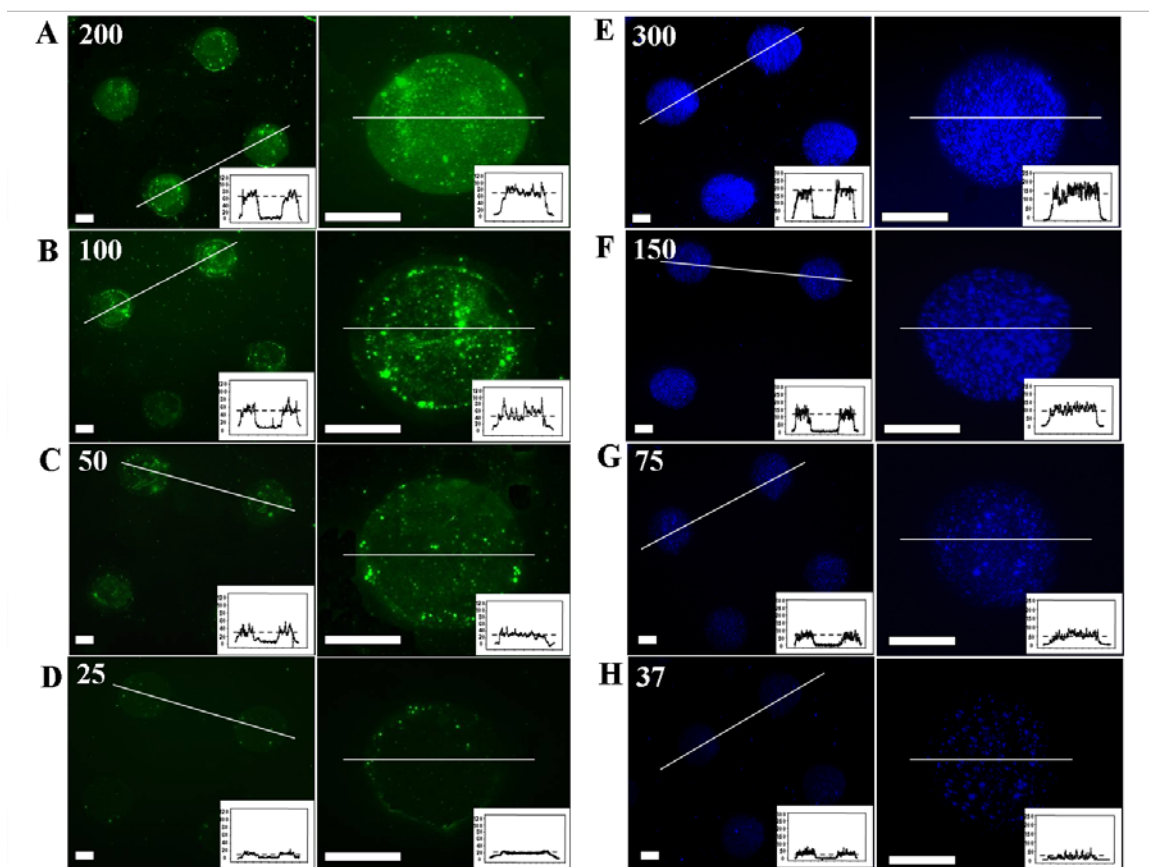


Figure A2.5. Pattern homogeneity is maintained over a range of tethered ligand density on μ -CP mixed SAM surfaces. Images are representative of patterns of specific antibody densities, including line intensity profiles at the indicated linear path. Scale bar is 8 μ m. **(A)** AF488, 200 μ g/mL. **(B)** AF488, 100 μ g/mL. **(C)** AF488, 50 μ g/mL. **(D)** AF488, 25 μ g/mL. **(E)** AF350, 300 μ g/mL. **(F)** AF350, 150 μ g/mL. **(G)** AF350, 75 μ g/mL. **(H)** AF350, 37 μ g/mL.

Controlling Multiple Antibody Tethering to μ -CP Mixed Alkanethiol Circular Patterns

We next determined whether multiple ligands (both AF350 and AF488) could be co-tethered to the same μ -CP patterns. We determined through pilot patterns that sequential incubation of activated patterns in each antibody solution would afford greater control over the relative tethered antibody density than one incubation of a single mixed solution of various concentrations of each antibody. Using identical protocol conditions (weight, stamp time, alkanethiol ratio) to the single ligand procedure, different combinations of exposure times of each antibody via sequential incubation were qualitatively evaluated (**Figure A2.2**). The optimal exposure time ratio was determined to be 40 min for the first ligand, followed by a full 60 min for the second ligand. Next, 25 combinations of different ratios of AF350 and AF488 coating concentrations were incubated on activated patterned substrates, and the total blue and green fluorescence intensity (corresponding to tethered AF350 and AF488 density, respectively) on each sample quantified by FIIQ (**Figure A2.6 E**). It would be expected that the AF488 green antibody densities would remain constant over all AF350 blue antibody concentrations - as the tethering process for each antibody is independent. However, since the coefficient of variation (standard deviation of the mean divided by the mean) for these measurements is $< 10\%$ (data not shown), the observed fluctuations in AF488 tethered densities over the range of blue AF350 coating concentrations are not statistically significant. Representative fluorescent images (**Figure A2.6 A-D**) at various AF350:AF488 coating concentration ratios reflect FIIQ antibody density data (**Figure A2.6 E**) and demonstrate our ability to control the density of tethered ligands on multiple ligand-tethered patterns.

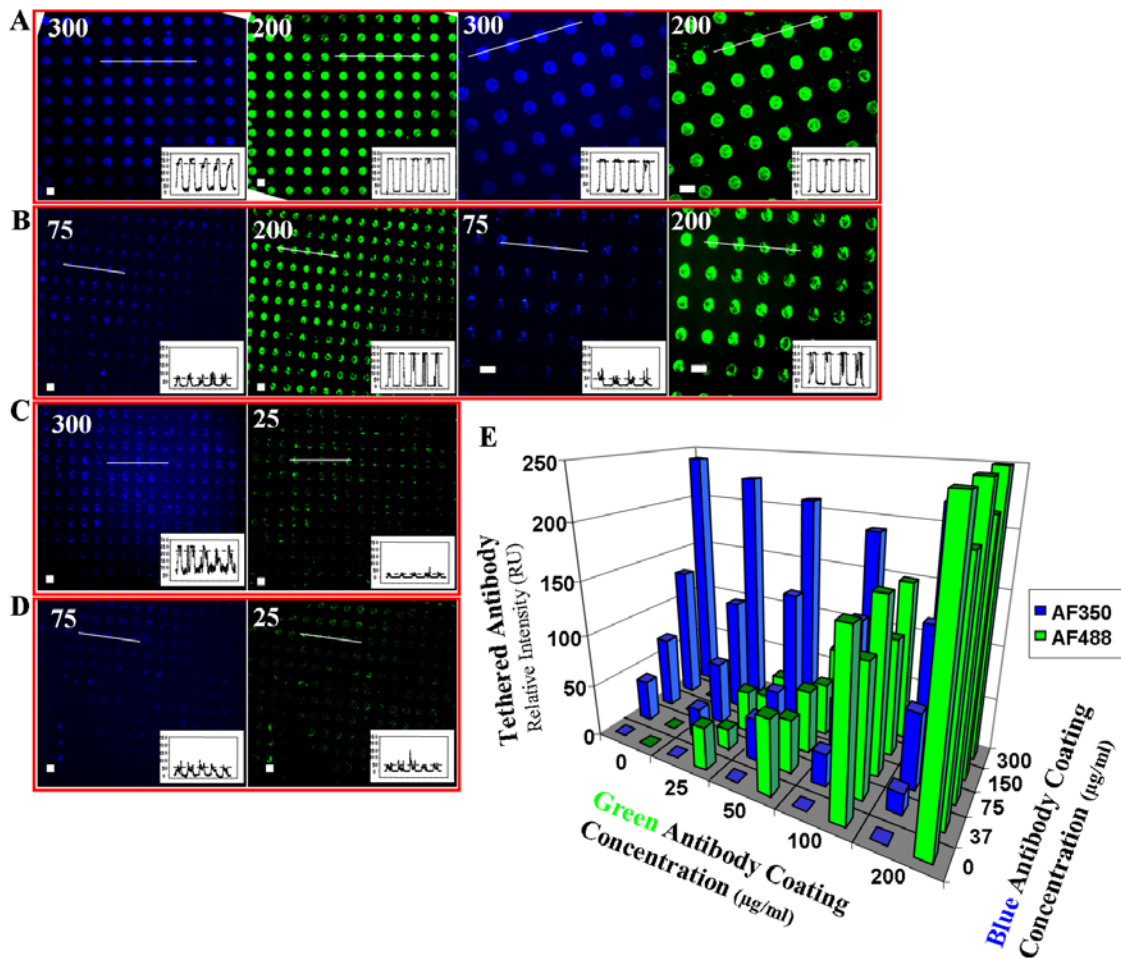


Figure A2.6. Multiple ligands can be tethered in a controlled manner to μ -CP mixed alkanethiol SAM islands. Representative fluorescent images of 4 extreme multi-ligand coating concentrations exemplify precise control over each antibody density on the same mixed alkanethiol SAM pattern. Scale bar is 25 μm . (A) AF350 (300 $\mu\text{g/mL}$), followed by AF488 (200 $\mu\text{g/mL}$). (B) AF350 (75 $\mu\text{g/mL}$), AF488 (200 $\mu\text{g/mL}$). (C) AF350 (75 $\mu\text{g/mL}$), AF488 (200 $\mu\text{g/mL}$). (D) AF350 (75 $\mu\text{g/mL}$), AF488 (25 $\mu\text{g/mL}$). (E) Controlled ratios of tethered AF350:AF488 on the same islands can be engineered by varying each antibody coating concentration and exposure time on activated mixed alkanethiol SAM patterns. 3-D plot of normalized relative surface density of tethered AF488 and AF350 antibodies on 25 different multi-antibody coating concentration combinations on μ -CP mixed alkanethiol patterns. (mean \pm st. error, $N = 4$).

μ-CP Using Mixed Alkanethiols is Applicable for Diverse Pattern Designs

To further examine the versatility of this system, other PDMS stamp designs were used to create antibody-tethered mixed alkanethiol patterns of different sizes and shapes. Multiple pattern designs were created on a single substrate in localized areas with excellent consistency and homogeneity (**Figure A2.7 A**). Rectangular (16 μm x 8 μm, **Figure A2.7 B**) and rod-shaped patterns (16 μm x 2 μm, **Figure A2.7 C**) were stamped, activated, and tethered with AF488, and linear intensity profiles revealed good surface and pattern homogeneity. While slightly fainter and less homogeneous across the surface, rectangular patterns (20 μm x 5 μm, **Figure A2.7 D**) of tethered AF350 were also created using this same optimized μ-CP protocol. Overall, we have demonstrated the utility of this μ-CP mixed alkanethiol system to generate well-defined and customizable patterns (size, shape, spatial locale) with controlled single or multiple ligand densities.

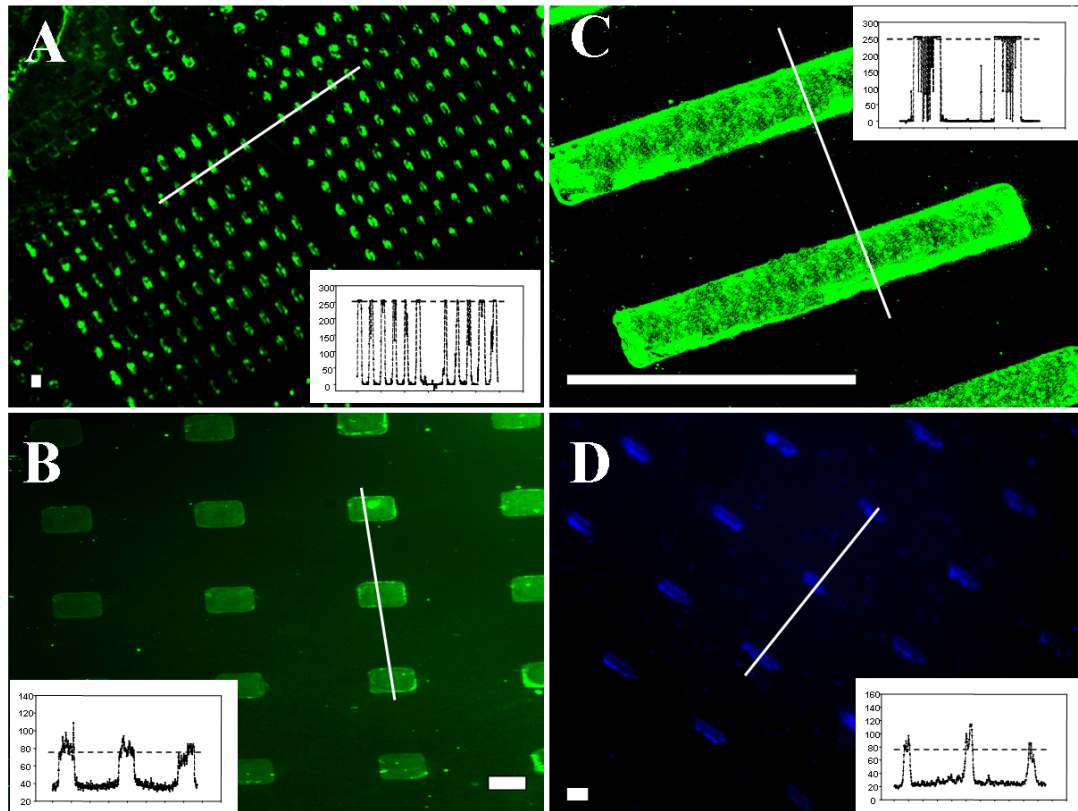


Figure A2.7. μ -CP mixed alkanethiol SAM patterns of different sizes and shapes can be prepared by modifying the stamp design. Representative images (scale bar is 5 μ m) and corresponding line profiles of: (A) Multi-shaped mixed alkanethiol patterns on one surface (AF488, 200 μ g/mL). (B) AF488-tethered rectangular islands (100 μ g/mL). (C) AF488-tethered rod-shaped islands (200 μ g/mL). (D) AF350-tethered long rectangular islands (150 μ g/mL).

Discussion

Development of effective surface patterning techniques to create micropatterned arrays with adjustable and controlled presentation of biological ligands is critical to the progress of a number of biotechnological applications, including biosensors, drug

delivery systems, and *in vitro* analyses of cell-material interactions. Moreover, recent studies have suggested that the surface density and stability of bioadhesive ligands play a central role in cell adhesion, migration, and downstream function, along with adhesive area and geometry [281,285-289]. Using a microcontact printing technique with mixed alkanethiol SAMs, we developed and optimized a hybrid ligand patterning protocol that affords controlled tethering of ligands in specific geometric patterns. The development of a simple, versatile, and high utility technique to generate micropatterned surfaces presenting tethered ligand is important to the engineering of platforms for rigorous studies of cell-material interactions and biotechnological/biomedical applications. The hybrid mixed alkanethiol μ -CP protocol presented takes advantage of the ligand tethering ability of COOH-terminated alkanethiolates, which can be modified to enable the immobilization of amine-presenting ligands [169,284,290]. Several recently developed 2-D patterning methods, such as the use of polymer films with ink-jet printer technology [291] and microfluidics networks [292], have focused on covalent, rather than adsorbed, ligand attachment on material surface patterns to better control surface density as well as afford control over multiple ligand patterning. However, considerable resources requirements and complex operation limit the everyday and widespread applicability of these methods. In contrast, the simplicity, speed, and minimal resources required of the modified μ -CP protocol presented in this study make it more appealing for many biotechnological and biomedical applications.

Many current ligand and cell patterning methods rely either on selective printing of ligand-adsorbing polymers into geometrically constrained wells/regions or direct printing of ligands onto substrates [266,280,283,291,293]. These methods generally

afford very precise ligand surface placement and are advantageous to screening combinatorial libraries of ligands. However, these techniques also share various key drawbacks, including lack of long-term stable ligand deposition (due to passive ligand adsorption) and precise manipulation of ligand density. These shortcomings hinder their applicability to rigorous studies of ligand-cell interactions, biosensors, and kinetic analyses that require more long-lasting, stable, and ligand-surface parameter controls. The hybrid mixed alkanethiol μ -CP system that is developed and optimized in this study directly solves this lack of control over ligand pattern density while maintaining the aforementioned beneficial features of micro-contact printing. Although not specifically examined in this study, a potential added benefit of this system is more robust control over ligand orientation. Moreover, the covalent tethering of ligands may afford more stable patterned surfaces in physiological media.

Since parameter optimization of this protocol was conducted with one set stamp size (and PDMS composition), it is possible that the optimal stamp time and weight may be slightly altered in systems utilizing alternate stamp size/PDMS volumes. Nonetheless, in our studies, we have typically noticed very little change in pattern integrity and quality with use of stamp sizes $\pm 50\%$ volume of the stamp used in this study (results not shown). In addition, stamp size did not seem to affect the quality of 5 μm or 20 μm patterns, although a meticulous analysis of these observations was not conducted. Therefore, it may be predicted that the stamping weight and time may need to be slightly increased for use of significantly larger volume stamps; vice versa for smaller volume stamps. Regardless, this study thoroughly delineates the major experimental parameters and general optimal values that should be used with this modified protocol.

This technique is applicable for controlled covalent patterning of a wide variety of ligands, including biomolecules such as proteins and peptides, polymers for drug delivery or sensing applications, antibodies for sensing arrays, and kinetic ligand analyses. This technique also could be easily applied to screening different densities and combinations of ligands on cells and testing potential drug compounds with controlled kinetic analysis. We present optimized parameters to generate spatially defined micropatterns with well defined surface densities of single and dual tethered ligands. While these optimized parameters were developed for two antibody ligands, it is possible that different processing parameters are needed to tether other ligands. A similar optimization strategy as that presented in this report could be easily adopted for other ligands as well as applications requiring more than two ligands tethered on single patterns.

Summary

Using microcontact printing techniques with mixed alkanethiol SAMs, we have developed and optimized a hybrid ligand patterning technique that affords controlled tethering of ligands in specific geometric patterns. We present optimized parameters to generate spatially defined micropatterns with well defined ligand densities of single and dual tethered ligands. This technique is applicable for controlled covalent patterning of a wide variety of ligands as well as screening combinatorial libraries of ligands in varying densities for study of cell-material interactions.

APPENDIX C

CONTROLLING CELL ADHESION TO TITANIUM: FUNCTIONALIZATION OF POLY(OLIGO(ETHYLENE GLYCOL) METHACRYLATE) BRUSHES WITH CELL ADHESIVE PEPTIDES

Introduction

Titanium and its alloys represent a major class of materials employed in orthopaedic and dental clinical applications. Although titanium-based implants can function effectively for a decade, the long-term clinical success of these devices is limited by implant loosening and wear, especially in younger patients [3,184]. Considerable efforts have focused on implant surface technologies, such as designing rough, porous coatings for bone ingrowth, and bone-bonding ceramic coatings to promote integration into the surrounding bone and thereby provide mechanical interlock [3,4,294]. However, slow rates of osseointegration, particularly in clinically challenging cases, currently restrict these approaches.

Biomimetic coatings, focusing on the presentation of biologically active molecules within a protein adsorption-resistant background, have recently emerged as a promising strategy to enhance osseointegration [28]. Self-assembled monolayers (SAMs) have been explored as a method to control biologically-related surface properties such as

*Modified from

J.E. Raynor, T.A. Petrie, A.J. García, D.M. Collard. *Controlling Cell Adhesion to Titanium: Functionalization of Poly[oligo(ethylene glycol)methacrylate] Brushes with Cell-Adhesive Peptides*. *Advanced Materials* 2007; 19:1724-1728. .

cell adhesion [278,286, 295-297]. For example, we have previously demonstrated control over protein adsorption and cell adhesion and function by modification of oligo(ethylene glycol)-substituted alkanethiol monolayers on gold with specific peptide sequences from adhesion proteins [108,169,170,298]. However, SAMs on gold and silver substrates suffer from long-term instability and loss of bioresistance, and there are severe limitations to the application of robust noble metal coatings on biomedical materials [278,286,295,296]. To overcome these shortcomings, several groups have concentrated on the engineering of polymeric films on titanium- and silicon-based surfaces to promote robust bioresistance [299-302]. For instance, adsorption of end-functionalized poly(ethylene glycol) (PEG) onto titanium metal (i.e., a “grafting to” approach to prepare polymer brushes) affords resistance to protein adsorption [297]. More recently, a “grafting-from” approach was developed based on surface-initiated atom transfer radical polymerization (SI-ATRP) of oligo(ethylene glycol) methacrylate (OEGMA) on gold modified with a thiol monolayer of a bromo ester initiator. An extensive study of the properties of these brushes was made as a function of polymerization time and the surface density of initiator. This afforded the ability to control the thickness of the poly(OEGMA) film and demonstrated the resistance of these surfaces to cell adhesion [296,301,303].

To build on these findings and to explore the development of stable surface modifications of titanium, we set out to establish routes to prepare protein adsorption-resistant polymer brushes that can be modified with peptide sequences that direct cell adhesion. We describe an approach to modify the surface of titanium with dense polymer brushes of poly(OEGMA) that resist protein adsorption and cell attachment. Furthermore,

conversion of the hydroxyl end groups of the oligo(ethylene glycol) (OEG) side chains to 4-nitrophenyl carbonate groups allows for tethering of bioactive peptide sequences and protein ligands such as adhesion domains from fibronectin and collagen. This procedure provides bioconjugate polymer brushes, **Figure A3.1**, which can be used to generate biomimetic coatings on titanium surfaces to promote bioactivity in biomedical and biotechnological applications.

Materials/ Results/ Discussion

To build on these findings and to explore the development of stable surface modifications of titanium, we set out to establish routes to prepare protein-adsorption-resistant polymer brushes that can be modified with peptide sequences that direct cell adhesion. We describe an approach to modify the surface of titanium with dense polymer brushes of poly(OEGMA) that resist protein adsorption and cell attachment. Furthermore, conversion of the hydroxyl end groups of the oligo(ethylene glycol) (OEG) side chains to 4-nitrophenyl carbonate groups allows for tethering of bioactive peptide sequences and protein ligands such as adhesion domains from fibronectin and collagen. This procedure provides bioconjugate polymer brushes, **Figure A3.1**, which can be used to generate biomimetic coatings on titanium surfaces to promote bioactivity in biomedical and biotechnological applications. Reaction of 2-bromo-2-methylpropionyl bromide with α -undecenyl alcohol to afford 10-undecen-1-yl 2-bromo-2-methylpropionate, followed by hydrosilylation with chlorodimethylsilane gave the initiator-substituted adsorbate, 11-(2-bromo-2-methyl)propionyloxy)undecenyl dimethylchlorosilane, (**Figure A3.2**) [304]. Titanium metal (2000 Å) was deposited onto clean glass coverslips by using electron-

beam evaporation. The titanium-coated coverslips were cleaned by treatment with piranha solution (50% H₂O₂, 50% concentrated H₂SO₄; 2 min, room temperature) followed by rinsing with copious amounts of distilled water then rinsing with acetone. The slides were dried at 125 °C for 2 h and immersed in a 1:1 solution of initiator-substituted adsorbate and dodecyldimethylchlorosilane (1.2 mmol of each in anhydrous hexane) to form a SAM on the titanium oxide surface, **Figure A3.1** [305,306].

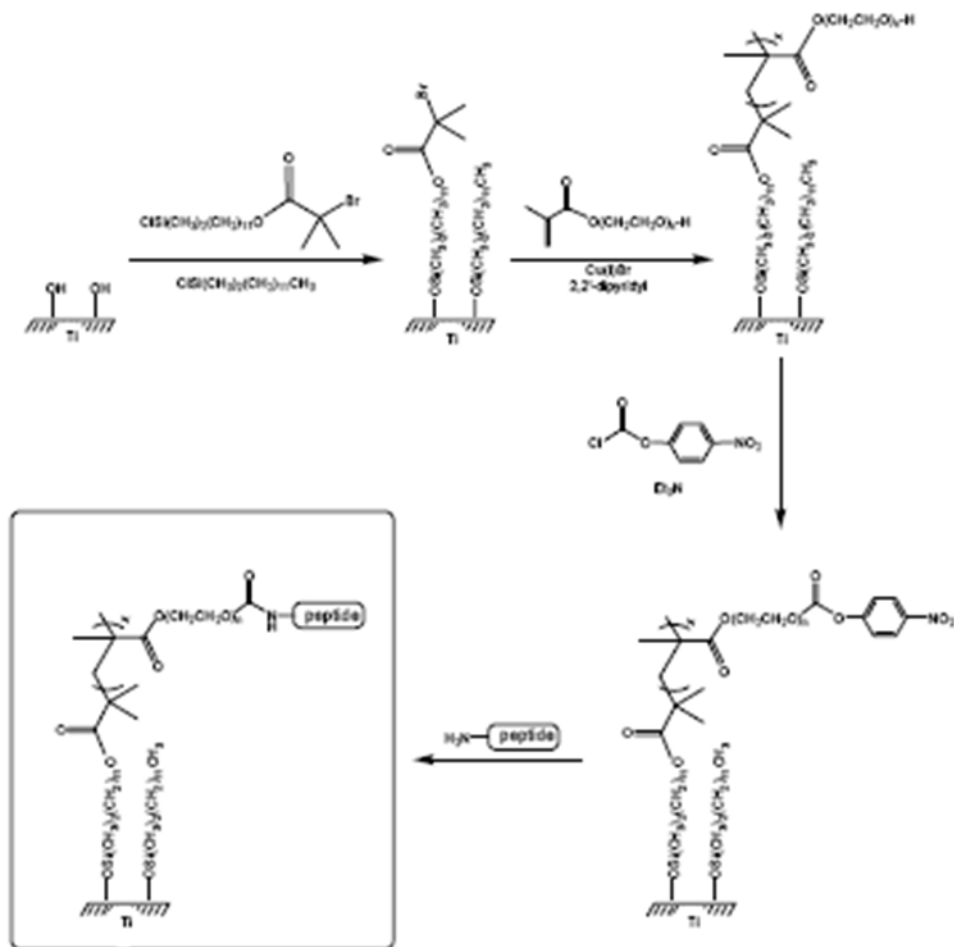


Figure A3.1. Poly(OEGMA) brush synthesis schematic. Formation of a peptide-modified poly(OEGMA) brush on titanium.

Formation of a monolayer of adsorbate was shown by the appearance of peaks at 809 (Si-O), 1738 (C=O), 1263 (O-C-O), and 1167 (O-C-O-C) cm^{-1} in the grazing angle (85°) specular reflection Fourier transform infrared reflectance (FTIR) spectrum, Figure 2A. The presence of bromine in the SAM was demonstrated by the appearance of a new peak in the X-ray photoelectron spectrum (XPS) at 103 eV (Br, 3d) (Supporting Information, Fig. S2). Polymer brushes of OEG-substituted polymethacrylate were prepared by immersing the SAM-modified slides into a solution of OEGMA (28.3 mmol), CuBr (1.6 mmol), 2,22-dipyridyl (2.8 mmol) in a 1:4 mixture of methanol (MeOH) and H₂O (37.5 mL) (**Figure A3.1**) [296,304]. Success of the polymerization was demonstrated by the appearance of a new peak in the FTIR spectrum at 1730 cm^{-1} corresponding to the carbonyl stretching vibration of the polymethacrylate backbone (**Figure A3.3 B**) and by the disappearance of the bromine peak in the XPS spectrum (**Figure A3.4**). The thickness of poly(OEGMA) brushes was monitored as a function of time using ellipsometry. The thickness of poly(OEGMA) increased linearly with the polymerization time for up to 4 h. Subsequent studies were conducted on slides subjected to SI-ATRP for 4 h, which afforded uniform films of poly(OEGMA) brushes with a thickness of approximately 135 Å (**Figure A3.5**).

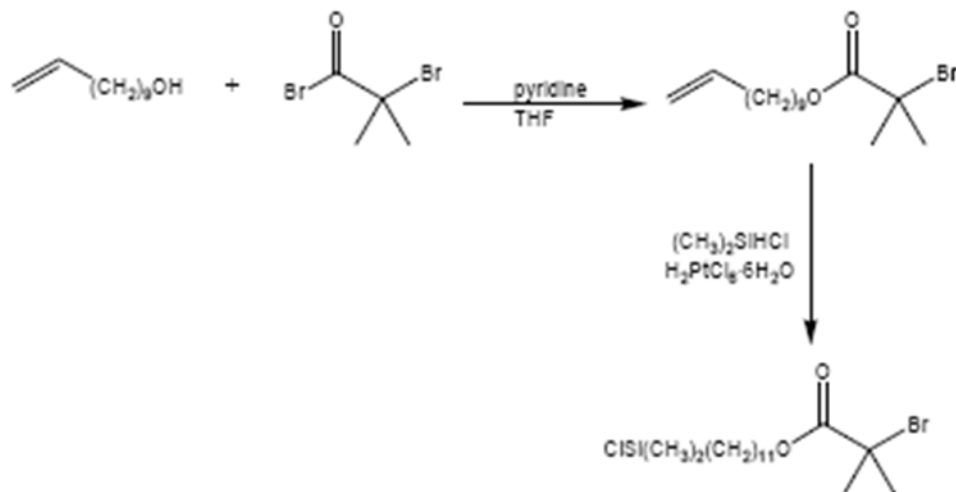


Figure A3.2. Synthesis schematic of initiator. Synthesis of chlorodimethyl(11-(2-bromo-2-methylpropionyloxy)undecyl)silane.

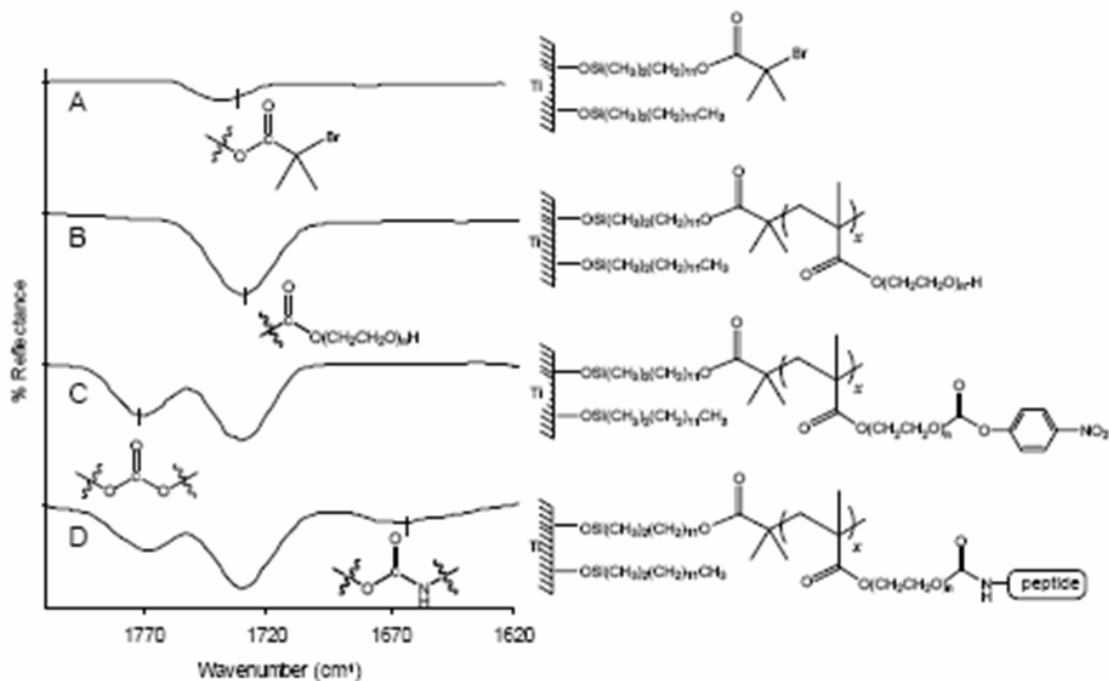
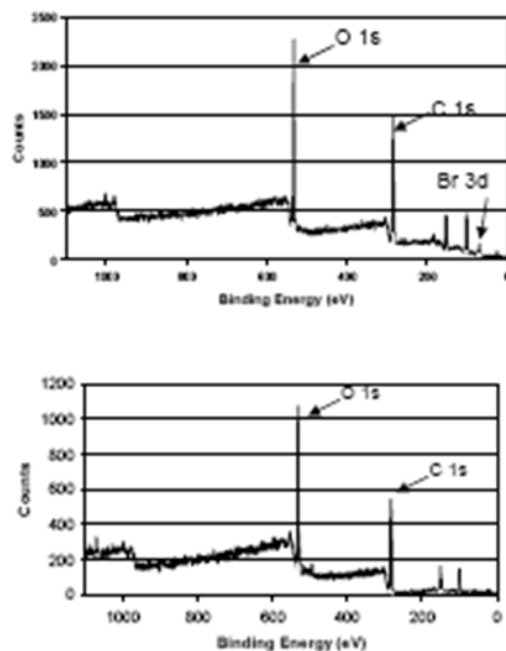


Figure A3.3. Carbonyl region of FTIR spectrum throughout formation of peptide-modified polymer brushes on titanium. A) 1:1 SAM of functionalized initiator **1**, and chlorododecyldimethylsilane; B) surfaces modified with poly(OEGMA) brushes; C) poly(OEGMA) brushes treated with NPC; and D) surfaces modified with GFOGER peptide.



Relative ratios of atoms present in a 1:1 SAM of functional initiator and nonfunctional spacer.				
	O 1s	C 1s	Br 3d	Si 2p
SAM of initiator and spacer	30	60	2	8
poly(OEGMA) brushes	37	47	0	16

Figure A3.4. XPS profiles of various stages of brush formation. XPS of SAM of □-bromo ester functionalized initiator on titanium (top) and poly(OEGMA) functionalized surface (bottom).

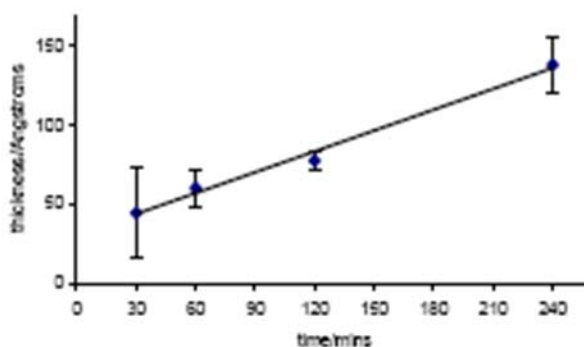


Figure A3.5. Control over brush thickness. Ellipsometric thickness of poly(OEGMA) brushes on titanium. Error bars indicate standard deviation from 3 measurements.

To evaluate the nonfouling properties and stability of the poly(OEGMA) brushes on titanium, surfaces were incubated for different time periods in Dulbecco's minimum essential medium (DMEM) culture medium supplemented with 10% fetal bovine serum and 1% penicillin–streptomycin. The serum contains adhesive proteins, such as vitronectin and fibronectin, which adsorb onto most synthetic materials and mediate cell adhesion [226]. Surface plasmon resonance (SPR) measurements of poly(OEGMA) brushes on titanium exposed to serum-containing media showed background levels (<0.2 ng/mm²) of protein adsorption, verifying the protein-adsorption-resistant nature of these films. For long-term cell-adhesion studies, the media was changed every seven days. After incubation in serum-containing media, titanium modified with poly(OEGMA) brushes was challenged with MC3T3-E1 osteoblast-like cells (RIKEN Cell Bank #RCB1126) for one hour. The slides were then rinsed with phosphate-buffered saline (PBS) buffer and the adherent cells were visualized using microscopy, **Figure A3.6 A**. Unmodified titanium-coated slides and SAMs of tri(ethylene glycol) (EG3)-terminated alkanethiol on Au were treated in the same way to demonstrate the effect of the poly(OEGMA) polymer brushes. Surfaces modified with poly(OEGMA) brushes on titanium were resistant to cell adhesion, **Figure A3.6 A**. After 56 days a few isolated cells that remained on the unfunctionalized poly(OEGMA)-grafted surfaces displayed a dendritic morphology indicative of poor adherence. In contrast to titanium surfaces modified with poly(OEGMA) brushes, cells adhered to and spread on unmodified titanium at all time periods. Notably, although SAMs of EG3-terminated alkanethiols on Au displayed resistance to cell adhesion at early time points, significant numbers of adherent cells were evident at 14 days. The resistance of poly(OEGMA) brushes on

titanium to cell adhesion over extended periods is in contrast to the loss of bioresistance of alkanethiols on gold, which has been well documented [278] The data from the long-term cell-adhesion studies was quantified in order to compare the resistance of poly(OEGMA) brushes to EG3 SAMs, **Figure A3.6 B**. The number of adherent cells on surfaces modified with poly(OEGMA) brushes and EG3 SAMs were normalized to the cell numbers on unmodified titanium surface. Poly(OEGMA) brushes and EG3 SAMs demonstrated comparable bioresistance for the 1 h and 7 day time points. However, at 14 days poly(OEGMA) maintained the ability to prevent cell adhesion, whereas EG3 SAMs showed an increase to 60% cell adhesion relative to the unmodified titanium standard, **Figure A3.6 B**.

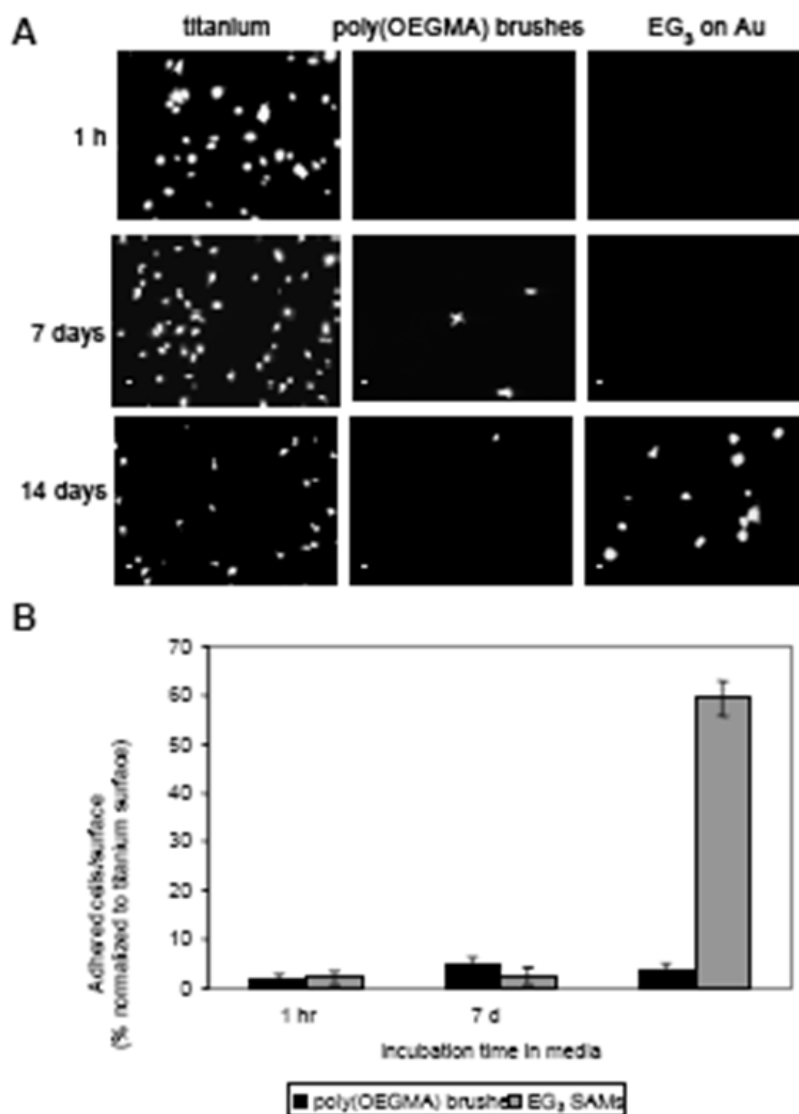


Figure A3.6. Poly(OEGMA) brushes on Ti resist cell adhesion. A) Micrographs of adhered cells on unmodified titanium slides (left column), poly(OEGMA)-modified titanium slides (center), and EG₃ thiol monolayers on Au surfaces (right) after incubation in media for up to 14 days and then incubated with fluorescence-labeled cells for 1 h. B) Plot of number of adhered cells as a function of time on poly(OEGMA) brushes and EG₃ SAMs.

Having demonstrated the resistance to cell adhesion and stability of poly(OEGMA) brushes in serum-containing media, we set out to explore methods to tether adhesive peptide sequences in order to impart biofunctionality and thereby attain control of cell adhesion. This was achieved by covalent immobilization of a triple helical peptide that contains the GFOGER sequence (GGYGGGPC(GPP)5(GFOGER)(GPP)5GPC, where O= hydroxyproline, G= glycine, F = phenylalanine, E= glutamic acid, and R= arginine) found in type I collagen, which selectively promotes cell adhesion [86]. Functionalization of the hydroxyl end groups of the poly(OEGMA) brushes was performed by immersion of the slides into a solution of 4-nitrophenyl chloroformate (NPC) (1.4 mmol in 60 mL of tetrahydrofuran (THF)) (**Figure A3.1**) [307]. Slides treated with NPC were then immersed in a 30 $\mu\text{g/mL}$ solution of GFOGER-containing peptide in PBS for 30 min. This process resulted in the displacement 4-nitrophenol and subsequent immobilization of the peptide via the N-terminus by formation of a urethane linkage. Thus, reaction of the polymer brushes with NPC resulted in the appearance of a second carbonyl peak at 1770 cm^{-1} (**Fig. A3.3 C**) because of the presence of the carbonate linkage. After treatment with the GFOGER-peptide an additional carbonyl peak was observed at 1668 cm^{-1} corresponding to the amide linkages in the oligopeptide, **Figure A3.3 D**. Effective tethering of adhesive peptides was also demonstrated by an enzyme-linked immunosorbent assay (ELISA). We examined tethering of a RGD-containing peptide since this sequence represents a common adhesion motif to render surfaces bioadhesive. Slides functionalized with NPC were treated with a GRGDSPC peptide sequence with a biotin label on the carboxy terminus. The slides were then incubated with a biotin antibody bearing an alkaline

phosphatase. Subsequent immersion of the slides into a solution of 4-methylumbelliferyl phosphate resulted in an increase in fluorescence relative to the amount of peptide on the surface. The peptide-modified slides demonstrated a threefold increase in fluorescence compared to slides for which the poly(OEGMA) brushes were unmodified, demonstrating both the success of the immobilization step and that the peptide retains a biologically active conformation.

The density of peptide tethered onto modified titanium surfaces was quantified by SPR. SPR chips were coated with titanium and modified with poly(OEGMA) brushes. Two conditions were analyzed: i) poly(OEGMA) brushes modified with NPC, and ii) poly(OEGMA) brushes that had not been treated with NPC (as a control). The modified SPR chips were exposed to GFOGER peptide (a 10 mL/min flow of a 30 $\mu\text{g/mL}$ solution for 25 min). Poly(OEGMA) brushes activated with NPC displayed a significant increase in mass when exposed to GFOGER peptide, indicating covalent tethering of the peptide onto NPC-modified brushes (**Figure A3.7**). Using a conversion factor (1000 RU= 1 ng/mm^2 , which is generally accepted for layers of adsorbed protein independent of their molecular weight, and has been validated for titanium surfaces using radiolabeled proteins), we estimate that a surface density of 27.8 pmol/cm^2 (i.e., 625 \AA of surface area per molecule of peptide) was obtained. In contrast, poly(OEGMA) brushes that had not been activated with NPC displayed essentially no increase in mass upon exposure to GFOGER peptide, reflecting the protein-adsorption-resistant nature of the unmodified brushes.

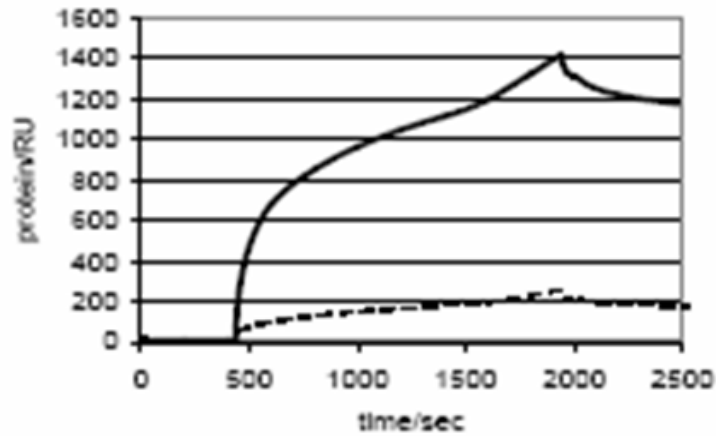


Figure A3.7. SPR profile of GFOGER-exposed poly(OEGMA) brushes. NPC-treated poly(OEGMA) brushes on Ti (solid line) and untreated brushes (dashed line) upon exposure to a solution of GFOGER-containing peptide.

As a final characterization of the peptide-functionalized surfaces, cells were seeded onto the engineered brushes. Cells adhered to and spread onto poly(OEGMA) brushes that had been activated with NPC and subsequently functionalized with the GFOGER peptide, **Figure A3.8 A**, demonstrating that the tethered peptide is in an active form that supports robust cell adhesion. Cells did not attach to poly(OEGMA) brushes that had not been activated with NPC, **Figure A3.8 B**, which is consistent with the SPR measurements and previous observations (i.e., **Figure A3.7**).



Figure A3.8. GFOGER immobilized on poly(OEGMA) brushes promotes cell adhesion. Micrographs of adhered cells on (left column), poly(OEGMA) brushes treated with NPC followed by GFOGER-containing peptide (left) and unmodified poly(OEGMA) brushes. Both slides were incubated in a cell solution for 1 hour.

Although a thorough evaluation of cytotoxicity is beyond the scope of this initial study, cells adhering to GFOGER-functionalized brushes exhibited a well spread morphology and we observed an increase in cell numbers with culture time, suggesting that these surfaces are cytocompatible. Ongoing in vitro as well as in vivo studies will examine this issue in more depth.

Summary

In conclusion, we present an approach to modify poly(OEGMA) brushes on titanium with peptide sequences from adhesion proteins to provide control over the adhesion of cells to the surfaces. The poly(OEGMA) brushes are stable, protein adsorption- and cell-adhesion-resistant surfaces. Functionalization with bioadhesive peptides selectively promotes cell adhesion. This approach provides a robust

methodology to generate coatings that present controlled densities of bioactive ligands within a nonfouling background on metal substrates. This represents a biomolecular strategy to impart biofunctionality to biomedical-grade titanium and thereby enhance the biological performance and osseointegration of titanium-based orthopedic and dental devices.

REFERENCES

1. American Academy of Orthopedic Surgeons. Arthroplasty and Total Joint Replacement Procedures: National Center for Health Statistics, 1991 to 2000 National Hospital Discharge Survey 2003.
2. Arthritis Foundation. National Arthritis Action Plan: A Public Health Strategy. CDC Web Page (www.cdc.gov) 1999.
3. Bauer TW, Schils J. The pathology of total joint arthroplasty. I. Mechanisms of implant fixation. *Skeletal Radiol.* 1999; 28:423-432.
4. Bauer TW, Schils J. The pathology of total joint arthroplasty. II. Mechanisms of implant failure. *Skeletal Radiol.* 1999; 28:483-497.
5. Ferris DM, Moodie GD, Dimond PM, Gioranni CW, Ehrlich MG, Valentini RF. RGD-coated titanium implants stimulate increased bone formation in vivo. *Biomaterials.* 1999; 20:2323-2331.
6. Alsberg E, Anderson KW, Albeiruti A, Rowley JA, Mooney DJ. Engineering growing tissues. *Proc Natl Acad Sci U S A.* 2002; 99:12025-12030.
7. Li F, Carlsson D, Lohmann C, Suuronen E, Vascotto S, Kobuch K, Sheardown H, Munger R, Nakamura M, Griffith M. Cellular and nerve regeneration within a biosynthetic extracellular matrix for corneal transplantation. *Proc Natl Acad Sci U S A.* 2003; 100:15346-1535.
8. Schense JC, Bloch J, Aebischer P, Hubbell JA. Enzymatic incorporation of bioactive peptides into fibrin matrices enhances neurite extension. *Nat Biotechnol.* 2000; 18:415-419.
9. Yu X, Bellamkonda RV. Tissue-engineered scaffolds are effective alternatives to autografts for bridging peripheral nerve gaps. *Tissue Eng.* 2003; 9:421-430.
10. Elmengaard B, Bechtold JE, Soballe K. In vivo study of the effect of RGD treatment on bone ongrowth on press-fit titanium alloy implants. *Biomaterials.* 2005; 26:3521-3526.
11. Schliephake H, Scharnweber D, Dard M, Rossler S, Sewing A, Meyer J, Hoogestraat D. Effect of RGD peptide coating of titanium implants on periimplant bone formation in the alveolar crest. An experimental pilot study in dogs. *Clin Oral Implants Res.* 2002; 13:312-319.

12. Barber TA, Ho JE, De Ranieri A, Viridi AS, Sumner DR, Healy KE. Peri-implant bone formation and implant integration strength of peptide-modified p(AAM-co-EG/AAC) interpenetrating polymer network-coated titanium implants. *J Biomed Mater Res A*. 2007; 80:306-320.
13. Aota S, Nomizu M, Yamada KM. The short amino acid sequence Pro-His-Ser-Arg-Asn in human fibronectin enhances cell-adhesive function. *J Biol Chem*. 1994; 269:24756-24761.
14. Emsley J, Knight CG, Farndale RW, Barnes MJ, Liddington RC. Structural basis of collagen recognition by integrin alpha2beta1. *Cell*. 2000; 101:47-56.
15. García AJ, Schwarzbauer JE, Boettiger D. Distinct activation states of alpha5beta1 integrin show differential binding to RGD and synergy domains of fibronectin. *Biochemistry*. 2002; 41:9063-9069.
16. Hynes RO. Integrins: bidirectional, allosteric signaling machines. *Cell*. 2002; 110:673-687.
17. Keselowsky BG, Collard DM, Garcia AJ. Integrin binding specificity regulate biomaterial surface chemistry effects on cell differentiation. *Proc Natl Acad Sci U S A*. 2005; 102: 5953 - 5957.
18. Lan MA, Gersbach CA, Michael KE, Keselowsky BG, Garcia AJ. Myoblast proliferation and differentiation on fibronectin-coated self assembled monolayers presenting different surface chemistries. *Biomaterials*. 2005; 26: 4523 - 4531.
19. Giancotti FG and Ruoslahti E. Integrin signaling. *Science*. 1999; 285: 1028 - 1032.
20. Schwartz MA and Assoian RK. Integrins and cell proliferation: regulation of cyclin-dependent kinases via cytoplasmic signaling pathways. *J Cell Sci*. 2001; 114: 2553 - 2560.
21. Temenoff JS and Mikos AG. *Biomaterials: The Intersection of Biology and Materials Science*. 2008.
22. Reichardt LF. *Introduction: Extracellular matrix molecules*. 1999; 2nd: 335 - 344.
23. Prockop DJ and Kivirikko KI. *Collagens: molecular biology, diseases, and potentials for therapy*. *Annu Rev Biochem*. 1995; 64: 403 - 434.
24. Reddi AH. Role of morphogenetic proteins in skeletal tissue engineering and regeneration. *Nat Biotechnol*. 1998; 16: 247 - 252.
25. Hynes RO. *Molecular biology of fibronectin*. *Annu Rev Cell Biol*. 1985; 1: 67 - 90.
26. De Arcangelis A and Georges-Labouesse E. Integrin and ECM functions: roles in vertebrate development. *Trends Genet*. 2000; 16: 389 - 395.

27. Danen EH and Sonnenberg A. Integrins in regulation of tissue development and function. *J Pathol.* 2003; 201: 632 - 641.
28. Garcia AJ and Reyes CD. Bio-adhesive surfaces to promote osteoblast differentiation and bone formation. *J Dent Res.* 2005; 84: 407 - 413.
29. Khan Y, Yaszemski MJ, Mikos AG, Laurencin CT. Tissue engineering of bone: material and matrix considerations. *J Bone Joint Surg Am.* 2008; 90 Suppl 1: 36 - 42.
30. Alberts B, Johnson A, Lewis J, Raff M, Roberts K, Walter P. 2007; 4th ed.
31. Lutolf MP and Hubbell JA. Synthetic biomaterials as instructive extracellular microenvironments for morphogenesis in tissue engineering. *Nat Biotechnol.* 2005; 23: 47 - 55.
32. Anderson JM. Biological responses to materials. *Annu Rev Mater Res.* 2001; 31: 81 - 110.
33. Hench LL and Polak JM. Third-generation biomedical materials. *Science.* 2002; 295: 1014 - 1017.
34. Vreeland WN and Barron AE. Functional materials for microscale genomic and proteomic analyses. *Curr Opin Biotechnol.* 2002; 13: 87 - 94.
35. Siebers MC, ter Brugge PJ, Walboomers XF, Jansen JA. Integrins as linker proteins between osteoblasts and bone replacing materials. A critical review. *Biomaterials.* 2005; 26: 137 - 146.
36. Moursi AM, Globus RK, Damsky CH. Interactions between integrin receptors and fibronectin are required for calvarial osteoblast differentiation in vitro. *J Cell Sci.* 1997; 110: 2187 - 2196.
37. Gronthos S, Simmons PJ, Graves SE, Robey PG. Integrin-mediated interactions between human bone marrow stromal precursor cells and the extracellular matrix. *Bone JID - 8504048.* 2001; 28: 174 - 181.
38. Gronowicz G and McCarthy MB. Response of human osteoblasts to implant materials: integrin-mediated adhesion. *J Orthop Res.* 1996; 14: 878 - 887.
39. Ruoslahti E and Pierschbacher MD. New perspectives in cell adhesion: RGD and integrins. *Science.* 1987; 238: 491 - 497.
40. Geiger B, Bershadsky A, Pankov R, Yamada KM. Transmembrane crosstalk between the extracellular matrix and the cytoskeleton. *Nat Rev Mol Cell Biol.* 2001; 2: 793 - 805.

41. Petit V and Thiery JP. Focal adhesions: structure and dynamics. *Biol Cell*. 2000; 92: 477 - 494.
42. Anselme K. Osteoblast adhesion on biomaterials. *Biomaterials JID* - 8100316. 2000; 21: 667 - 681.
43. Takeuchi Y, Suzawa M, Kikuchi T, Nishida E, Fujita T, Matsumoto T. Differentiation and transforming growth factor-beta receptor down-regulation by collagen-alpha2beta1 integrin interaction is mediated by focal adhesion kinase and its downstream signals in murine osteoblastic cells. *J Biol Chem*. 1997; 272: 29309 - 29316.
44. Nykvist P, Tasanen K, Viitasalo T, Kapyla J, Jokinen J, Bruckner-Tuderman L, Heino J. The cell adhesion domain of type XVII collagen promotes integrin-mediated cell spreading by a novel mechanism. *J Biol Chem*. 2001; 276: 38673 - 38679.
45. Moursi AM, Damsky CH, Lull J, Zimmerman D, Doty SB, Aota S, Globus RK. Fibronectin regulates calvarial osteoblast differentiation. *J Cell Sci*. 1996; 109: 1369 - 1380.
46. Lan MA, Gersbach CA, Michael KE, Keselowsky BG, Garcia AJ. Myoblast proliferation and differentiation on fibronectin-coated self assembled monolayers presenting different surface chemistries. *Biomaterials*. 2005; 26: 4523 - 4531.
47. Stephansson SN, Byers BA, García AJ. Enhanced expression of the osteoblastic phenotype on substrates that modulate fibronectin conformation and integrin receptor binding. *Biomaterials*. 2002; 23: 2527 - 2534.
48. Mizuno M, Fujisawa R, Kuboki Y. Type I collagen-induced osteoblastic differentiation of bone-marrow cells mediated by collagen-alpha2beta1 integrin interaction. *J Cell Physiol*. 2000; 184: 207 - 213.
49. Reyes CD, Petrie TA, Burns KL, Schwartz Z, Garcia AJ. Biomolecular surface coating to enhance orthopaedic tissue healing and integration. *Biomaterials*. 2007; 28: 3228 - 3235.
50. Cheng SL, Lai CF, Blystone SD, Avioli LV. Bone mineralization and osteoblast differentiation are negatively modulated by integrin alpha(v)beta3. *J Bone Miner Res*. 2001; 16: 277 - 288.
51. Sung V, Stubbs JT, III, Fisher L, Aaron AD, Thompson EW. Bone sialoprotein supports breast cancer cell adhesion proliferation and migration through differential usage of the alpha(v)beta3 and alpha(v)beta5 integrins. *J Cell Physiol*. 1998; 176: 482 - 494.

52. Niu JX, Zhang WJ, Ye LY, Wu LQ, Zhu GJ, Yang ZH, Grau GE, Lou JN. The role of adhesion molecules, alpha v beta 3, alpha v beta 5 and their ligands in the tumor cell and endothelial cell adhesion. *Eur J Cancer Prev.* 2007; 16: 517 - 527.
53. Zhou X, Murphy FR, Gehdu N, Zhang J, Iredale JP, Benyon RC. Engagement of alphavbeta3 integrin regulates proliferation and apoptosis of hepatic stellate cells. *J Biol Chem.* 2004; 279: 23996 - 24006.
54. Tang L, Ugarova TP, Plow EF, Eaton JW. Molecular determinants of acute inflammatory responses to biomaterials. *J Clin Invest.* 1996; 97: 1329 - 1334.
55. Flick MJ, Du X, Witte DP, Jirouskova M, Soloviev DA, Busuttill SJ, Plow EF, Degen JL. Leukocyte engagement of fibrin(ogen) via the integrin receptor alphaMbeta2/Mac-1 is critical for host inflammatory response in vivo. *J Clin Invest.* 2004; 113: 1596 - 1606.
56. Garcia AJ. *Advanced Polymer Science.* 2006; 172 - 190.
57. Vogel V, Thomas WE, Craig DW, Krammer A, Baneyx G. Structural insights into the mechanical regulation of molecular recognition sites. *Trends Biotechnol.* 2001; 19: 416 - 423.
58. Xu LC and Siedlecki CA. Effects of surface wettability and contact time on protein adhesion to biomaterial surfaces. *Biomaterials.* 2007; 28: 3273 - 3283.
59. Sinha RK and Tuan RS. Regulation of human osteoblast integrin expression by orthopedic implant materials. *Bone.* 1996; 18: 451 - 457.
60. Ter Brugge PJ, Torensma R, de Ruijter JE, Figdor CG, Jansen JA. Modulation of integrin expression on rat bone marrow cells by substrates with different surface characteristics. *Tissue Eng.* 2002; 8: 615 - 626.
61. Ter Brugge PJ, Dieudonne S, Jansen JA. Initial interaction of U2OS cells with noncoated and calcium phosphate coated titanium substrates. *J Biomed Mater Res.* 2002; 61: 399 - 407.
62. Kilpadi KL, Chang PL, Bellis SL. Hydroxylapatite binds more serum proteins, purified integrins, and osteoblast precursor cells than titanium or steel. *J Biomed Mater Res JID - 0112726.* 2001; 57: 258 - 267.
63. Yamamoto H, Shibata Y, Miyazaki T. Anode glow discharge plasma treatment of titanium plates facilitates adsorption of extracellular matrix proteins to the plates. *J Dent Res.* 2005; 84: 668 - 671.
64. Brodbeck WG, Shive MS, Colton E, Nakayama Y, Matsuda T, Anderson JM. Influence of biomaterial surface chemistry on the apoptosis of adherent cells. *J Biomed Mater Res.* 2001; 55: 661 - 668.

65. Keselowsky BG, Collard DM, Garcia AJ. Surface chemistry modulates fibronectin conformation and directs integrin binding and specificity to control cell adhesion. *J Biomed Mater Res A*. 2003; 66: 247 - 259.
66. Keselowsky BG, Collard DM, Garcia AJ. Surface chemistry modulates focal adhesion composition and signaling through changes in integrin binding. *Biomaterials*. 2004; 25: 5947 - 5954.
67. Michael KE, Vernakar VN, Keselowsky BG, Meredith JC, Latour RA, Garcia AJ. Adsorption-induced conformational changes in fibronectin due to interactions with well-defined surface chemistries. *Langmuir*. 2003; 19: 8033 - 8040.
68. Lee MH, Ducheyne P, Lynch L, Boettiger D, Composto RJ. Effect of biomaterial surface properties on fibronectin- α 5 β 1 integrin interaction and cellular attachment. *Biomaterials*. 2006; 27: 1907 - 1916.
69. Lange R, Luthen F, Beck U, Rychly J, Baumann A, Nebe B. Cell-extracellular matrix interaction and physico-chemical characteristics of titanium surfaces depend on the roughness of the material. *Biomol Eng*. 2002; 19: 255 - 261.
70. Keselowsky BG, Wang L, Schwartz Z, Garcia AJ, Boyan BD. Integrin α (5) controls osteoblastic proliferation and differentiation responses to titanium substrates presenting different roughness characteristics in a roughness independent manner. *J Biomed Mater Res A*. 2006; 80A: 700 - 710.
71. Lincks J, Boyan BD, Blanchard CR, Lohmann CH, Liu Y, Cochran DL, Dean DD, Schwartz Z. Response of MG63 osteoblast-like cells to titanium and titanium alloy is dependent on surface roughness and composition. *Biomaterials*. 1998; 19: 2219 - 2232.
72. Anselme K, Bigerelle M, Noel B, Dufresne E, Judas D, Iost A, Hardouin P. Qualitative and quantitative study of human osteoblast adhesion on materials with various surface roughnesses. *J Biomed Mater Res*. 2000; 49: 155 - 166.
73. Rezanian A and Healy KE. Biomimetic peptide surfaces that regulate adhesion, spreading, cytoskeletal organization, and mineralization of the matrix deposited by osteoblast-like cells. *Biotechnol Prog*. 1999; 15: 19 - 32.
74. Gronthos S, Stewart K, Graves SE, Hay S, Simmons PJ. Integrin expression and function on human osteoblast-like cells. *J Bone Miner Res*. 1997; 12: 1189 - 1197.
75. Jimbo R, Sawase T, Shibata Y, Hirata K, Hishikawa Y, Tanaka Y, Bessho K, Ikeda T, Atsuta M. Enhanced osseointegration by the chemotactic activity of plasma fibronectin for cellular fibronectin positive cells. *Biomaterials*. 2007; 28: 3469 - 3477.

76. Geissler U, Hempel U, Wolf C, Scharnweber D, Worch H, Wenzel K. Collagen type I-coating of Ti6Al4V promotes adhesion of osteoblasts. *J Biomed Mater Res.* 2000; 51: 752 - 760.
77. Bierbaum S, Hempel U, Geissler U, Hanke T, Scharnweber D, Wenzel KW, Worch H. Modification of Ti6AL4V surfaces using collagen I, III, and fibronectin. II. Influence on osteoblast responses. *J Biomed Mater Res A.* 2003; 67: 431 - 438.
78. Karadag A and Fisher LW. Bone sialoprotein enhances migration of bone marrow stromal cells through matrices by bridging MMP-2 to alpha(v)beta3-integrin. *J Bone Miner Res.* 2006; 21: 1627 – 1636.
79. O'Toole GC, Salih E, Gallagher C, FitzPatrick D, O'Higgins N, O'Rourke SK. Bone sialoprotein-coated femoral implants are osteoinductive but mechanically compromised. *J Orthop Res.* 2004; 22: 641 - 646.
80. Cheng SL, Lai CF, Fausto A, Chellaiah M, Feng X, McHugh KP, Teitelbaum SL, Civitelli R, Hruska KA, Ross FP, Avioli LV. Regulation of alphaVbeta3 and alphaVbeta5 integrins by dexamethasone in normal human osteoblastic cells. *J Cell Biochem.* 2000; 77: 265 - 276.
81. Langer R and Tirrell DA. Designing materials for biology and medicine. *Nature.* 2004; 428: 487 - 492.
82. Humphries MJ. Peptide recognition motifs involved in the binding of integrins to their ligands. *Kidney Int.* 1992; 41: 645 - 649.
83. Merrill EW. Poly(ethylene oxide) and blood contact: a chronicle of one laboratory. 1992; 199 - 220.
84. Garcia AJ, Vega MD, Boettiger D. Modulation of cell proliferation and differentiation through substrate-dependent changes in fibronectin conformation. *Mol Biol Cell.* 1999; 10: 785 - 798.
85. Hodde J, Record R, Tullius R, Badylak S. Fibronectin peptides mediate HMEC adhesion to porcine-derived extracellular matrix. *Biomaterials.* 2002; 23: 1841 - 1848.
86. Reyes CD and Garcia AJ. Alpha2beta1 integrin-specific collagen-mimetic surfaces supporting osteoblastic differentiation. *J Biomed Mater Res.* 2004; 69A: 591 - 600.
87. Gilbert M, Giachelli CM, Stayton PS. Biomimetic peptides that engage specific integrin-dependent signaling pathways and bind to calcium phosphate surfaces. *J Biomed Mater Res.* 2003; 67A: 69 - 77.
88. Sanchez-Aparicio P, Dominguez-Jimenez C, Garcia-Pardo A. Activation of the alpha 4 beta 1 integrin through the beta 1 subunit induces recognition of the RGDS sequence in fibronectin. *J Cell Biol.* 1994; 126: 271 - 279.

89. Horton MA, Nesbit MA, Helfrich MH. Interaction of osteopontin with osteoclast integrins. *Ann N Y Acad Sci.* 1995; 760: 190 - 200.
90. Weber LM, Hayda KN, Haskins K, Anseth KS. The effects of cell-matrix interactions on encapsulated beta-cell function within hydrogels functionalized with matrix-derived adhesive peptides. *Biomaterials.* 2007; 28: 3004 - 3011.
91. Shin H, Jo S, Mikos AG. Biomimetic materials for tissue engineering. *Biomaterials.* 2003; 24: 4353 - 4364.
92. Hersel U, Dahmen C, Kessler H. RGD modified polymers: biomaterials for stimulated cell adhesion and beyond. *Biomaterials.* 2003; 24: 4385 - 4415.
93. Shin H, Temenoff JS, Bowden GC, Zygorakis K, Farach-Carson MC, Yaszemski MJ, Mikos AG. Osteogenic differentiation of rat bone marrow stromal cells cultured on Arg-Gly-Asp modified hydrogels without dexamethasone and beta-glycerol phosphate. *Biomaterials.* 2005 Jun;26(17):3645-54.
94. Liu JC, Heilshorn SC, Tirrell DA. Comparative cell response to artificial extracellular matrix proteins containing the RGD and CS5 cell-binding domains. *Biomacromolecules.* 2004; 5: 497 - 504.
95. Harbers GM and Healy KE. The effect of ligand type and density on osteoblast adhesion, proliferation, and matrix mineralization. *J Biomed Mater Res A.* 2005; 75: 855 - 869.
96. Schense JC and Hubbell JA. Three-dimensional migration of neurites is mediated by adhesion site density and affinity. *J Biol Chem.* 2000; 275: 6813 - 6818.
97. Takagi J. Structural basis for ligand recognition by RGD (Arg-Gly-Asp)-dependent integrins. *Biochem Soc Trans.* 2004; 32: 403 - 406.
98. Pakalns T, Haverstick KL, Fields GB, McCarthy JB, Mooradian DL, Tirrell M. Cellular recognition of synthetic peptide amphiphiles in self-assembled monolayer films. *Biomaterials.* 1999; 20: 2265 - 2279.
99. Dahmen C, Auernheimer J, Meyer A, Enderle A, Goodman SL, Kessler H. Improving implant materials by coating with nonpeptidic, highly specific integrin ligands. *Angew Chem Int Ed Engl.* 2004; 43: 6649 – 6652.
100. Lieb E, Hacker M, Tessmar J, Kunz-Schughart LA, Fiedler J, Dahmen C, Hersel U, Kessler H, Schulz MB, Gopferich A. Mediating specific cell adhesion to low-adhesive diblock copolymers by instant modification with cyclic RGD peptides. *Biomaterials.* 2005; 26: 2333 – 2341.
101. Marchi-Artzner V, Lorz B, Hellerer U, Kantlehner M, Kessler H, Sackmann E. Selective adhesion of endothelial cells to artificial membranes with a synthetic RGD-lipopeptide. *Chemistry.* 2001; 7: 1095 - 1101.

102. Hennessy KM, Clem WC, Phipps MC, Sawyer AA, Shaikh FM, Bellis SL. The effect of RGD peptides on osseointegration of hydroxyapatite biomaterials. *Biomaterials*. 2008; 29: 3075 - 3083.
103. Petrie TA, Raynor JE, Reyes CD, Burns KL, Collard DM, Garcia AJ. The effect of integrin-specific bioactive coatings on tissue healing and implant osseointegration. *Biomaterials*. 2008; 29: 2849 - 2857.
104. Elmengaard B, Bechtold JE, Soballe K. In vivo effects of RGD-coated titanium implants inserted in two bone-gap models. *J Biomed Mater Res A*. 2005; 75: 249 - 255.
105. Schliephake H, Scharnweber D, Dard M, Rossler S, Sewing A, Meyer J, Hoogestraat D. Effect of RGD peptide coating of titanium implants on periimplant bone formation in the alveolar crest. An experimental pilot study in dogs. *Clin Oral Implants Res*. 2002; 13: 312 - 319.
106. Ferris DM, Moodie GD, Dimond PM, Gioranni CW, Ehrlich MG, Valentini RF. RGD-coated titanium implants stimulate increased bone formation in vivo. *Biomaterials*. 1999; 20: 2323 - 2331.
107. Tosatti S, Schwartz Z, Campbell C, Cochran DL, VandeVondele S, Hubbell JA, Denzer A, Simpson J, Wieland M, Lohmann CH, Textor M, Boyan BD. RGD-containing peptide GCRGYGRGDSPG reduces enhancement of osteoblast differentiation by poly(L-lysine)-graft-poly(ethylene glycol)-coated titanium surfaces. *J Biomed Mater Res*. 2004; 68A: 458 - 472.
108. Petrie TA, Capadona JR, Reyes CD, Garcia AJ. Integrin specificity and enhanced cellular activities associated with surfaces presenting a recombinant fibronectin fragment compared to RGD supports. *Biomaterials*. 2006; 27: 5459 - 5470.
109. Lee MH, Adams CS, Boettiger D, DeGrado WF, Shapiro IM, Composto RJ, Ducheyne P. Adhesion of MC3T3-E1 cells to RGD peptides of different flanking residues: detachment strength and correlation with long-term cellular function. *J Biomed Mater Res A*. 2007; 81: 150 - 160.
110. Aota S, Nomizu M, Yamada KM. The short amino acid sequence Pro-His-Ser-Arg-Asn in human fibronectin enhances cell-adhesive function. *J Biol Chem*. 1994; 269: 24756 - 24761.
111. Petrie TA, Reyes CD, Raynor JE, Burns KL, Collard DM, Garcia AJ. Biointerfaces promoting tissue healing. *J Musculoskelet Neuronal Interact*. 2007; 7: 332.
112. Lee MH, Ducheyne P, Lynch L, Boettiger D, Composto RJ. Effect of biomaterial surface properties on fibronectin- α 5 β 1 integrin interaction and cellular attachment. *Biomaterials*. 2006 Mar;27(9):1907-16.

113. Altroff H, Schlinkert R, van der Walle CF, Bernini A, Campbell ID, Werner JM, Mardon HJ. Interdomain tilt angle determines integrin-dependent function of the ninth and tenth FIII domains of human fibronectin. *J Biol Chem.* 2004; 279: 55995 - 56003.
114. Krammer A, Craig D, Thomas WE, Schulten K, Vogel V. A structural model for force regulated integrin binding to fibronectin's RGD-synergy site. *Matrix Biol.* 2002; 21: 139 - 147.
115. Friedland JC, Lee MH, Boettiger D. Mechanically activated integrin switch controls alpha5beta1 function. *Science.* 2009 Jan 30;323(5914):642-4.
116. Kokkoli E, Mardilovich A, Wedekind A, Rexeisen EL, Garg A, Craig JA. Self-assembly and applications of biomimetic and bioactive peptide-amphiphiles. *Soft Matter.* 2006; 2: 1015 - 1024.
117. Dillow AK, Ochsenhirt SE, McCarthy JB, Fields GB, Tirrell M. Adhesion of alpha5beta1 receptors to biomimetic substrates constructed from peptide amphiphiles. *Biomaterials.* 2001; 22: 1493 - 1505.
118. Kokkoli E, Ochsenhirt SE, Tirrell M. Collective and single-molecule interactions of alpha5beta1 integrins. *Langmuir.* 2004; 20: 2397 - 2404.
119. Ochsenhirt SE, Kokkoli E, McCarthy JB, Tirrell M. Effect of RGD secondary structure and the synergy site PHSRN on cell adhesion, spreading and specific integrin engagement. *Biomaterials.* 2006; 27: 3863 - 3874.
120. Mardilovich A and Kokkoli E. Biomimetic peptide-amphiphiles for functional biomaterials: the role of GRGDSP and PHSRN. *Biomacromolecules.* 2004; 5: 950 - 957.
121. Mardilovich A, Craig JA, McCammon MQ, Garg A, Kokkoli E. Design of a novel fibronectin-mimetic peptide-amphiphile for functionalized biomaterials. *Langmuir.* 2006; 22: 3259 - 3264.
122. Benoit DS and Anseth KS. The effect on osteoblast function of colocalized RGD and PHSRN epitopes on PEG surfaces. *Biomaterials.* 2005; 26: 5209 - 5220.
123. Jensen TW, Hu BH, Delatore SM, Garcia AS, Messersmith PB, Miller WM. Lipopeptides incorporated into supported phospholipid monolayers have high specific activity at low incorporation levels. *J Am Chem Soc.* 2004; 126: 15223 - 15230.
124. Cutler SM and García AJ. Engineering cell adhesive surfaces that direct integrin alpha5beta1 binding using a recombinant fragment of fibronectin. *Biomaterials.* 2003; 24: 1759 - 1770.

125. Richards J, Miller M, Abend J, Koide A, Koide S, Dewhurst S. Engineered fibronectin type III domain with a RGDWXE sequence binds with enhanced affinity and specificity to human α 5 β 3 integrin. *J Mol Biol.* 2003; 326: 1475 - 1488.
126. Mould AP, Komoriya A, Yamada KM, Humphries MJ. The CS5 peptide is a second site in the IIICS region of fibronectin recognized by the integrin α 4 β 1. Inhibition of α 4 β 1 function by RGD peptide homologues. *J Biol Chem.* 1991; 266: 3579 - 3585.
127. Dufour S, Duband JL, Humphries MJ, Obara M, Yamada KM, Thiery JP. Attachment, spreading and locomotion of avian neural crest cells are mediated by multiple adhesion sites on fibronectin molecules. *EMBO J.* 1988 Sep; 7(9):2661-71.
128. Raynor JE, Petrie TA, García AJ, Collard DM. Controlling cell adhesion to titanium: Functionalization of poly[oligo(ethylene glycol methacrylate)] brushes with cell-adhesive peptides. *Adv Mater.* 2007; 19(33): 1724-1728.
129. Mizuno M and Kuboki Y. Osteoblast-related gene expression of bone marrow cells during the osteoblastic differentiation induced by type I collagen. *J Biochem (Tokyo).* 2001; 129: 133 - 138.
130. Knight CG, Morton LF, Peachey AR, Tuckwell DS, Farndale RW, Barnes MJ. The collagen-binding A-domains of integrins α (1) β (1) and α (2) β (1) recognize the same specific amino acid sequence, GFOGER, in native (triple-helical) collagens. *J Biol Chem.* 2000; 275: 35 - 40.
131. Knight CG, Morton LF, Onley DJ, Peachey AR, Messent AJ, Smethurst PA, Tuckwell DS, Farndale RW, Barnes MJ. Identification in collagen type I of an integrin α 2 β 1-binding site containing an essential GER sequence. *J Biol Chem.* 1998; 273: 33287 - 33294.
132. Morton LF, Peachey AR, Zijenah LS, Goodall AH, Humphries MJ, Barnes MJ. Conformation-dependent platelet adhesion to collagen involving integrin α 2 β 1-mediated and other mechanisms: multiple α 2 β 1-recognition sites in collagen type I. *Biochem J.* 1994; 299 (Pt 3): 791 - 797.
133. Reyes CD and Garcia AJ. Engineering integrin-specific surfaces with a triple-helical collagen-mimetic peptide. *J Biomed Mater Res A.* 2003; 65: 511 – 523.
134. Koide T. Triple helical collagen-like peptides: engineering and applications in matrix biology. *Connect Tissue Res.* 2005; 46: 131 - 141.
135. Khew ST and Tong YW. The specific recognition of a cell binding sequence derived from type I collagen by Hep3B and L929 cells. *Biomacromolecules.* 2007; 8: 3153 - 3161.

136. Khew ST, Zhu XH, Tong YW. An integrin-specific collagen-mimetic peptide approach for optimizing Hep3B liver cell adhesion, proliferation, and cellular functions. *Tissue Eng.* 2007; 13: 2451 - 2463.
137. Khew ST and Tong YW. Template-assembled triple-helical peptide molecules: mimicry of collagen by molecular architecture and integrin-specific cell adhesion. *Biochemistry.* 2008; 47: 585 - 596.
138. Baronas-Lowell D, Lauer-Fields JL, Fields GB. Induction of endothelial cell activation by a triple helical alpha2beta integrin ligand, derived from type I collagen alpha1(I)496-507. *J Biol Chem.* 2004; 279: 952 - 962.
139. Baronas-Lowell D, Lauer-Fields JL, Borgia JA, Sferrazza GF, Al-Ghoul M, Minond D, Fields GB. Differential modulation of human melanoma cell metalloproteinase expression by alpha2beta1 integrin and CD44 triple-helical ligands derived from type IV collagen. *J Biol Chem.* 2004; 279: 43503 - 43513.
140. Malkar NB, Lauer-Fields JL, Juska D, Fields GB. Characterization of peptide-amphiphiles possessing cellular activation sequences. *Biomacromolecules.* 2003; 4: 518 - 528.
141. Reyes CD, Petrie TA, Burns KL, Garcia AJ. Mixed ECM ligands synergistically modulate integrin adhesion and signaling. *Journal of Cell Physiology.* 2008 Nov;217(2):450-8.
142. Colombi M, Zoppi N, De PG, Marchina E, Gardella R, Tavian D, Ferraboli S, Barlati S. Matrix assembly induction and cell migration and invasion inhibition by a 13-amino acid fibronectin peptide. *J Biol Chem.* 2003; 278: 14346 - 14355.
143. Sechler JL and Schwarzbauer JE. Control of cell cycle progression by fibronectin matrix architecture. *J Biol Chem.* 1998; 273: 25533 - 25536.
144. Schwarzbauer JE and Sechler JL. Fibronectin fibrillogenesis: a paradigm for extracellular matrix assembly. *Curr Opin Cell Biol.* 1999; 11: 622 - 627.
145. Sechler JL, Corbett SA, Schwarzbauer JE. Modulatory roles for integrin activation and the synergy site of fibronectin during matrix assembly. *Mol Biol Cell.* 1997; 8: 2563 - 2573.
146. Takahashi S, Leiss M, Moser M, Ohashi T, Kitao T, Heckmann D, Pfeifer A, Kessler H, Takagi J, Erickson HP, Fassler R. The RGD motif in fibronectin is essential for development but dispensable for fibril assembly. *J Cell Biol.* 2007; 178: 167 - 178.
147. Sechler JL, Takada Y, Schwarzbauer JE. Altered rate of fibronectin matrix assembly by deletion of the first type III repeats. *J Cell Biol.* 1996; 134: 573 - 583.

148. Sechler JL, Cumiskey AM, Gazzola DM, Schwarzbauer JE. A novel RGD-independent fibronectin assembly pathway initiated by alpha4beta1 integrin binding to the alternatively spliced V region. *J Cell Sci.* 2000; 113 (Pt 8): 1491 – 1498.
149. Capadona JR, Petrie TA, Fears KP, Latour RA, Collard DM, Garcia AJ. Surface-nucleated assembly of fibrillar extracellular matrices. *Advanced Materials.* 2005; 17: 2604 - 2608.
150. Gallant ND, Michael KE, Garcia AJ. Cell adhesion strengthening: contributions of adhesive area, integrin binding, and focal adhesion assembly. *Mol Biol Cell.* 2005; 16: 4329 - 4340.
151. Koo LY, Irvine DJ, Mayes AM, Lauffenburger DA, Griffith LG. Co-regulation of cell adhesion by nanoscale RGD organization and mechanical stimulus. *J Cell Sci.* 2002; 115: 1423 - 1433.
152. Maheshwari G, Brown G, Lauffenburger DA, Wells A, Griffith LG. Cell adhesion and motility depend on nanoscale RGD clustering. *J Cell Sci.* 2000; 113: 1677 - 1686.
153. Villard V, Kalyuzhnyi O, Riccio O, Potekhin S, Melnik TN, Kajava AV, Ruegg C, Corradin G. Synthetic RGD-containing alpha-helical coiled coil peptides promote integrin-dependent cell adhesion. *J Pept Sci.* 2006; 12: 206 - 212.
154. Garanger E, Boturyn D, Dumy P. Tumor targeting with RGD peptide ligands-design of new molecular conjugates for imaging and therapy of cancers. *Anticancer Agents Med Chem.* 2007; 7: 552 - 558.
155. Garanger E, Boturyn D, Coll JL, Favrot MC, Dumy P. Multivalent RGD synthetic peptides as potent alphaVbeta3 integrin ligands. *Org Biomol Chem.* 2006; 4: 1958 - 1965.
156. Coussen F, Choquet D, Sheetz MP, Erickson HP. Trimers of the fibronectin cell adhesion domain localize to actin filament bundles and undergo rearward translocation. *J Cell Sci.* 2002; 115: 2581 - 2590.
157. Buckwalter JA, Glimcher MJ, Cooper RR, Recker R. Bone biology. I: Structure, blood supply, cells, matrix, and mineralization. *Instr Course Lect.* 1996; 45:371-386.
158. Buckwalter JA, Glimcher MJ, Cooper RR, Recker R. Bone biology. II: Formation, form, modeling, remodeling, and regulation of cell function. *Instr Course Lect.* 1996; 45:387-399.
159. Mollano AV, Sheu TJ, Puzas JE. Localization of bone formation to areas of bone resorption: osteoporosis and coupling. *Curr Opin Ortho.* 2001; 12:371-377.

160. Raisz LG. Physiology and pathophysiology of bone remodeling. *Clin Chem.* 1999; 45: 1353-1358.
161. Cohen MM. Merging the old skeletal biology with the new: Intramembranous ossification, endochondral ossification, ectopic bone, secondary cartilage, and pathologic considerations. *J Craniofac. Genet. Dev. Biol.* 2000; 20: 84-93.
162. Harada S, Rodan GA. Control of osteoblast function and regulation of bone mass. *Nature.* 2003; 423: 349-355.
163. Ducy P, Zhang R, Geoffroy V, Ridall AL, Karsenty G. *Osf2/Cbfa1*: A transcriptional activator of osteoblast differentiation. *Cell.* 1997; 89: 747-754.
164. Karsenty G. *Cbfa1* as a regulator of osteoblast differentiation and function. *Bone.* 1999; 25: 107-108.
165. Redick SD, Settles DL, Briscoe G, Erickson HP. Defining fibronectin's cell adhesion synergy site by site-directed mutagenesis. *J Cell Biol.* 2000; 149:521-527.
166. Humphries JD, Askari JA, Zhang XP, Takada Y, Humphries MJ, Mould AP. Molecular basis of ligand recognition by integrin $\alpha 5 \beta 1$. II. Specificity of arg-gly-Asp binding is determined by Trp157 OF THE α subunit. *J Biol Chem,* 2000; 275:20337-20345.
167. Feng Y, Mrksich M. The synergy peptide PHSRN and the adhesion peptide RGD mediate cell adhesion through a common mechanism. *Biochemistry.* 2004; 43:15811-15821.
168. Kao WJ, Lee D, Schense JC, Hubbell JA. Fibronectin modulates macrophage adhesion and FBGC formation: the role of RGD, PHSRN, and PRRARV domains. *J Biomed Mater Res.* 2001; 55:79-88.
169. Lahiri J, Isaacs L, Tien J, Whitesides GM. A strategy for the generation of surfaces presenting ligands for studies of binding based on an active ester as a common reactive intermediate: a surface plasmon resonance study. *Anal Chem.* 1999; 71:777-790.
170. Capadona JR, Collard DM, García AJ. Fibronectin adsorption and cell adhesion to mixed monolayers of tri(ethylene glycol)- and methyl-terminated alkanethiols. *Langmuir.* 2003; 19:1847-1852.
171. Reyes CD, García AJ. A centrifugation cell adhesion assay for high-throughput screening of biomaterial surfaces. *J Biomed Mater Res.* 2003; 67A:328-333.
172. Keselowsky BG, García AJ. Quantitative methods for analysis of integrin binding and focal adhesion formation on biomaterial surfaces. *Biomaterials.* 2005; 26:413-418.

173. Leahy DJ, Aukhil I, Erickson HP. 2.0 A crystal structure of a four-domain segment of human fibronectin encompassing the RGD loop and synergy region. *Cell*. 1996; 84:155-164.
174. Schoen RC, Bentley KL, Klebe RJ. Monoclonal antibody against human fibronectin inhibits cell attachment. *Hybridoma*. 1982; 1:99-108.
175. Hanks SK, Ryzhova L, Shin NY, Brabek J. Focal adhesion kinase signaling activities and their implications in the control of cell survival and motility. *Front Biosci*. 2003; 8: 982-996.
176. Wozniak MA, Modzelewska K, Kwong L, Keely PJ. Focal adhesion regulation of cell behavior. *Biochim Biophys Acta*. 2004; 1692:103-119.
177. Mi J, Zhang X, Giangrande PH, McNamara JO, Nimjee SM, Sarraf-Yazdi S, Sullenger BA, Clary BM. Targeted inhibition of alphavbeta3 integrin with an RNA aptamer impairs endothelial cell growth and survival. *Biochem Biophys Res Commun*. 2005; 338:956-963.
178. Cowles EA, Brailey LL, Gronowicz GA. Integrin-mediated signaling regulates AP-1 transcription factors and proliferation in osteoblasts. *J Biomed Mater Res*. 2000; 52:725-737.
179. Massia SP, Hubbell JA. An RGD spacing of 440 nm is sufficient for integrin alpha v beta 3-mediated fibroblast spreading and 140 nm for focal contact and stress fiber formation. *J Cell Biol*. 1991; 114:1089-1100.
180. Shin H, Jo S, Mikos AG. Modulation of marrow stromal osteoblast adhesion on biomimetic oligo[poly(ethylene glycol) fumarate] hydrogels modified with Arg-Gly-Asp peptides and a poly(ethyleneglycol) spacer. *J Biomed Mater Res*. 2002; 61:169-179.
181. Silva GA, Czeisler C, Niece KL, Beniash E, Harrington DA, Kessler JA, Stupp SI. Selective differentiation of neural progenitor cells by high-epitope density nanofibers. *Science*. 2004; 303:1352-1355.
182. Rowley JA, Mooney DJ. Alginate type and RGD density control myoblast phenotype. *J Biomed Mater Res*. 2002; 60:217-223.
183. Heilshorn SC, DiZio KA, Welsh ER, Tirrell DA. Endothelial cell adhesion to the fibronectin CS5 domain in artificial extracellular matrix proteins. *Biomaterials*. 2003; 24:4245-4252.
184. Pilliar RM. Cementless implant fixation--toward improved reliability. *Orthop Clin North Am*. 2005; 36:113-119.
185. Hubbell JA. Biomaterials science and high-throughput screening. *Nat Biotechnol*. 2004; 22:828-829.

186. García AJ. Get a grip: integrins in cell-biomaterial interactions. *Biomaterials*. 2005; 26:7525-7529.
187. Cheng SL, Lou J, Wright NM, Lai CF, Avioli LV, Riew KD. In vitro and in vivo induction of bone formation using a recombinant adenoviral vector carrying the human BMP-2 gene. *Calcif Tissue Int*. 2001; 68:87-94.
188. Tamura Y, Takeuchi Y, Suzawa M, Fukumoto S, Kato M, Miyazono K, Fujita T. Focal adhesion kinase activity is required for bone morphogenetic protein--Smad1 signaling and osteoblastic differentiation in murine MC3T3-E1 cells. *J Bone Miner Res*. 2001; 16:1772-1779.
189. Rammelt S, Heck C, Bernhardt R, Bierbaum S, Scharnweber D, Goebbels J, Ziegler J, Biewener A, Zwipp H. In vivo effects of coating loaded and unloaded Ti implants with collagen, chondroitin sulfate, and hydroxyapatite in the sheep tibia. *J Orthop Res*. 2007; 25:1052-1061.
190. Wang H, Eliaz N, Xiang Z, Hsu HP, Spector M, Hobbs LW. Early bone apposition in vivo on plasma-sprayed and electrochemically deposited hydroxyapatite coatings on titanium alloy. *Biomaterials*. 2006; 27:4192-4203.
191. Siebers MC, Wolke JG, Frank W, X, Leeuwenburgh SC, Jansen JA. In vivo evaluation of the trabecular bone behavior to porous electrostatic spray deposition-derived calcium phosphate coatings. *Clin Oral Implants Res*. 2007; 18:354-361.
192. Kanagaraja S, Lundstrom I, Nygren H, Tengvall P. Platelet binding and protein adsorption to titanium and gold after short time exposure to heparinized plasma and whole blood. *Biomaterials*. 1996; 17:2225-2232.
193. Nakamura I, Pilkington MF, Lakkakorpi PT, Lipfert L, Sims SM, Dixon SJ, Rodan GA, Duong LT. Role of alpha(v)beta(3) integrin in osteoclast migration and formation of the sealing zone. *J Cell Sci*. 1999; 112:3985-3993.
194. Engleman VW, Nickols GA, Ross FP, Horton MA, Griggs DW, Settle SL, Ruminski PG, Teitelbaum SL. A peptidomimetic antagonist of the alpha(v)beta3 integrin inhibits bone resorption in vitro and prevents osteoporosis in vivo. *J Clin Invest*. 1997; 99:2284-2292.
195. Hutchinson JH, Halczenko W, Brashear KM, Breslin MJ, Coleman PJ, Duong IT, Fernandez-Metzler C, Gentile MA, Fisher JE, Hartman GD, Huff JR, Kimmel DB, Leu CT, Meissner RS, Merkle K, Nagy R, Pennypacker B, Perkins JJ, Prueksaritanont T, Rodan GA, Varga SL, Wesolowski GA, Zartman AE, Rodan SB, Duggan ME. Nonpeptide alphavbeta3 antagonists. 8. In vitro and in vivo evaluation of a potent alphavbeta3 antagonist for the prevention and treatment of osteoporosis. *J Med Chem*. 2003; 46:4790-4798.
196. Carron CP, Meyer DM, Engleman VW, Rico JG, Ruminski PG, Ornberg RL, Westlin WF, Nickols GA. Peptidomimetic antagonists of alphavbeta3 inhibit bone

resorption by inhibiting osteoclast bone resorptive activity, not osteoclast adhesion to bone. *J Endocrinol.* 2000; 165:587-598.

197. Ducheyne P, Qiu Q. Bioactive ceramics: the effect of surface reactivity on bone formation and bone cell function. *Biomaterials.* 1999; 20: 2287 - 03.
198. Ripamonti U, Richter PW, Nilen RW, Renton L. The induction of bone formation by smart biphasic hydroxyapatite tricalcium phosphate biomimetic matrices in the non-human primate *Papio ursinus*. *J Cell Mol Med.* 2008; 12: 1029-48.
199. Chung EH, Gilbert M, Viridi AS, Sena K, Sumner DR, Healy KE. Biomimetic artificial ECMs stimulate bone regeneration. *J Biomed Mater Res A.* 2006; 79: 815 - 26.
200. Hubbell JA. Materials as morphogenetic guides in tissue engineering. *Curr Opin Biotechnol.* 2003; 14: 551 - 8.
201. Bernhardt R, Van Den DJ, Bierbaum S, Beutner R, Scharnweber D, Jansen J, Beckmann F, Worch H. Osteoconductive modifications of Ti-implants in a goat defect model: characterization of bone growth with SR μ CT and histology. *Biomaterials.* 2005; 26: 3009 - 19.
202. Becker D, Geissler U, Hempel U, Bierbaum S, Scharnweber D, Worch H, Wenzel KW. Proliferation and differentiation of rat calvarial osteoblasts on type I collagen-coated titanium alloy. *J Biomed Mater Res.* 2002; 59: 516 - 27.
203. De RA, Viridi AS, Kuroda S, Shott S, Leven RM, Hallab NJ, Sumner DR. Local application of rhTGF-beta2 enhances peri-implant bone volume and bone-implant contact in a rat model. *Bone.* 2005; 37: 55 - 62.
204. Sumner DR, Turner TM, Urban RM, Viridi AS, Inoue N. Additive enhancement of implant fixation following combined treatment with rhTGF-beta2 and rhBMP-2 in a canine model. *J Bone Joint Surg Am.* 2006; 88: 806 - 17.
205. Ho JE, Chung EH, Wall S, Schaffer DV, Healy KE. Immobilized sonic hedgehog N-terminal signaling domain enhances differentiation of bone marrow-derived mesenchymal stem cells. *J Biomed Mater Res A.* 2007; 83: 1200 - 08.
206. Muller P, Bulnheim U, Diener A, Luthen F, Teller M, Klinkenberg ED, Neumann HG, Nebe B, Liebold A, Steinhoff G, Rychly J. Calcium phosphate surfaces promote osteogenic differentiation of mesenchymal stem cells. *J Cell Mol Med.* 2008; 12: 281 - 91.
207. Logeart-Avramoglou D, Anagnostou F, Bizios R, Petite H. Engineering bone: challenges and obstacles. *J Cell Mol Med.* 2005; 9: 72 - 84.
208. Kneser U, Schaefer DJ, Polykandriotis E, Horch RE. Tissue engineering of bone: the reconstructive surgeon's point of view. *J Cell Mol Med.* 2006; 10: 7 - 19.

209. Ripamonti U. Osteoinduction in porous hydroxyapatite implanted in heterotopic sites of different animal models. *Biomaterials*. 1996; 17: 31 - 5.
210. Adams JC, Watt FM. Regulation of development and differentiation by the extracellular matrix. *Development*. 1993; 117: 1183 - 98.
211. Damsky CH. Extracellular matrix-integrin interactions in osteoblast function and tissue remodeling. *Bone*. 1999; 25: 95 - 96.
212. Clark EA, Brugge JS. Integrins and signal transduction pathways: the road taken. *Science*. 1995; 268: 233 - 39.
213. Takeuchi Y, Suzawa M, Kikuchi T, Nishida E, Fujita T, Matsumoto T. Differentiation and transforming growth factor-beta receptor down-regulation by collagen-alpha2beta1 integrin interaction is mediated by focal adhesion kinase and its downstream signals in murine osteoblastic cells. *J Biol Chem*. 1997; 272: 29309 - 16.
214. Mizuno M, Fujisawa R, Kuboki Y. Type I collagen-induced osteoblastic differentiation of bone-marrow cells mediated by collagen-alpha2beta1 integrin interaction. *J Cell Physiol*. 2000; 184: 207 - 13.
215. Luthen F, Lange R, Becker P, Rychly J, Beck U, Nebe JG. The influence of surface roughness of titanium on beta1- and beta3-integrin adhesion and the organization of fibronectin in human osteoblastic cells. *Biomaterials*. 2005; 26: 2423 - 40.
216. Roche P, Goldberg HA, Delmas PD, Malaval L. Selective attachment of osteoprogenitors to laminin. *Bone*. 1999; 24: 329 - 36.
217. Garcia AJ, Keselowsky BG. Biomimetic surfaces for control of cell adhesion to facilitate bone formation. *Crit Rev Eukaryot Gene Expr*. 2002; 12: 151 - 62.
218. Schneider GB, Zaharias R, Stanford C. Osteoblast integrin adhesion and signaling regulate mineralization. *J Dent Res*. 2001; 80: 1540 - 4.
219. Docheva D, Popov C, Mutschler W, Schieker M. Human mesenchymal stem cells in contact with their environment: surface characteristics and the integrin system. *J Cell Mol Med*. 2007; 11: 21 - 38.
220. Guillot PV, Cui W, Fisk NM, Polak DJ. Stem cell differentiation and expansion for clinical applications of tissue engineering. *J Cell Mol Med*. 2007; 11: 935 - 44.
221. Liu YK, Uemura T, Nemoto A, Yabe T, Fujii N, Ushida T, Tateishi T. Osteopontin involvement in integrin-mediated cell signaling and regulation of expression of alkaline phosphatase during early differentiation of UMR cells. *FEBS Lett*. 1997; 420: 112 - 16.

222. Lynch MP, Stein JL, Stein GS, Lian JB. The influence of type I collagen on the development and maintenance of the osteoblast phenotype in primary and passaged rat calvarial osteoblasts: modification of expression of genes supporting cell growth, adhesion, and extracellular matrix mineralization. *Exp Cell Res.* 1995; 216: 35 - 45.
223. Healy KE, Rezanian A, Stile RA. Designing biomaterials to direct biological responses. *Ann N Y Acad Sci.* 1999; 875: 24 - 35.
224. Krebsbach PH, Kuznetsov SA, Bianco P, Robey PG. Bone marrow stromal cells: characterization and clinical application. *Crit Rev Oral Biol Med.* 1999; 10: 165 - 81.
225. Aubin JE. Osteoprogenitor cell frequency in rat bone marrow stromal populations: role for heterotypic cell-cell interactions in osteoblast differentiation. *J Cell Biochem.* 1999; 72: 396 - 410.
226. Garcia AJ. Get a grip: integrins in cell-biomaterial interactions. *Biomaterials.* 2005; 26: 7525 - 29.
227. Aubin JE, Liu F. The osteoblast lineage. In: Bilezikien JP, Raisz LG, Rodan GA, editors. *Principles of Bone Biology.* San Diego: Academic Press; 1996. p. 69 - 88.
228. Ripamonti U, Richter PW, Thomas ME. Self-inducing shape memory geometric cues embedded within smart hydroxyapatite-based biomimetic matrices. *Plast Reconstr Surg.* 2007; 120: 1796 - 807.
229. Ripamonti U. Soluble osteogenic molecular signals and the induction of bone formation. *Biomaterials.* 2006; 27: 807 - 22.
230. Miyamoto S, Akiyama SK, Yamada KM. Synergistic roles for receptor occupancy and aggregation in integrin transmembrane function. *Science.* 1995; 267:883-885.
231. Miyamoto S, Teramoto H, Coso OA, Gutkind JS, Burbelo PD, Akiyama SK, Yamada KM. Integrin function: molecular hierarchies of cytoskeletal and signaling molecules. *J Cell Biol.* 1995; 131:791-805.
232. Huang J, Grater SV, Corbellini F, Rinck S, Bock E, Kemkemer R, Kessler H, Ding J, Spatz JP. Impact of order and disorder in RGD nanopatterns on cell adhesion. *Nano Lett.* 2009 Mar; 9(3):1111-6.
233. Petrie TA, Reyes CD, Burns KL, García AJ. Simple application of fibronectin-mimetic coating enhances osseointegration of titanium implants. *J Cell Mol Med.* 2008 Aug 21.
234. Garanger E, Boturyn D, Dumy P. Tumor targeting with RGD peptide ligands-design of new molecular conjugates for imaging and therapy of cancers. *Anticancer Agents Med Chem.* 2007; 7:552-558.

235. Garanger E, Boturyn D, Jin Z, Dumy P, Favrot MC, Coll JL. New multifunctional molecular conjugate vector for targeting, imaging, and therapy of tumors. *Mol Ther*. 2005; 12:1168-1175.
236. Basha S, Rai P, Poon V, Saraph A, Gujraty K, Go MY, Sadacharan S, Frost M, Mogridge J, Kane RS. Polyvalent inhibitors of anthrax toxin that target host receptors. *Proc Natl Acad Sci USA*. 2006; 103:13509-13513.
237. Rai P, Padala C, Poon V, Saraph A, Basha S, Kate S, Tao K, Mogridge J, Kane RS. Statistical pattern matching facilitates the design of polyvalent inhibitors of anthrax and cholera toxins. *Nat Biotechnol*. 2006; 24:582-586.
238. Petrie TA, Stanley BT, García AJ. Micropatterned surfaces with controlled ligand tethering. *J Biomed Mater Res A*. 2008 Jun 20.
239. Beck K, Gambée JE, Bohan CA, Bächinger HP. The C-terminal domain of cartilage matrix protein assembles into a triple-stranded alpha-helical coiled-coil structure. *J Mol Biol*. 1996; 256(5):909-23.
240. Yamada KM. Functions of integrins in cell adhesion and migration. *AIDS Res Hum Retroviruses*. 1992; 8(5):786-93.
241. Brinkerhoff CJ, Linderman JJ. Integrin dimerization and ligand organization: key components in integrin clustering for cell adhesion. *Tissue Eng*. 2005; 11(5-6):865-76.
242. Brinkerhoff CJ, Woolf PJ, Linderman JJ. Monte Carlo simulations of receptor dynamics: insights into cell signaling. *J Mol Histol*. 2004; 35(7):667-77.
243. Irvine DJ, Hue KA, Mayes AM, Griffith LG. Simulations of cell-surface integrin binding to nanoscale-clustered adhesion ligands. *Biophys J*. 2002; 82(1 Pt 1):120-32.
244. Zhao T, Li Y, Dinner AR. How focal adhesion size depends on integrin affinity. *Langmuir*. 2009; 25(3):1540-6.
245. Brinkerhoff CJ, Linderman JJ. Integrin dimerization and ligand organization: key components in integrin clustering for cell adhesion. *Tissue Eng*. 2005; 11(5-6):865-76
246. French-Constant C, Colognato H. Integrins: versatile integrators of extracellular signals. *Trends Cell Biol*. 2004; 14(12):678-86.

247. Charest JL, García AJ, King WP. Myoblast alignment and differentiation on cell culture substrates with microscale topography and model chemistries. *Biomaterials*. 2007; 28(13):2202-10.
248. Somerman M, Hewitt AT, Varner HH, Schiffmann E, Termine J, Reddi AH. Identification of a bone matrix-derived chemotactic factor. *Calcif Tissue Int*. 1983; 35(4-5):481-5.
249. Coyer SR, García AJ, Delamarche E. Facile preparation of complex protein architectures with sub-100-nm resolution on surfaces. *Angew Chem Int Ed Engl*. 2007; 46(36):6837-40.
250. Petersen S, Alonso JM, Specht A, Duodu P, Goeldner M, del Campo A. Phototriggering of cell adhesion by caged cyclic RGD peptides. *Angew Chem Int Ed Engl*. 2008; 47(17):3192-5.
251. Raimondi MT. Engineered tissue as a model to study cell and tissue function from a biophysical perspective. *Curr Drug Discov Technol*. 2006; 3(4):245-68.
252. Smith DM, Cooper GM, Mooney MP, Marra KG, Losee JE. Bone morphogenetic protein 2 therapy for craniofacial surgery. *J Craniofac Surg*. 2008; 19(5):1244-59.
253. Phillips JE, Burns KL, Le Doux JM, Guldberg RE, García AJ. Engineering graded tissue interfaces. *Proc Natl Acad Sci U S A*. 2008; 105(34):12170-5.
254. Humes HD, Buffington DA, MacKay SM, Funke AJ, and Weitzel WF. Replacement of renal function in uremic animals with a tissue-engineered kidney. *Nat Biotechnol* 1999; 17:451-455.
255. Bhatia SN, Balis UJ, Yarmush ML, and Toner M. Microfabrication of hepatocyte/fibroblast co-cultures: role of homotypic cell interactions. *Biotechnol Prog* 1998; 14:378-387.
256. Huynh T, Abraham G, Murray J, Brockbank K, Hagen PO, and Sullivan S. Remodeling of an acellular collagen graft into a physiologically responsive neovessel. *Nat Biotechnol* 1999; 17:1083-1086.
257. Chen CS, Mrksich M, Huang S, Whitesides G, and Ingber DE. Geometric control of cell life and death. *Science* 1997; 276:1425-1428.
258. Singhvi R, Kumar A, Lopez GP, Stephanopoulos GN, Wang DI, Whitesides GM, and Ingber DE. Engineering cell shape and function. *Science* 1994; 264:696-698.
259. Kane RS, Takayama S, Ostuni E, Ingber DE, and Whitesides GM. Patterning proteins and cells using soft lithography. *Biomaterials* 1999; 20:2363-2376.
260. Bhatia SN, Yarmush ML, and Toner M. Controlling cell interactions by micropatterning in co-cultures: hepatocytes and 3T3 fibroblasts. *J Biomed Mater Res* 1997; 34:189-199.

261. Anamelechi CC, Truskey GA, and Reichert WM. Mylar and Teflon-AF as cell culture substrates for studying endothelial cell adhesion. *Biomaterials* 2005; 26:6887-6896.
262. Borkholder DA, Bao J, Maluf NI, Perl ER, and Kovacs GT. Microelectrode arrays for stimulation of neural slice preparations. *J Neurosci Methods* 1997; 77:61-66.
263. Kato K, Toda M, and Iwata H. Antibody arrays for quantitative immunophenotyping. *Biomaterials* 2007; 28:1289-1297.
264. Park TH and Shuler ML. Integration of cell culture and microfabrication technology. *Biotechnol Prog* 2003; 19:243-253.
265. Lehnert D, Wehrle-Haller B, David C, Weiland U, Ballestrem C, Imhof BA, and Bastmeyer M. Cell behaviour on micropatterned substrata: limits of extracellular matrix geometry for spreading and adhesion. *J Cell Sci* 2004; 117:41-52.
266. Brock A, Chang E, Ho CC, Leduc P, Jiang XY, Whitesides GM, and Ingber DE. Geometric determinants of directional cell motility revealed using microcontact printing. *Langmuir* 2003;19:1611-1617.
267. Wang N, Ostuni E, Whitesides GM, and Ingber DE. Micropatterning tractional forces in living cells. *Cell Motility and the Cytoskeleton* 2002; 52:97-106.
268. Milner KR and Siedlecki CA. Fibroblast response is enhanced by poly(L-lactic acid) nanotopography edge density and proximity. *Int J Nanomedicine* 2007; 2:201-211.
269. Milner KR and Siedlecki CA. Submicron poly(L-lactic acid) pillars affect fibroblast adhesion and proliferation. *J Biomed Mater Res A* 2007; 82:80-91.
270. Maskarinec SA and Tirrell DA. Protein engineering approaches to biomaterials design. *Curr Opin Biotechnol* 2005; 16:422-426.
271. Boontheekul T and Mooney DJ. Protein-based signaling systems in tissue engineering. *Curr Opin Biotechnol* 2003; 14:559-565.
272. Whitesides GM, Ostuni E, Takayama S, Jiang X, and Ingber DE. Soft lithography in biology and biochemistry. *Annu Rev Biomed Eng* 2001; 3:335-373.
273. Truskett VN and Watts MPC. Trends in imprint lithography for biological applications. *Trends in Biotechnology* 2006; 24:312-317.
274. Blawas AS and Reichert WM. Protein patterning. *Biomaterials* 1998; 19:595-609.
275. Gallant ND, Capadona JR, Frazier AB, Collard DM, and García AJ. Micropatterned surfaces for analyzing cell adhesion strengthening. *Langmuir* 2002; 18:5579-5584.

276. Gallant ND, Charest JL, King WP, and Garcia AJ. Micro- and nano-patterned substrates to manipulate cell adhesion. *J Nanosci Nanotechnol* 2007; 7:803-807.
277. Prime KL and Whitesides GM. Self-assembled organic monolayers: model systems for studying adsorption of proteins at surfaces. *Science* 1991; 252:1164-1167.
278. Mrksich M, Dike LE, Tien J, Ingber DE, and Whitesides GM. Using microcontact printing to pattern the attachment of mammalian cells to self-assembled monolayers of alkanethiolates on transparent films of gold and silver. *Exp Cell Res* 1997; 235:305-313.
279. Mrksich M and Whitesides GM. Patterning self-assembled monolayers using microcontact printing: a new technology for biosensors. *Trends in Biotechnology* 1995; 13:228-235.
280. Chen CS, Mrksich M, Huang S, Whitesides GM, and Ingber DE. Micropatterned surfaces for control of cell shape, position, and function. *Biotechnol Prog* 1998; 14:356-363.
281. Roberts C, Chen CS, Mrksich M, Martichonok V, Ingber DE, and Whitesides GM. Using mixed self-assembled monolayers presenting RGD and (EG)3OH groups to characterize long-term attachment of bovine capillary endothelial cells to surfaces. *J Am Chem Soc* 1998; 120:6548-6555.
282. Takayama S, Ostuni E, LeDuc P, Naruse K, Ingber DE, and Whitesides GM. Subcellular positioning of small molecules. *Nature* 2001; 411:1016-
283. Ostuni E, Chen CS, Ingber DE, and Whitesides GM. Selective deposition of proteins and cells in arrays of microwells. *Langmuir* 2001; 17:2828-2834.
284. Lahiri J, Ostuni E, and Whitesides GM. Patterning Ligands on Reactive SAMs by Microcontact Printing. *Langmuir* 1999; 15:2055-2060.
285. Ingber DE. Fibronectin controls capillary endothelial cell growth by modulating cell shape. *Proc Natl Acad Sci U S A* 1990; 87:3579-3583.
286. Nelson CM, Raghavan S, Tan JL, and Chen CS. Degradation of micropatterned surfaces by cell-dependent and -independent processes. *Langmuir* 2003; 19:1493-1499.
287. Smith JT, Elkin JT, and Reichert WM. Directed cell migration on fibronectin gradients: effect of gradient slope. *Exp Cell Res* 2006; 312:2424-2432.
288. Smith JT, Tomfohr JK, Wells MC, Beebe TP, Jr., Kepler TB, and Reichert WM. Measurement of cell migration on surface-bound fibronectin gradients. *Langmuir* 2004; 20:8279-8286.

289. Re F, Zanetti A, Sironi M, Polentarutti N, Lanfranccone L, Dejana E, and Colotta F. Inhibition of anchorage-dependent cell spreading triggers apoptosis in cultured human endothelial cells. *J Cell Biol* 1994; 127:537-546.
290. Gujraty KV, Ashton R, Bethi SR, Kate S, Faulkner CJ, Jennings GK, and Kane RS. Thiol-Mediated Anchoring of Ligands to Self-Assembled Monolayers for Studies of Biospecific Interactions. *Langmuir* 2006; 22:10157-10162.
291. Gauvreau V and Laroche G. Micropattern printing of adhesion, spreading, and migration peptides on poly(tetrafluoroethylene) films to promote endothelialization. *Bioconjug Chem* 2005; 16:1088-1097.
292. Jiang X, Xu Q, Dertinger SK, Stroock AD, Fu TM, and Whitesides GM. A general method for patterning gradients of biomolecules on surfaces using microfluidic networks. *Anal Chem* 2005; 77:2338-2347.
293. Kam L, Boxer SG. Cell adhesion to protein-micropatterned-supported lipid bilayer membranes. *J Biomed Mater Res.* 2001; 55:487-495.
294. Ducheyne P, Cuckler JM. Bioactive ceramic prosthetic coatings. *Clin Orthop Relat Res.* 1992; 276:102-14.
295. Flynn NT, Tran TNT, Cima MJ, Langer R. Long-term stability of self-assembled monolayers in biological media. *Langmuir* 2003; 19(26):10909-10915.
296. Ma HW, Wells M, Beebe TP, Chilkoti A. Surface-initiated atom transfer radical polymerization of oligo(ethylene glycol) methyl methacrylate from a mixed self-assembled monolayer on gold. *Adv Funct Materials* 2006; 16(5):640-648.
297. Fan XW, Lin LJ, Dalsin JL, Messersmith PB. Biomimetic anchor for surface-initiated polymerization from metal substrates. *J Amer Chem Society* 2005; 127(45):15843-15847.
298. Lahiri J, Isaacs L, Grzybowski B, Carbeck JD, Whitesides GM. Biospecific binding of carbonic anhydrase to mixed SAMs presenting benzenesulfonamide ligands: A model system for studying lateral steric effects. *Langmuir* 1999; 15(21):7186-7198.
299. Ma HW, Li DJ, Sheng X, Zhao B, Chilkoti A. Protein-resistant polymer coatings on silicon oxide by surface-initiated atom transfer radical polymerization. *Langmuir* 2006; 22(8):3751-3756.
300. Barber TA, Harbers GM, Park S, Gilbert M, Healy KE. Ligand density characterization of peptide-modified biomaterials. *Biomaterials* 2005; 26(34):6897-6905.
301. Dalsin JL, Lin LJ, Tosatti S, Voros J, Textor M, Messersmith PB. Protein resistance of titanium oxide surfaces modified by biologically inspired mPEG-DOPA. *Langmuir* 2005; 21(2):640-646.

302. Andruzzi L, Senaratne W, Hexemer A, Sheets ED, Ilic B, Kramer EJ, Baird B, Ober CK. Oligo(ethylene glycol) containing polymer brushes as bioselective surfaces. *Langmuir* 2005; 21(6):2495-2504.
303. Barber TA, Golledge SL, Castner DG, Healy KE. Peptide-modified p(AAm-co-EG/AAc) IPNs grafted to bulk titanium modulate osteoblast behavior in vitro. *J Biomed Mater Res.* 2003; 64A(1):38-47.
304. Matyjaszewski K, Miller PJ, Shukla N, Immaraporn B, Gelman A, Luokala BB, Siclovan TM, Kickelbick G, Vallant T, Hoffmann H, Pakula T. Polymers at interfaces: Using atom transfer radical polymerization in the controlled growth of homopolymers and block copolymers from silicon surfaces in the absence of untethered sacrificial initiator. *Macromolecules* 1999; 32(26):8716-8724.
305. Nanci A, Wuest JD, Peru L, Brunet P, Sharma V, Zalzal S, McKee MD. Chemical modification of titanium surfaces for covalent attachment of biological molecules. *J Biomed Mater Res.* 1998; 40(2):324-335.
306. Lee JP, Jang YJ, Sung MM. Atomic layer deposition of TiO₂ thin films on mixed self-assembled monolayers studied as a function of surface free energy. *Adv Funct Materials* 2003; 13(11):873-876.
307. Tugulu S, Arnold A, Sielaff I, Johnsson K, Klok HA. Protein-functionalized polymer brushes. *Biomacromolecules* 2005; 6(3):1602-1607.

VITA

TIMOTHY ANDREW PETRIE

Timothy is from Southern California, a land far, far away - a magical place of sunshine, great mexican food, beaches, unicorns, and incredibly overpriced housing and state tax. He was fortunate to be born and brought up in San Diego, where both outdoor activities, including basketball, running, surfing, swimming, hiking, and football, and Roberto's Taco Shop became a large part of his happy childhood and young life. He participated in many varsity sports as well as science and math activites at La Jolla High School, and when he wasn't coming into 2nd period late from the beach or down at the taco shop, he enjoyed mathematics and science classes. He made the magnificent choice of attending UC Berkeley (Go Bears!) for his undergraduate education, spurning many absurd institutions like Stanford (whose mascot is... a Pine Tree). Participating in wide-ranging research in cell biology, imaging and electrosopy, and biomaterials during his four-year tenure, he developed a passion for crazy ideas, hard work, and scientific discovery that has persisted throughout his academic career. He met his current PhD advisor at the most marvelous place in the western hemisphere, where magic goes to rest in peace - Reno, Nevada – at a biomaterials conference and was introduced by Dr. Kevin Healy of UC Berkeley. Timothy enjoyed this loud and brazen Puerto Rican genius, and applied to Georgia Institute of Technology to conduct research in his lab, blissfully unaware of where Georgia Tech or Georgia was located. Despite finding out he would be living next to Alabama and Tennessee, he still decided to work in Dr. Garcia's laboratory in the ATL. His time at Tech was eye-opening and incredibly worthwhile, and his colleagues and friends made the experience an absolute blast. He even began enjoying southern food, the Tennessee and South Carolina landscapes, and the dirty south lifestyle. Timothy continues to run, weightlift, swim, bike, attend road San Diego Charger football games with his amazing brother Jon, and procrastinate for pleasure. He hopes to return to his roots in the West and continue his academic career in California, after postdocing in Randall Moon's laboratory in U Washington.